CFD SIMULATIONS IN SUPPORT OF WIND TUNNEL TESTING

by

Wanan SHENG

Dissertation submitted to the Department of Aerospace Engineering, Faculty of Engineering, University of Glasgow, for the Degree of Doctor of Philosophy

November, 2003

To my wife Xiaoyun and son Ziyan with love

PREFACE

The work described in this dissertation was carried out by the author in the Department of Aerospace Engineering of the University of Glasgow, during the period January 2000 to November 2003, the dissertation is original in content except where otherwise stated.

Wanan Sheng

July, 2003

CONTENTS

Lists of Figures viii

Lists of Tables xii

Acknowledgements xiii

Abstract xiv

Nomenclature xvi

Chapter 1 Introduction

1.1 Overview 1

1.2 Computational Fluid Dynamics 4

1.2.1 Grid Generation 4

1.2.2 Turbulence Modelling 7

1.2.3 Large Eddy Simulation-LES 10

1.2.4 Direct Numerical Simulation-DNS 12

1.3 CFD Applications 13

1.4 CFD for Aerodynamic Design 16

1.5 Roles of Wind Tunnel Test 20

1.6 Concluding Remarks 22

Figures of Chapter 1 24

Chapter 2 CFD Applications in Wind Tunnels

2.1 Introduction 33

2.2 CFD Applications in Wind Tunnel Experiments 35

2.2.1 Model Design and Fabrication 35
2.2.2 Experiment Set-up 37
2.2.3 Experiment Monitoring 38
2.2.4 Data Analysis 39
2.3 CFD Applications in Data Correction of Wind Tunnel Test 39
2.4 CFD Applications in Wind Tunnel Design 40
2.5 CFD Applications in Virtual Wind Tunnel 41
2.6 CFD in Support of Wind Tunnel 42
2.7 Concluding Remarks 43
Figures of Chapter 2 44

Chapter 3 Numerical Simulation (I): Working Section

3.1 Introduction 47
3.2 Boundary Layer Simulation 48
3.3 Simulation of the Working Section 52
3.4 Improvements of Boundary Layer Removal 54
3.5 Calibration of Working Section 55
3.6 Concluding Remarks 57
Figures of Chapter 3 58

Chapter 4 Numerical Simulation (II): A Car in Working Section

4.1 Introduction 70
4.2 Numerical Simulation of Car in Free Air 74
4.3 Numerical Simulation of a Car in Working Section 75
4.3.1 Grid 75
4.3.2 A Car in Working Section (no Strut) 76

4.3.3 A Car in Working Section (with Strut) 77

4.4 Result Analysis of Numerical Simulation 78

4.4.1 Strut and Tunnel Wall Effect on Drag and Lift 78

4.4.2 Effect of Strut Position on Drag and Lift 78

4.4.3 Effect of Ground Clearances 79

4.5 Concluding Remarks 80

Figures of Chapter 4 81

Chapter 5 Blockage Corrections and CFD

5.1 Introduction 99

5.2 Blockage Correction Methods 102

5.2.1 Classical Methods 102

5.2.2 Boundary Measurement Methods 105

5.2.3 Computational Fluid Dynamics (CFD) Methods 106

5.3 Blockage Correction for Bluff Bodies 107

5.4 CFD applications in Blockage Corrections 108

5.5 Concluding Remarks 110

Figures of Chapter 5 111

Chapter 6 Numerical Simulation (III): Working Section with Diffuser/Contraction/Settling Chamber

6.1 Introduction 115

6.2 The Effect of Test Model on Inlet and Exit Conditions 117

6.3 Numerical Simulation of Working Section with Diffuser/Contraction/ Settling Chamber 118

6.4 Concluding Remarks 120

Figures of Chapter 6 121

Chapter 7 Model Testing of a Car in Wind Tunnel

7.1 Introduction 131

7.2 Methodologies of Model Test 132

7.3 Use of Wind Tunnel Data 133

7.4 Car Model 134

7.5 Aerodynamics Test of Car 136

7.6 Flow Visualization 137

7.7 Concluding Remarks 139

Figures of Chapter 7 140

Chapter 8 Conclusions and Future Work

8.1 Conclusions 146

8.2 Future Work 149

References 151

Appendix A: N-S equations and Turbulence Models 160

Appendix B: Near-Wall Treatments 170

Appendix C: Dimensional Analysis and Similitude Laws 176

LISTS OF FIGURES

Figure 1.1 Numerical Computation of MD-11 ····24

Figure 1.2 CFD analysis of F-18 E aircraft ····25

Figure 1.3 Hierarchy of Computational Fluid Dynamics ····26

Figure 1.4 Approximation of sphere in Cartesian co-ordinates ···· 27

Figure 1.5 Structured grids ····27

Figure 1.6 3D unstructured grid ····28

Figure 1.7 Hybrid grid around an airfoil ····28

Figure 1.8 Grid Adaptation ····29

Figure 1.9 Time-average velocity along centerline of square cylinder ···· 30

Figure 1.10 Simulation of flow past circular cylinder by various approaches ···· 30

Figure 1.11 DNS of turbulent flow over a backward-facing step ····31

Figure 1.12 Torpedo launch from a submarine bay ····31

Figure 1.13 A naval destroyer moving at 20 kn, with smoke from the stacks and an approaching helicopter ····32

Figure 1.14 Pressure and velocity vector for the flow over the Mir Space Station at 110km ····32

Figure 2.1 Pressure tap arrangements ····44

Figure 2.2 Comparison of wind tunnel and CFD predicted pressure ···· 44

Figure 2.3 Upper surface *Cp* distribution (Lamar et al 2001) ···· 45

Figure 2.4 Superposition of liquid crystal and tuft image data for F-16XL-1 airplane at $\alpha \approx 13^0$, $M_\infty = 0.28$, and $Re = 47 \times 10^6$···· 45

Figure 2.5 Wind tunnel data (uncorrected) ····46

Figure 2.6 Wind tunnel data after correction ····46

Figure 2.7 The completed wind/water tunnel ····46

Figure 3.1 Glasgow University Argyll Wind Tunnel ···· 58

Figure 3.2 Moving belt system of the Argyll Wind Tunnel ···· 58

Figure 3.3 Multi-Suction-and-Blowing methods ···· 58

Figure 3.4 Boundary layer removal methods ···· 59

Figure 3.5 Boundary layer simulation using different turbulence models ····· 59
Figure 3.6 Pressure distributions along the working section ····· 60
Figure 3.7 Boundary layer simulations in different near-wall-treatments ····· 60
Figure 3.8 Coarse grid with 78925 elements ····· 60
Figure 3.9 Fine grid with 123750 elements ····· 61
Figure 3.10 Boundary layer simulation with different coarse and fine grid ····· 61
Figure 3.11 Inlet and outlet of the working section with an expansion ····· 61
Figure 3.12 Static pressure along the working section with/without an expansion ··· 62
Figure 3.13 Velocity distribution along the central line of working section ····· 62
Figure 3.14 Velocity distributions above tunnel floor ····· 62
Figure 3.15 Velocity profiles with vent exit ····· 63
Figure 3.16 Velocity and pressure coefficient in the WS ····· 64
Figure 3.17 Comparisons of the velocity distributions above moving ground ····· 65
Figure 3.18 Improved moving ground (flush with tunnel floor) ····· 65
Figure 3.19 Boundary layer removal for the improved moving ground ····· 66
Figure 3.20 The comparison of flush floor, all moving ground and the experiment ··67
Figure 3.21 "Empty tunnel" calibration ····· 67
Figure 3.22 Velocity and pressure coefficient contours of working section with strut (longitudinal) ····· 68
Figure 3.23 Pressure contours of working section with strut ····· 69

Figure 4.1 Ahmed's Automotive-like Bluff Body ····· 81
Figure 4.2 Increment in total coefficient ····· 81
Figure 4.3 Flowfield over the car in open air (Scale=30%) ····· 83
Figure 4.4 Flowfield over the car in open air (Scale=60%) ····· 84
Figure 4.5 Flow ribbons over the car (Scale=30%) ····· 84
Figure 4.6 Flow ribbons over the car (Scale=60%) ····· 85
Figure 4.7 Drag coefficients in different scales ····· 85
Figure 4.8 Grids are used in the research ····· 86
Figure 4.9 Car in the tunnel (no Strut, Scale=30%) ····· 89
Figure 4.10 Car in the tunnel (no Strut, Scale=60%) ····· 90
Figure 4.11 Velocity Vectors behind the car ····· 91
Figure 4.12 Velocity vectors (transverse section) behind the car ····· 93
Figure 4.13 Car in the tunnel (with Strut, Scale=30%) ····· 95

Figure 4.14 Car in the tunnel (with Strut, Scale=60%) 96
Figure 4.15 Coefficient comparison 96
Figure 4.16 Support systems used in conventional aircraft testing 97
Figure 4.17 Photography of the strut 97
Figure 4.18 Effect of strut position on the drag and lift 98
Figure 4.19 Clearance height effect on the coefficients 98

Figure 5.1 Model representation with elementary singularities 111
Figure 5.2 Image System for a Model in the Rectangular Working Section 111
Figure 5.3 Panel discretisation of the wind tunnel settling chamber, contraction, working section and diffuser 112
Figure 5.4 Typical orifice locations for the pressure signature method 112
Figure 5.5 Boundary interference correction method 113
Figure 5.6 Numerical results of drag coefficient in different cases 113
Figure 5.7 Drag coefficients after correction (numerical results) 114

Figure 6.1 Velocity and pressure contours of the working section, 1st diffuser and contraction 121
Figure 6.2 Velocity and Pressure Contours at Inlet and Outlet of the Working Section (case: no model, no strut, but with diffuser and contraction) 123
Figure 6.3 Velocity and Pressure Contours at Inlet and Outlet of the Working Section (case: with model, strut, diffuser and contraction) 124
Figure 6.4 velocity and pressure contours at inlet and exit of the working section (case: no diffuser, no contraction, but with model and strut) 125
Figure 6.5 Velocity and pressure contours of the working section, 1st diffuser and contraction 126
Figure 6.6 Velocity contours at the symmetrical plan in the working section (Scale=30%) 127
Figure 6.7 Velocity contours at the symmetrical plan in the working section (Scale=55%) 128
Figure 6.8 Wake behind the car model (scale=30%) 129
Figure 6.9 Wake behind the car model (scale=55%) 130

Figure 7.1 Image of the car (numerical model) 140
Figure 7.2 The section view of the 30% scaled car 140
Figure 7.3 Some sections of the 30% car 141
Figure 7.4 The manufactured 30% car model 141
Figure 7.5 A Car Model in the Working Section..... 142
Figure 7.6 A Car Model in the Working Section (Numerical Model) 142
Figure 7.7 Drag and lift coefficient against the air speed 143
Figure 7.8 Drag and lift coefficients against the clearance 143
Figure 7.9 Flow visualization by fluorescent oil on car surface 144
Figure 7.10 Pathlines over the car surface 144
Figure 7.11 Flow visualization by fluorescent oil on car surface 145
Figure 7.12 Pathlines over the car surface 145

Figure B1 Subdivisions of the Near-Wall Region 175

LISTS OF TABLES

Table1.1 Advantages and Disadvantages of Various SGS Models 11

Table 6.1 Drag Coefficient Comparisons 119

Table 7.1 Test Cases 136

Acknowledgements

First and foremost, I would like to thank my supervisor Professor R. A. McD. Galbraith for his supervision over the past three years. He has supported my research work in many ways. With his encouragement, the research work was carried out smoothly; with his support, the author has a good time staying in Glasgow.

Second, I would like to express my appreciation to Professor F. Coton and Dr. M. Vezza. With whom, my supervisor Prof. Galbraith secured a project funding to support my writing-up of dissertation. I would also like to thank Dr. G. N. Barakos, who gave me the good suggestions to conduct CFD simulations in the early stage of the research work.

Third, I would like to thank Dr. J. Yang, who used to be my second supervisor when he was in the University, with whom I discussed the many problems in the research, particularly in the early stage of the research work.

Finally, I wish to thank Andrew Fleming, who helped me to photograph during wind tunnel testing, and with whom I discussed many technical problems in numerical simulations and in wind tunnel testing. And I would like to thank Mr. R. Gilmour for his support in the wind tunnel testing.

ABSTRACT

In many aspects CFD has made great progress during the past decades. With the advances in computer speed and memory, now a desktop computer or a workstation can run a CFD package for many practical problems. Meanwhile, the accuracy and reliability of CFD prediction have improved, even though there are many improvements needed.

Wind tunnels have been, and will be, very important facilities in aerodynamic development. CFD has replaced some wind tunnel tests during the aerodynamic design process, but wind tunnel test in the final design is requisite. The role of the wind tunnel is expanding towards phenomena-based testing and development of code validation databases.

CFD and wind tunnel simulations are complementary due to their inherent limitations. Wind tunnel tests apply to any hypothesis, but are limited by the tunnel wall interference/blockage, the model details, and even the distortion of the model. CFD are not limited in any of these ways, but limited in speed and memory and the lack of determinate set of equations. Theoretically, CFD can provide an assessment of any problem in fluid dynamics (Direct Numerical Simulation), but the requirements of speed and memory are far from being met presently, or even in the foreseeable future. Of necessity, present CFD applications, however, employ a turbulence model, which limits its application due to the problems in accuracy and reliability.

Given the power of CFD, however, the work contained herein makes use of the advantages of CFD and also the wind tunnel, to form a powerful facility for aerodynamic test, i.e., CFD was used to complement and enhance the wind tunnel test, so producing an integrated test facility.

The present research work included CFD in support of wind tunnel test: numerical simulation of working section (first diffuser, contraction and settling chamber), blockage correction and support system effect.

For the numerical simulation of wind tunnel, the pressure and velocity distributions were investigated, and for auto sport work, the removal of boundary layer was also numerically modelled. CFD simulations predicted the uniform flow in the working section when the diffuser and contraction were included in the simulation.

A very important aspect in this work is that CFD was used to investigate the blockage correction for wind tunnel tests. By using CFD, the blockage correction could be made directly, in terms of representing the test model and tunnel walls in high fidelity. Meanwhile, the effect of support system on the test model was also investigated by CFD. The numerical results showed significant effect of the strut on the test model in the Argyll Wind Tunnel (Glasgow University), and an interesting result showed that different positions of support system had different effects.

This research aimed to utilize CFD to support wind tunnel testing, and its ultimate purpose is to form a powerful facility for aerodynamic test by combining CFD and wind tunnel. The contributions are summarized as follows:

- The calibrations of wind tunnel by CFD simulations
- A proposed improvement for moving belt system by CFD tools
- Blockage correction of wind tunnel by CFD method
- The confirmation of CFD results by wind tunnel model test

NOMENCLATURE

A	Projected frontal area of car
C_d	Drag coefficient ($C_d = \frac{F_x}{\frac{1}{2}\rho V^2 A}$)
C_{du}	Uncorrected drag coefficient
C_l	Lift coefficient ($C_l = \frac{F_y}{\frac{1}{2}\rho V^2 A}$)
C_p	Pressure coefficient ($C_p = \frac{p - p_\infty}{\frac{1}{2}\rho V^2}$)
F_x, F_y	Forces on car in x, y direction, i.e. the drag and lift forces respectively
L	Length or Characteristic length
l_{mix}	Prandtl mixing length
M	Mach number
MG	Moving ground
M_∞	Free-stream Mach number
P	Average pressure
p	Pressure
p_∞	Pressure for the oncoming flow
p'	Fluctuation pressure
R_e	Reynolds number
S_{ij}	Strain rate tensor, $S_{ij} = \frac{1}{2}(\frac{\partial U_i}{\partial x_j} + \frac{\partial U_j}{\partial x_i})$
V	Wind speed
V_∞	Upstream flow speed
U_i	Average velocity in i direction
U^+	Dimensionless velocity ($U^+ = U / u_\tau$)
u_τ	Friction velocity ($u_\tau = \sqrt{\tau_w / \rho}$)
u_i	Velocity in i direction
u_i'	Fluctuation velocity in i direction

u_w, v_w, w_w	Three components of the velocity due to the wall interference potential
u_m, v_m, w_m	Three components of the velocity due to the model potential
y^+	Normal distance ($y^+ = u_\tau y/\nu$)
AOA	Angle of attack
CFD	Computational Fluid Dynamics
DGV	Doppler Global Velocimetry
LDV	Laser Doppler velocimetry
N-S	Navier-Stokes
PIV	Particle Image Velocimetry
RANS	Reynolds-averaged Navier-Stokes
RSM	Reynolds Stress Method
WS	Working section
WT	Wind tunnel

Greek symbols

ρ	Density of air
ε	Blockage Ratio or Turbulent Dissipation Rate
ε_s	Solid Blockage Ratio
ε_w	Wake Blockage Ratio
κ	Turbulent Kinetic Energy
μ	Kinematic viscosity
μ_T	Turbulence viscosity
ν	Kinetic viscosity
λ	Scale ratio
τ_w	Sum of the viscous and Reynolds shear stress at the wall
Π	Buckingham Pi symbol
τ_{ij}	Reynolds stress tensor ($\tau_{ij} = -\overline{\rho u_i' u_j'}$)
Ω_{ij}	Rotation tensor ($\Omega_{ij} = \frac{1}{2}(\frac{\partial U_i}{\partial x_j} - \frac{\partial U_j}{\partial x_i})$

Subscript:

m	Model

CHAPTER 1

INTRODUCTION

1.1 Overview

Over the past four decades there have been enormous strides in the development of computational fluid dynamics (CFD) in a broad variety of scientific research and engineering applications. These have been made in all aspects of CFD techniques, including the geometry modelling and grid generation, the numerical algorithms for solving the governing equations, turbulence modelling, flow visualization and data post-processing, and even the practical applications. Now, CFD techniques have covered many domains of science and engineering, from under the sea, to the sea, to the land, to the near space, to the sun, to the stars, and even beyond (Oran 2002). The detailed subjects include aerospace, ship, marine, automobile, combustion, environment, oil recovery, oceanography, meteorology, and astrophysics etc.

From numerous publications, such as books, journal and conference papers, technical reports, it can be seen that many examples have shown the great success of CFD applications. For example, in his review of computational fluid dynamics of whole-body aircraft, Agarwal (1999) summarized the 'state of the art' of CFD applications in the aircraft industry, including the progress in CFD techniques of the geometry and grid generation, N-S equation solution, turbulence modelling, convergence acceleration methods, near-wall treatments etc. Some excellent results of CFD analysis on the whole-body aircraft were also given. Fig 1.1 and 1.2 are the examples of CFD computations of

whole-body aircraft. The numerical results have shown very good agreement with the experiment.

In the long history of fluid mechanics, much effort has been afforded to solve the Navier-Stokes equations, the governing equations of fluid mechanics. In mathematics, they are a set of nonlinear partial differential equations. The difficulty is that there is no effective closed set of equations that can represent turbulent flow. In physics, too many factors and too complicated phenomena are involved in the fluid dynamics, while the understanding of the turbulence in the flows is very limited. In reality, although much effort, and great progress has been made in tackling the problems of turbulence, the science is far from the complete; possibly even in the near future. Summarily, the bottlenecks are factually existing: first, limited analytical methods have been developed to solve the non-linear partial differential equations; second, the high-Reynolds-number turbulent flows and the flows around complicated configurations can't be solved directly because of the wide range of excited length and time scales; third, the poor mathematical and physical understandings of turbulence lead to all the modelling ways limited to some specified problems, and at present, no universal turbulence model exists.

Due to the difficulties in solving the N-S equations, people have developed a hierarchy method to cope with the practical problems; Figure 1.3 shows the hierarchy structure. For instance, in the early days, for some practical problems, the fluid can be regarded as inviscid and irrotational, and the potential flows dominated the flowfield. In such 'potential' flows, the fluid dynamic equations reduced to the Laplace or Poisson equation. These are linear partial differential equations, and so superposition methods can be used. But, when the complexity of the practical problems is severe, the full potential methods, or even Euler's equations, are required. When the viscosity takes an important role in the

fluids, the boundary layer must be considered. When the problems became more complicated, or the more accurate predictions were desired, the modern one-, two-equation turbulence models and even Reynolds-stress models were employed. The details of turbulence models are given in Appendix A.

Today, after a lengthy development period, CFD applications are becoming more and more mature. The activities in CFD benchmarking are an indication of just how far CFD has developed. For example, Taniguchi etc (2002) reported that the Society of Automotive Engineers of Japan (JSAE) has organized a validation for main commercial CFD codes sold in Japan, and 14 commercial codes took part in the activity, including 3 individual codes for preprocessing and post-processing. The benchmark problems comprised four major aspects in vehicle flow design: the vehicle aerodynamics, engine cylinder flow, air-conditioning and defroster duct flow. These code vendors performed their predictions based on various selections of grids, turbulence models and the equation discretization. A concluding remark was made that only few codes performed all the four objects very well, but the capability of CFD applications in industry was confirmed. It's interesting to notice that most of them tend to use the hybrid grid of tetra/prism, in which the prisms are generated near the vehicle surface while they were able to automatically fill the other region with unstructured mesh.

With the rapid advances of computers in both speed and memory, two other sophisticated techniques of computational fluid dynamics have seen some use: large eddy simulation (LES) and direct numerical simulation (DNS). The former model, based on the filtering approach calculates the large eddies directly, and only small eddies need to be modelled. The latter method is to solve the Navier-Stokes equations directly; nothing to be modelled.

From the limited studies, these two methods have shown such promise, but suffer from too big a requirement of computer resources.

1.2 Computational Fluid Dynamics (CFD)

CFD techniques have progressed a great deal in the past 40 years, and made a significant success in engineering and academic applications. Even so, the CFD is still in its development. Urgent and important advances are still needed in grid generating and turbulence modelling. In this section, some relevant information pertaining to the above is given.

1.2.1 Grid Generation

Grid generation is one of the most important steps in any successful CFD computations. It is not only the process of generating the mesh, but the synthesis of planning and balancing of the CFD computation. Generally, the grid generation for a complicated geometry is very time-consuming. At present, different gridding methods have been developed and used, such as Cartesian grids, structured and unstructured grids, hybrid gridding etc.

Cartesian Grids

The Cartesian grid is the simplest grid and the straightest grid in sense. The extant difficulties in implementing the boundary conditions on the boundaries or surfaces have limited its current use. None the less, some researchers are making efforts to alleviate

these difficulties. Lin et al (1998) developed an automatic grid generation method in Cartesian co-ordinates. The main idea was to use diagonal segments for the approximations of complex geometries, Fig. 1.4 shows the comparison of a sphere based on the diagonal approach and the conventional saw-tooth approximation. Still, however, the practical applications of Cartesian grid in complicated geometry need significant development.

Structured Grids

Structured grids are formed by a series of curvilinear coordinate lines, where the one-to-one mapping can be established between the physical and computational domains. The curvilinear grid points conform to the boundaries, surfaces, or both and therefore provide an excellent way of specifying the boundary conditions.

For complex geometrical configurations such as that of the whole-body aircraft, the physical region is usually divided into subregions, and within each subregion a structured grid is generated. The resulting subgrids may then be patched together at common interfaces to form the entire computational region. Figure 1.5 shows the 2D and 3D multi-block structured grids.

The structured multi-block grids represent the most widely used strategy during the past 20 years for both 2D and 3D grid generation about complex configurations. The major difficulty in generating the structured grids is their automation. Recent research activities in this area have been directed toward the development of algorithms to perform automatic blocking and grid generation. It should be noted that the user interaction and graphical

user interfaces (GUI) are extremely important in generation of structured grids (Agarwal 1999).

From the standpoint of numerical simulation, high quality grids are requisite for any successful CFD computations. Therefore, user's ingenuity and experience are becoming critical in generating grids and in governing the time required in grid generation.

Unstructured Grids

Unstructured grids are composed of triangles in 2D and tetrahedrons in 3D. The grid information is provided by a set of nodes and the connectivity between the nodes. A connectivity table describes connections and provides the appropriate neighborhood information among nodes and cells. Figure 1.6 shows a 3D unstructured grid.

The unstructured grids are increasingly used in CFD simulations. However, due to current computers, memory limitations, the generation of high-quality grids for turbulent-flow simulations require high aspect ratio cells near the body surface; this is not available in unstructured grids and so remains a major difficulty. The major advantages of the unstructured grids are, however, the potential for automation, adaptation, and the greater geometric flexibility.

Hybrid Grids

In present CFD computations, hybrid grids are becoming more and more popular. The hybrid grids are actually the combinations of structured and unstructured grids. They use high aspect ratio structured grids near the solid boundaries for viscous flow simulations,

while the other region is filled with the unstructured grids. This approach offers the potentials both in greater geometric flexibility and in high-quality grids with automation. Figure 1.7 is an example of hybrid grid generated around an airfoil.

Grid Adaptation

Reynolds averaged Navier-Stokes (RANS) simulations about complicated configurations require more and more grid points. This is especially so when some important flow features need to be captured, such as shocks, contact discontinuities, boundary layers, wakes, and separated and vortical flow regions et al where very fine grids are needed, and so is a very large memory. But, the most popular way to reduce the grid requirement is to include a grid adaptation strategy in which grid clustering is automatically achieved in the regions of steep flow gradients and relatively fewer grid points in the rest of the computational domain. Figure 1.8 shows the grid before and after adaptation.

The major difficulty with many structured grid algorithms, when used for generating adaptive grids about bodies with large curvature, is that the initial grid about the body needs to be chosen with great care so that the subsequent adaptation of this grid to the flow does not cause points to move inside the body.

1.2.2 Turbulence Modelling

Complex turbulence is an irregular motion in the fluid flows, which may be the most difficult problem in the classical physics due to its complexity and the limited understanding of it. In the history of over 100 years, many approaches have been

developed for the practical problem solving, from the simplified analytical solution to full direct numerical computation of Navier-Stokes equations. The physics of fluid dynamics is very complicated, consisting of variety components of different spatial and temporal scales. Fortunately, in most industrial engineering, only the averaged values are of technological importance. Therefore, the time averaging solutions have been pursued, changing the conventional Navier-Stokes equations into the Reynolds-averaged N-S equations (RANS). But this brings in an additional Reynolds stress term and renders the equations indeterminate. To close the equations, the Reynolds stress must be modelled to provide the necessary equation closure; this is the problem of turbulence modelling. A variety of turbulence models of various complexities have been developed over decades. These turbulence models include: (1) algebraic (zero-equation models), (2) one-equation models, (3) two-equation models, and (4) second-order closure models (Appendix A gives the details).

In the zero-equation models, the turbulent length scale and timescale are algebraically specified, usually by using Prandtl's mixing-length hypothesis. These models are formally valid for thin turbulent shear flows, near a wall, where the mean velocity is primarily unidirectional. The main deficiency of these models is that they require a specification of the turbulent length scale l_0, which may be impossible to do reliably in complex turbulent flows.

In the one-equation models, a transport equation for the turbulent kinetic energy is resolved, while the turbulent length scale is required to be specified. But, Baldwin & Barth, and Spalart & Allmaras have developed their improved one-equation models based on the solution of a modelled transport equation for the eddy viscosity ν_t, which alleviates

the problem of having to specify the turbulent length scale in their definition of the eddy viscosity ν_t.

In the two-equation models, these usually referred to as the complete turbulence models. Two of the most widely known and extensively employed models are the κ-ε models (turbulent kinetic energy-turbulent dissipation rate) and the κ-ω models (turbulent kinetic energy-rate of dissipation per unit turbulent kinetic energy). In each of the categories, many other improved turbulence models have been developed for some specified problems.

Reynolds stress models (RSM) have been developed to solve model transport equations for individual stresses in the Reynolds-stress tensor, abandoning the Boussinesq's eddy viscosity hypothesis which is used in the other RANS methods. For the 3D flows, RSM models introduce seven equations, one for the turbulent length scale and six for the components of the Reynolds stress tensor. In principle, they are better suited for computing complex 3D turbulent flows with the effects of streamline curvature, swirl, rotation, and rapid changes in strain rate. They may be the potential models to give accurate predictions for complex flows. It is believed that the modelling of the pressure-strain and dissipation-rate terms is really challenging, and so is often considered to be responsible for compromising the accuracy of RSM predictions.

NASA organized a workshop for the assessment of the direction of CFD research for the design of future generations of transportation aircraft (Rubinstein et al 2001). From the two-day discussion about the needs of aircraft manufacturers, the need for further developments of single-point turbulence models stood out in clear light. The major points were as follows:

- Advances in turbulence modelling are needed in order to calculate high Reynolds number flows near the onset of separation and beyond
- NASA should support long-term research on Algebraic Stress Models (ASM) and Reynolds Stress Models (RSM)
- Turbulence modelling development, validation and implementation should include DNS, LES and hybrid method approaches.

The discussion between model developers, aircraft designers, program managers etc should be regarded as the basic directions of the turbulence model development and validation.

1.2.3 Large Eddy Simulation-LES

Strictly speaking, LES is one of the methods of turbulence modelling, but it is significantly different from the RANS methods in both the general principle and the practical applications. RANS methods compute an ensemble average of the flowfield, in which the average physics is resolved from the averaged Navier-Stokes equations, with the fluctuating physics included via a turbulence model. LES resolves the mean and large eddies (energy carrying and transferring structures) directly. In LES filtering methods are used. It's generally believed that the small eddies tend to be homogeneous and universal, and less affected by the boundary conditions. Therefore, there is hope that their models can be simpler and require fewer adjustments in different flows (Piomelli 1999). This may be the reason that LES generally gives much better simulation results than RANS in many

complex flows. The only problem for LES is the huge requirement of computer resources, which is usually impossible in the practical applications.

Since 1970s, the standard Smagorinsky model has been widely used in the computation of LES until the dynamic SGS model was proposed. Then the improvement of SGS models is continuing, and many variations of dynamic SGS model have been proposed. Murakami (1997) summarized the advantages and disadvantages of various SGS models and these are given in the table1.1.

Table 1.1 Advantages and disadvantages of various SGS models (from Murakami 1997)

	Consideration to non-equilibrium effect	Consideration to transition	Stability of computation
Smagorinsky Model (static type)	×	×	O*
Scale similarity model (static type)	Δ	O	×
Mixed model (mixed type)	Δ	Δ, O	O
Dynamic SGS model	Δ	O	Δ
Dynamic mixed model	Δ, O	O	Δ, O
Lagrangian dynamic SGS model	Δ, O	O	O
Lagrangian Dynamics mixed model	O	O	O*

Note: O*: function very well; O: function well; Δ: function insufficiently; ×: function poorly

In his paper, Murakami (1997) also reported the comparison between RANS and LES in the computational wind engineering. For flowfield around the bluff bodies, LES gave the most accurate prediction of the flowfield, much better than the κ-ε models and RSM models, Figure 1.9 shows the flowfield predictions with different turbulence models, in which κ-ε model tends to overpredict the wake of the bluff body.

It's well known that in full LES, the grid spacing would scale with the boundary-layer thickness for a given accuracy, and the requirement restricts the LES applications. Therefore, some researchers tried LES simulation on the coarse grid. Spalart (2000) gave a comparison of the flow past a circle cylinder, and Figure 1.10 shows the comparisons. The LES simulation on coarse grid gave very similar results with the fine grid. The drag prediction for RANS is too low at $C_d \approx 0.9$, URANS (unsteady RANS) gives too high result at $C_d \approx 1.7$, while LES methods give much better predictions: $C_d = 1.05$ for coarse grid, $C_d = 1.32$ for fine grid (the experiment gives $C_d = 1.2$).

Most successful LES has been done using high-order spatial discretization, with great care being taken to resolve all scales larger than the inertial subrange. The degradation of accuracy in the mean flow quantities with poorly resolved LES is not well documented. In addition, the use of wall functions with LES is an approximation that requires further validation.

1.2.4 Direct Numerical Simulation-DNS

In DNS, the Navier-Stokes equations are discretized and solved directly; nothing to be modelled. Theoretically, if the mesh is fine enough to resolve even the smallest scales of motion, and the scheme is designed to minimize the numerical dispersion and dissipation errors, the 3D time dependent accurate solutions can be obtained. In practice, there are some limitations: the accurate, high order schemes designed to reduce the dispersion and dissipation errors tend to have little flexibility in handling complex geometries and the boundary conditions; a number of grid points proportional to the 9/4 power of Reynolds

number are also required to resolve all scales of motion: too much computer resources are required.

Presently, DNS is not a development tool, but a very useful tool in the research of transitional and turbulent flows. Moin et al (1998) stressed that DNS is a research tool. In their paper, some related numerical issues, such as boundary conditions and the spatial and temporal discretization were discussed, illustrating that DNS is a useful tool to complement the experiments and get the turbulence physics that was not easily attained in the laboratory. Figure 1.11 shows all the terms in the Reynolds stress equations computed directly by DNS. Hwang et al (1998) compared the data of several second-order closure turbulence models to the DNS predictions of a channel flow, and Suga (1998) used DNS data of a channel flow to develop a nonlinear eddy viscosity turbulence model.

DNS has a much higher cost than LES simulation for the same Reynolds number. But, Spalart (2000) suggested that it's possible that DNS simulation can finish the task in a lower Reynolds number at the same cost of LES simulation, then an extrapolation method is used to extrapolate the DNS results into the LES Reynolds number with confidence. Moreover, the extrapolation can reach any Reynolds number. If this can be done with confidence, DNS simulation will be superior to LES, even at the same computational cost.

1.3 CFD Applications

CFD applications are becoming more and more popular, and the application areas spread from the under sea, to the sea, to the land, to near space, to the sun, to the stars, and even beyond (Oran 2002). Oran also illustrated various CFD applications by a number of

examples. Figure 1.12 is a torpedo launch from a submarine bay, where flow complications arises as water moves into the bay when the torpedo is launched, as flow is induced by the relative motion of the submarine and the torpedo and the due to the effects of the water jet used to propel the torpedo. Figure 1.13 shows a destroyer moving at 20 kn, with smoke from the stacks and an approaching helicopter with rotating blades. Wind and smoke passing over the ship create rapid background fluctuations in which a helicopter must land. Simulations were used to create background airflows for virtual reality training for helicopter pilots and to design deflectors to keep the gases out of open bays. Figure 1.14 shows the pressure and velocity vector for the flow over the Space Station. The low density of the upper atmosphere put this problem in a range where fluid dynamics is not equilibrated, and particle-based methods give more accurate solutions. It may be considered, therefore, that CFD has emerged as a powerful tool in many applications. In this research, CFD applications are focused on the automotive aerodynamics.

The aerodynamics is a very important aspect in the design of road vehicles, particularly after two crises of oil in 1970s. A vehicle with a low drag coefficient is becoming one of the major selling points. Before CFD techniques and powerful computers were available, the development of vehicle aerodynamics was heavily dependent on wind tunnel testing. Generally, in the process of the production design, several different scaled models must be built for wind tunnel testing in the different stage of development. It's a reliable procedure, but a costly and time-consuming procedure. People have been looking for a replacement or complementary tool. Fortunately, CFD happens to be the tool.

As early as in 1989, Han (1989) used an incompressible RANS method to simulate the flows around an Ahmed's vehicle-like body, and Han et al (1996) made the further research on the automotive aerodynamics, where they investigated three type vehicles:

Square-back (SB), Fast-back (FB) and fast-back boat-tail ramp (FBR). They concluded that CFD could track relative changes in drag between the three type vehicles with acceptable engineering accuracy (less than 4% percent error of the relative drag).

Keller et al (1999) used a CFD tool to study the Formula 1 car wheel aerodynamics. The computational flow visualization tool combined with the experimental visualization study enable a new wing geometry to be designed, which may lead to a significant reduction in the drag of the wheel. Basara (2000) emphasized the applications of second moment closure (SMC) in automotive flows, and used CFD with SMC to predict the external aerodynamics, car compartment and in-cylinder flow, where he studied some important and complicated flow features: separation and recirculation, impingement, swirl and streamline curvature etc.

Aroussi et al (2000) compared the results of CFD and PIV measurements for the flowfield in a vehicle when both windshield defroster and instrument panel (IP) registers are open. They illustrated although there were differences between the experimental and computational results in locating, the core of the jets issuing from the IP registers, the macroscopic features in terms of shape, size and intensity were correctly predicted. They concluded the use of CFD as a design tool in the field of vehicle climate control was justified.

Okada et al (2002) used CFD to predict the water condensation in an automotive headlamp. The numerical and experimental results showed the consistency.

It's widely accepted that most of the CFD predictions for road vehicle aerodynamics can be done in the steady manner, although the flowfield around the road vehicles are

unsteady. But Person et al (2000) completed the CFD simulations of the transient flows of vehicles. Since the flows around a vehicle are very complicated and inherently unsteady, and the numerical problems may occur when the mesh resolution becomes very fine in the separation regions, a converged solution may not be attainable. They pointed out that this approach might benefit both from stability and physics. For the stability, there is always a solution, however transient the flow is. For the physics, it gives fewer assumptions in the numerical computation.

1.4 CFD for Aerodynamic Design

In recent years, there has been significant progress in the development of techniques for aerodynamic shape optimization by using the advanced CFD methods. These techniques can be broadly categorized into direct and inverse design methods. Traditionally, the direct approach of optimizing design has been carried out by trial and error, which is heavily relied on the intuition and experience of the designer. One of the disadvantages of the method is, that repeated trials in an interactive design and analysis procedure could not lead to a truly optimum design. In order to take full advantage of the possibility of examining a large design space, the numerical simulations need to be combined with automatic search and optimization approaches. Another disadvantage is, that the method needs extremely intensive computation when the number of variations is large.

Another approach is the inverse design method. The design problem is cast as an inverse problem involving the research for a shape that will generate the desired pressure distribution. This approach requires knowledge of the pressure distribution a priori by the designer that will lead to the desired performance. The method has the advantage that only

one flow solution is required to obtain the desired design, the disadvantage is that the desired shape may not exist unless the pressure distribution satisfies certain constraints. Jameson (1994) formulated the inverse design optimization problem in terms of control theory, and developed an adjoint equation to determine the gradient of the cost function. The adjoint equation is always linear and has coefficients defined by the solution of the flow equations. The cost of solving the adjoint equation is comparable to that of solving the flow equation. Thus the gradient can be determined with roughly the computational cost of two flow solutions, independent of the number of design variables. The method shows very promising future for full configuration vehicle design.

The primary purpose of engineering research and development is to provide new information and tools for the analysis and design of new systems and the concepts to meet certain human needs (Kumar 2000). In the typical design of a fluid dynamic machine, the process is usually accomplished in three major steps: conceptual design, preliminary design and final design.

In the conceptual design stage, the main overall dimensions of the machine are determined by using dimensionless coefficients from accumulated experience. Typical coefficients are those of the drag or lift. Typically, this stage involves the applications of low fidelity but very fast tools to examine a large design space, in which many design iterations can be performed quickly. The tools may provide approximate changes in performance due to changes in design.

In the preliminary design stage, the detailed design of the machine's components follows an iterative process between analytical design and experimental verification. The major task in this stage is to produce an overall design that can meet the mission requirements

within the given constraints, therefore, higher fidelity tools are used to assess the performance within sufficient accuracy. Presently, CFD has accelerated the convergence of this process significantly, and it permits interference effects among the components to be taken into account.

In the final design stage, the separated optimized components are put together in a prototype system, and the complete details are designed. In this stage, the highest fidelity tools are needed.

In aerodynamic design, CFD tools are taking a more and more important role thanks to the advances in computer platforms and the numerical techniques in CFD. In many cases, CFD has been successfully used in the preliminary design stages and replaced a lot of wind tunnel testing, and it can reduce the cost and shorten the design circle significantly.

If CFD is used in the design process, the following three factors must be considered (Agarwal 1999, Jameson et al 2000):

- Sufficient accuracy
- Acceptable computational and manpower costs
- Fast turnaround time

Jameson et al (2000) pointed out that for the civil aircraft, CFD prediction of the drag coefficient should be the order of 1%, i.e., the drag prediction has to be within the accuracy of 1-2 counts. Kumar et al (2000) pointed out that for the transonic transport aircraft, cruise drag can be predicted by CFD techniques only in 10-20 counts, or 3.5 to 8% accuracy of total drag. But the more difficult thing is to reach the same level of

accuracy in off-design conditions, such as buffet onset or high-lift configurations where the flow may be highly separated and unsteady.

Although the Navier-Stokes equations can predict the unsteady, separated flows for a complete configuration (DNS computation), the requirements of huge computer resources make it impractical to resolve all the relevant scales in such flows. It is, therefore, necessary to model the unresolved scales. RANS equations are the conventional approaches, with the introduction of the turbulence models. Jameson et al (2000) reported that to allow the completion of the major design cycle in 4-6 months, the cycle time for the multidisciplinary loop should not be longer than about 2 weeks. Therefore, the turnaround time for aerodynamic analyses is only a few hours. The biggest problem in aerodynamic analyses may be the geometry processing and the surface grid generation. It's reported that 80-90% of total grid generation time is spent on them (Agarwal 1999).

In the design of road vehicles, the development process is significantly different from that of aircraft, where the aerodynamic development is performed in a closed loop containing aesthetic, functional and aerodynamic considerations. Both the number of iterations necessary and the quality of the final result depend on the ability of the aerodynamicist to recognize the intentions of the exterior designer, and to find solutions within the designer's limits of acceptability (Hucho & Sovran 1993).

Beccaria et al (1999) developed a software system which is capable of quickly performing a semi-automatic optimization of the shape of sport cars with respect to their aerodynamic properties. The system utilized the aerodynamic solver based on the assumption of attached flow along the body except its aftermost part. This assures a good prediction of the pressures almost up to the separation region, and in particular a good evaluation of the

vertical pressure loads if the wake is modelled properly. In their parallel computing, a full optimization cycle, of the order of 1000 iterations over the car shape, can be performed on a workstation cluster in order of 10 hours.

1.5 Roles of Wind Tunnel Test

As early as 1975, Chapman et al (1975) surmised that "computers should begin to supplant wind tunnels in the aerodynamic design and testing process", and pointed out that computers would provide a numerical wind tunnel to obtain aerodynamic flow simulation in less time and at lower cost for the design of new aerospace vehicles. Indeed, several breakthroughs of computational fluid dynamics during the 1970's and 1980's, especially the development of the two-equation turbulence model and Reynolds stress methods, made the prediction of fluid dynamics automatic and successful in many practical problems. Unfortunately, the situation didn't happen, even when the capabilities of computers are increasing in geometric series. The superficial understanding of the turbulence mechanism made the numerical methods applicable only to simple fluid problems. So, the wind tunnel is still an indispensable tool in fluid dynamics. Sawley etc (1997) reported that the Sauber Petronas Engineering AG (Swiss) spends about 33 weeks of wind tunnel testing each year to test their race cars, this is a good example to show the importance of the wind tunnel.

In the general use of wind tunnels, Squire (1998) gave a review of small high speed wind tunnels in aeronautical research. He suggested that small tunnels can make significant contributions to aeronautical research in the following areas: boundary layer measurements; shock/boundary layer interactions; the parametric study of the

aerodynamics of wings of unusual planform; the investigation of complex viscous flows for development and validation of CFD and the development of new techniques.

In some specific applications, wind tunnels sometimes show their advantages in the whole design process of the aircraft. Niewald et al (2000) used wind tunnels to develop the F/A-18E fighter. In the different development stages, different scale models were used. At the stage of aerodynamic configuration development, a relatively small model (5% scale model) was utilized to permit low-cost evaluation of numerous configuration refinements. Then an 8% scale model was used to support verification and documentation testing. Then, a 15% scale model was manufactured to provide corrections for support system effects. In the last stage, a 17.6% scale model with the high-fidelity inlet/airframe was used for the preflight performance testing.

Landman et al (2000) used wind tunnel testing to optimize the geometry of the multi-element airfoils. Combining the optimization methods, the wind tunnel model was used to get the optimum lift as a function of flap position.

The inherent limitations of computational and wind tunnel simulations make them complementary. Wind tunnels are limited by the size of the models that can be placed in them and by the density, temperature, and velocity of the flow that they can sustain, with the consequence that flight Reynolds numbers cannot be realized with complete models. Their accuracy is also limited by wall and support interference and by aeroelastic distortion. Whilst computers are not limited in any of these ways, but in speed and memory, which in turn limit the attainable complexity and resolution of simulations (Agarwal 1999).

As the computational tools become increasingly reliable in predicting system performance, the role of wind tunnels will shift towards physics based testing for increased understanding of various flow phenomena and for developing high fidelity data for physical model development and validation. As the physical understanding grows, more and more flow interactions can be included in a given test, such as vortical flow interactions, massively separated flow, wing/control surface interactions etc (Kumar et al 2000). An important requirement for accurate code validation data is the characterization of the wind tunnel flow in the working section, and the global wind tunnel calibration data must be available over the entire operating envelope of the facility, and must be shown repeatable at all times between calibration.

1.6 Concluding Remarks

CFD has been made a great progress during the past decades, and actually emerged as a powerful tool in academic and engineering applications. Presently, many three dimensional complex flows can be solved efficiently and accurately with Euler or Navier-Stokes equation, and it is to be expected that CFD will be use for wider and wider applications in practical problems.

The present difficulties of CFD applications lie in the turbulence modelling and the set-up time for the geometry modelling and mesh generation for the treatment of complete configurations. For the former difficulty, people need to go further to the understanding of the phenomena of turbulence, by advanced CFD simulations (i.e. LES and DNS), and by the delicate wind tunnel test. Much effort is still needed in the improvement of the turbulence modelling, particular the Reynolds stress models. For the latter difficulty,

people are working on the Computer-Aided Geometric Design (CAGD) techniques for more efficient and accurate geometry modelling, aiming to reduce the unacceptably large geometry processing time of the current systems and remove one of the major bottlenecks in acceptance of CFD in industry (Agarwal 1999).

CFD and wind tunnel simulations can be complementary due to their inherent limitations. Therefore, it's possible to use CFD simulation to complement and enhance wind tunnel testing, and form a more powerful overall facility for aerodynamic test (Campbell et al 2003). This research work is on CFD in support of wind tunnel testing, including the investigation of the flowfield in the working section, the strut effect on the test model, the blockage correction etc. Next few chapters will give the details of the research work.

Figures of Chapter 1

(a)

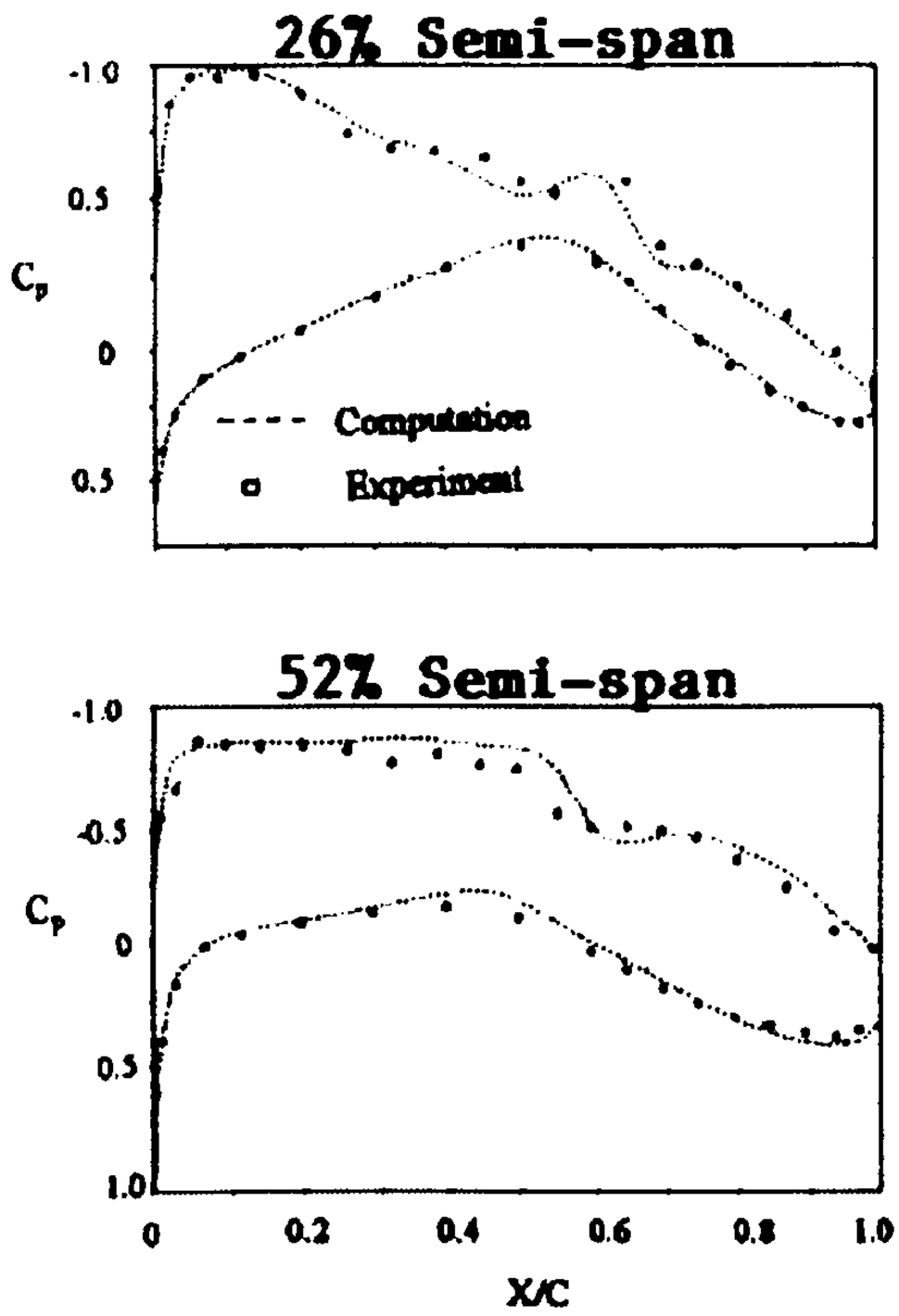

(b)

Figure 1.1 Numerical Computation of MD-11 (from Agarwal 1999)
(a) Structured surface grid; *(b)* Comparison of computed and experimental surface pressure at two-wing locations, M_0=0.85, α=1.8^0

(a)

(b)

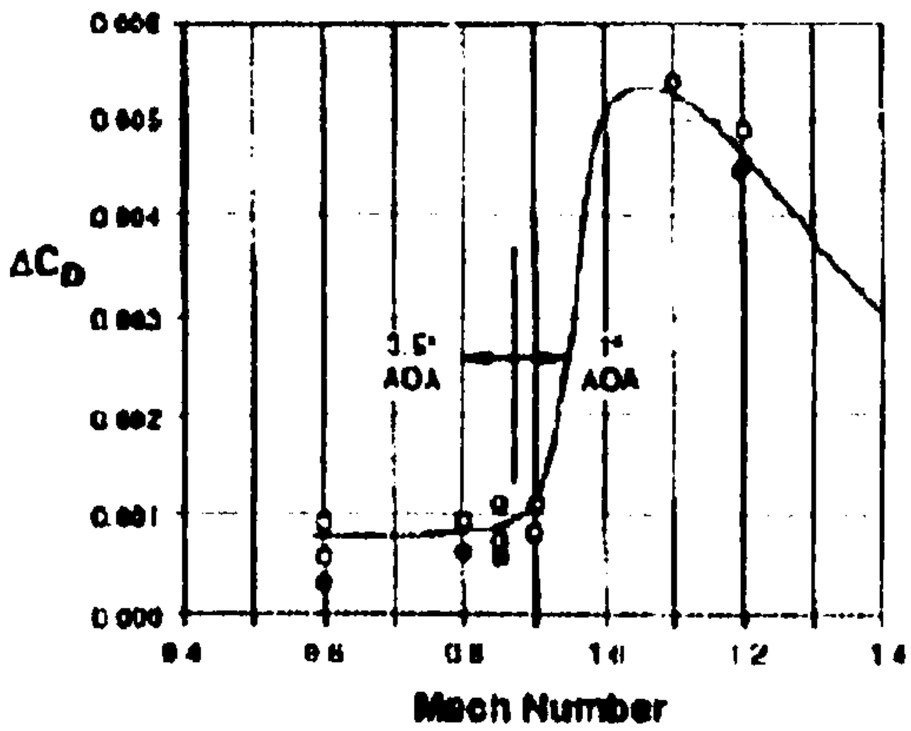

(c)

Figure 1.2 CFD analysis of F-18 E aircraft (from Agarwal 1999)

(a) Unstructured surface mesh
(b) Surface pressure distribution
(*c*) Drag increment curve

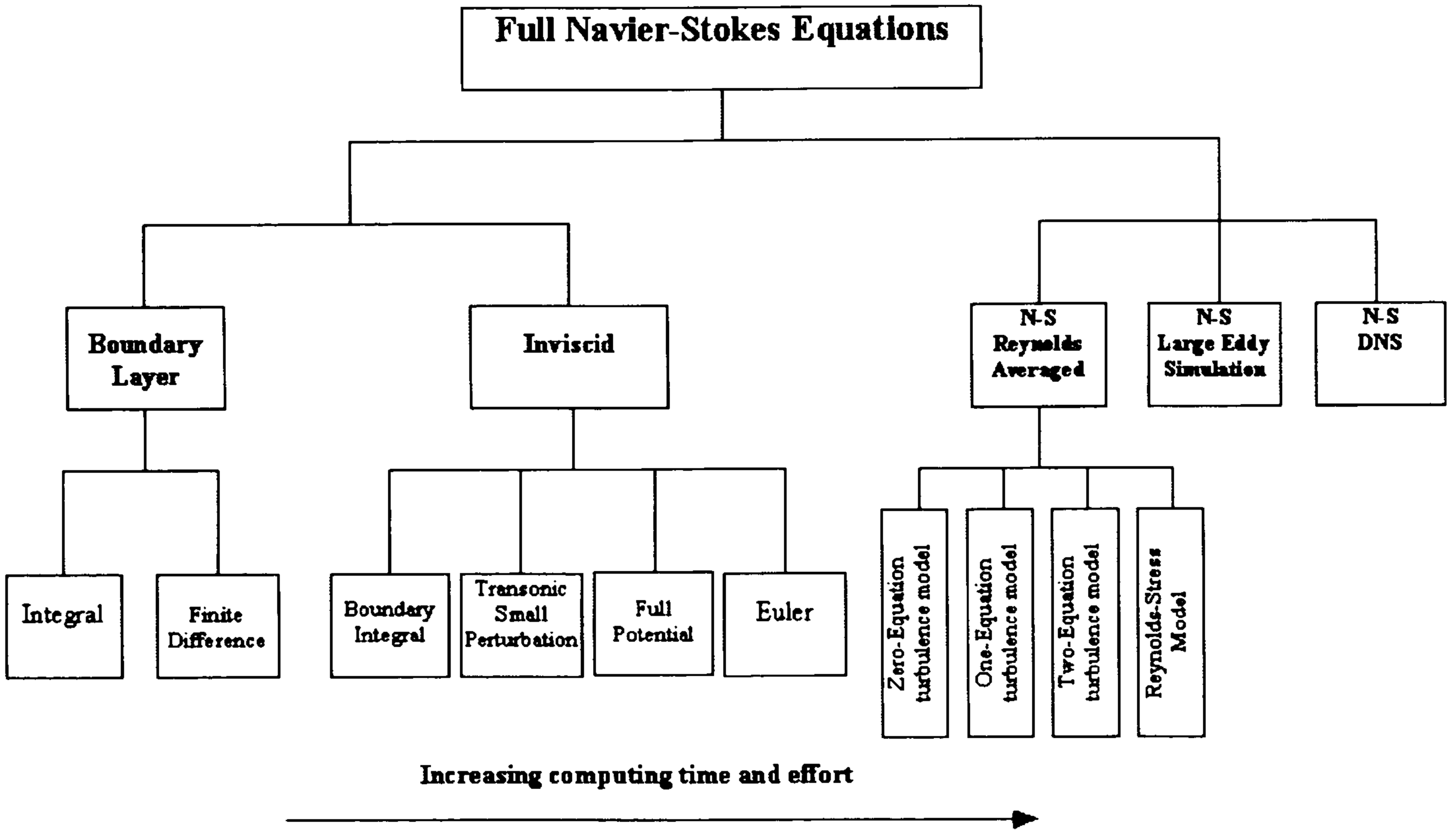

Figure 1.3 Hierarchy of Computational Fluid Dynamics

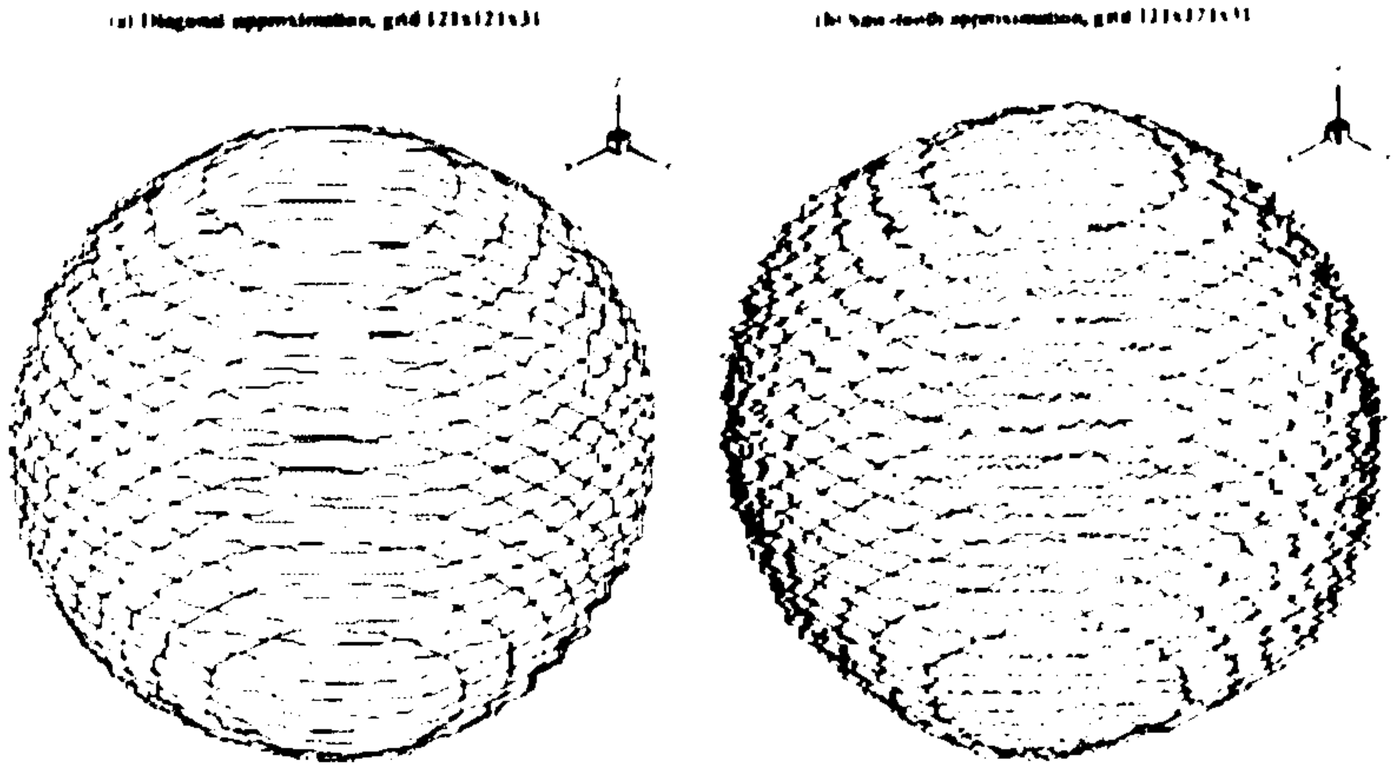

Figure 1.4 Approximation of sphere in Cartesian co-ordinates (from Lin 1998)

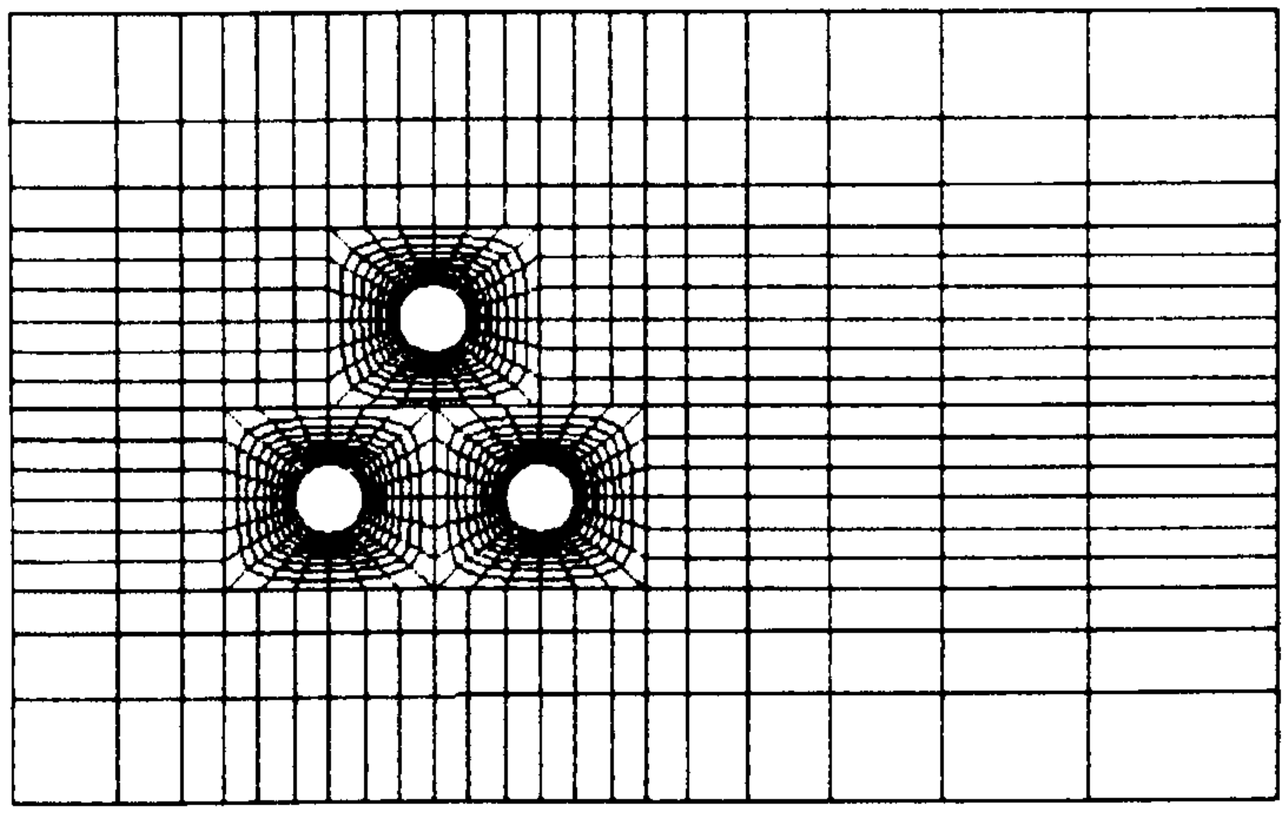

(a) 2D multiblock grid

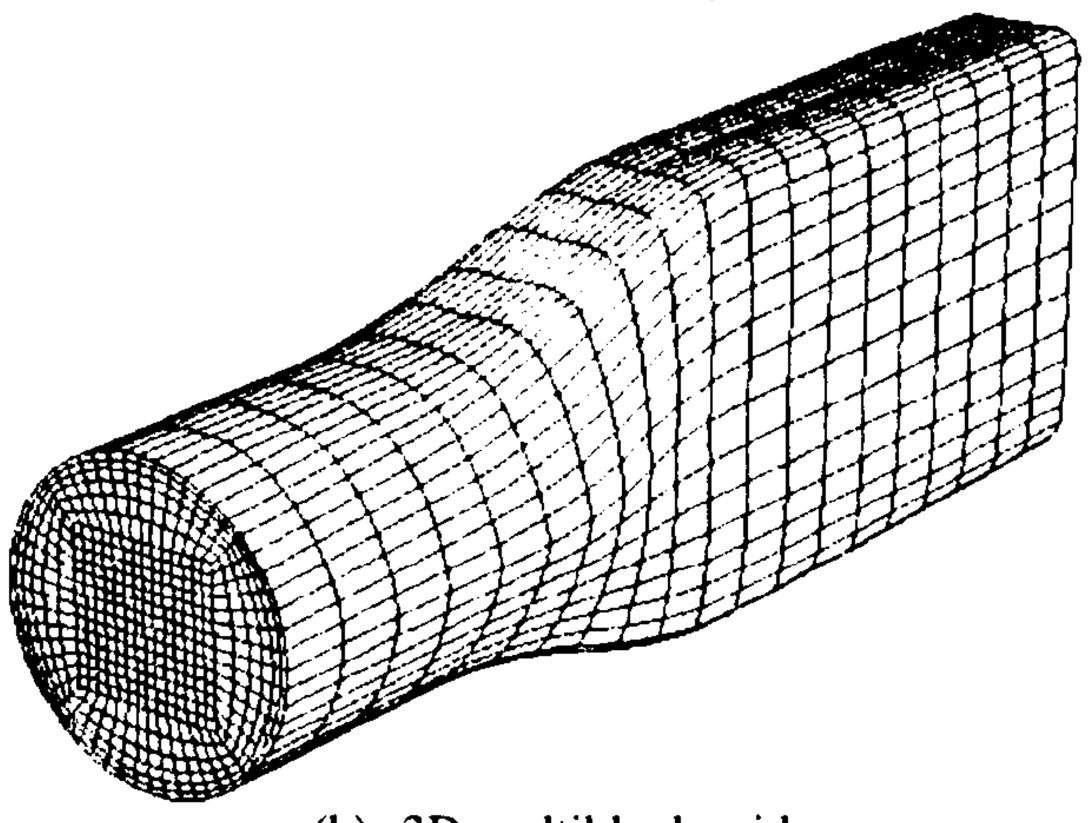

(b) 3D multiblock grid

Figure 1.5 Structured grids (from Fluent Manual)

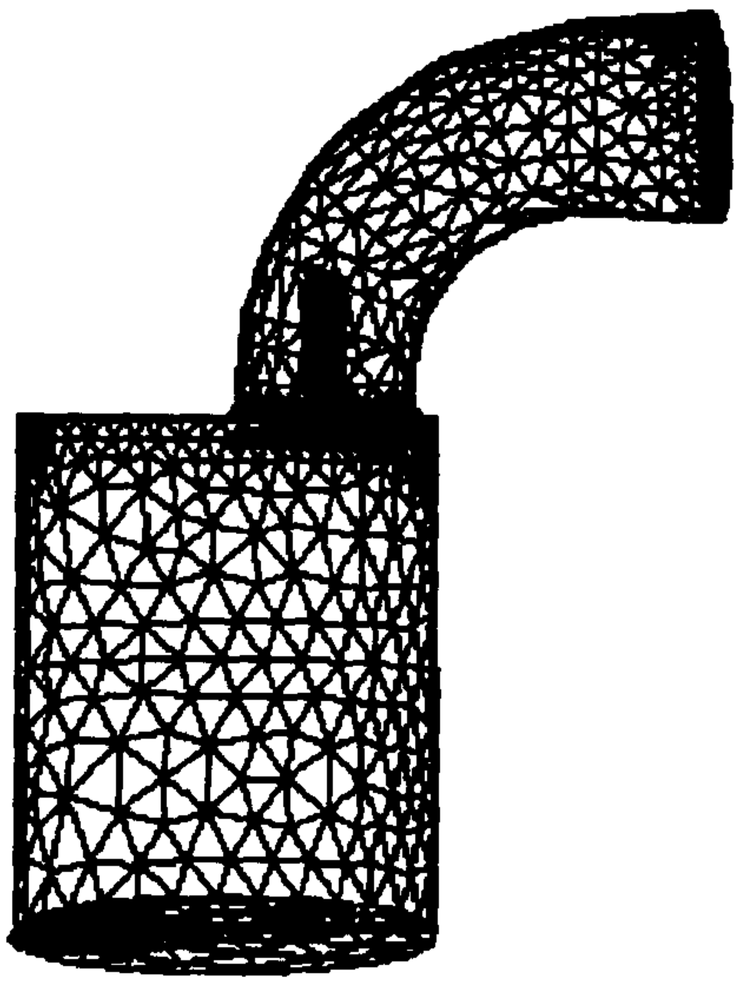

Figure 1.6 3D unstructured grid (from Fluent Manual)

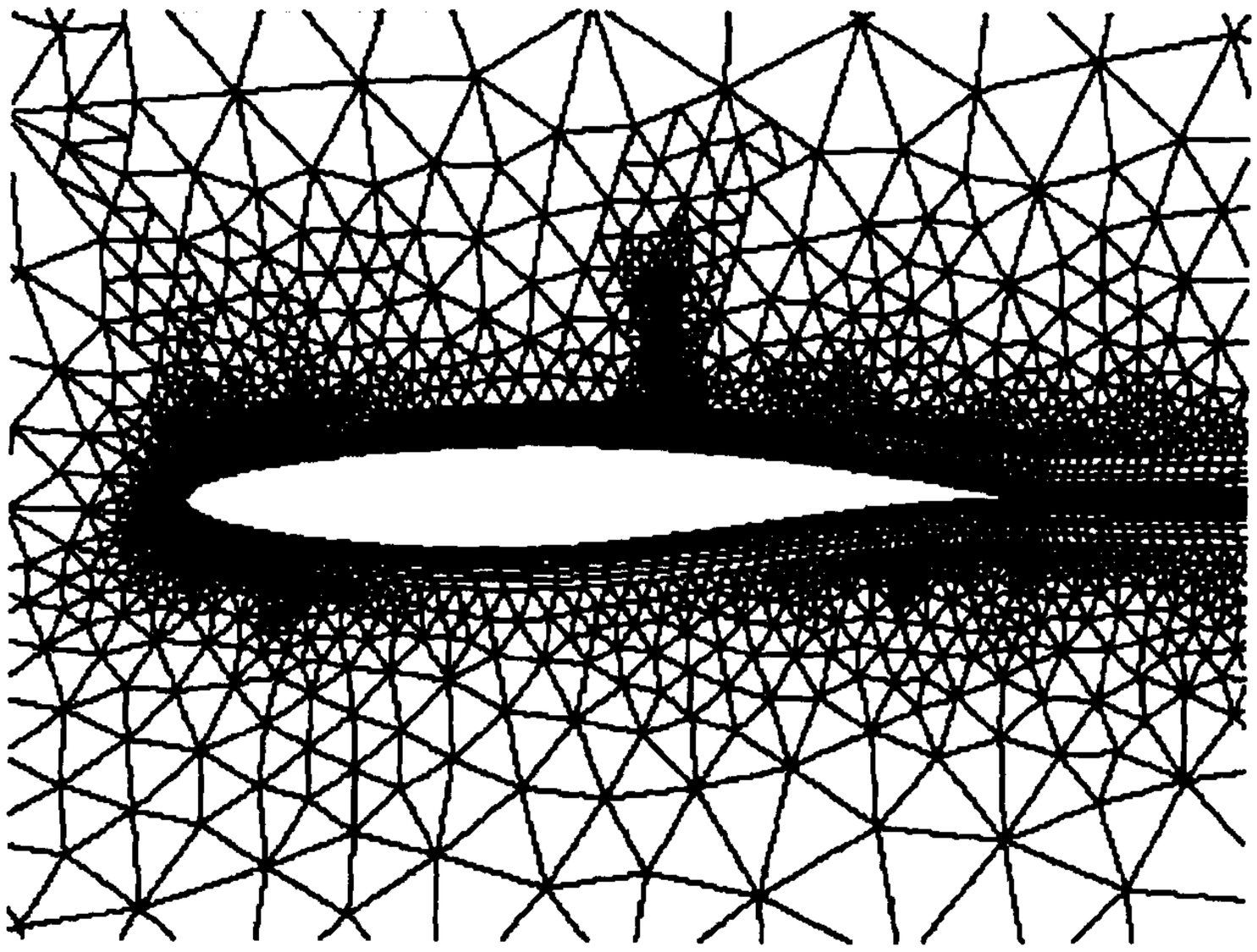

Figure 1.7 Hybrid grid around an airfoil (from Fluent Manual)

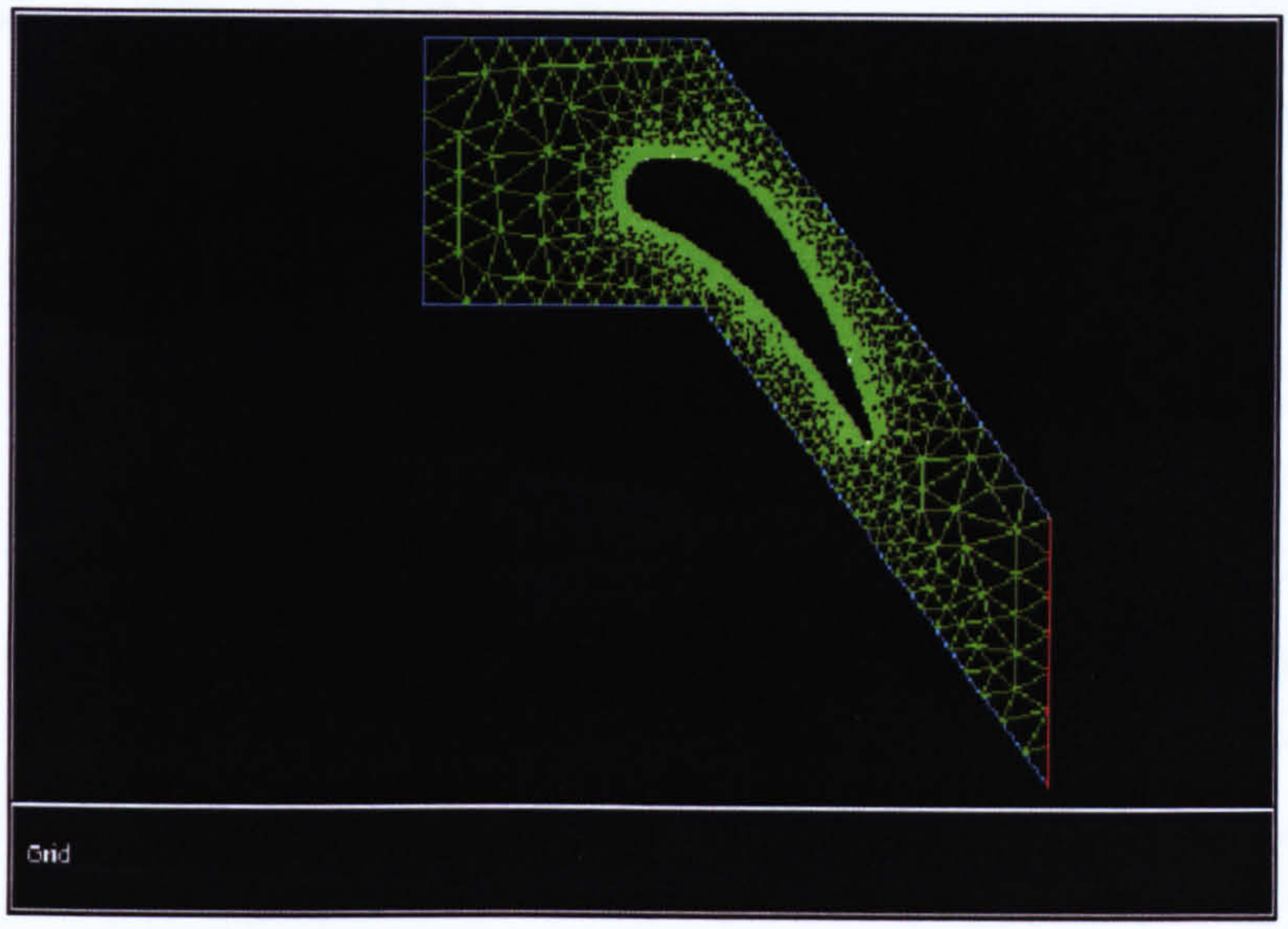

(a) Normal Grid

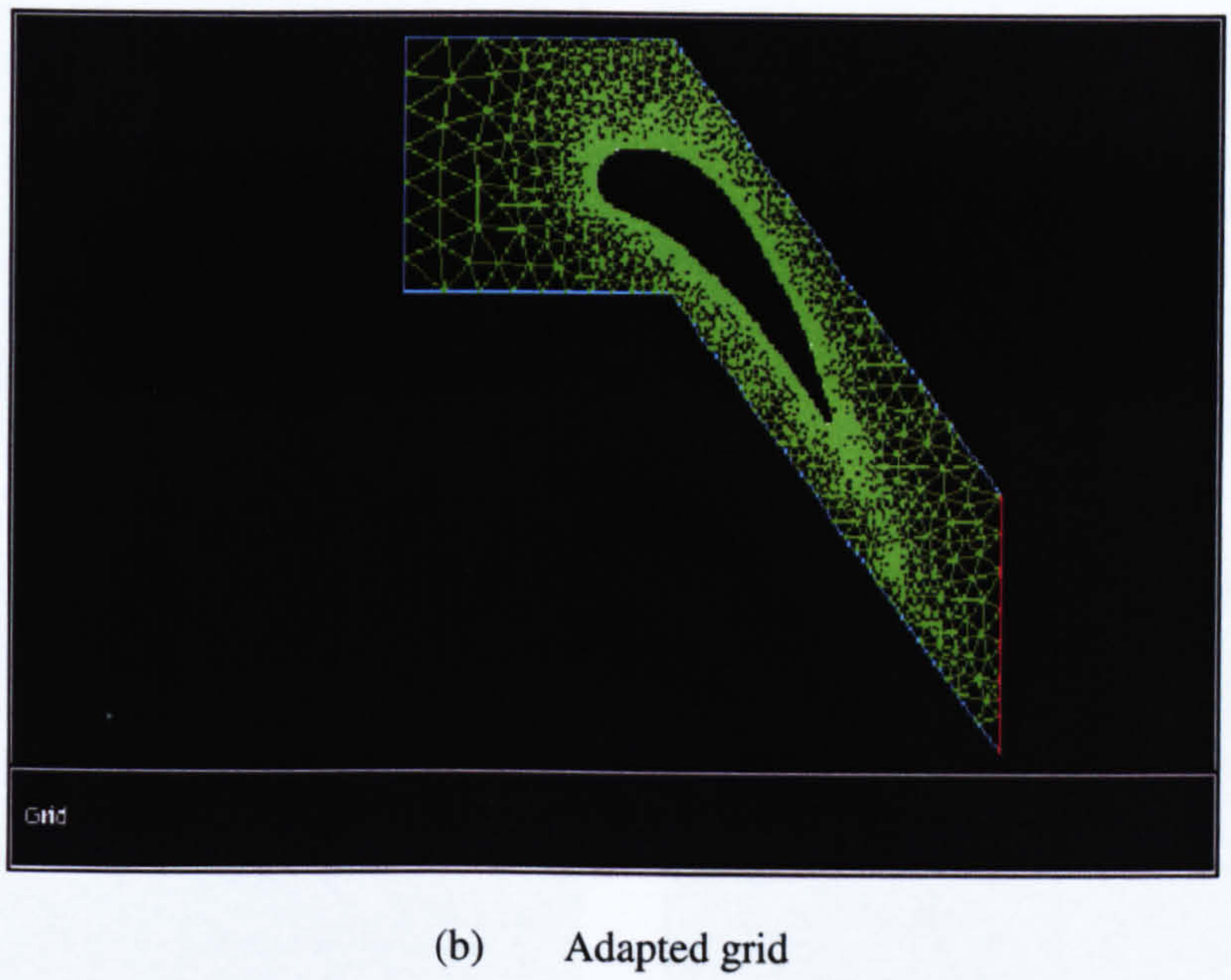

(b) Adapted grid

Figure 1.8 Grid Adaptation (Fluent Manual)

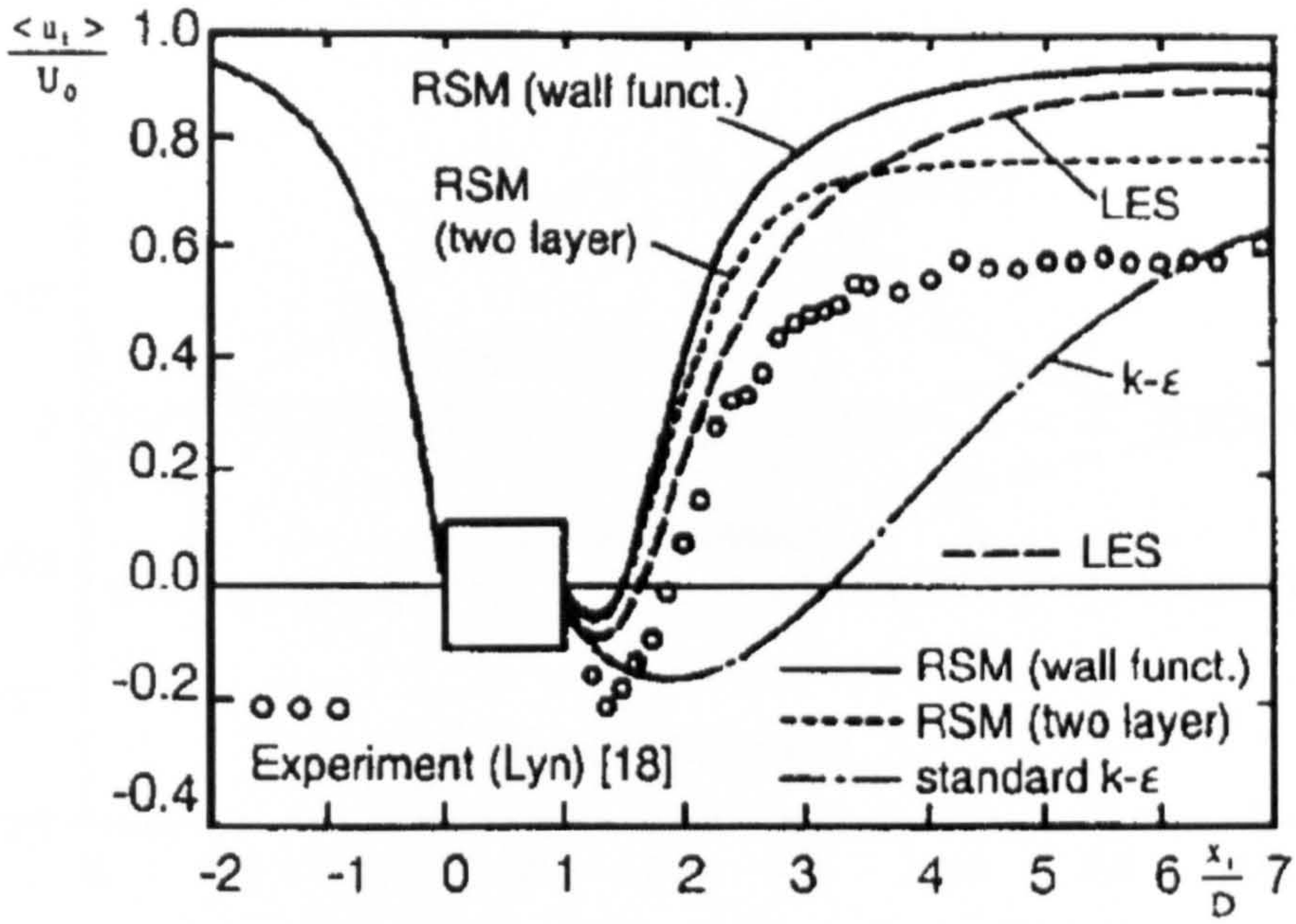

Figure 1.9 Time-average velocity along centerline of square cylinder (Murakami 1997)

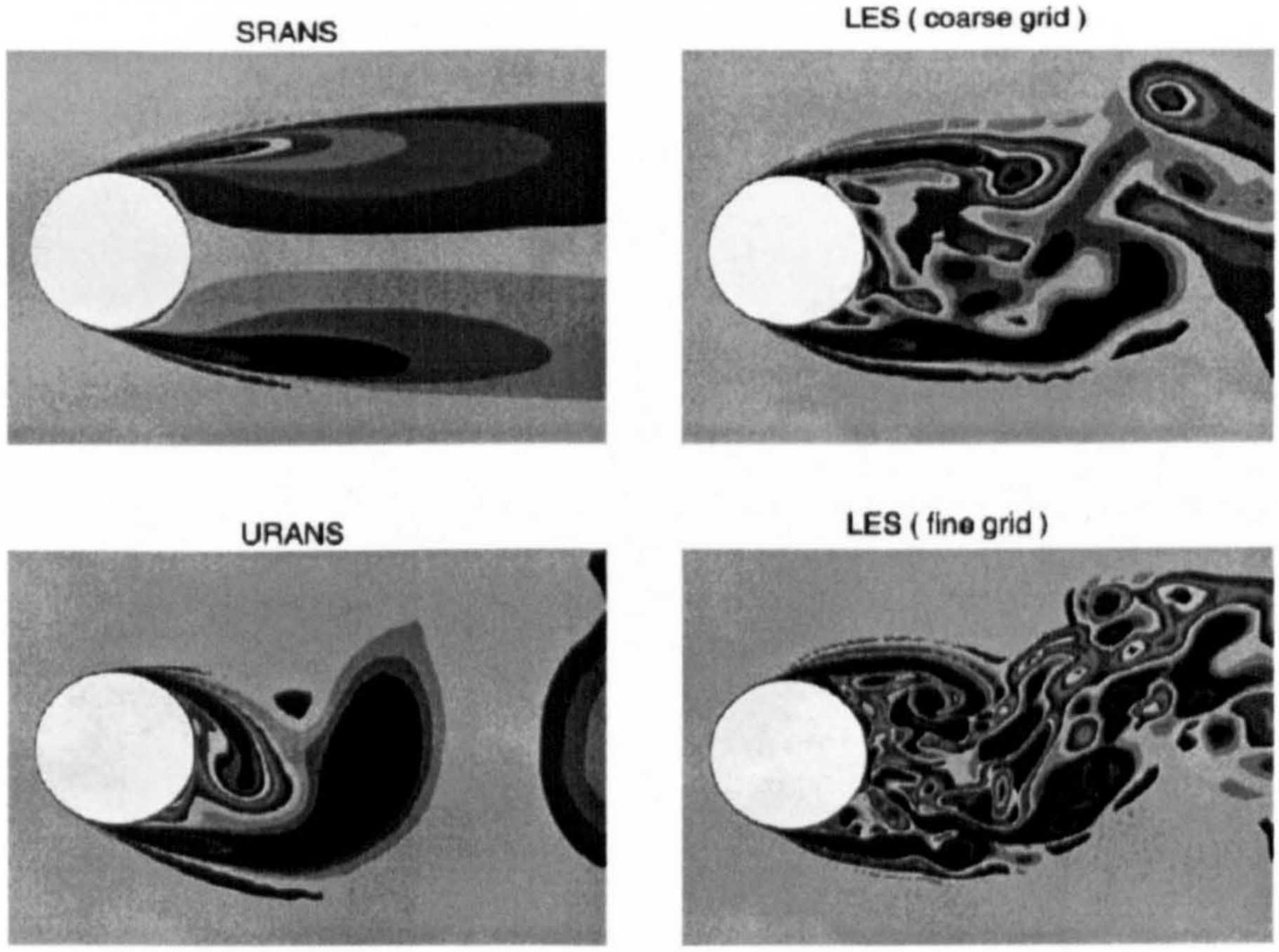

Figure 1.10 Simulation of flow past circular cylinder by various approaches (Spalart 2000)

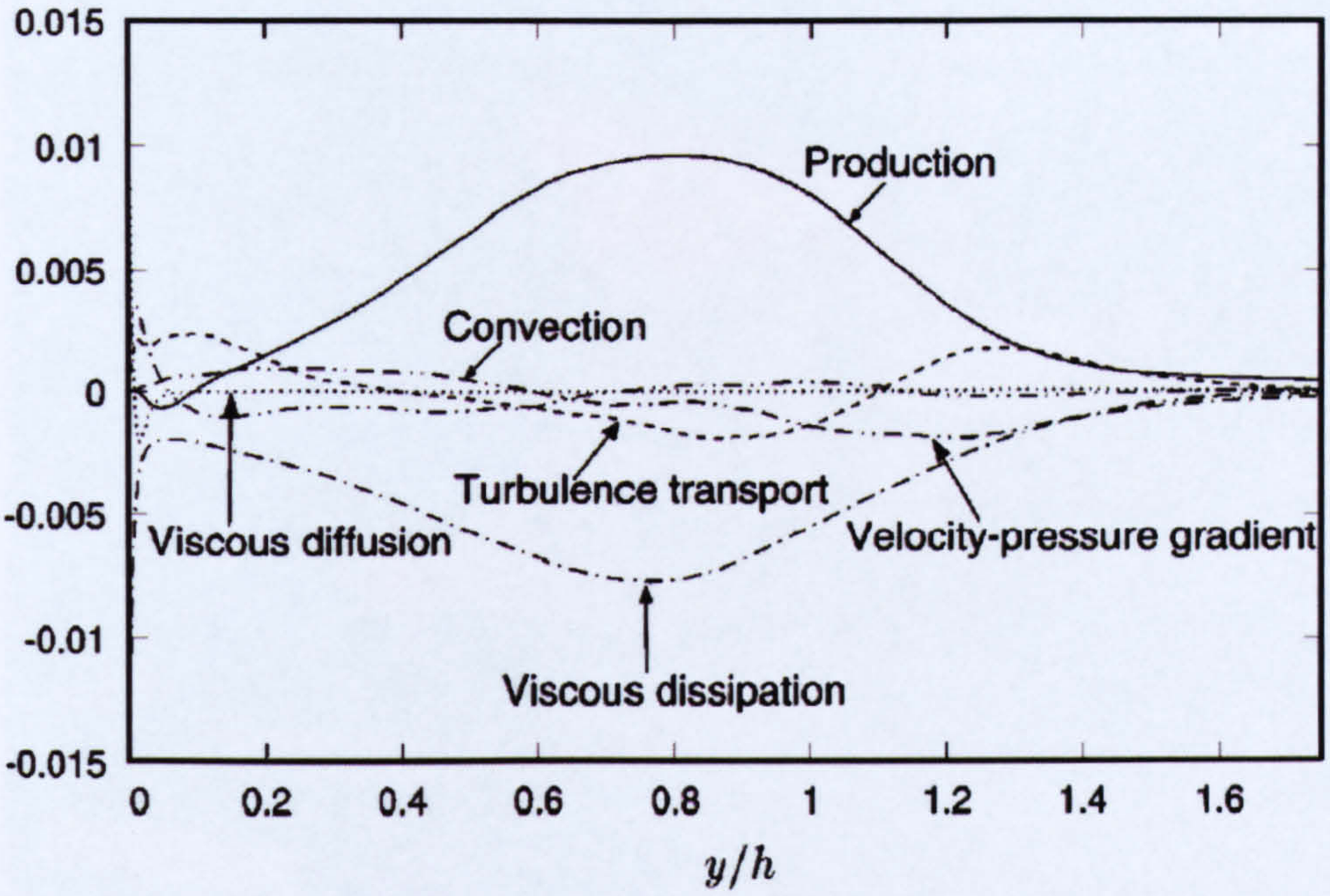

Figure 1.11 DNS of turbulent flow over a backward-facing step (Moin etc 1998), all the terms in the Reynolds stress equations computed directly

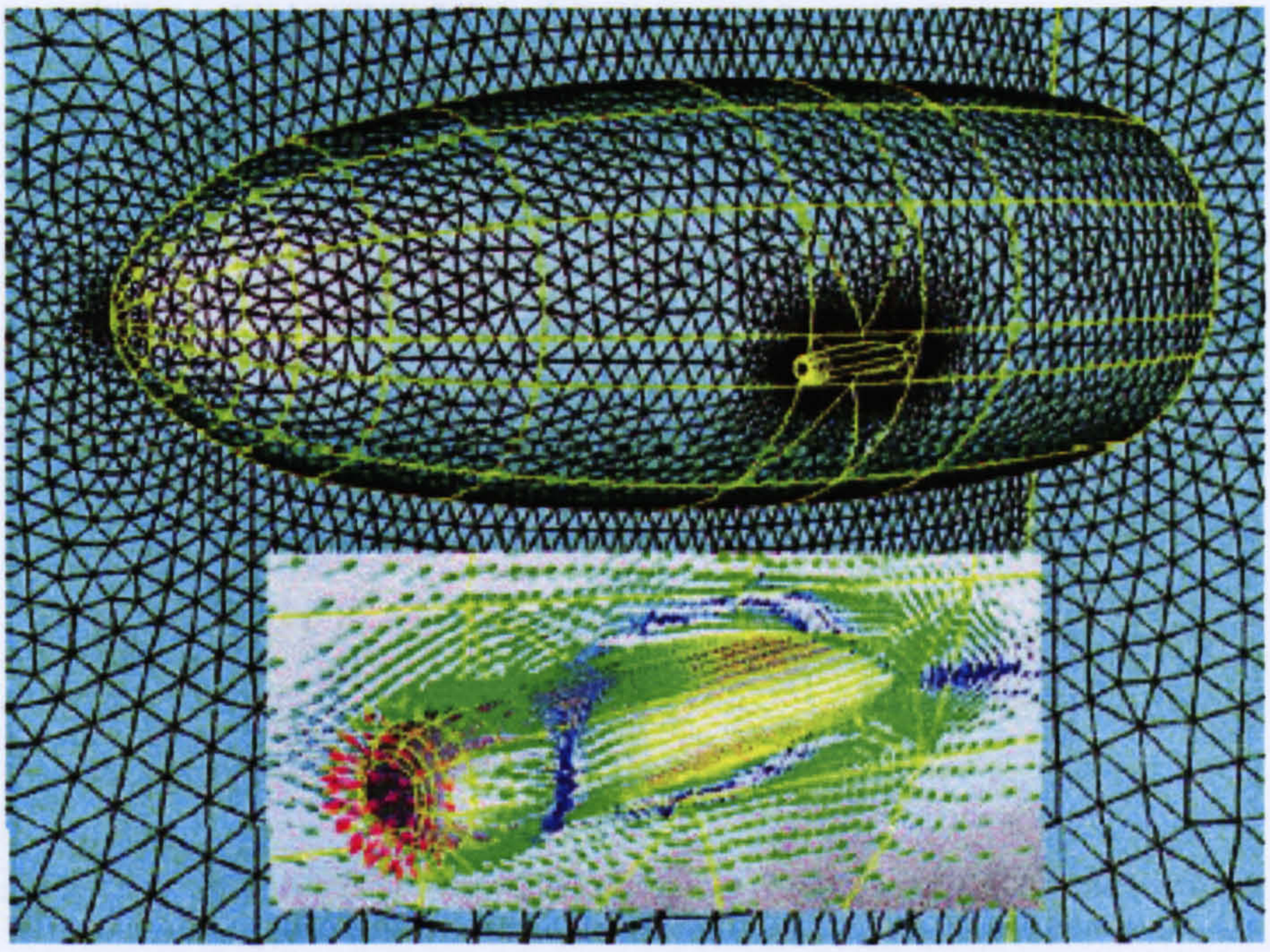

Figure 1.12 Torpedo launch from a submarine bay (Oran 2002)

Figure 1.13 A naval destroyer moving at 20 kn, with smoke from the stacks and an approaching helicopter (Oran 2002)

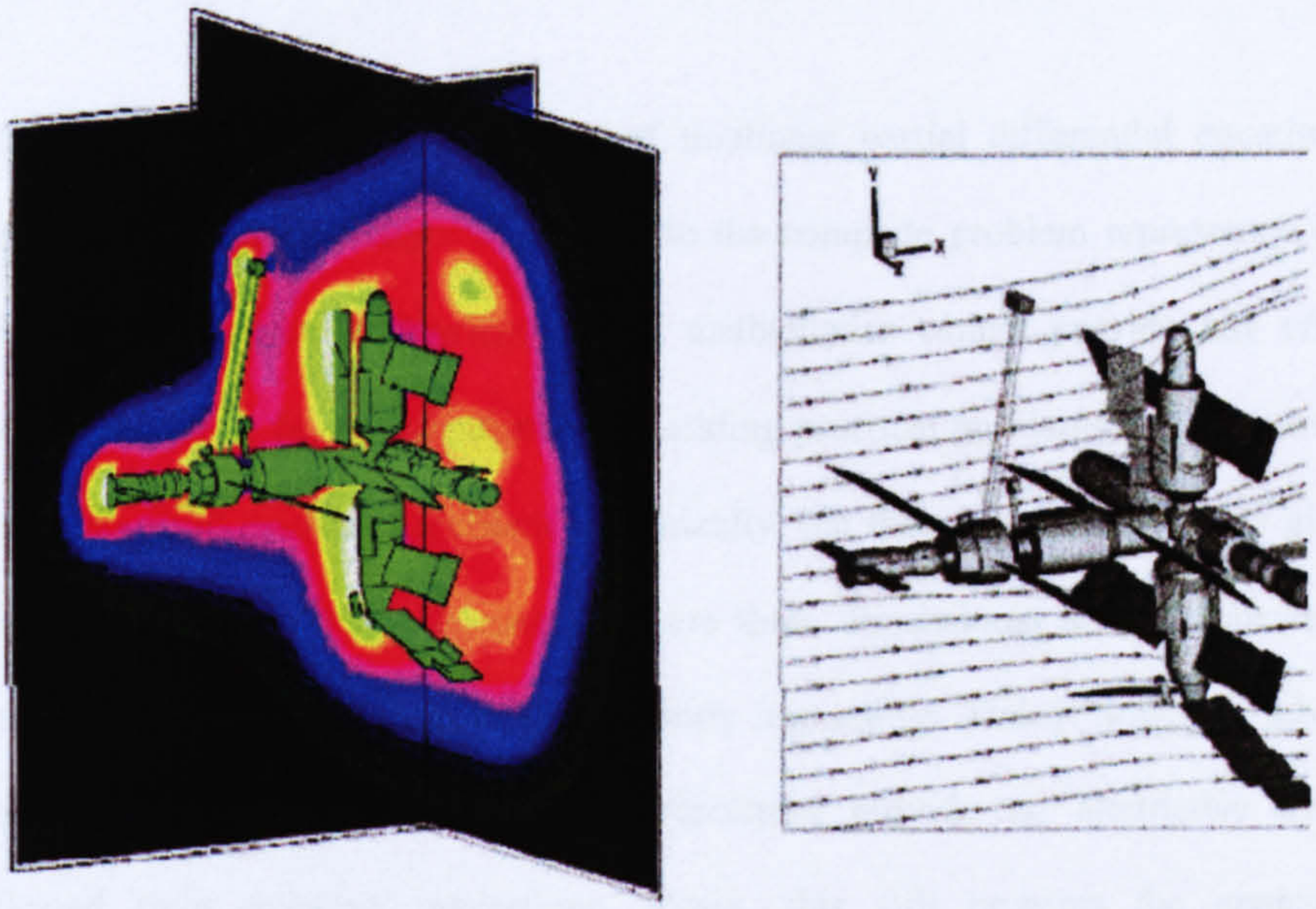

Figure 1.14 Pressure and velocity vector for the flow over the Mir Space Station at 110km (Oran 2002)

CHAPTER 2

CFD APPLICATIONS IN WIND TUNNELS

2.1 Introduction

Wind tunnels have been and will be the very important tools for development of aerodynamics, hydrodynamics and other fluid dynamics. Through the breakthroughs in CFD techniques in the 1960s-1970s, people once thought the wind tunnel as a tool would be obsolete (Ewald 1998), but it has never happened. The fact is that CFD development, though powerful, is far away from the early expectations. This is as a consequence of a limited understanding of turbulence. The current models tend to be limited, both in physical mechanism and in mathematical analysis.

The fluid dynamics equations are a set of nonlinear partial differential equations. In mathematics, there is no analytical solution to the complete problem represented by the equations, i.e., the present development of mathematics cannot provide any efficient theoretical tool for it. In the long history of tackling practical problems, people have tried to resolve the fluid dynamics problems empirically, but these methods can only give the approximate solutions. When the problems are three dimensional and complicated, the solutions become more difficult, if not currently impossible. Today, however, advanced computer platforms and the numerical techniques provide an alternative tool for complicated fluid dynamic predictions. Again, this still presents the approximate solutions, and the accuracy and reliability may become problematic for complex configurations, such as the flows for large AOA flight and bluff bodies et al. In many cases, people would like to use wind tunnel as the final development tool.

It is believed that wind tunnels can provide reliable data under the well-controlled environments and well-conducted measurements. Some practical difficulties in wind tunnel testing, however, always haunt tunnel engineers: blockage or wall interference, Reynolds number effect and even physical modelling.

Firstly, when the test model is in working section, it will reduce the area of the flow passage, accelerate the flow which passes the test model, and cause a blockage in working section. It's obvious that the blockage may change the flow field and the testing results. Blockage is usually defined by the ratio of the model frontal area and the working section cross area, therefore, for a given working section, the bigger the model is, the bigger the blockage. When the blockage is small, the effect of blockage on the test results is either small or can be corrected by a conventional linear method or more advanced approach. When the blockage is too big, say, bigger than 7.5% (the maximum blockage ratio Rae & Pope (1984) recommended), it will have a bigger effect on the results, and the correction methods must be applied, but the correction procedure may be problematic or even uncorrectable.

Secondly, the Reynolds number of the model is usually much smaller than the prototype since the testing model is usually scaled. For example, for road vehicle test, a 25-30% scale model is usually used in Europe, and 40% model in America (Hucho & Sovran 1993). The Reynolds number for prototype may be an order greater than that for typical wind tunnel model. To increase Reynolds number in wind tunnel, increasing the wind speed in the tunnel is one way, but may be problematic. Think about a simple example, if the model is one fourth of prototype and supposed the speed of the prototype is 100m/s (223mph) (a very high speed car). In order to reach the prototype Reynolds number, the air speed in wind tunnel should increase to 400m/s (it's supersonic!). In this case, the

flows around the test model are totally different from those around the prototype. Obviously, the physical modelling can not be successful.

Third, the model manufacturing may not be as exact as the prototype, especially for some small parts. One reason is that the small parts are not easy to manufacture, another reason is that even if the small parts are physically modelled, but it's still unclear for their effects due to the Reynolds number effect. It must be kept in mind, however, that in some cases the some small parts may cause the significant difference for the flows between scaled model and the prototype.

In summary, CFD techniques and wind tunnels have their own advantages and disadvantages, and they are complementary in many ways. This research aims to combine CFD tools and wind tunnel into a more powerful facility for aerodynamics testing, i.e., CFD to complement and, therefore, to enhance the wind tunnel testing.

2.2 CFD Applications in Wind Tunnel Experiments

CFD has been employed to support wind tunnel experiments in many aspects, such as test model design and fabrication, experimental set-up, experiment monitor, and data analysis and visualization etc. Some details are given as follows.

2.2.1 Model Design and Fabrication

When the model is being designed, the first thing is the selection of the model scale. From the standpoints of measurement and modelling, the model should be manufactured as big

as possible, for the bigger the model is, the better the test results are. From the standpoints of model blockage and the cost of model building, the smaller the model is, the smaller the blockage is and the less the cost. Therefore, in wind tunnel testing, there is always a compromise for the model scale, usually depending on the wind tunnel engineer's experience. To be independent of engineer's experience for the selection of the model ratio, some researchers suggest the general rules for the testing model. Rae and Pope (1984) recommended that the maximum model frontal area should not exceed 7.5% of the test section, and they also suggested that the blockage effect can be removed by semi-empirical correction methods. Hucho and Sovran (1993) reported that a blockage ratio of 5% has been appropriate for the vehicle aerodynamic testing for a long time. Accordingly, very few automotive wind tunnels in the world can meet the requirement for a typical car prototype testing, which will require the test section area of about $40m^2$. Normally, the blockage of slightly more than 5% has been used in practice. But, when the blockage ratio is more than 10%, the testing results will be very doubtful.

Now, CFD techniques may lead to a better selection for test model ratio. Niewald and Parker (2000) used a CFD tool to check up the blockage and the wall interference for their different sized model testing in wind tunnels during the development of F/A-18E fighter. They carried on the wind tunnel testing of 5%, 8%, 15% and 17.6% model scales in different project development stages and CFD ensures them that the wind tunnel wall has no apparent effect on the test data for the different scale models.

CFD techniques may allow people to select model ratio more scientifically. Generally, a bigger scale for model fabrication is expected since the tunnel engineers tend to be conservative in selection of model ratio. The bigger model may produce threefold benefits: bigger Reynolds number can be reached; the manufacturing of a higher-fidelity model

may become feasible; and the bigger model may provide more space for the onboard instrumentation.

2.2.2 Experiment Set-up

Experiment setup is a very important stage for any model test. The experimental preparations, such as the measurement locations, the transducer range selection and model support approach, are included.

The reasonable measurement locations are of vital importance in the measurement of the test data. To get reliable and reasonable data from test, the more measurements there are, the better, at least theoretically. But, too many measurements during the tests may not be the best solution. Because too many measurements may increase the cost in buying the sensors, and increase the test data which may cause the difficulties in data processing and management, and even difficulties in operating or recording. In practice, people developed the methods for reducing the measurements in certain areas where the parameters change smoothly, and increasing the measurements where the parameters change quickly. Good CFD results can be most beneficial in the placement of sensors etc.

Niewald and Parker (2000) used CFD results to determine the proper number and concentration of pressure taps required to accurately measure sting and distortion effects over the range of test conditions. Figure 2.1 shows that approximately 1050 pressure taps distributed over the external surface of the testing model. Pressure taps were concentrated in the region where CFD predicted the complicated flows occurred and a sparse distribution of taps was in the region only for the requirement of pressure integration. This

approach would minimize the effect of measurement system bias on the results on the limited measurements.

Once the measurement locations have been decided, the next step is to decide the range of the transducers. Transducers usually have limited overloading capabilities, especially for the transducers with high accuracy, which tend to be expensive. In the past, when the measuring value is often unknown, large range transducers were used to keep the maximum sensed value within the overload range. This approach, however, reduces the measurement accuracy.

CFD techniques can guide to determine the ranges of the transducers efficiently, even though CFD cannot give the accurate prediction. Bosniakov (1998) used CFD results in several ways in preparing for the experimental tests, including the choice of transducers or gauges for the tests.

2.2.3 Experiment Monitoring

Real-time (online) monitoring of wind tunnel test is a good way to ensure the reliable test results. Niewald et al (2000) used a continuous online monitoring system in their wind tunnel experiment. The real-time 3D surface pressure color contour displays, compared to CFD results, were monitored to access data quality and to support elimination and substitution of faulty pressure measurements, if necessary. Online correlation of pretest N-S CFD solutions and test data led to high confidence throughout the test, Figure 2.2 shows the comparison of the pressure predictions of CFD and wind tunnel.

2.2.4 Data Analysis

CFD can provide more details of the flowfield than the tunnel data, particularly in the areas of test or measuring difficulties. Therefore, the comparison and fusion (overlaying) of the data from tunnel and CFD simulation may provide additional insight into the data sets. Lamar et al (2001) summarized the comparisons of the flight, wind tunnel and CFD data for craned arrow wing (F-16XL-1), including the test conditions of subsonic and transonic speeds. And with the aid of data fusion (overlaying), the resulting highly diverse types of data sets were obtained over a wide range of test conditions, and have produced some novel results. Figure 2.3 shows the comparison of upper surface Cp distribution of CFD and flight, and Figure 2.4 shows the data fusion method.

2.3 CFD Applications in Data Corrections of Wind Tunnel Test

Corrections of wind tunnel test data have remained an unsolved problem for all wind tunnel engineers. Many researchers proposed their correction methods of wind tunnel data, which were mainly based on semi-empirical methods. In many circumstances, these correction methods are quite effective. Figure 2.5 shows the uncorrected data obtained from different wind tunnels, where the data are not correlative at all, while Figure 2.6 shows the corresponding results after correction; very consistent results are found for the different wind tunnels.

The most conventional corrections of wind tunnel data are the linear correction methods based on potential theory, and these methods give the very good corrections for small blockage and the simple flows. With advances in computer capabilities and numerical

techniques, the more sophisticated wall correction methods have been or are being developed, such as boundary-measurement methods and CFD methods. The former are based on the assumption that the wall-induced flowfield satisfies the Prandtl-Glauert equation, and utilization of the measurements of the flow at or near the tunnel walls. The latter cover a large range of numerical techniques, from the linear potential theory to Navier-Stokes equations in RANS.

Rogers and Roth (2000) showed the CFD validation of high-lift flows with significant wind-tunnel effects, and then compared the test data from two different size wind tunnels and CFD results. Finally, they concluded that current CFD techniques could predict accurate forces and pressures at low to moderate AOA. McDonald etc (2000) investigated the correlation between the wind tunnels and flight, and presented their improvement on the understanding of the pertinent aerodynamics and the extrapolation methods. Their report included many experiment examples on improving the understanding of various aspects of aerodynamics pertinent to design and testing at NASA Ames Research Centre.

2.4 CFD Applications in Wind Tunnel Design

In the history of wind tunnel, design methods have been well documented, Bradshaw & Pankhurst (1964) summarized the aerodynamic and structural design from the viewpoint of the prospective tunnel designer, and the practice in the wind tunnel design, then outlined the features of general use wind tunnels. Later on, Mehta and Bradshaw (1979) further formed the design rules for small low speed wind tunnels. The rules have been accepted widely. A typical example is the wind tunnel built up in Tohoku University, Japan (Ito et al 1992). This is a general-purpose low turbulence wind tunnel, with

longitudinal component of turbulence intensity at the center of the closed working section is less than 0.02%, and mean velocity variation across the working section are within ±0.1% of the mean velocity.

Although the general rules of wind tunnel design are widely accepted, these rules are mainly based on the simplified analytical or experimental results. Gordon and Imbabi (1998) employed CFD techniques to optimize the design of a wind/water tunnel. In order to achieve the goal of building a compact and cost-effective tunnel, they employed CFD techniques to modify some components design, significantly different from those of the conventional tunnel. The significant modifications included: two smooth 180^0 bends in place of four sharp 90^0 square bends; cascaded diffuser/contraction with no intermediate settling chamber; and the use the guiding vanes at diffuser/contraction inlet, to diffuse the flow more effectively over a wide range of Reynolds numbers. As a result, a compact wind/water tunnel was built. The assembled tunnel is shown in Figure 2.7.

2.5 CFD Applications in Virtual Wind Tunnel

Virtual wind tunnels or numerical wind tunnels are taking a more important role in analysis of the associated flow fields. When the complicated geometrical and topological situations are considered, the 3D flow fields are very complicated, and some complex or small turbulent structures are not easy to visualize in the tunnels, while numerical simulations may give more details in the flow fields. For example, multiple vortices, recirculation bubbles and chaotic flows within vortex breakdown have been all observed in computer simulations of steady 3D fluid flows (Bryson et al 1992). Besides, more complicated phenomena in unsteady 3D flows are required to be visualised.

Computers have become the main tools to display the complicated flow fields, representing the real (physical) wind tunnel in numerical methods or the data obtained from the wind tunnel test. Many techniques have been implemented in the computer software, and include isosurfaces, streamlines, ribbons, particle pathlines, rendering of vectors, tufts etc. These can all be reached in the high-performance graphics workstations as well as in some desktop PCs.

2.6 CFD in Support of Wind Tunnel

After several breakthroughs during the 60-70s of the last century, CFD techniques became more applicable to a whole variety of the fluid dynamic problems. It had been suggested that wind tunnels, as development tools, would become obsolete (Ewald 1998). The development of CFD techniques, however, was far slower than expected. The main difficulties lay in the modelling of turbulence, both the physical mechanism and mathematical expressions. So, wind tunnels are still the indispensable tools for fluid dynamic scientists and engineers.

Since the increasing testing time and the requirement of predicting the accurate characteristics of military and civil aircrafts, wind tunnel testing is facing the requirement of providing more accurate and reliable data for customers. Advanced techniques are needed for wind tunnel testing, in either the improvement of measurement methods, or the complementarities by other tools. Fortunately, CFD happens to be the complementary tool. Sheng et al (2002), Campbell et al (2003), and Sheng et al (2003a, 2003b) used CFD to complement and, therefore, enhance the wind tunnel test, including the numerical

simulation of wind tunnel, the blockage correction and even the support system effect. This research aims at forming a more powerful facility for aerodynamic test by combining CFD tool and wind tunnel.

2.7 Concluding Remarks

From the statements above, we can conclude the following remarks:

- CFD has been used as a powerful tool in enhancing and complementing wind tunnel testing, i.e., CFD provides a more detailed flow field than current wind tunnels. Also CFD can enhance the wind tunnel test by being used during the whole process, from model preparation to the data analysis.

- Combining CFD into the wind tunnel testing forms a more powerful facility for aerodynamic research and design, making full use of the strengths of wind tunnels and CFD.

- CFD applications in the design of wind tunnels have a promising future. Of course, CFD techniques may be used to check the design of the existing wind tunnels and may provide the detailed information for the wind tunnel update.

Figures of Chapter 2

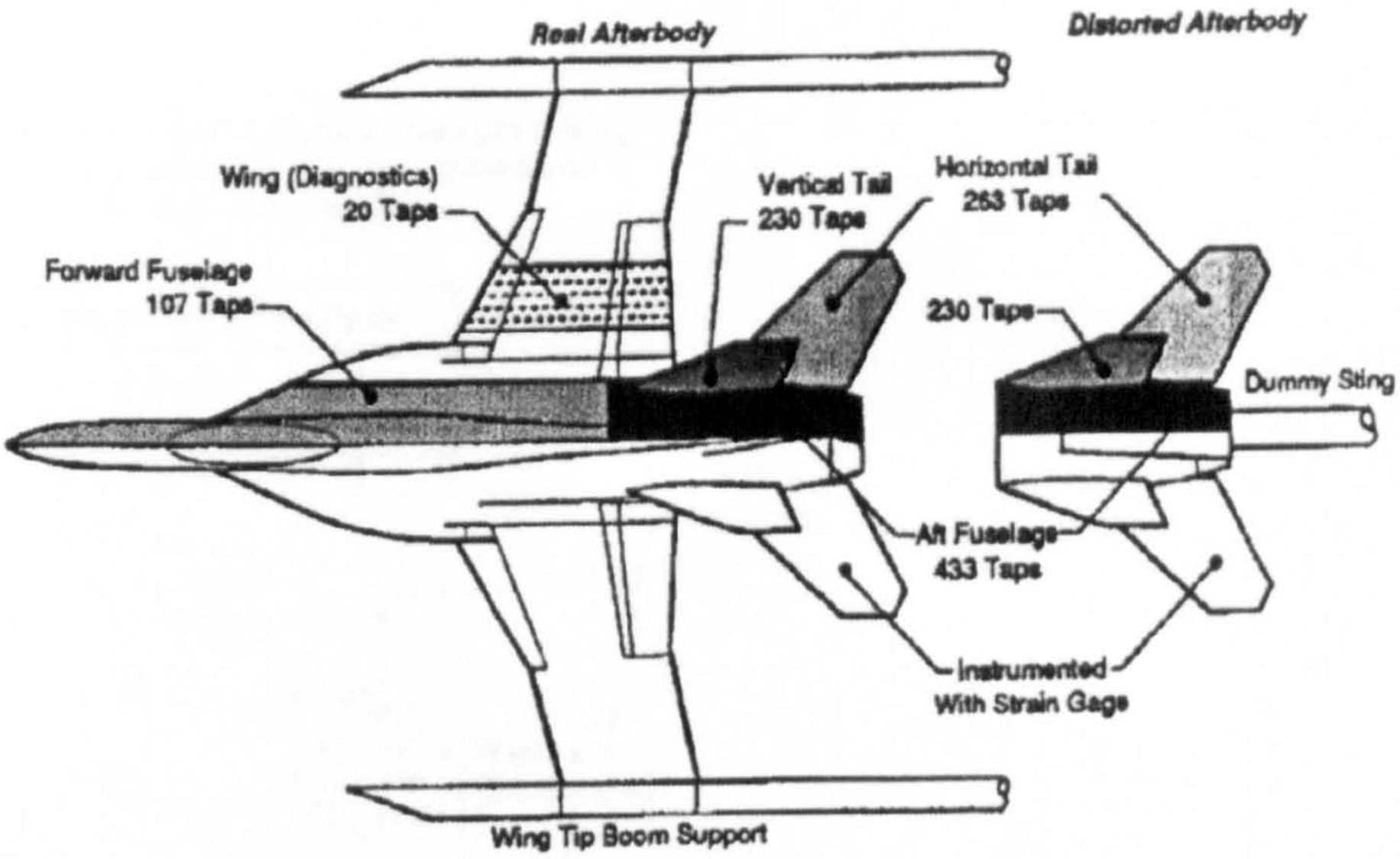

Figure 2.1 Pressure tap arrangements (From Niewald 2000)

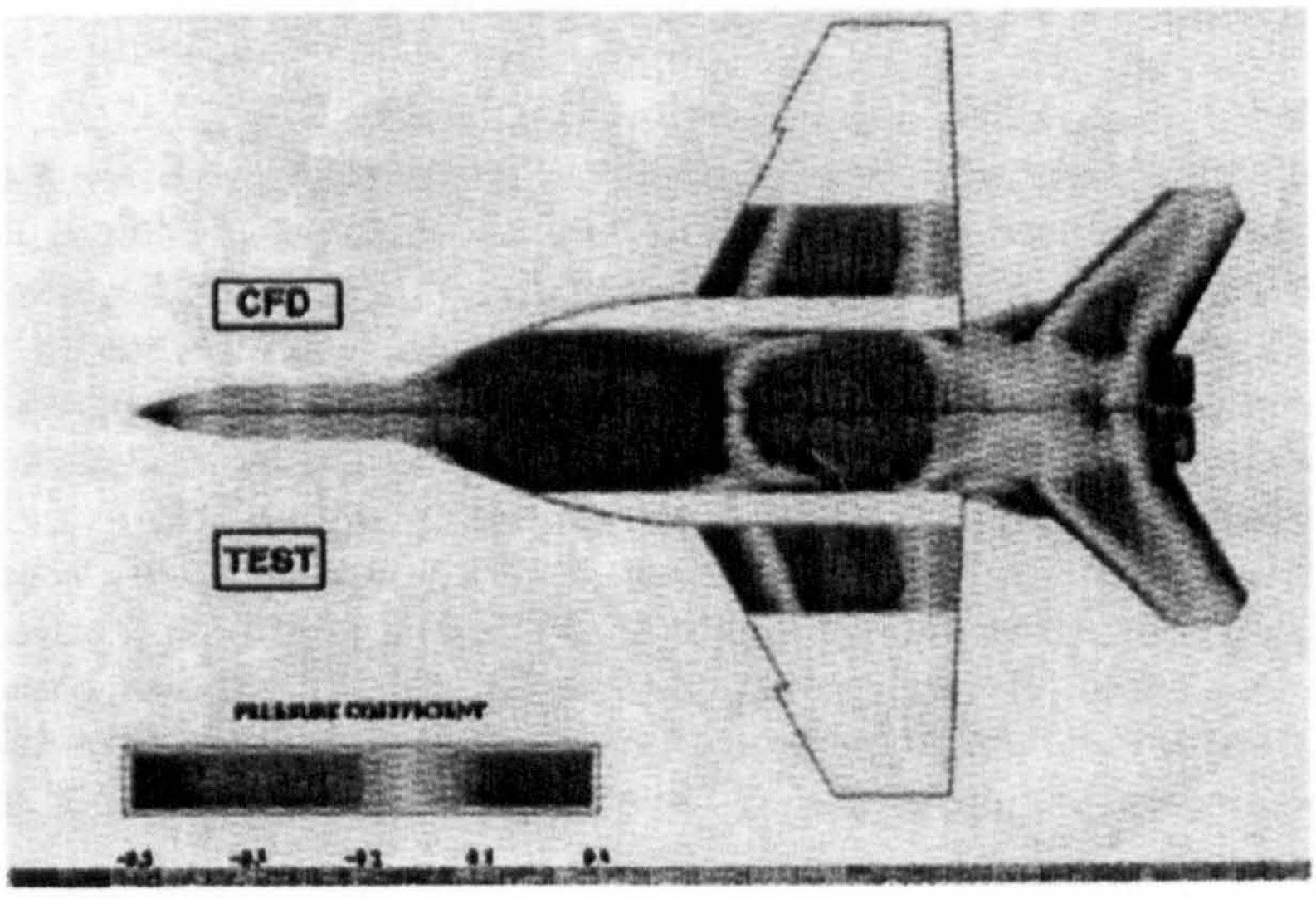

Figure 2.2 Comparison of wind tunnel and CFD predicted pressure (From Niewald et al 2000)

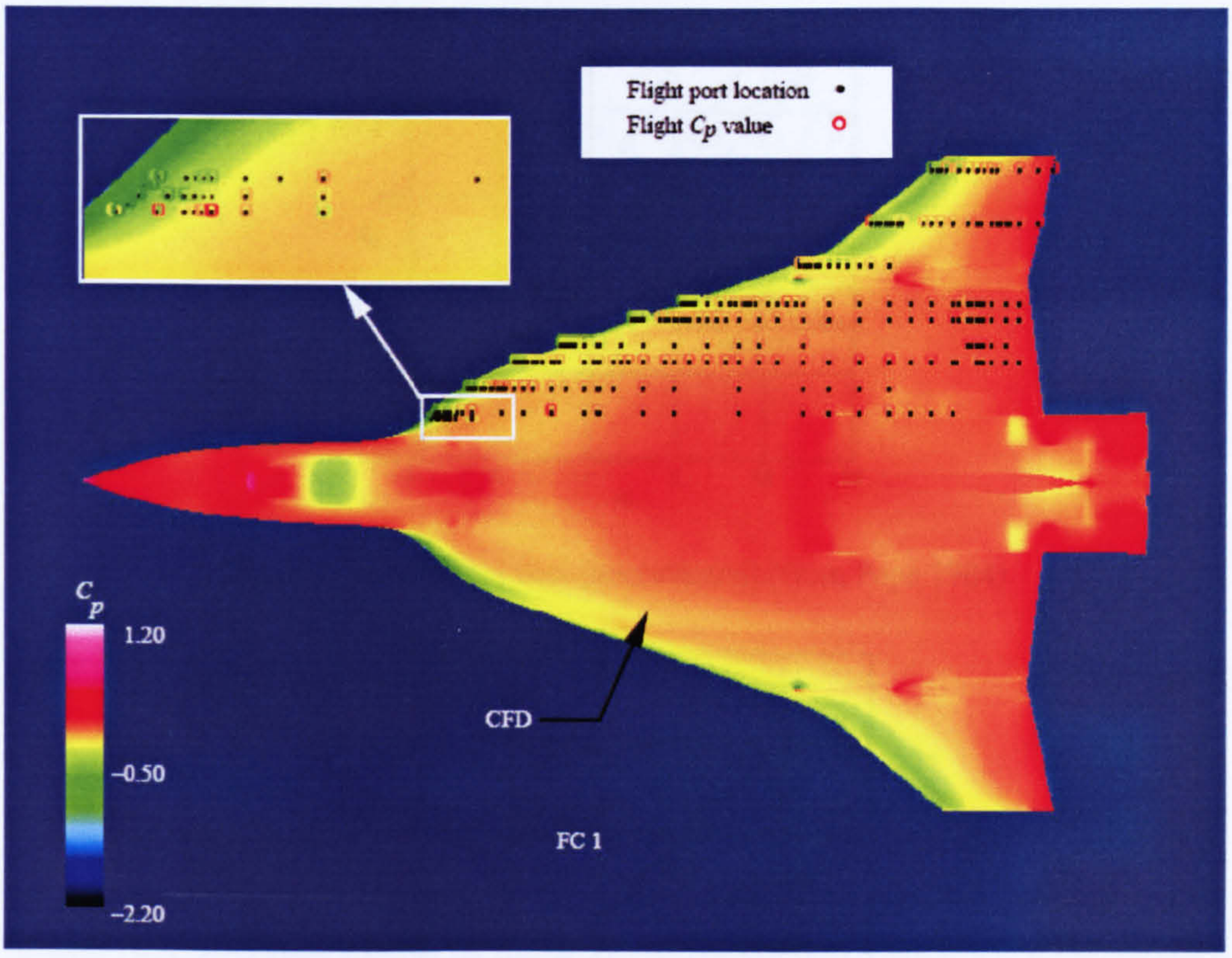

Figure 2.3 Upper surface *Cp* distribution (Lamar et al 2001)

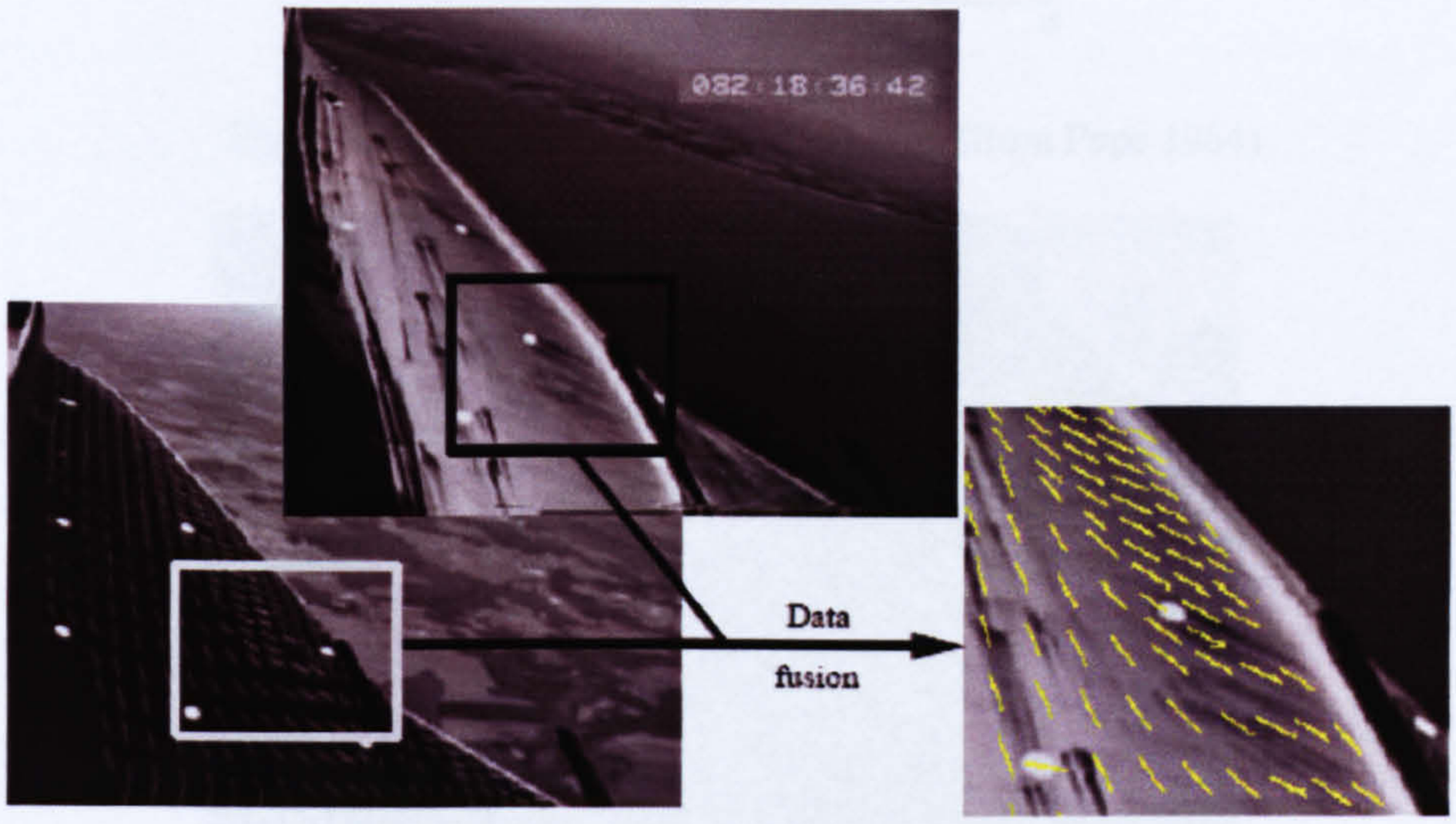

Figure 2.4 Superposition of liquid crystal and tuft image data for F-16XL-1 airplane at $\alpha \approx 13^0$, $M_\infty = 0.28$, and $Re = 47 \times 10^6$ (Lamar et al 2001)

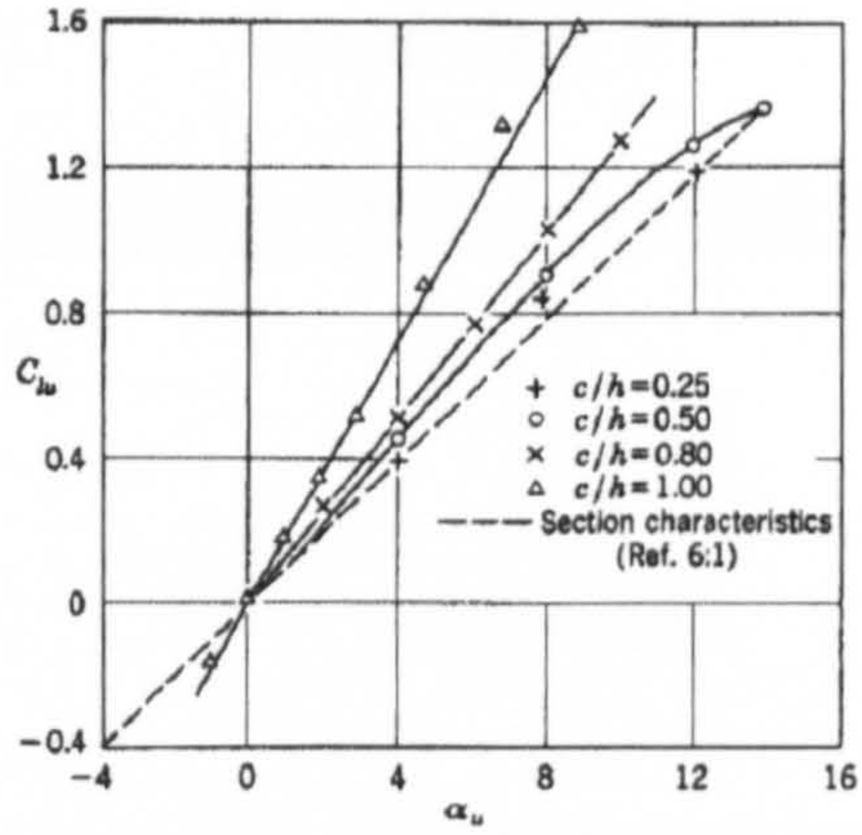

Fig.2.5 Wind tunnel data (uncorrected) (from Pope 1984)

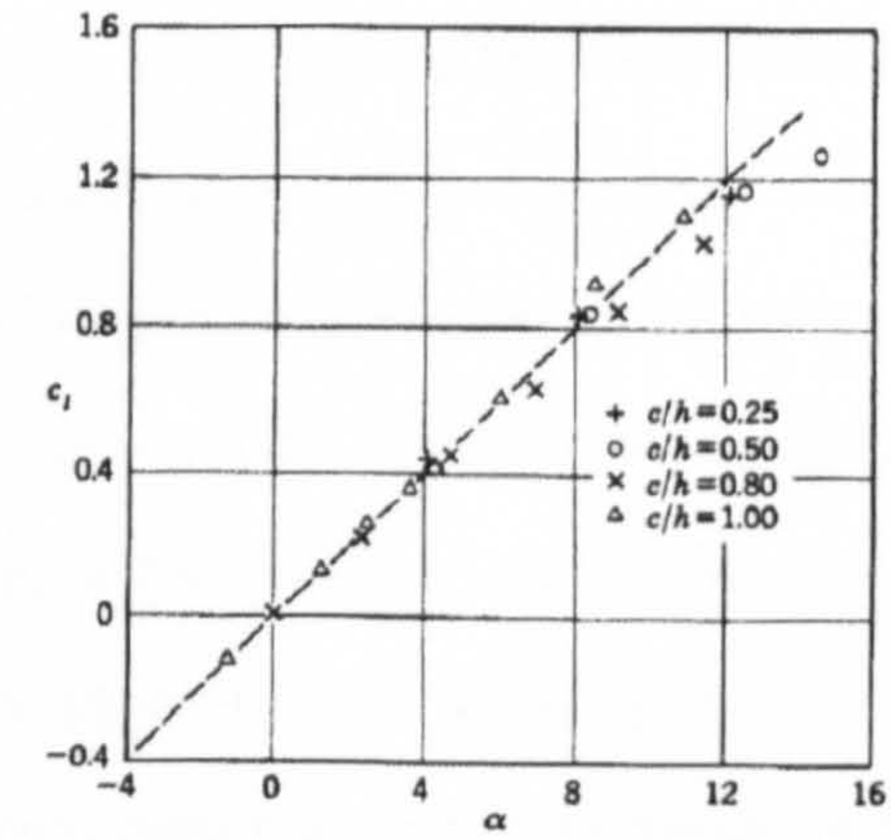

Fig.2.6 Wind tunnel data after correction (from Pope 1984)

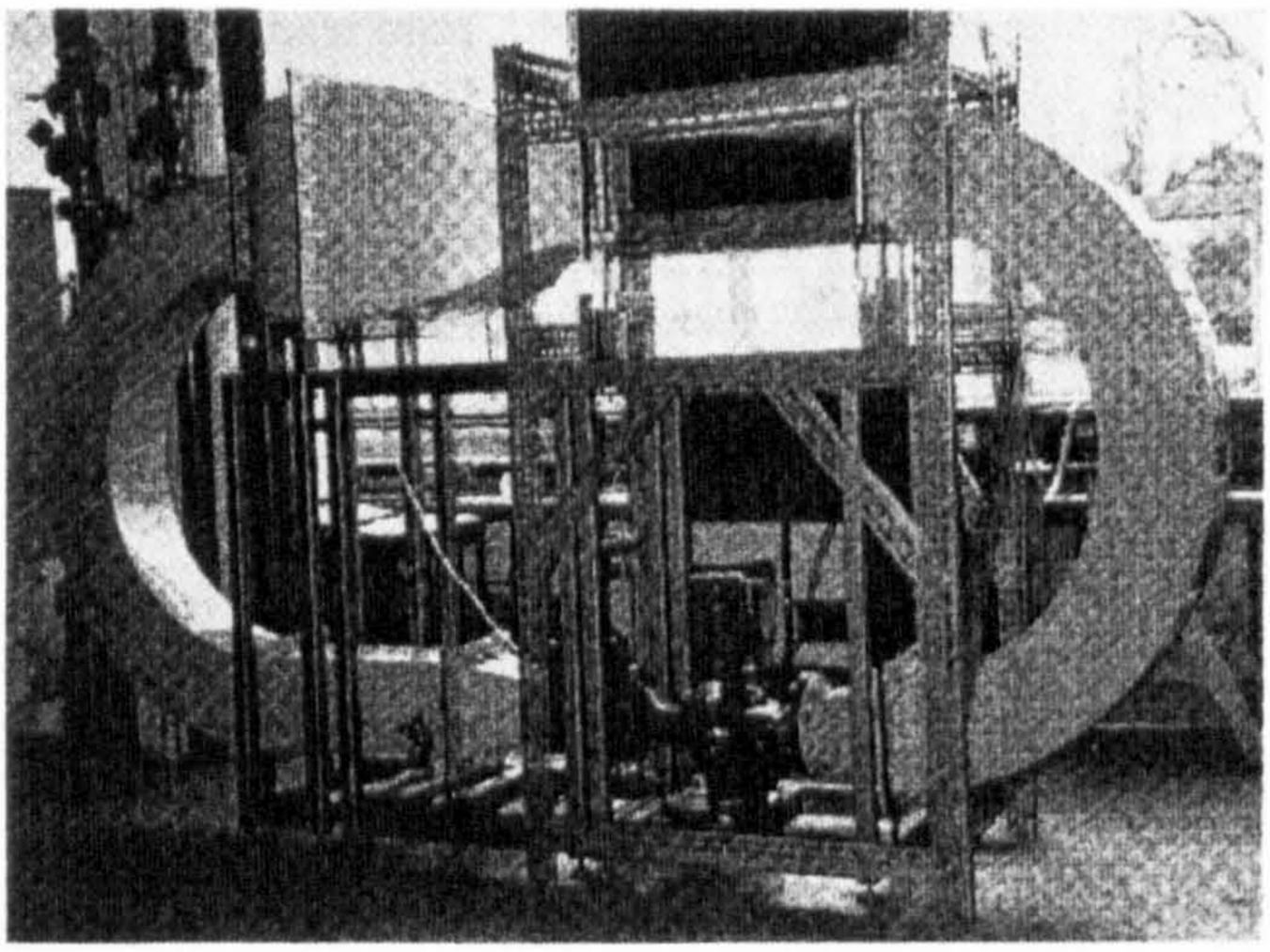

Figure 2.7 The completed wind/water tunnel (From Gordon et al 1998)

CHAPTER 3

NUMERICAL SIMULATION (I): WORKING SECTION

3.1 Introduction

The main objective of the design and build of wind tunnels is to provide a well-controlled environment for aerodynamic testing. Any wind tunnel may be the production of necessary compromises, such as the building field limitation and cost, the operation cost, maximum wind speed, velocity uniformity and turbulence intensity etc. Flow uniformity in the working section is the normal expectation of any good wind tunnel design. In the history of wind tunnel design and build, experience has been widely accumulated. A good example, is the design rules for small low speed wind tunnel formed by Mehta and Bradshaw (1979). Now people are trying to use advanced CFD techniques in wind tunnel design to enhance or indeed replace the empirical design methods. Gordon and Imbabi (1998) employed CFD to design a wind/water tunnel, and they successfully built a high performance wind/water tunnel at reasonable cost. In this chapter, the research will focus on the use of CFD tool to investigate the design of the Argyll Wind Tunnel at Glasgow University.

The wind tunnel to be simulated is a closed return type wind tunnel, which is shown schematically in Figure 3.1. The wind tunnel was formally housed at BAE Systems Hatfield site with its origins steeped in the historic DeHaviland company. Indeed, much of the early Airbus wing work was carried out in that tunnel and so it is a high quality industrial production facility. The wind tunnel had two changeable working sections, one is the normal working section, used for conventional aerodynamic experiments, another is

the one with a moving belt and boundary layer removal system, specially designed for the road vehicles testing. The boundary layer removal system in the working section is shown in Figure 3.2.

Generally, road vehicles are bluff bodies in very close proximity to the ground. The road vehicle tests in wind tunnels are quite different from the aeronautic experiments. In most cases of vehicle test, the road representation (boundary layer removal) is necessary. The most popular moving ground modelling system is a moving belt, which represents the almost perfect moving ground in the working section. The other modeling methods include multi-tangential-blowing system, boundary layer suction system or their combinations. Imaizumi (1996) developed a multi-suction & blowing (MSB) system, and compared the results of MSB and moving belt and concluded that the MSB ground plane can replace the moving belt system (Figure 3.3). Some other boundary layer removal systems are shown in Figure 3.4(a)-(d) (Barnard 1996).

In the chapter, CFD numerical simulation of wind tunnel contains following cases:

- Simulation of boundary layer
- Numerical investigation of working section design
- Removal of boundary layer

3.2 Boundary Layer Simulation

As mentioned above, road vehicles are bluff bodies in very close proximity to the ground. Therefore, the ground effect may have obvious effect on the performance of the vehicles, especially on its aerodynamic characteristics. When the underbody is very close to the

ground, there will be a strong Venturi effect between the underbody and ground, in that case, the boundary layer will take an important part in the underbody flow. As a result, in the actual wind tunnel modeling of ground, some measures must be taken, such as the moving belt method and suction and blowing method etc.

In this section, some factors affecting CFD performance were first considered, such as the turbulence models, near wall treatments and grid independence, before the boundary layer simulations were conducted.

- **Case 1: Turbulence Models**

In modern fluid dynamics, turbulence modelling is very difficult. The problem is currently universal and, as previously mentioned, understanding of it is limited, both in physical mechanism and in mathematical expressions. Progress was made however in the last century, especially during the 1960-70s. Unfortunately, the big breakthroughs that were expected, never happened. Today, however, many varieties of turbulence models have been proposed, and demonstrated the difficulties encountered. At present, no turbulence model is universally superior to others, and every turbulence model may be effective only in some cases, but not in others.

In the Fluent package, the solver has integrated several different turbulence models: one-, two-equation and RSM turbulence models. Besides, the laminar and inviscid flow, and even LES are also provided for selection. For the purpose of comparison herein, only RANS with turbulence models have been used, including Spalart-Alamass (S-A) one-equation model, standard κ-ε model, RNG κ-ε model, Realizable κ-ε model and

Reynolds-stress model (RSM). When the package was used to assess the velocity distributions above the tunnel working section floor, all the turbulence models considered gave very similar, if not identical results (Figure 3.5).

For static pressure distributions along the central line of the working section, different turbulence models give some differences; but the differences were small (Figure 3.6). From the figure, S-A model, Standard κ-ε model and RNG κ-ε model give the close results, and realizable κ-ε model and RSM give a little different results. The differences, relative to atmospheric pressure, were of the order of 0.003%. Note that in the calculation the working section was considered to be section-equal for the comparison, the whole pressure drop in the working section was about 0.03% of the atmosphere pressure.

- **Case 2: Near-Wall Treatments**

In fluid dynamics, flows are always affected by some kind of boundary conditions (restrictions). Walls may be the most ordinary boundary conditions. For example, when an airplane flies in the air, the surface of the airplane is a wall boundary; when fluid flows in the pipes, the pipe wall is a wall boundary; when a car runs on the ground, the car surface and the ground surface are all the wall boundaries.

The boundary layer simulation is a very difficult and important task for any CFD computation, for the boundary layers are usually the determined factor for a successful numerical computation of the flow field. The structure of the boundary layer is very complicated. Generally, when very close to the wall, viscous damping reduces the tangential velocity fluctuations, and kinematic blocking reduces the normal fluctuations.

Toward the outer part of the near-wall region, however, the turbulence is rapidly augmented by the production of turbulent kinetic energy due to the large gradients in mean velocity in the boundary layer. In present practice, the near-wall can be treated in three ways: standard wall functions, special wall functions (non-equilibrium) and hybrid methods (two zonal layer). The details of near wall treatments are given in Appendix B.

Figure 3.7 gives the simulation results with three different near-wall treatments. In this simple situation, all different near-wall treatments gave the same results for the velocity profile.

- **Case 3: Grid Independence**

Grid independence is an important aspect in CFD numerical computation. From the standpoint of numerical computation, it is normally agreed that, within limits, the finer the grid is, the better the computational results will be. For complicated flows, a very fine grid is needed, and very useful to capture the small physical structures, which are usually lost when using coarse grid. But a finer grid requires more computer resources, sometimes it's impractical to use too fine a grid in complicated flow computations and, if too fine, can lead to large errors and instabilities in some cases. Therefore, in practical applications, the grid generation is always an informed compromise between fine and coarse grid, i.e. the accuracy and the computer capabilities.

A general idea is to carry on the grid dependence computation, in which the results of coarse and fine grid are compared. When the coarse grid gives the very near results with

fine grid, it's believed the grid is fine enough. Now, grid adaptation makes the process easier.

Figure 3.8 and 3.9 show the coarse and the fine grid, having elements of 78,925 and 123,750 respectively. Figure 3.10 is the comparison of the results under two different grids, showing the very good agreement. So in this simple case, the coarse grid is believed to be fine enough.

3.3 Simulation of the Working Section

When air flows through the working section, the boundary layer will be developed on the tunnel walls, and cause a blockage and an associated pressure drop. Accordingly, a buoyancy force will be exerted on the test model. But for the well-designed working section, the buoyancy effect has been removed by the expansion of the working section. Like the Argyll Wind Tunnel at Glasgow University, the working section has an expansion. Figure3.11 shows the inlet and exit sections, and the exit is 1.4% larger than the inlet in area.

Numerical simulation (Figure3.12) shows the working section with an expansion has a much better static pressure distribution along the working section. This figure illustrates the comparison of static pressure distributions for the working section with/without an expansion. The static pressure drop in the working section with an expansion is very small, and can be neglected. Unfortunately no experimental data exist for comparison.

The velocity distributions along the working section can also benefit from the expansion design. Figure 3.13 gives the velocity distributions. The equal section design gives an increase in the velocity along the working section, as expected with a dropping pressure, but the expansion design gives almost constant distributions. Figure 3.14 shows the comparison of the velocity distributions above tunnel floor at the middle of the working section. Close inspection will reveal the differences in the profiles.

The modelling of the working section then considered the inclusion of a moving ground and a vent at the front. Generally, the moving ground had little effect on the working section flow profiles, while the forward configuration of the vent did.

When the vent is added on, the velocity profiles may be a little different from that of the normal working section (no vent). Figure 3.15a gives the result of the case without porous suction, and Figure 3.15b the result with porous suction. It can be seen that the vent didn't improve the boundary layer over tunnel floor in the working section. In the contrary, when the suction is off, the boundary layer became thicker, and the velocity beyond the boundary layer was a little larger than expected (figure 3.15a). When the suction is on, the case was improving and the velocity profile was closer to that of the normal working section (figure 3.15b).

Figure 3.16 gives the velocity and pressure coefficient contours with the vent. We can see the flow field is not so uniform, but still acceptable. Figure 3.17 gives the velocity distributions above the moving ground, it can be seen that the case with suction shows a good removal for the boundary layer (fig. 3.17b), but the numerical computation predicted a little different result from the experiment (fig.3.17a).

3.4 Improvements of Boundary Layer Removal

The vent exit at the front of the working section had been designed to remove the boundary layer development from the contraction, while the porous suction was used to further remove the boundary layer development after the vent (see Figure 3.2).

From standpoint of the numerical simulation, the vent exit design will increase the complexity of the geometrical configuration, and the difficulties in grid generation. In order to simplify the numerical computation of the working section and, therefore, simplify the design of the boundary layer removal system, a modification was proposed, and numerical simulation was carried out for the modification. This modification removed the vent at the front of the working section, and the moving belt was lowered down to be flush with the tunnel floor (Figure 3.18). The working section with a moving ground had the same shape as the original one, the only differences were the moving belt system and the porous suction.

Figure 3.19 shows the comparisons of measurement and simulation. The simulation results show a quite good agreement for the case with porous suctions.

Further, a simpler moving belt system in the numerical simulation was supposed for numerical computation, i.e., it simply took the whole working section floor as a moving ground, and removed the porous suctions (All MG in Figure 3.20). Again, numerical simulation shows a very good agreement with the measurement.

The numerical simulation results showed the possibility to simplify the design of the moving ground system in Argyll Wind Tunnel. Generally, porous suctions are necessary

to remove the boundary layer effectively. From numerical simulation, the vent exit can be removed, and twofold benefits can be obtained from it- simplifying the design of moving system, and improving the overall flow field in the working section.

3.5 Calibration of Working Section

For the completeness of the numerical simulation of the working section, the calibration of the wind tunnel further included the model support system. The support system considered herein was the strut support system, which is from the ceiling of the working section. The support system may have significant effect on the test results. Therefore, how to remove the effect from the testing results is a problem of the tunnel calibration.

Generally, the tunnel calibration establishes quantitative relationship between the flow conditions in working section and reference measurements. The flow conditions of primary interest are wind speed and direction and variations of these quantities over the region normally occupied by the test model. The reference measurements which relate to the wind speed are usually total and static pressure, the calibration is intended to provide "tunnel-empty" data as a reference base for corrections which allow for the constraining effects of the wall.

In the conventional wind tunnel testing, the model must be constrained by a support system, such as sting support system, strut/post support system or tip support system etc. So, the "empty tunnel" for the model testing calibration may be one of following cases:

a) The "truly empty tunnel" (figure 3.21a): the support system is taken as part of testing model.

b) The "combining empty tunnel" (figure 3.21b): the combination of the tunnel and the support system is taken as the "empty tunnel".

For the "truly empty tunnel", the calibration data must be corrected to a tunnel configuration. This means that the measurements of pressure on the support system should be corrected for the blockage of the support system. If the method of constraint correction is based on the measurements of pressure changes at the tunnel walls, the wall pressure measurements must be included in the calibration and the datum measurement at these points should also be corrected for the direct and wall-induced effects of the support system.

For the "combining empty tunnel", the working section with the support system is defined as the empty tunnel. When classical methods are used to calculate the model blockage, the appropriate source distributions should be those of the difference between the displacement flows of the model. Since the balance does not measure the loads on the support system, the "combining empty tunnel" is properly better, but the correct choice may be influenced by the method used to account for the support system interference.

For the Argyll Wind Tunnel, the working section calibration was carried out for working section and support system (strut). Figures 3.22(a) and 3.22(b) give the velocity and pressure coefficient contours at the longitudinal symmetrical planes in working section, and figure 3.23(a) and (b) show the transversal distributions. From these figures, the big influence of support system on the test results is expected.

3.6 Concluding Remarks

Numerical simulations of working section have been conducted, including the working section with expansion, moving ground system, and the tunnel calibration. The general concluding remarks can be drawn as following:

- The working section with expansion in Argyll Wind Tunnel has both good static pressure and velocity distributions along the working section, according to CFD predictions
- CFD simulation gives very good predictions for the boundary layer removal, especially for the case of porous suction on.
- The moving belt system may be designed more compactly according to CFD simulation. The simplified design, by removing the vent exit and lowering the moving belt, might give the good removal of the boundary layer.
- CFD provides a powerful tool to analysis the flows in the wind tunnels.
- CFD simulation shows the strut has significant influence on the flow field in working section.

Figures of Chapter 3

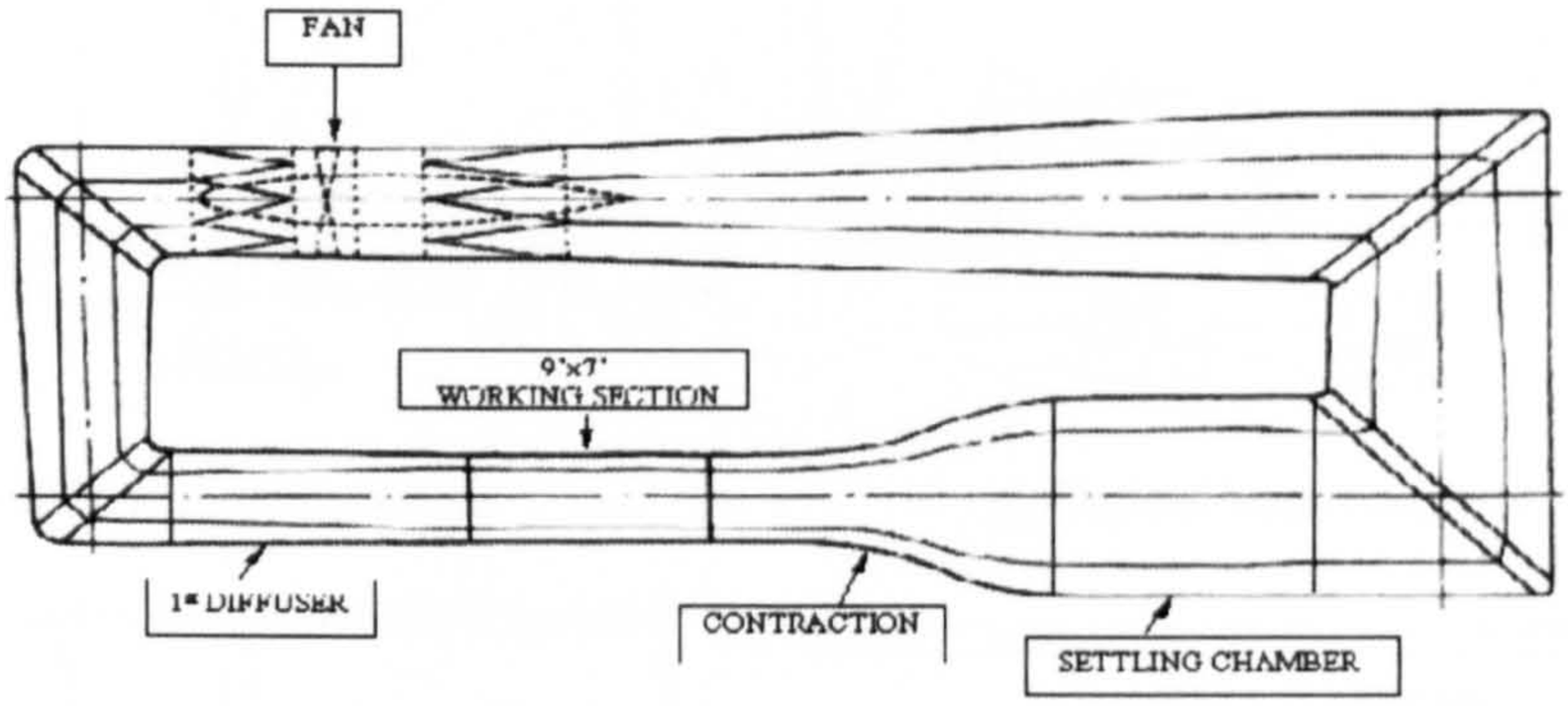

Figure 3.1 Glasgow University Argyll Wind Tunnel

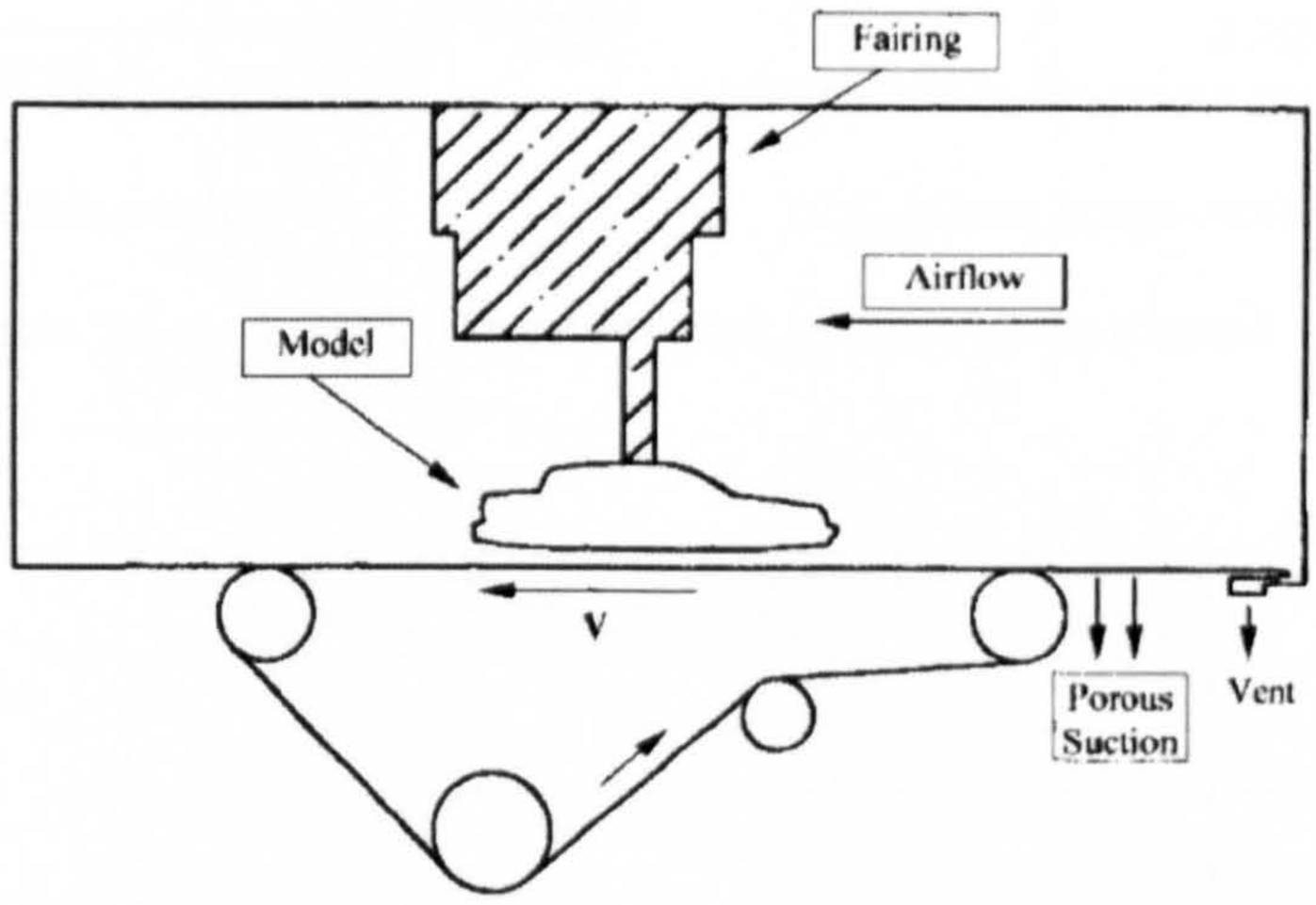

Figure 3.2 Moving belt system of the Argyll Wind Tunnel

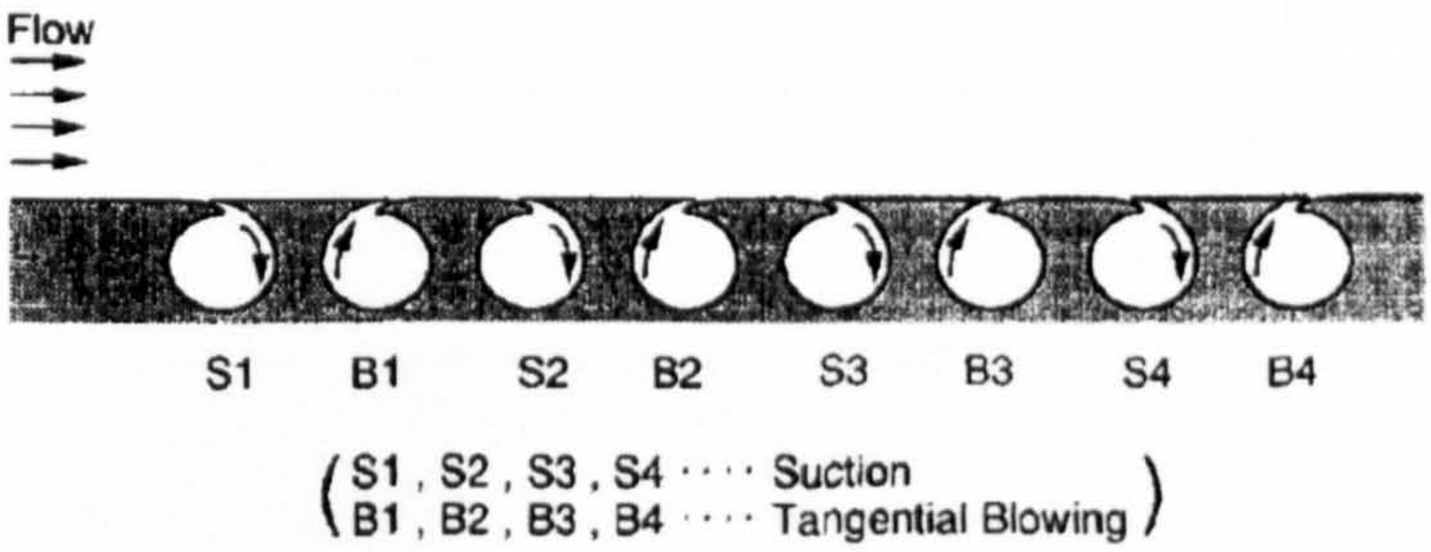

Figure 3.3 Multi-Suction-and-Blowing methods (Imaizumi 1996)

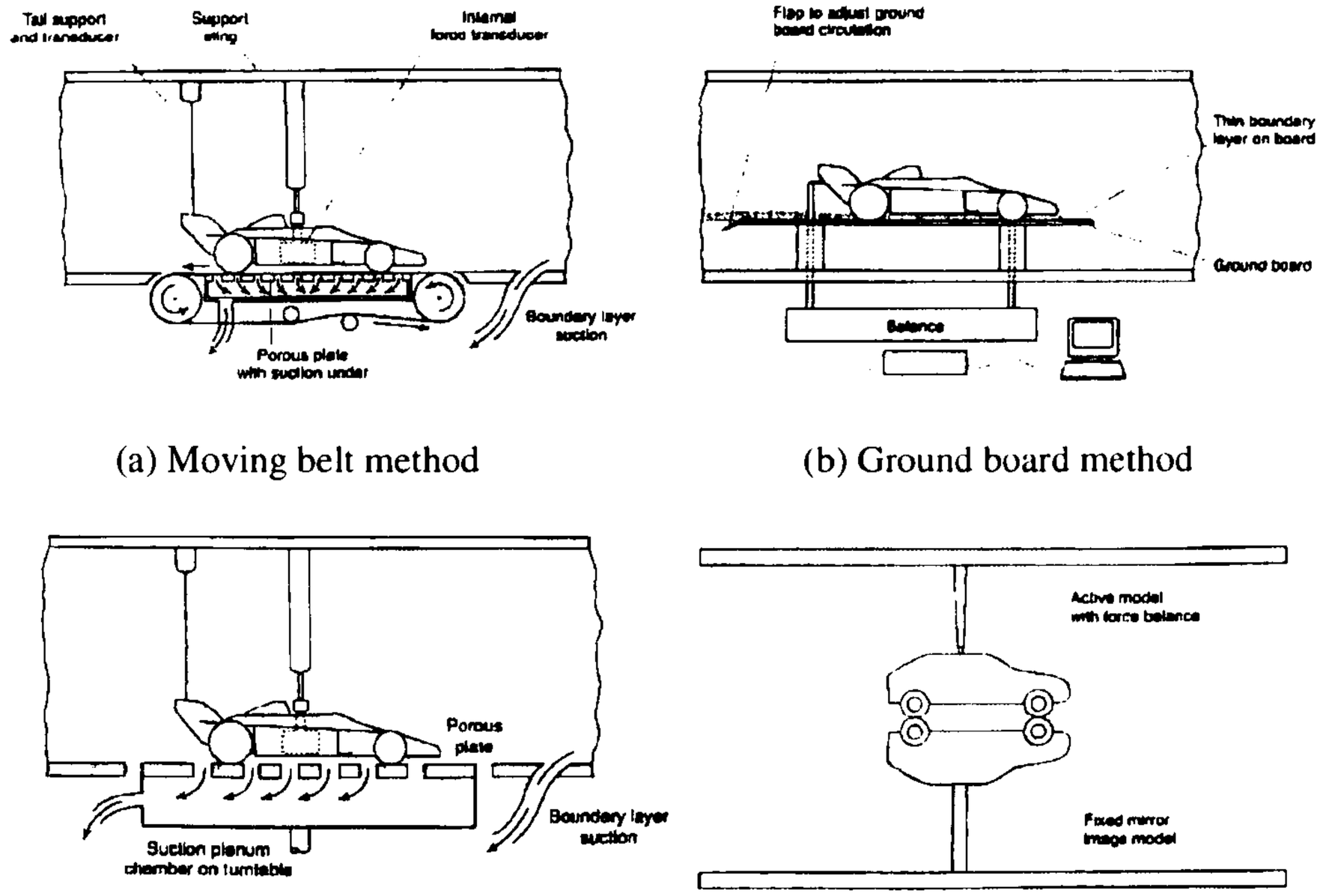

(a) Moving belt method (b) Ground board method

(c) Suction method (d) Mirror image method

Figure 3.4 Boundary layer removal methods (from Barnard 1996)

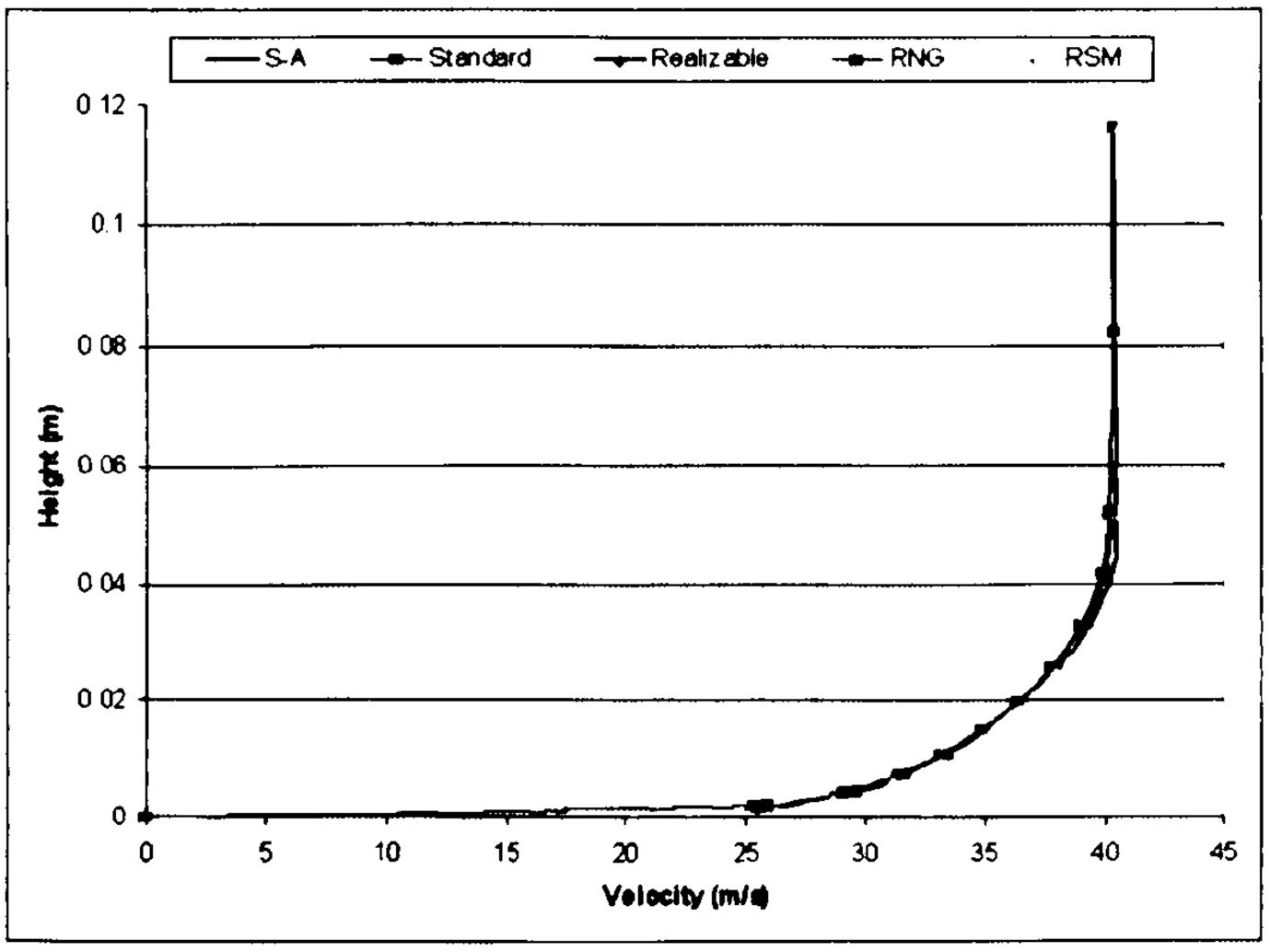

Figure 3.5 Boundary layer simulation using different turbulence models

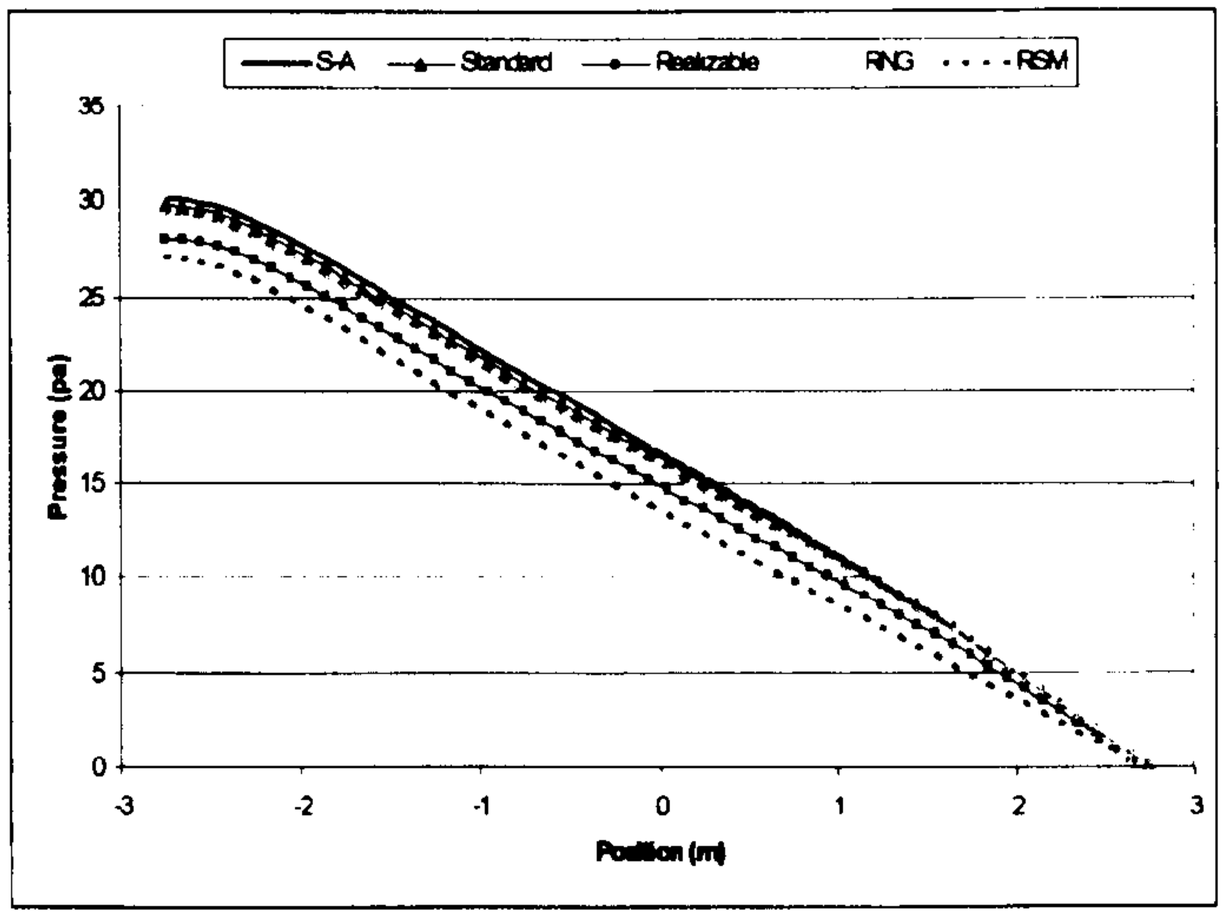

Figure 3.6 Pressure distributions along the working section

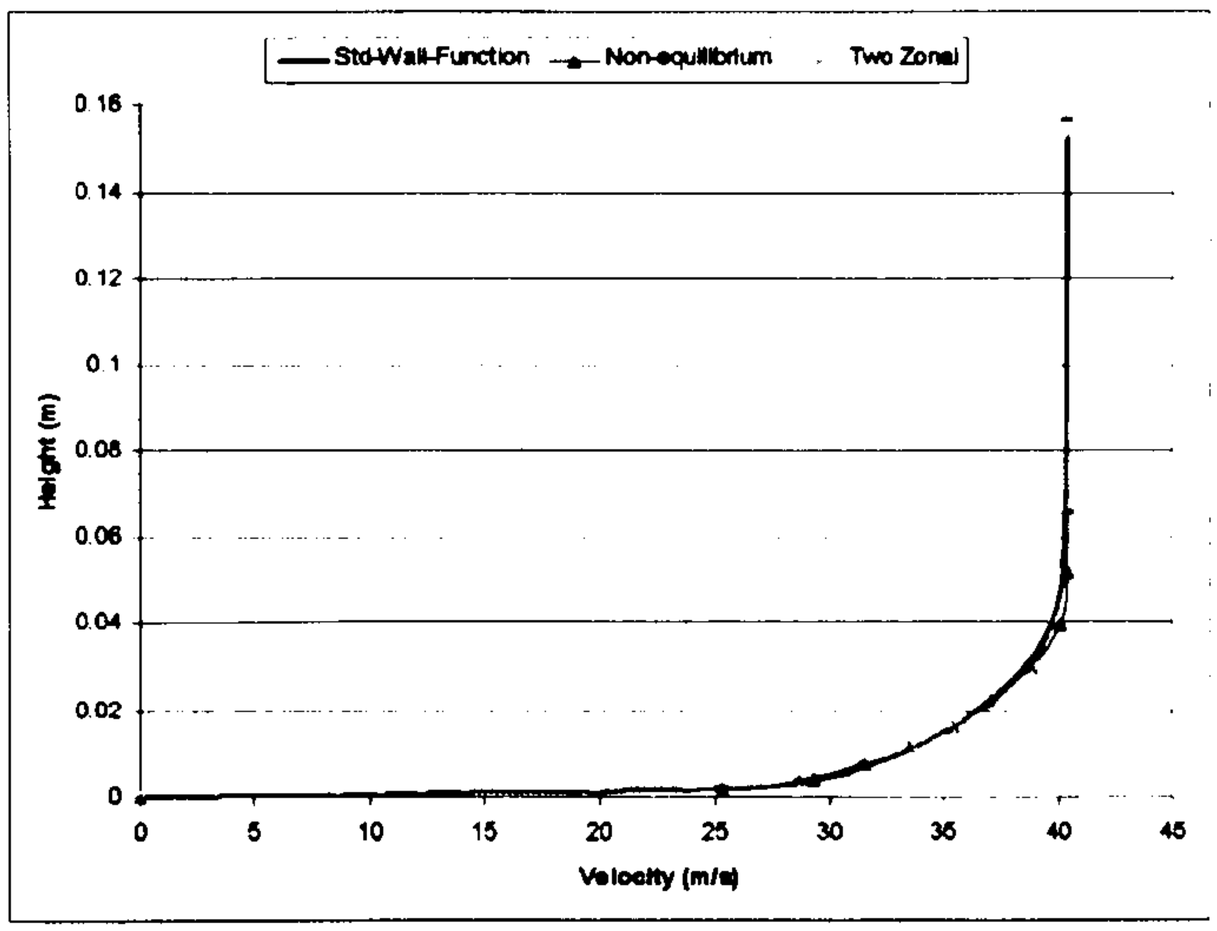

Figure 3.7 Boundary layer simulations in different near-wall-treatments

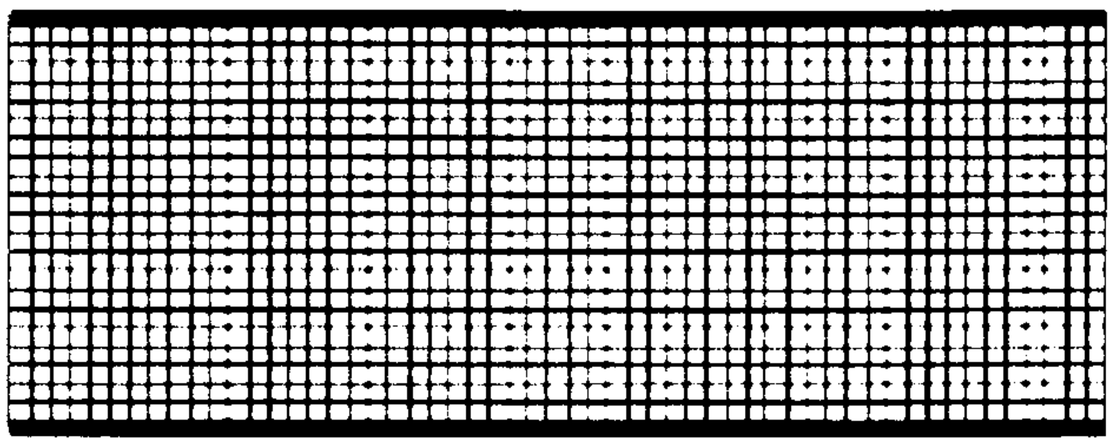

Figure 3.8 Coarse grid with 78,925 elements

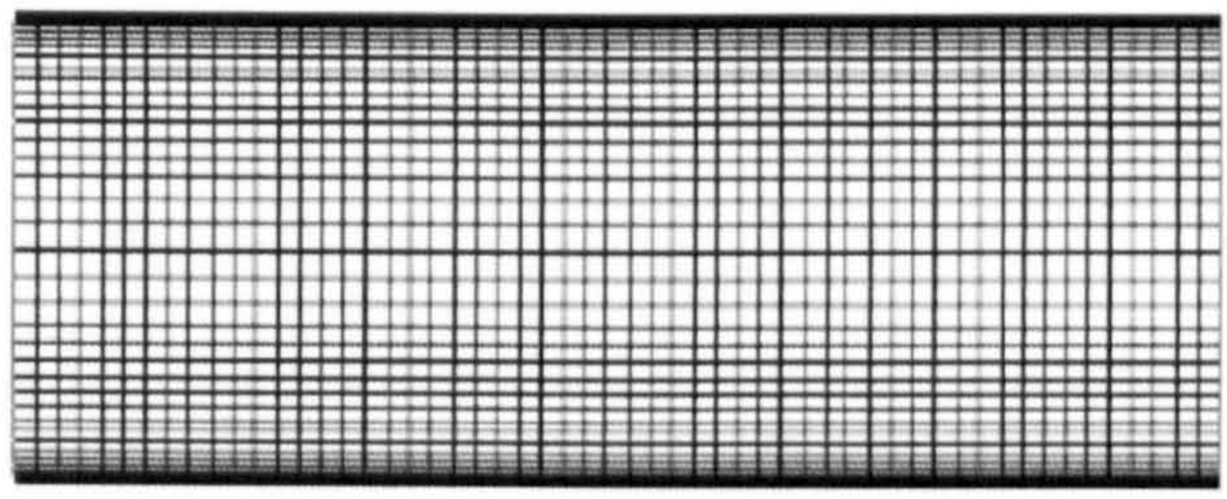

Figure 3.9 Fine grid with 123,750 elements

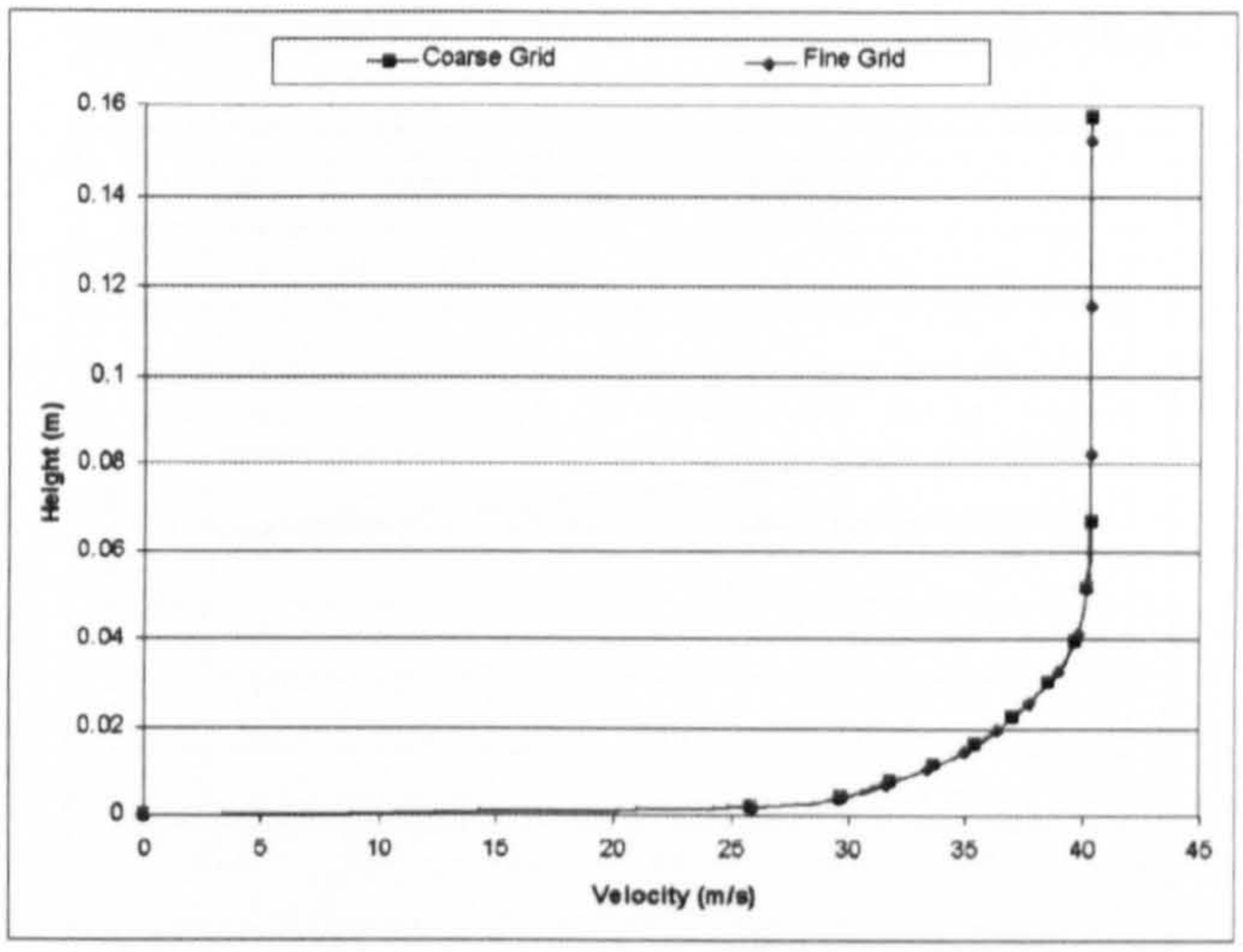

Figure 3.10 Boundary layer simulation with different coarse and fine grid

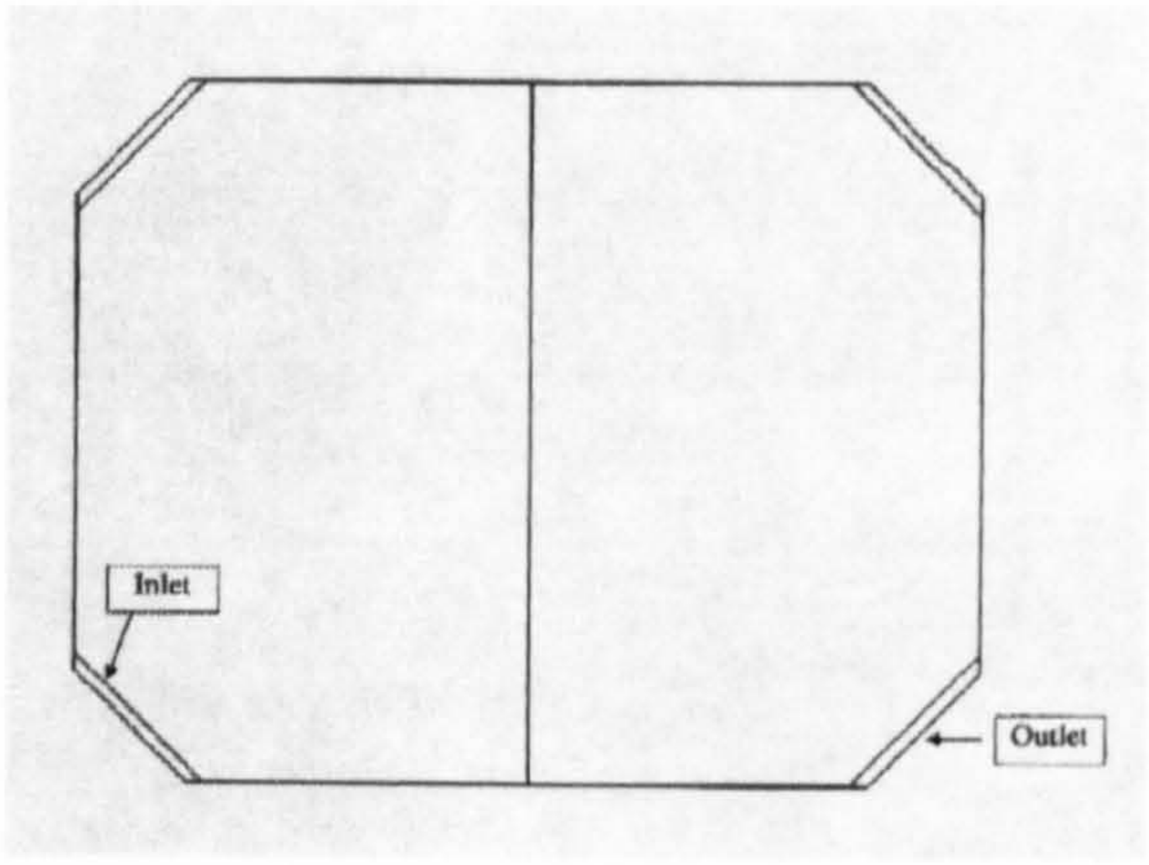

Figure 3.11 Inlet and outlet of the working section with an expansion

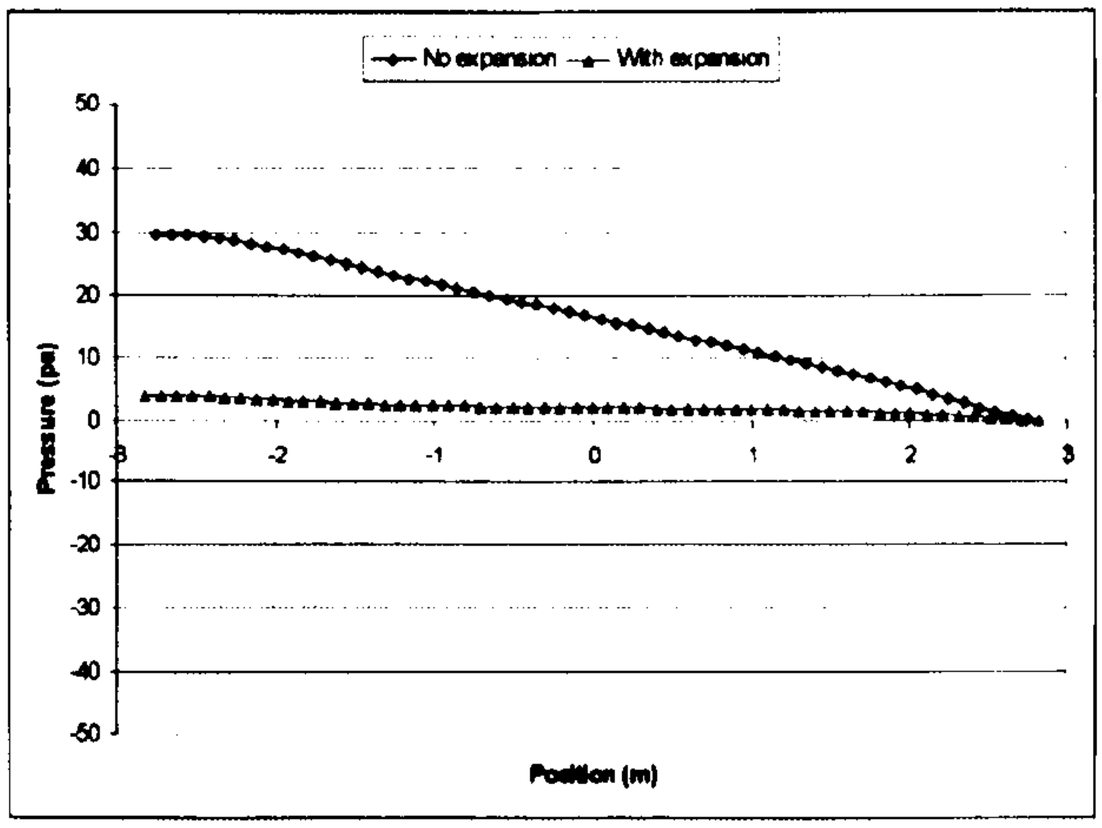

Figure 3.12 Static pressure along the working section with/without an expansion

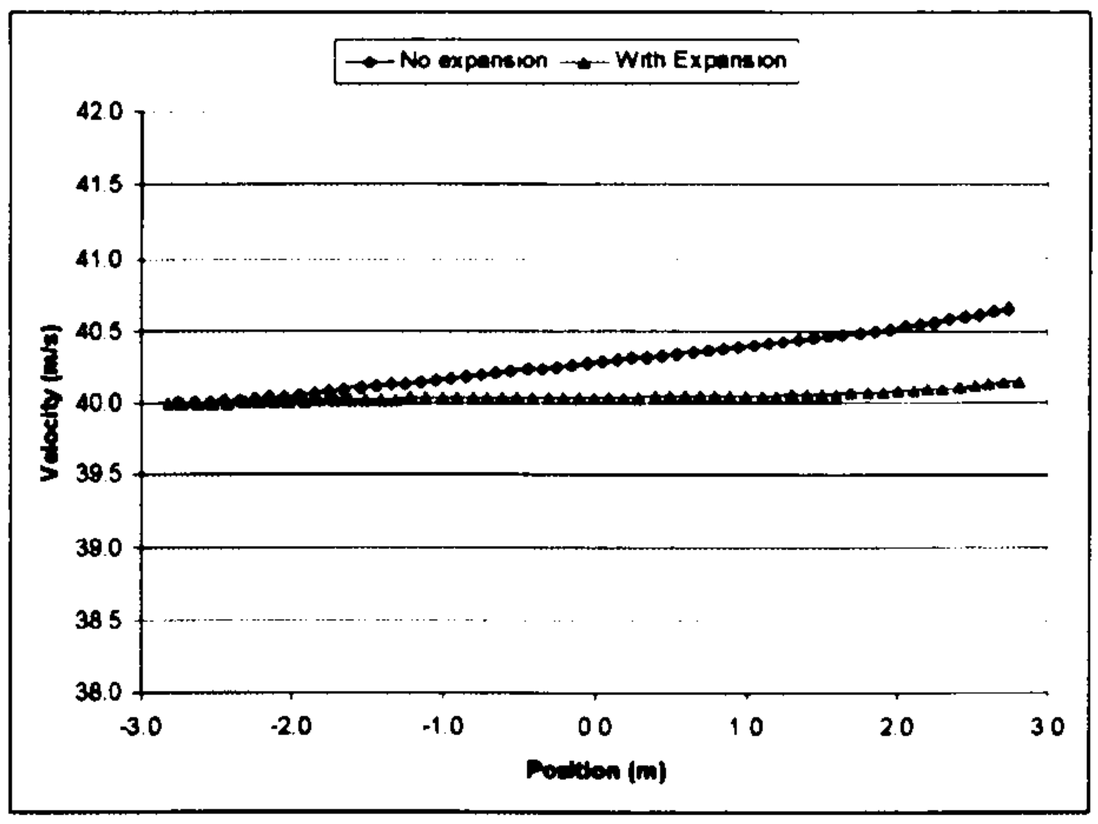

Figure 3.13 Velocity distribution along the central line of working section

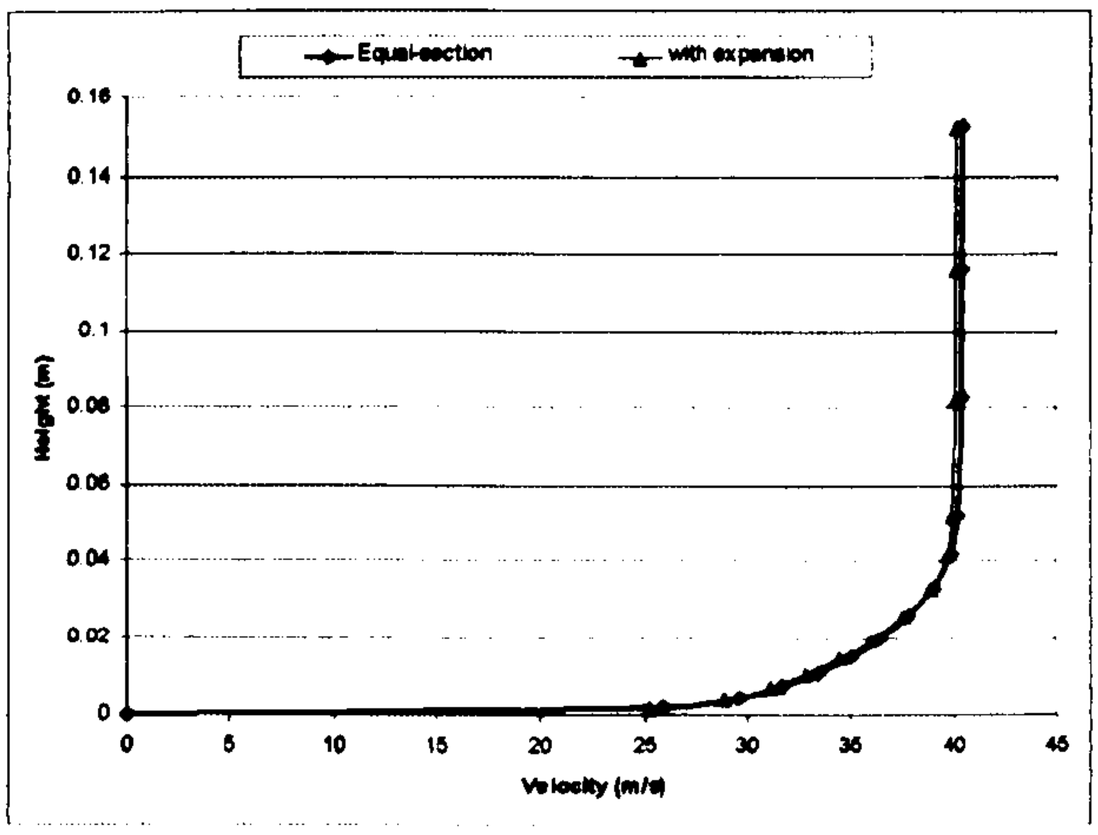

Figure 3.14 Velocity distributions above tunnel floor

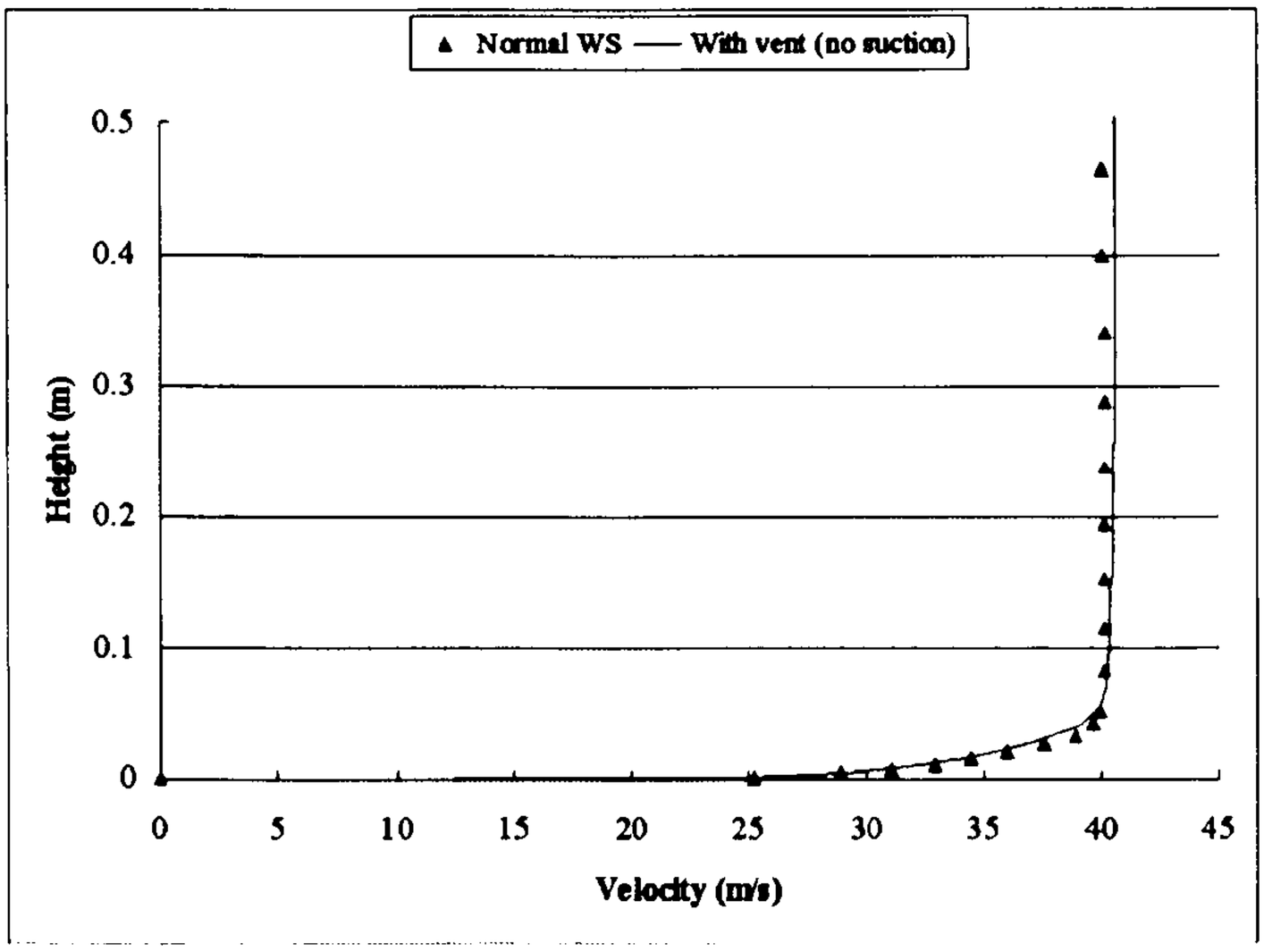

(a) Velocity profile with vent (no suction)

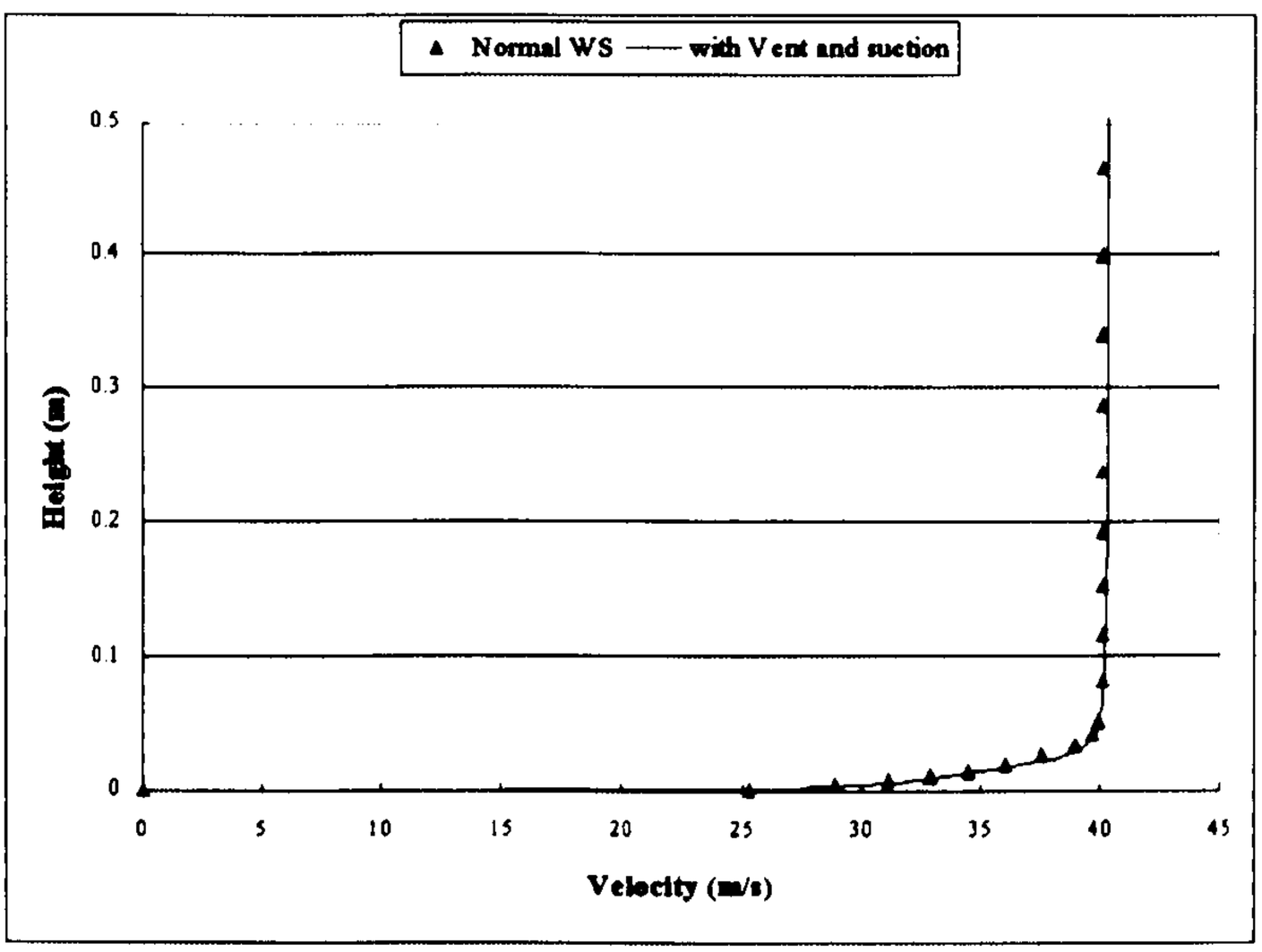

(b) Velocity profile with vent and suction

Figure 3.15 Velocity profiles with vent exit

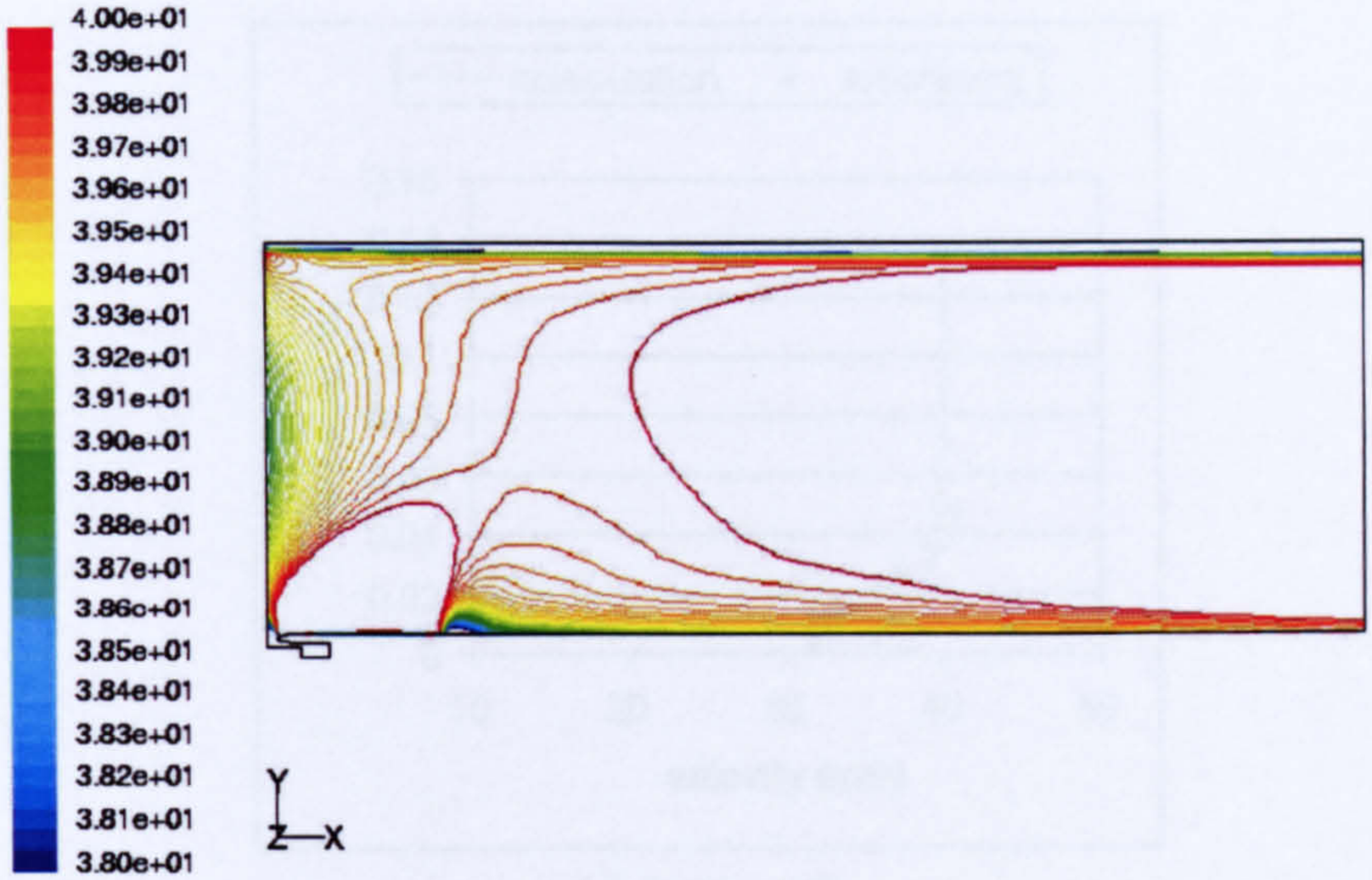

(a) Velocity (m/s)

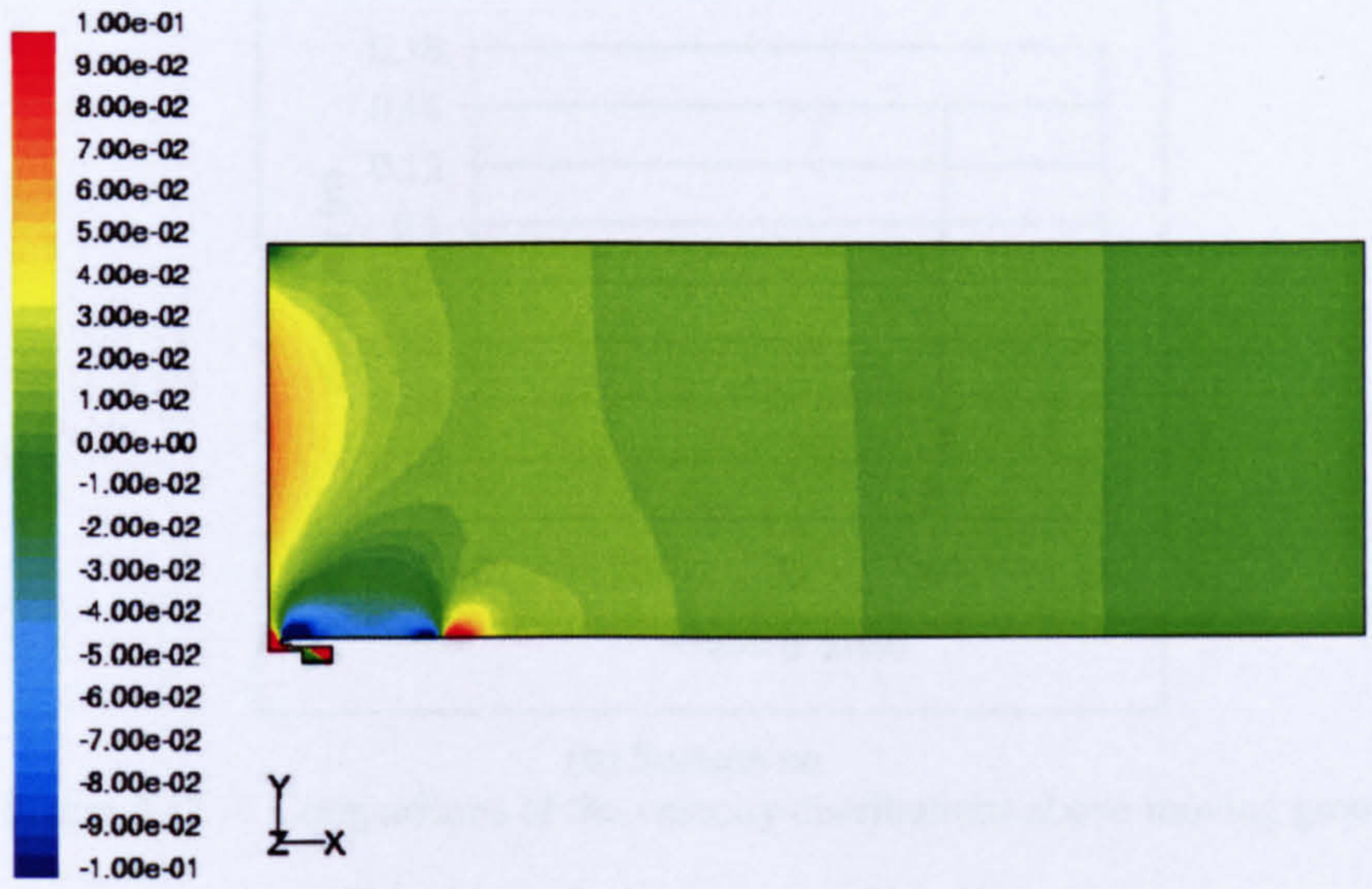

(b) Pressure coefficient

Figure 3.16 Velocity and pressure coefficient contours in the working section

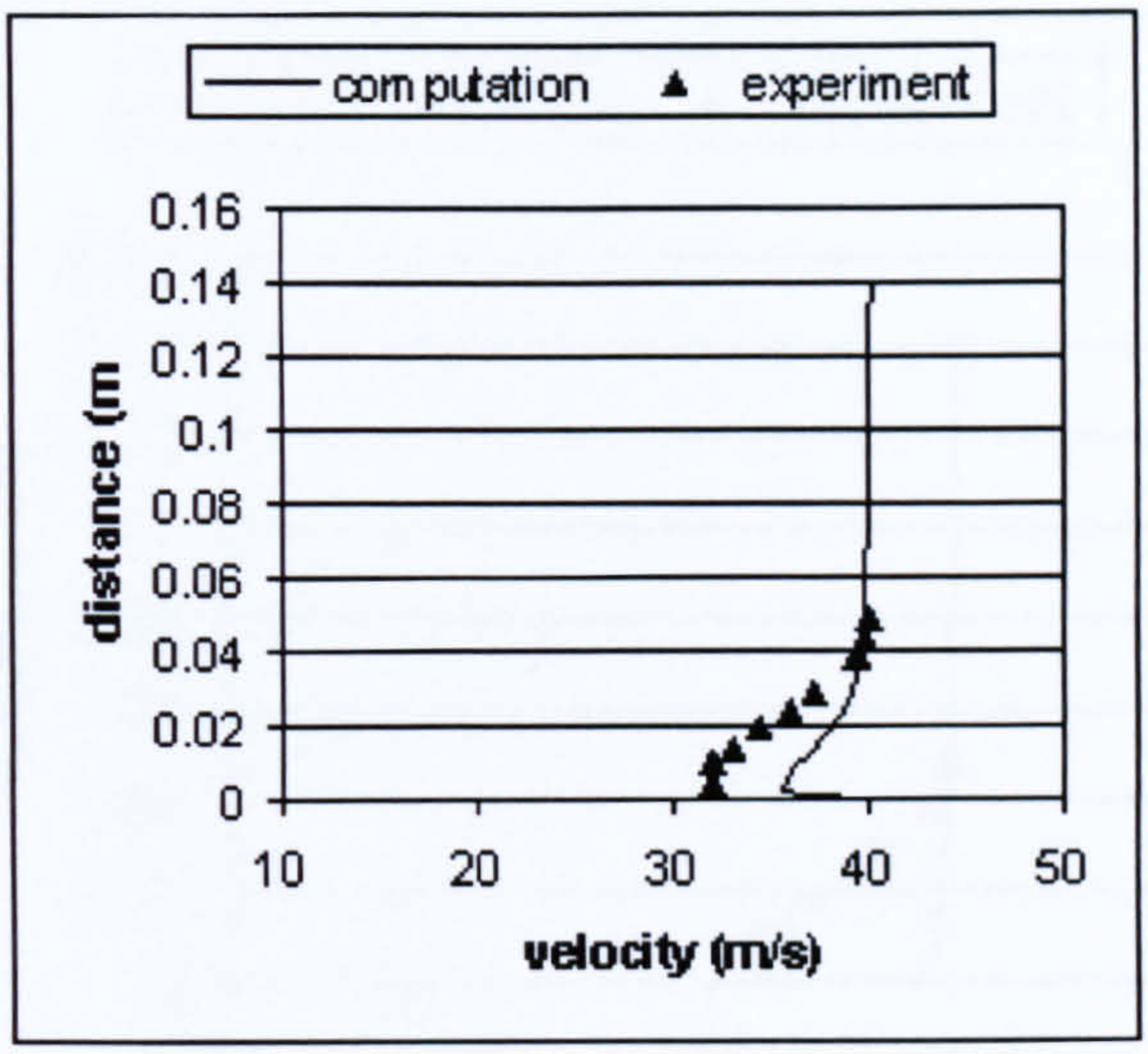

(a) Suction off

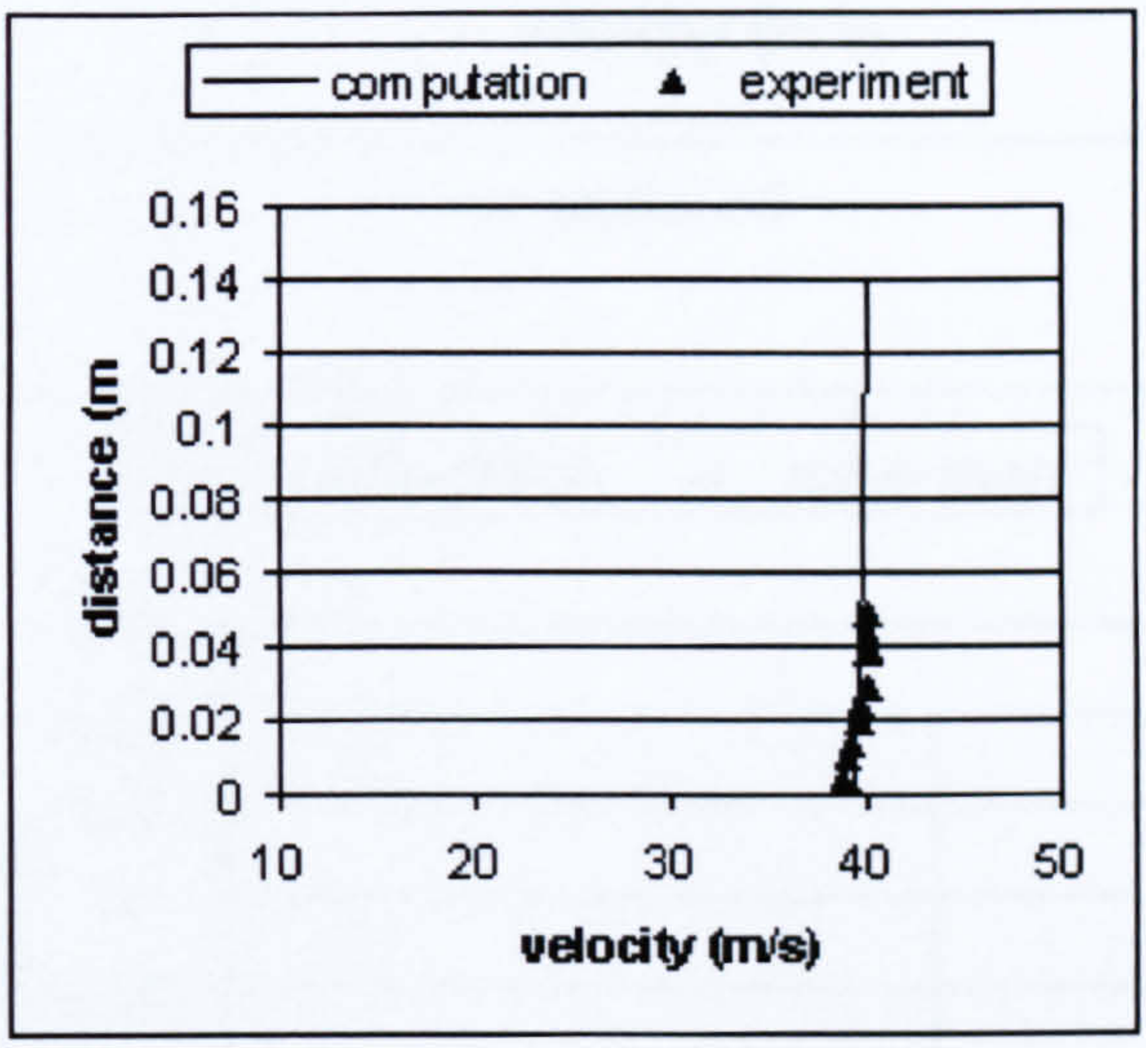

(b) Suction on

Figure 3.17 Comparisons of the velocity distributions above moving ground

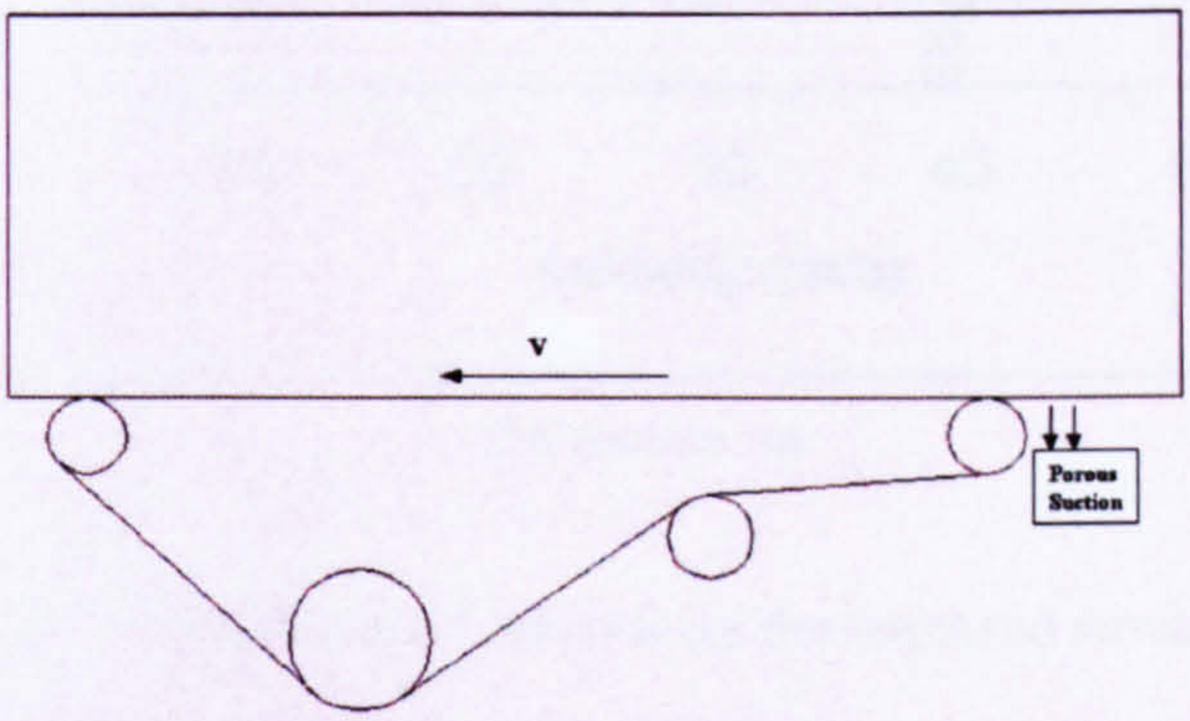

Figure 3.18 Improved moving ground (flush with tunnel floor)

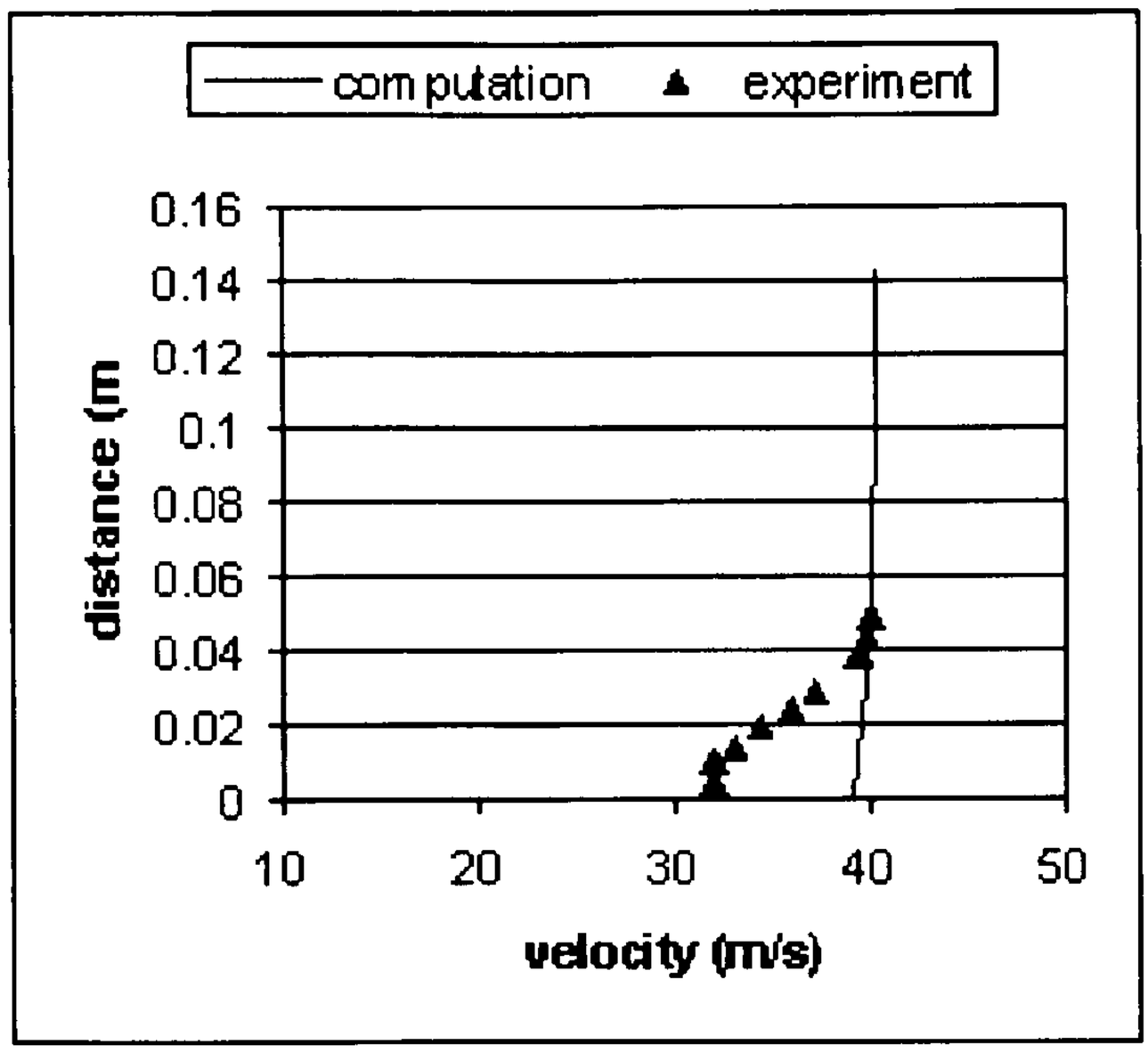

(a) suction off

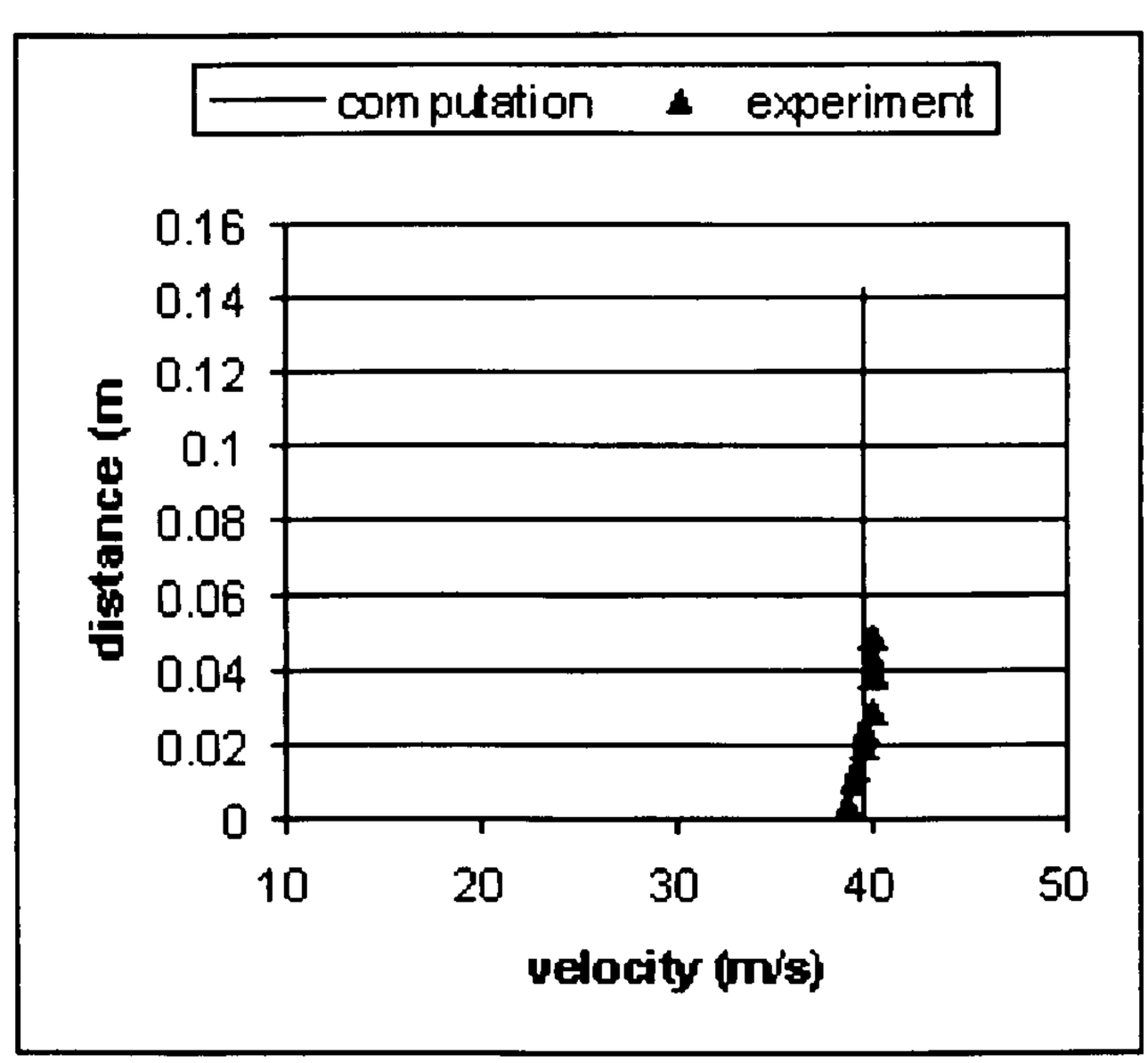

(b) suction on

Figure 3.19 Boundary layer removal for the improved moving ground

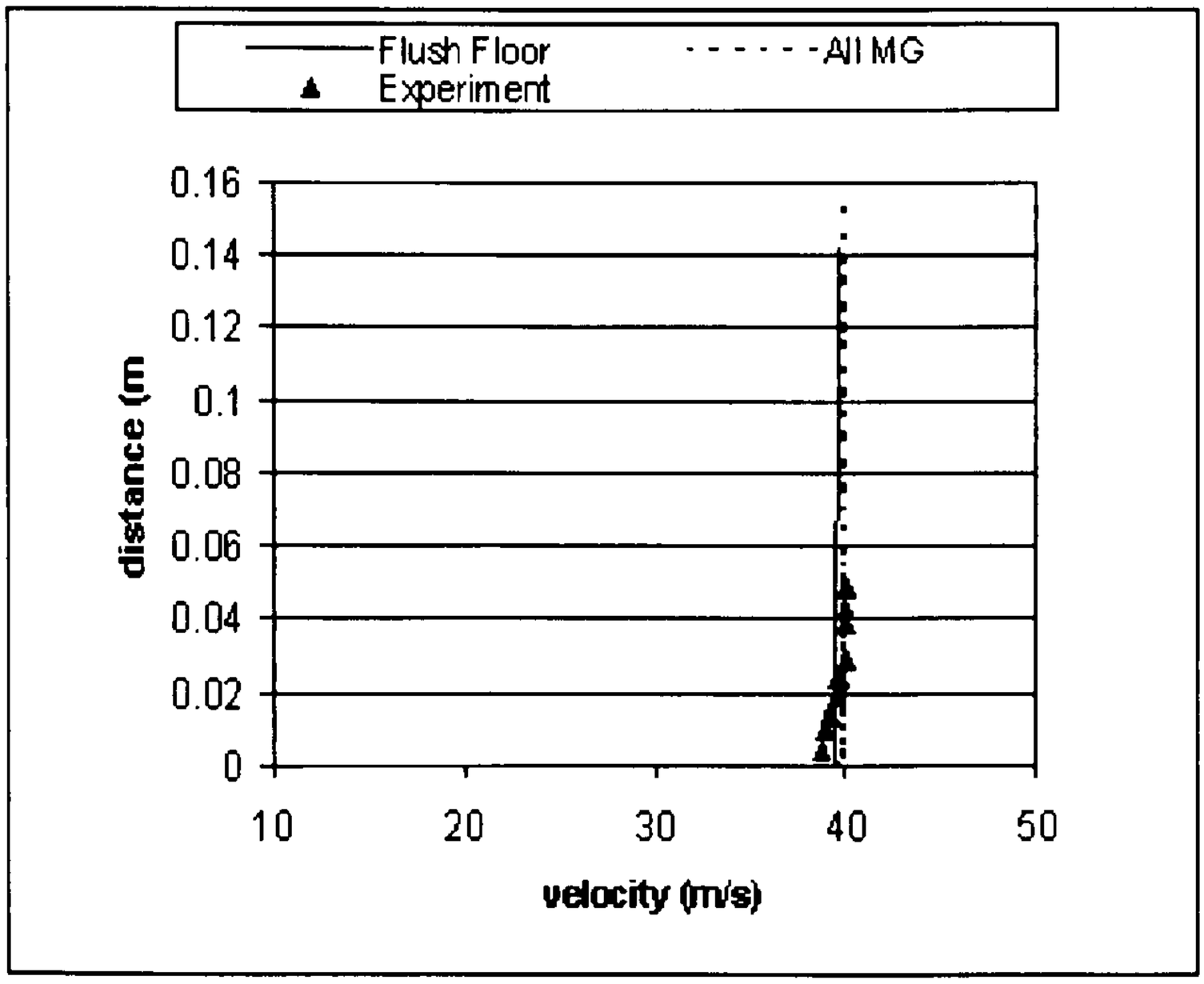

Figure 3.20 The comparison of flush floor, all moving ground and the experiment

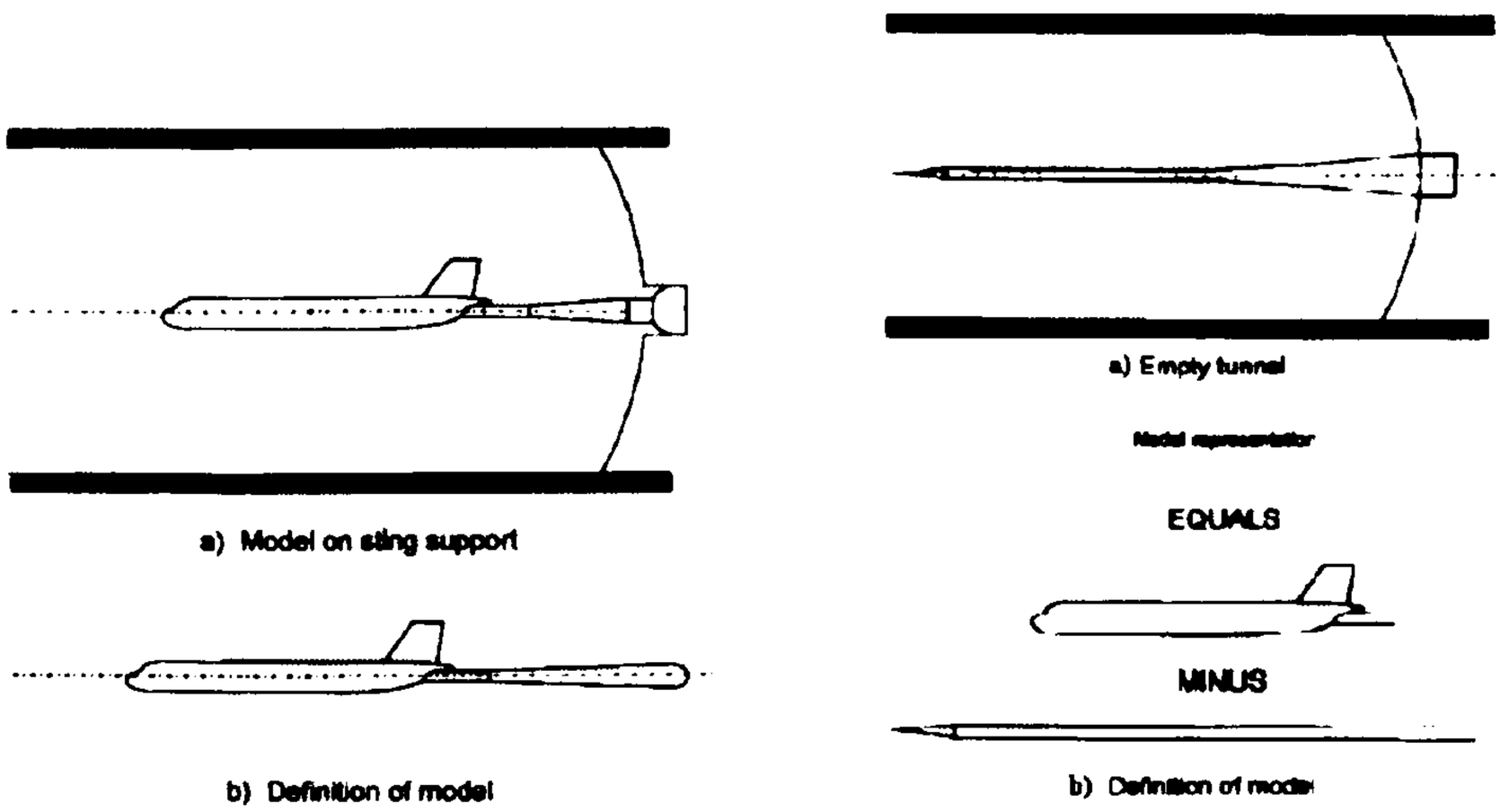

(a) Truly Empty Tunnel (b) Combining empty tunnel

Figure 3.21 "Empty tunnel" calibration (from Ewald 1998)

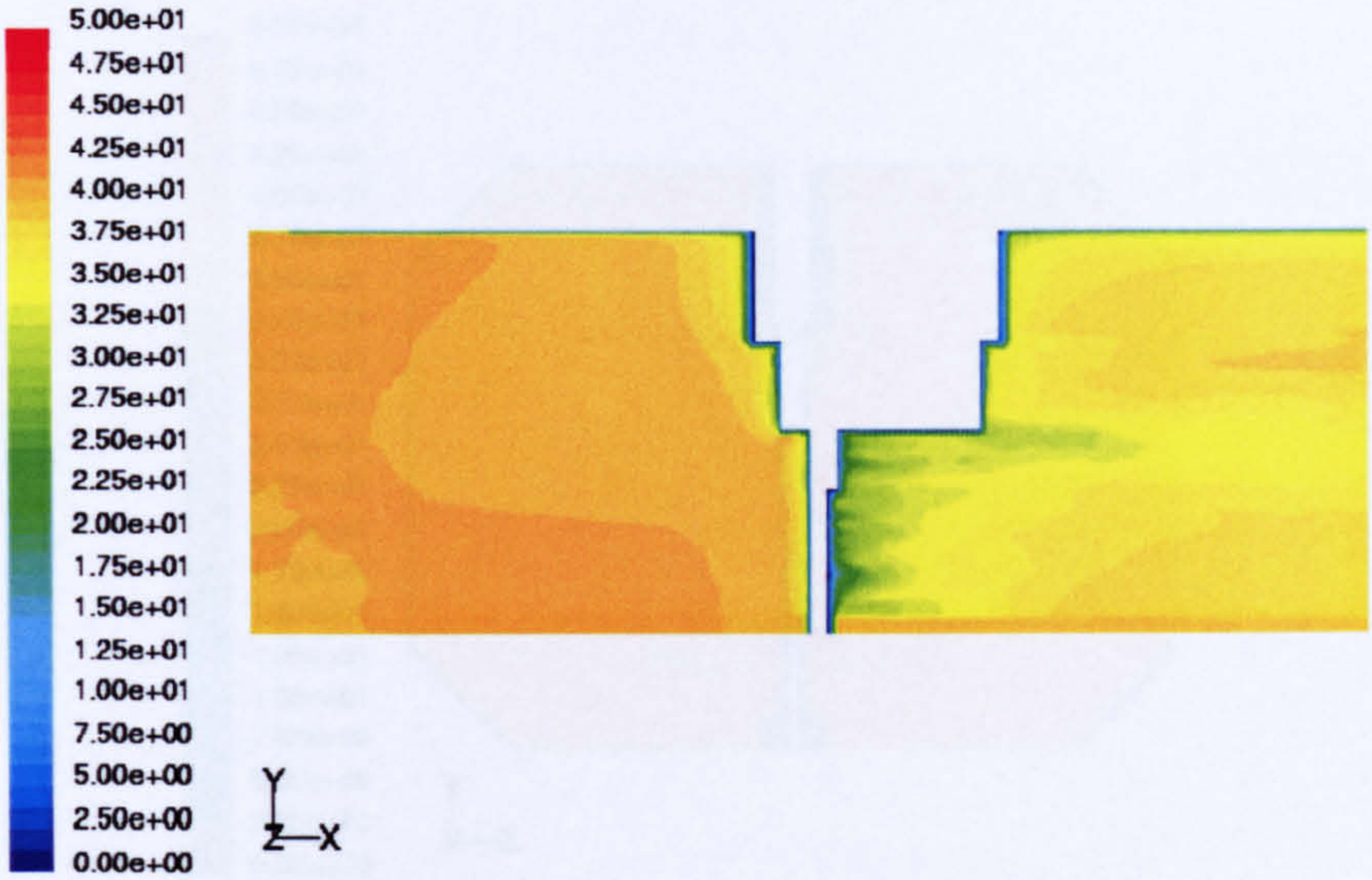

(a) Velocity (m/s)

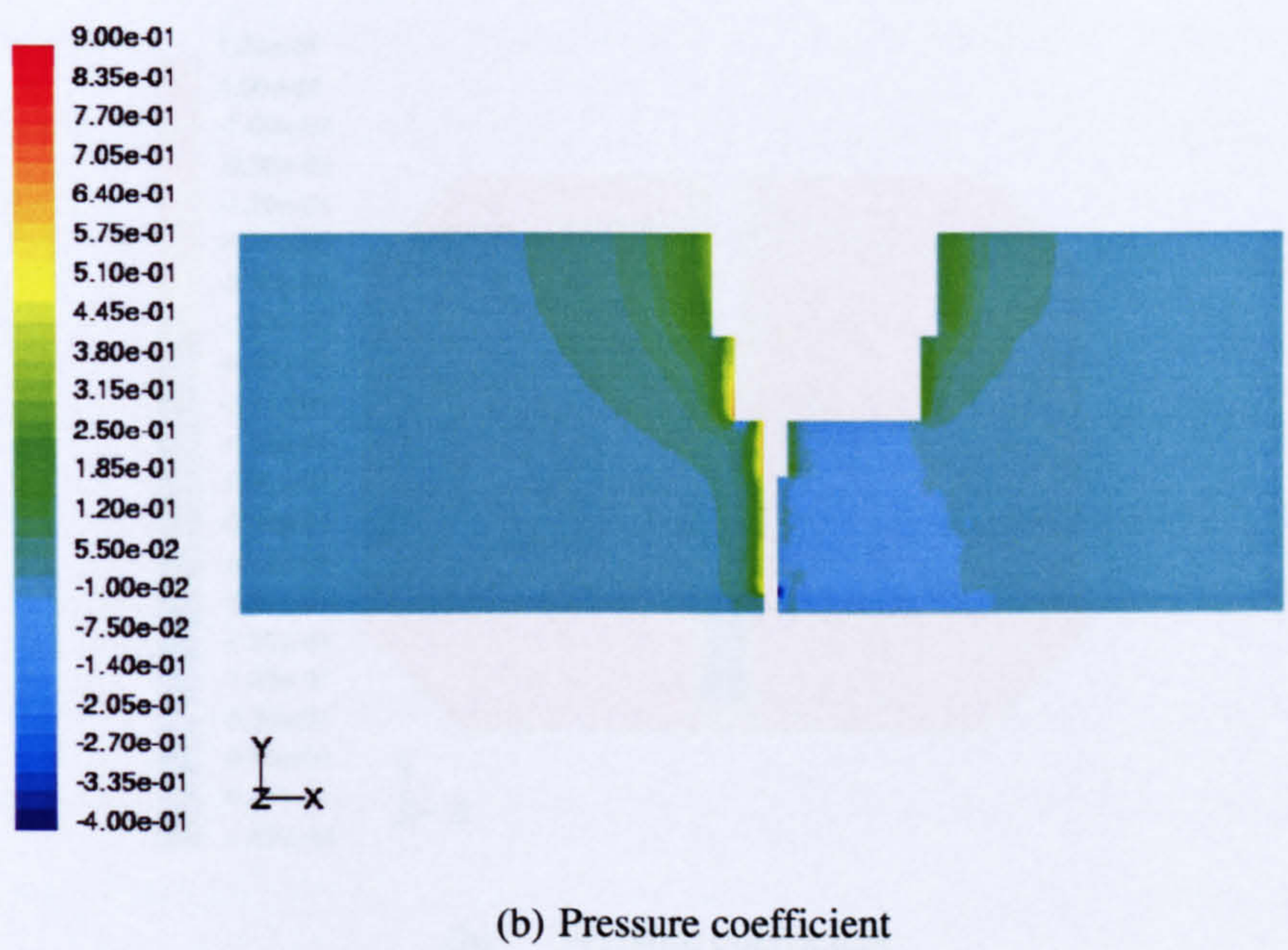

(b) Pressure coefficient

Figure 3.22 Longitudinal distributions in working section with strut

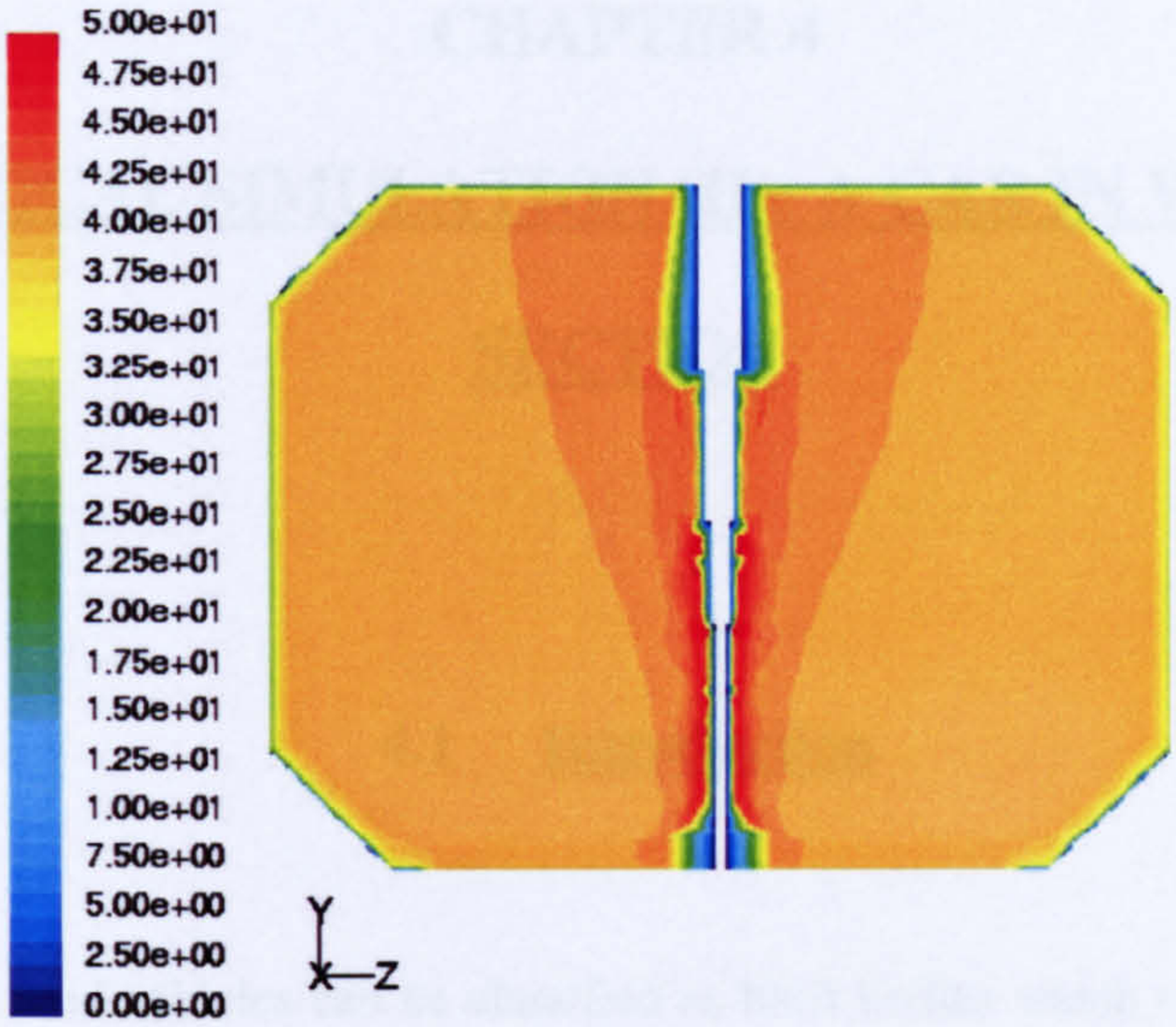

(a) Velocity

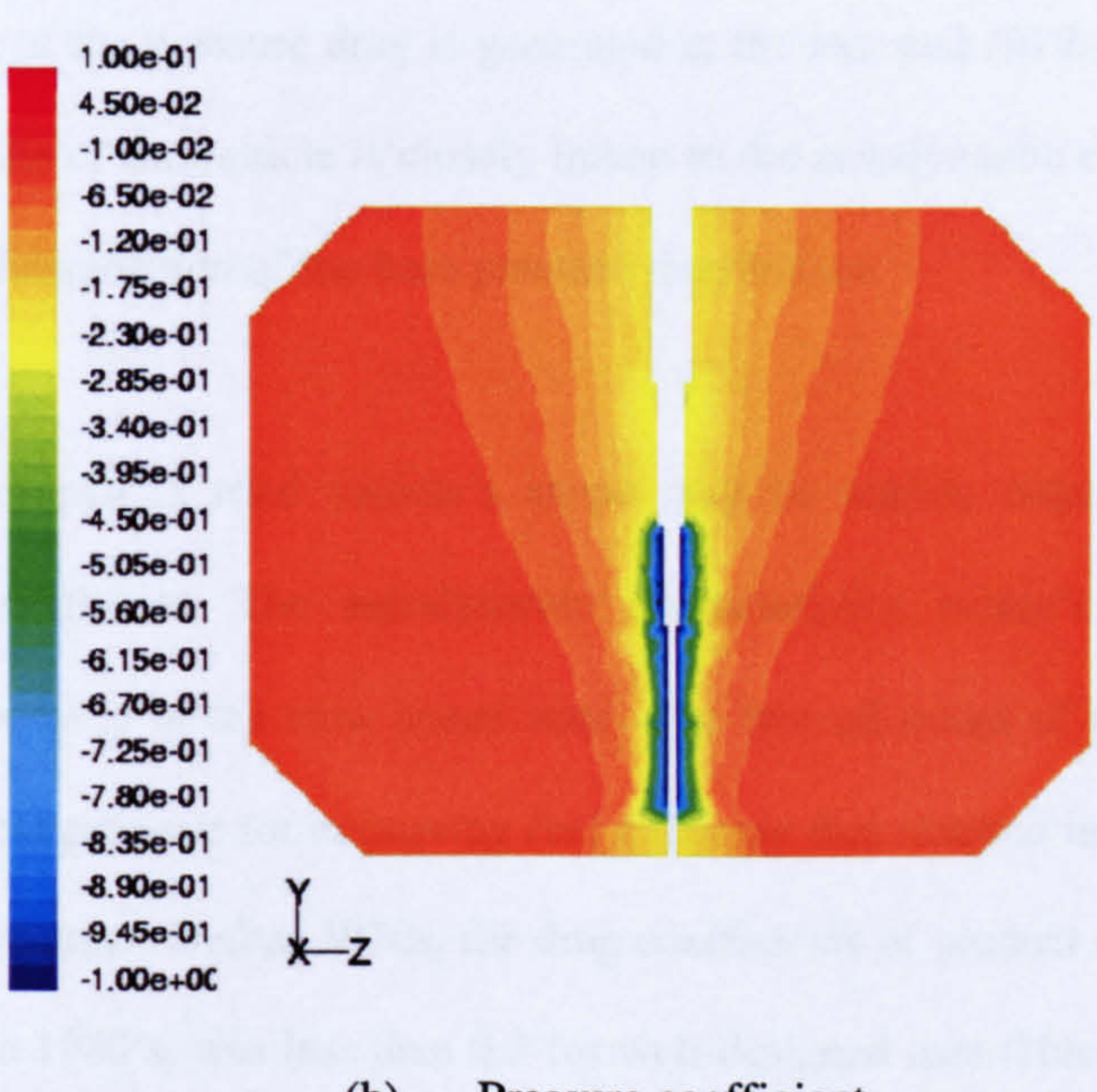

(b) Pressure coefficient

Figure 3.23 Transversal distributions in working section with strut

CHAPTER 4

NUMERICAL SIMULATION (II): A CAR IN WORKING SECTION

4.1 Introduction

As most of the road vehicles can be classified as bluff bodies which move in the ground vicinity, a major contribution to the aerodynamic drag stems from pressure drag created by the low pressure prevalent in the separated flow region base. Ahmed et al (1984) estimated that pressure drag is the dominant components (85%) of the total drag on the car body, and the major part of the pressure drag is generated at the rear end (91%). The kinematics of flow in the wake of the vehicle is closely linked to the aerodynamic drag and governs the magnitude and disposition of the base pressure distribution.

In the medium past, a road vehicle's shape may be mainly determined by function, economy or aesthetics. The aerodynamic characteristics weren't deemed to be so important, especially in the slow speed state. The two oil crises of the 1970s, however, produced a great pressure for improving fuel economy that resulted in the huge interest in vehicle aerodynamics. Before 1970s, the drag coefficients of product cars were about 0.5, but, by the late 1980's, was less than 0.3 for well-designed cars (Hucho & Sovran 1993). In order to reduce the aerodynamic drag of their cars, the main manufacturers built wind tunnels and spent much time in testing.

For some special vehicles, such as Formula One race cars and solar powered vehicles, aerodynamic characteristics are far more important than for production cars. Formula One runs at high speed and the aerodynamic lift and drag may be the vital determined factor to win the race. Even a little improvement in aerodynamic performance could produce winner. Sawley et al (1997) reported Sauber Petronas Engineering AG spent 33 weeks of wind tunnel testing each year.

Solar cars are powered using solar energy. The flux intensity of this energy forces designers to seek extreme low drag configurations. Ozawa et al (1998) reported that Honda "Dream" solar race car ('96 model) had a very low drag coefficient of 0.101. The car won the World Solar Challenge race for a distance of 3,010km at the average speed of 89.76km/h in Australia (1996).

Originally, much of the research on vehicle aerodynamics was restricted to the force and moment studies and the pressure evaluations in the wind tunnel testing of road vehicles. The generality of these results was often narrowed down due to the specialized project oriented geometries investigated. But still a few flow field measurements were available which could serve as a basis for modelling the flow around vehicles or to gain insight into the drag creating mechanisms at work in the flow field.

Ahmed (1981) made a wide measurement of wake structure for three typical automobile shapes: Estate (Squareback), Fastback and Notchback. A nine-hole probe was used to conduct the measurements of the wake structure. Further more, in 1983 he systematically measured the wake structure and the drag, and the influence of the base slant.

The high cost and long period of wind tunnel testing forced researchers to look for better development tools. Fortunately, CFD happened to be the developing tool, thanks to the advances in computer capabilities and numerical techniques. As early as 1989, Han used an incompressible RANS method, including a k-ε turbulence model, to simulate the flow about Ahmed's vehicle-like body (Figure 4.1). For the Ahmed-type bluff body, its forebody had rounded edges whereas the center section and afterbody had sharp edges. The slant angle θ of the afterbody could be varied and the flow as well as the drag was strongly influenced by this angle. All afterbody configurations have the same base slant length of 0.222 m. The total drag coefficient (based on frontal area) was predicted to be 0.33 (Han 1989) for a slant angle of 0^0, whereas the experimental value was 0.272 (Ahmed 1983). Han pointed out the source of this problem may have been the k- turbulence model which failed to respond properly to the adverse pressure gradients on the afterbody. But, as shown in Figure 4.2, the incremental change of the total drag coefficient, with slant angle, was shown to have good agreement with experiment, especially for the slant angles less than or equal to 20^0. The simulations, however, failed to predict the rapid increase in drag beyond this slant angle together with the breakdown of the vortex system combined with a sharp drop in drag at 30^0. At $\theta=30^0$, the wake of the bluff body is in an unstable condition, where the stable low-drag condition (the black symbol) may be destroyed by a small disturbance leading to an unstable high-drag flow condition (the cycle symbol).

Han et al. (1996) studied the aerodynamic characteristics of three simplified vehicle models: a square-back (S-B) configuration, a fastback (F-B) configuration, and a fastback boat-tail ramp (F-B-R) configuration. Two turbulence models were used: the standard κ-ε and the RNG κ-ε turbulence model. From the numerical results, the RNG model gave slightly better drag predictions. He concluded CFD simulations might not be able to accurately predict the aerodynamic properties of very different vehicle shapes, they were

able to track, with acceptable engineering accuracy (less than 4% error of relative drag), relative changes in drag between the three models

Grun (1996) developed a zonal approach to simulate exterior aerodynamics for road vehicles. The method incorporated two components for the inviscid and viscous domains of the flow field at high Reynolds numbers. For the inviscid part of the flow field, a first order panel method was used, which also accounted for the simulation of separated flow downstream incorporating the vehicle's free shear layers. For the viscous part of flow field, a 3D integral boundary layer method was used. As a result, the approach required only a discretisation of the vehicle's surface, therefore, reduced the turnaround time greatly.

Barasa (2000) stressed the utilization of the second moment closure (SMC) in automotive industry. He investigated the exterior flows, car heat, vent, and air-conditioning (HVAC) and the flows inside engine. His results indicated that SMC was better than most of two-equation turbulence models; especially for complicated flows around road vehicles.

In his review paper, Dhaubhadel (1996) summarised the CFD applications in automotive industry. He pointed out that CFD had emerged as a powerful tool for predicting flow and thermal distributions in vehicle systems. Also the proper applications of CFD would decrease the dependence on wind tunnel test, and so, reduce the cost and cycle time of design.

In order to escape the problem of computation convergence, Perzon et al (2000a, b) used CFD to investigate the transient flow around vehicles, which benefited in numerical stability and modelling physics. For the transient flows, there is always a solution to the

problem; and also, there is one less assumption made just because the flows around road vehicles are inherently unsteady.

Beccaria et al (1999) reported that the HIPEROAD project had integrated the design and development environment for optimizing car aerodynamics and other features, which resulted in a reduction of car development time, i.e. a full optimization cycle was performed on a workstation cluster in O(10) hours, and so rapidly provided feedback to the styling group, compared to more than 10 days using the traditional methods.

4.2 Numerical Simulation of a Car in Free Air

The considered numerical simulation of a car in free air used boundaries of a virtual tunnel of 10×5×5m for the half model (symmetrical model), which had a cross section of $25m^2$. For the 30% model, the solid blockage was 0.705%, and blockage 2.82% for the 60% model. In the numerical simulations, it is normally desirable that the modelling should not be subjected to any blockage corrections. Figure 4.3 and 4.4 are the velocity and pressure coefficient contours of 30% and 60% model, respectively. From the figures, the 30% scale model has a small wake, and the reattached flows are formed very quickly behind the car, while for the 60% scale model, the wake is much larger. There are obvious differences between the wakes of 30% and 60% scale models.

Figure 4.5 and 4.6 give the flow streamlines over the car. The ribbons behind the 30% model are not so complicated as that of 60% model. In the wake of 30% model, few vortices are formed, but for 60% model, the ribbons in the wake become much more complicated.

Figure 4.7 shows little change of drag coefficients from 30% to 60% model, even although their wake structures are very different (compare Figure 4.5 and 4.6).

4.3 Numerical Simulation of a Car in Working Section

4.3.1 Grid

In this research, three grids were used for the comparisons of the influence of grid quality for the numerical simulation of the flowfield of car in the working section, they were the unstructured grid, the multi-block grid and the hybrid grid, respectively. Most numerical computations were conducted on the hybrid grids.

Unstructured grid:

This was generated by filling the unstructured tetrahedral grid in all computational regions. To generate high quality unstructured grid, a fine grid is usually generated in the region of complicated flows, while other region can be filled with coarse grid. For this case, near the car and the strut, fine grids were generated, but near the tunnel walls, they were coarse. Therefore, the boundary layers on the tunnel walls can not be simulated properly due to insufficient nodes in that region. The grid is shown in Figure 4.8a. The relative coarse grids can be seen underbody. Of course, we can use very fine grid underbody, but it's not a good choice obviously, since it will cause some problems in generating grids sometimes.

Multi-block grid:

For the multi-block grids, the computational region was first split into several sub-regions. In the regular sub-regions, the structured grids were generated, while the other sub-regions were filled with unstructured grids. Generally, the grids were of high fidelity, but were very time-consuming to generate. The grids are shown in Figure 4.8b.

Hybrid grid:

For hybrid grid, prisms with high aspect ratio were generated near the walls, while unstructured grids fill the remaining regions. Generally, the grids are straightforward to generate. The potential advantages are the geometrical flexibility and grid adaptation. The grid is shown in Figure 4.8c.

4.3.2 A Car in Working Section (no Strut)

One advantage of CFD simulation over the wind tunnel testing is the car can be modelled in the wind tunnel without the support system, therefore, to eliminate the influence of the support system.

Figure 4.9 illustrates the difference in the case of 30% scale for two different grids. The case of unstructured grid results in a very thick boundary layer on the tunnel walls, see Figure 4.9(a) and 4.9(e). For the hybrid grid, no such layer was produced, see Figure 4.9(b) and 4.9(f). From the velocity and pressure coefficient contours, it can be seen that the thick boundary layers caused by the grid have a significant effect on the flow field

after the center of car. The thick boundary layer blocks the flow passage and tends to suppress the wake development both in the cases of 30% scale and 60% scale models, also see figure 4.10. But in both cases of 30% and 60% car model, the different grids seem to have little effect on the upstream flows.

The wakes of different scale models show significant differences since the Reynolds number is different (all numerical simulations were conducted at the airspeed of 40m/s). Figure 4.11 show the velocity vectors in the symmetrical plan behind the car. Obviously, the wake of 60% scale model is much larger than that of 30% scale model.

Figure 4.12 show the velocity vectors in the transverse plane behind the car. For the 30% scale model, the wake at xb=470mm behind the car is greatly diminished in intensity (Figure 4.12b). For 60% scale model, however, even at the xb=1040mm behind the car, the wake is still visible (Figure 4.12f).

4.3.3 A Car in Working Section (with Strut)

The case of a car in the working section with the strut support system is presented here. The case models the wind tunnel testing. Figure 4.13 and 4.14 show the velocity and pressure coefficient contours of 30% and 60% scale models in the tunnel. The contours show that the strut has significant effect on the velocity distribution, compared to Figure 4.9 and 4.10, while strut influencing the aerodynamics of car will be shown in the next section.

4.4 Analysis of Numerical Simulation

4.4.1 Strut and Tunnel Wall Interference on Drag

Figure 4.15 shows the drag coefficient comparison for the cases with the car in free air, car in tunnel (no strut) and a car in tunnel with the support system. It's interesting to note how the drag coefficient changes with regard to the model size. Generally, it may be seen that the drag coefficient of 30% scale model shows good agreement between the car in free air and the car in the tunnel, but with no strut.

The figure shows the effect of the strut is significant. The drag coefficient with strut is larger than the case without strut. The difference is almost kept the same without regard to the model size (up to 60% model), indicating that a possible interference correction could be generated/developed.

4.4.2 Effect of Strut Position on Drag and Lift

For wind tunnel testing, there are several model supporting systems. Niewald et al (2000) outlined three conventional support systems used in aeronautic tunnel testing, see Figure 4.16 giving the support system: wing-tip, sting and strut. Every support system has their advantages and disadvantages.

The wind tunnel testing of road vehicles, however, is quite different from the conventional aeronautic wind tunnel testing, since the road vehicle testing needs the road modelling facilities, such as the moving belt system. In the Argyll Wind Tunnel, a moving belt system is used and for the safety of test, a very strong support is required. The strut in the

above wind tunnel is shown in Figure 4.17 (the model support method in the working section is also sketched in Figure 3.2).

From the numerical simulation, it's interesting to notice that the strut position has significant effect on both the drag and lift, see Figure 4.18. The drag coefficient can vary from –14% to 3% due to the strut position, compared to the normal support.

4.4.3 Effect of Ground Clearances

The road vehicles usually run in very close proximity to the ground, so the ground effect may be very important. Figure 4.19 shows the drag and lift coefficients against the clearance height, both with and without moving ground.

From Figure 4.19, it can be seen the moving ground has significant effect only when the clearance height is smaller than 0.05m, while the scaled clearance is 0.076m, which is used for aerodynamic computation of the car model elsewhere. The moving ground has different effect on the drag and lift, i.e. drag is decreased and the lift is increased.

4.5 Concluding Remarks

- The significant wall interference on the flowfield suppresses the wake structure, especially for the big model. The car in free air has a much larger wake structure than that in working section.

- The strut has the obvious effect on the vehicle aerodynamics, not only blocking the passage area of the flow, but also changing the flow pattern. The significant feature of the effect of the strut position on the drag and lift coefficient is also presented numerically. This may guide the strut installation in order to reduce its effect.

Figures of Chapter 4

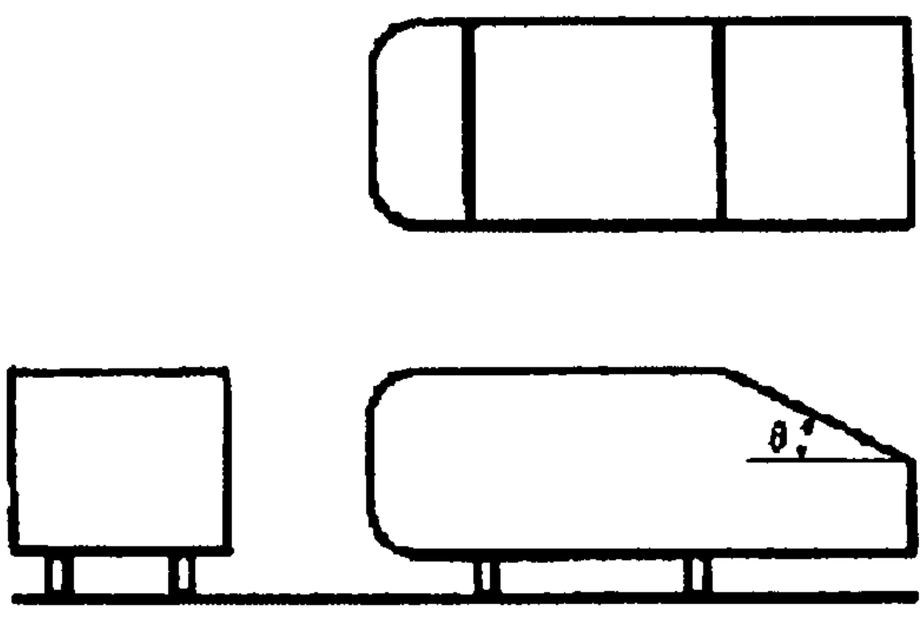

Figure 4.1 Ahmed's Automotive-like Bluff Body (from van Dam 1999)

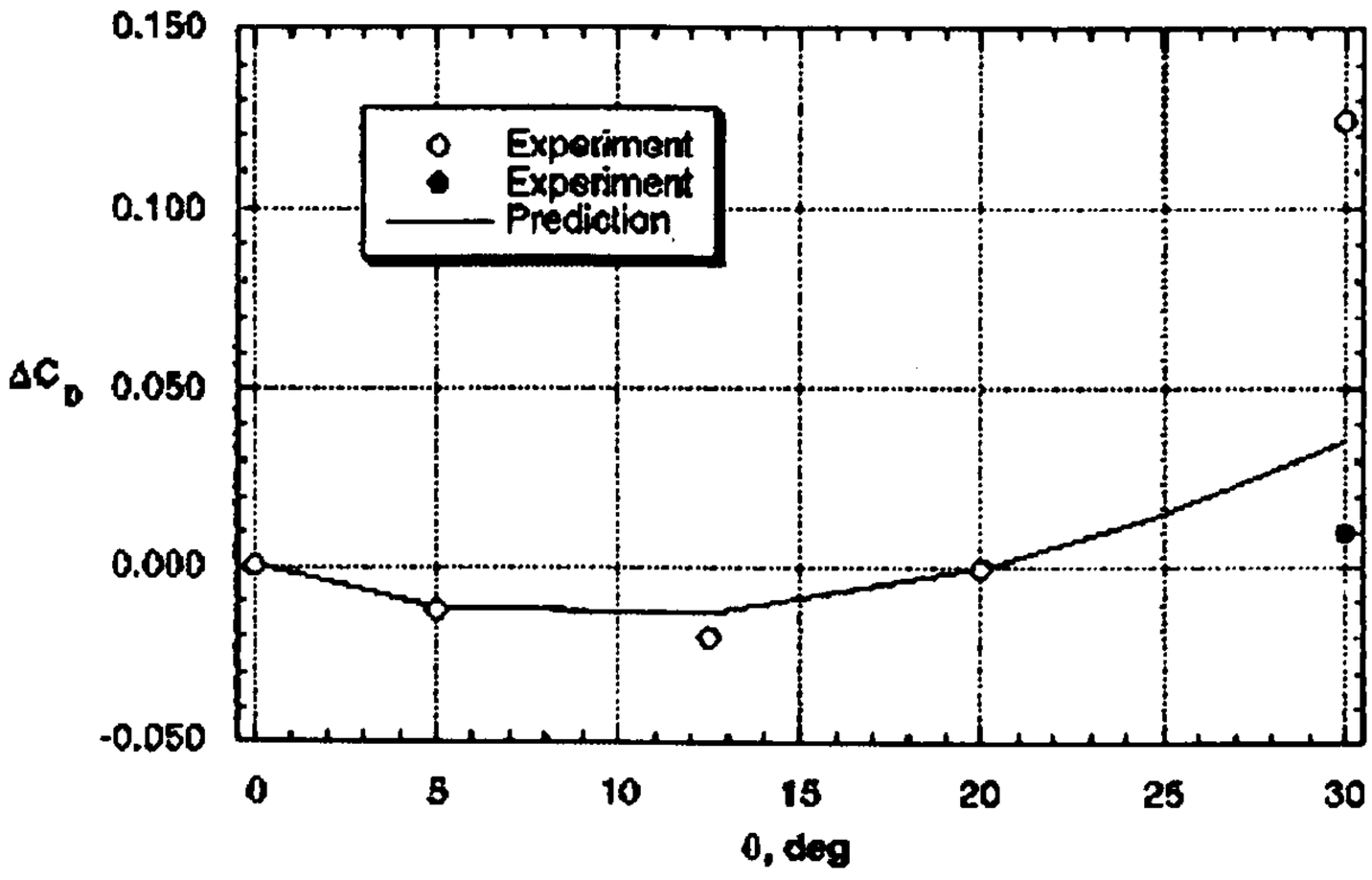

Figure 4.2 Increment in total coefficient (from Han 1989)

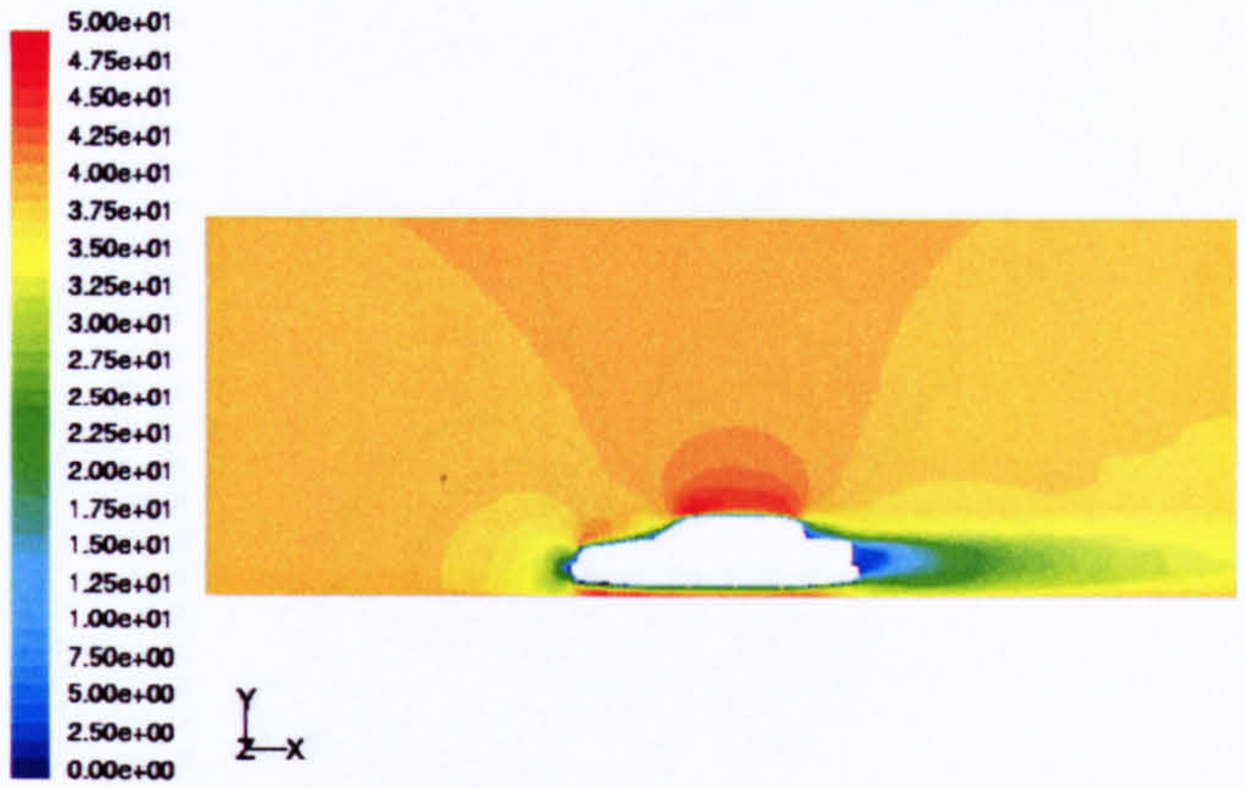

(a) Velocity contours (m/s)

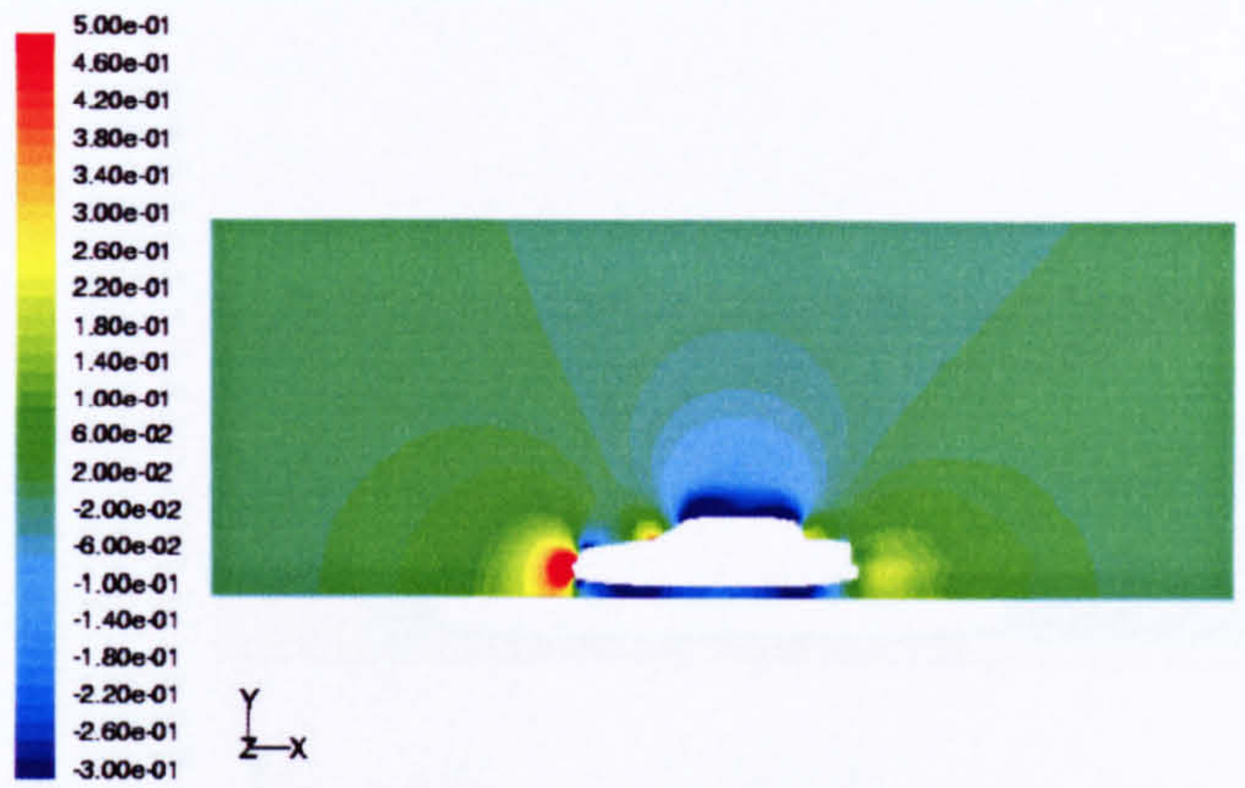

(b) Pressure coefficient contours

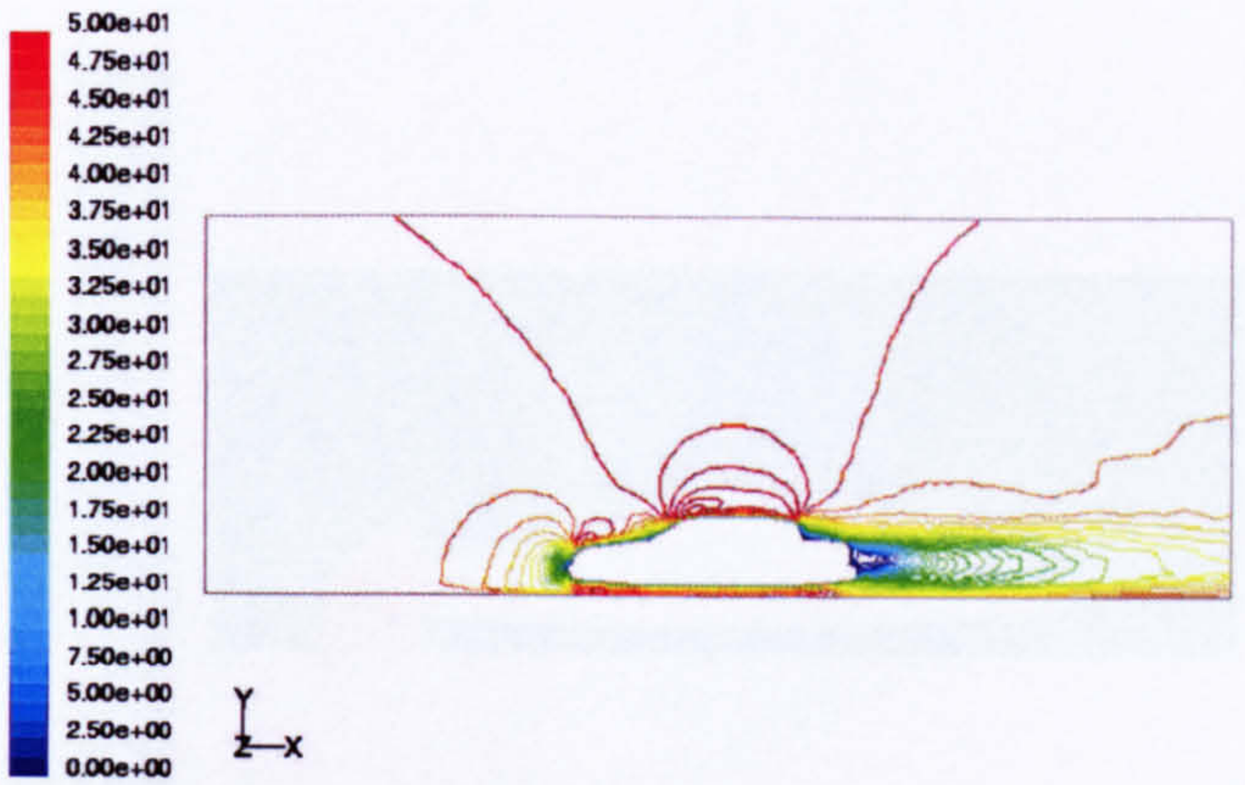

(c) velocity (m/s)

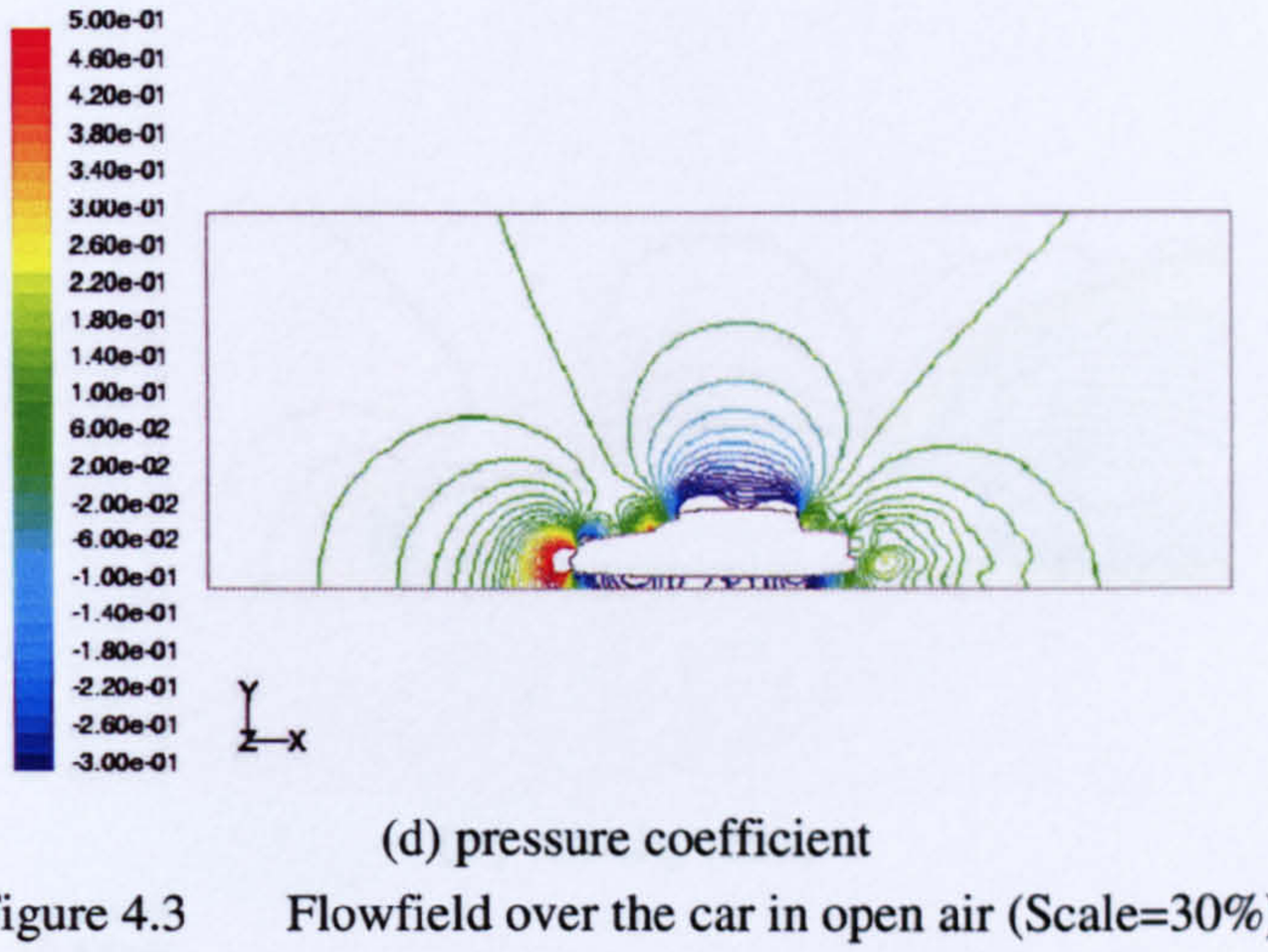

(d) pressure coefficient

Figure 4.3 Flowfield over the car in open air (Scale=30%)

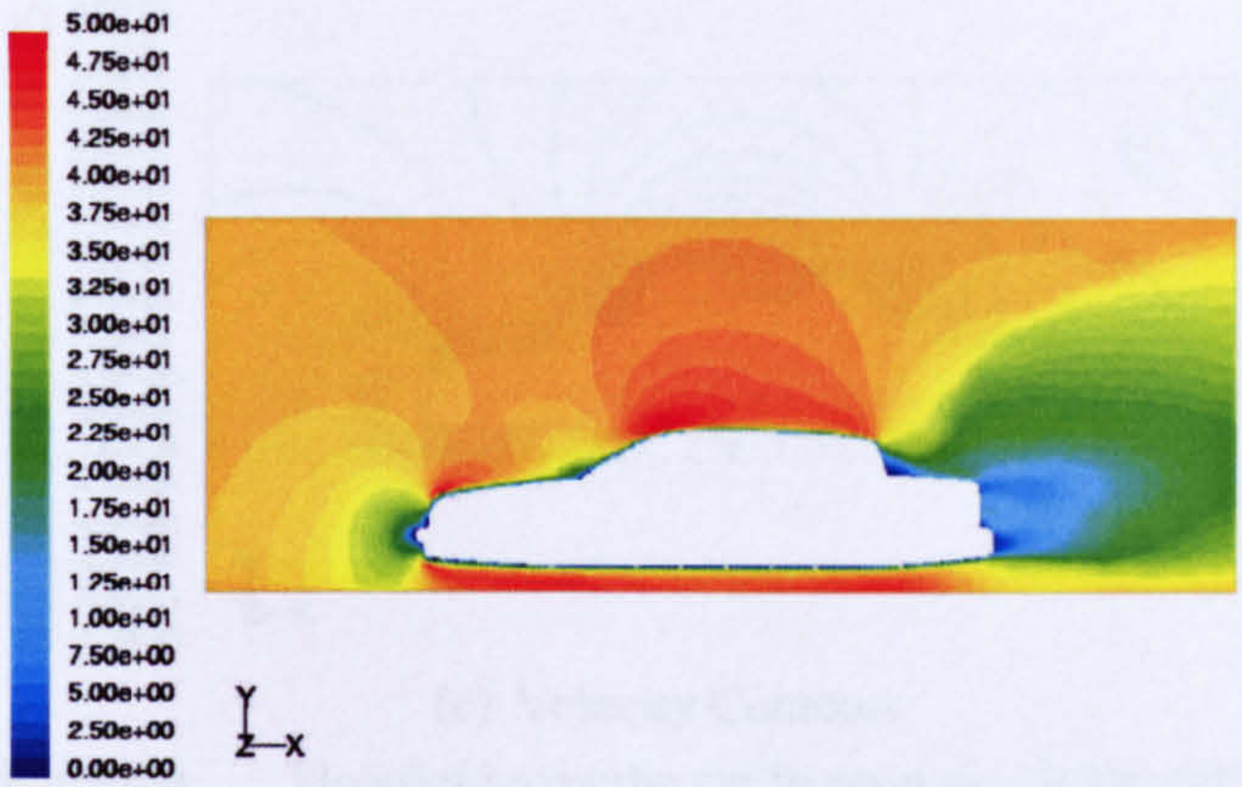

(a) Velocity (m/s)

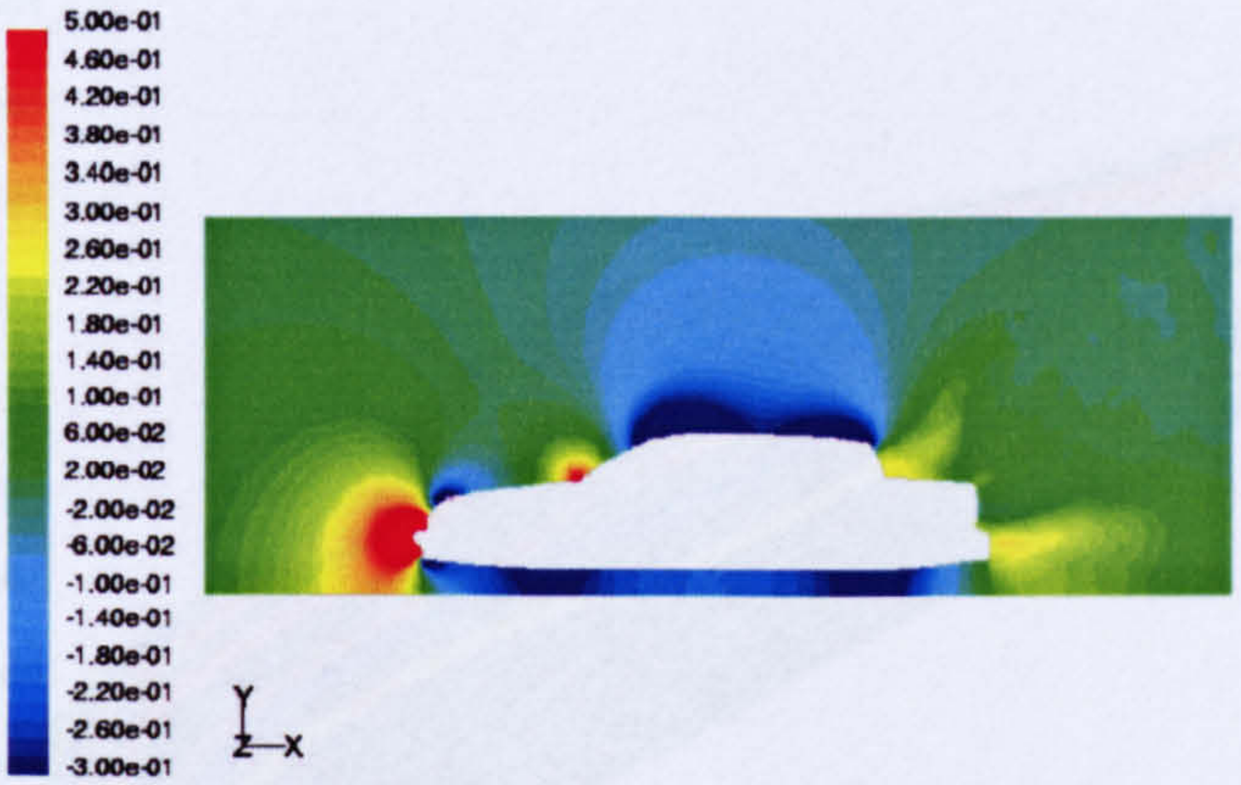

(b) Pressure Coefficient

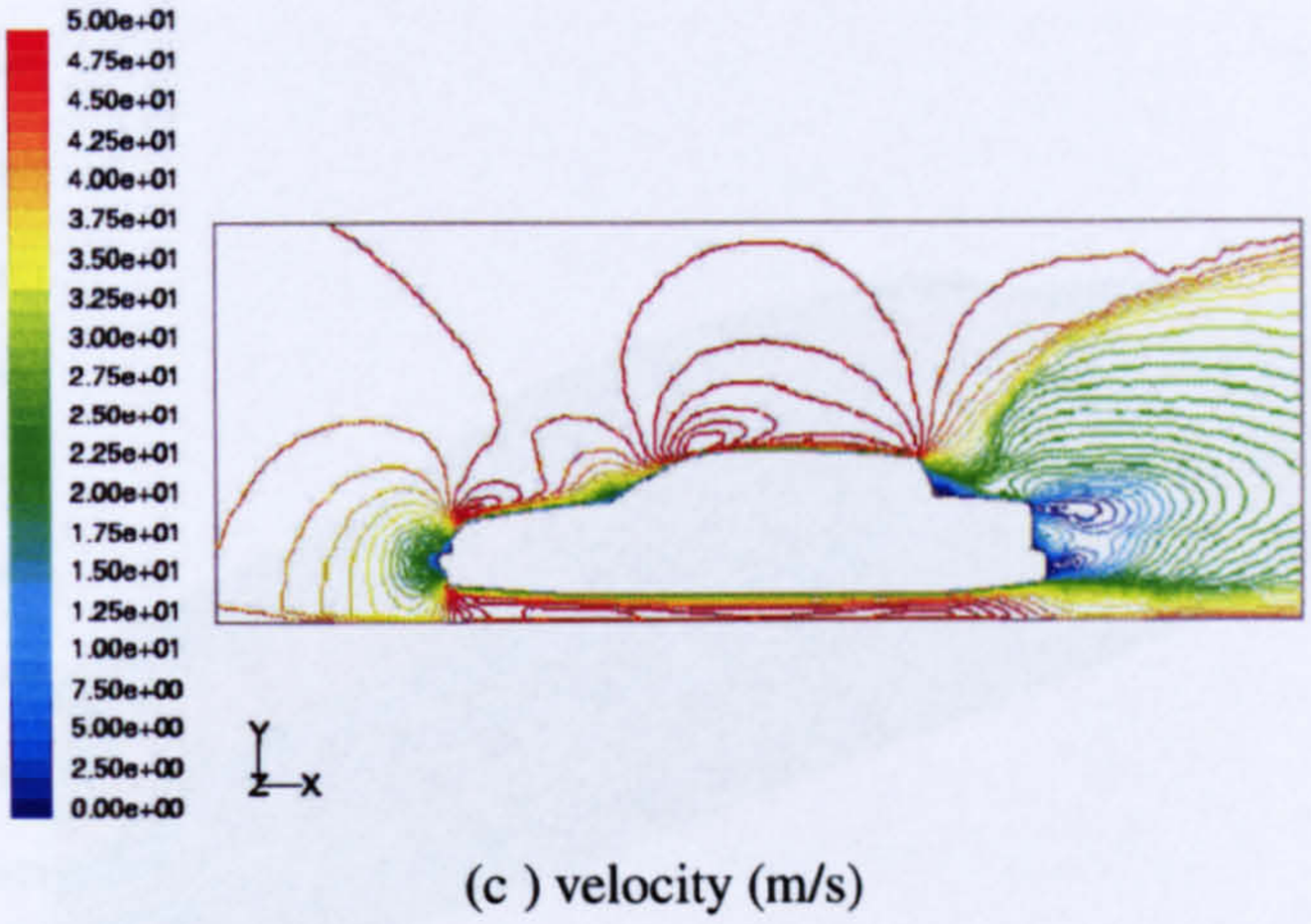

(c) velocity (m/s)

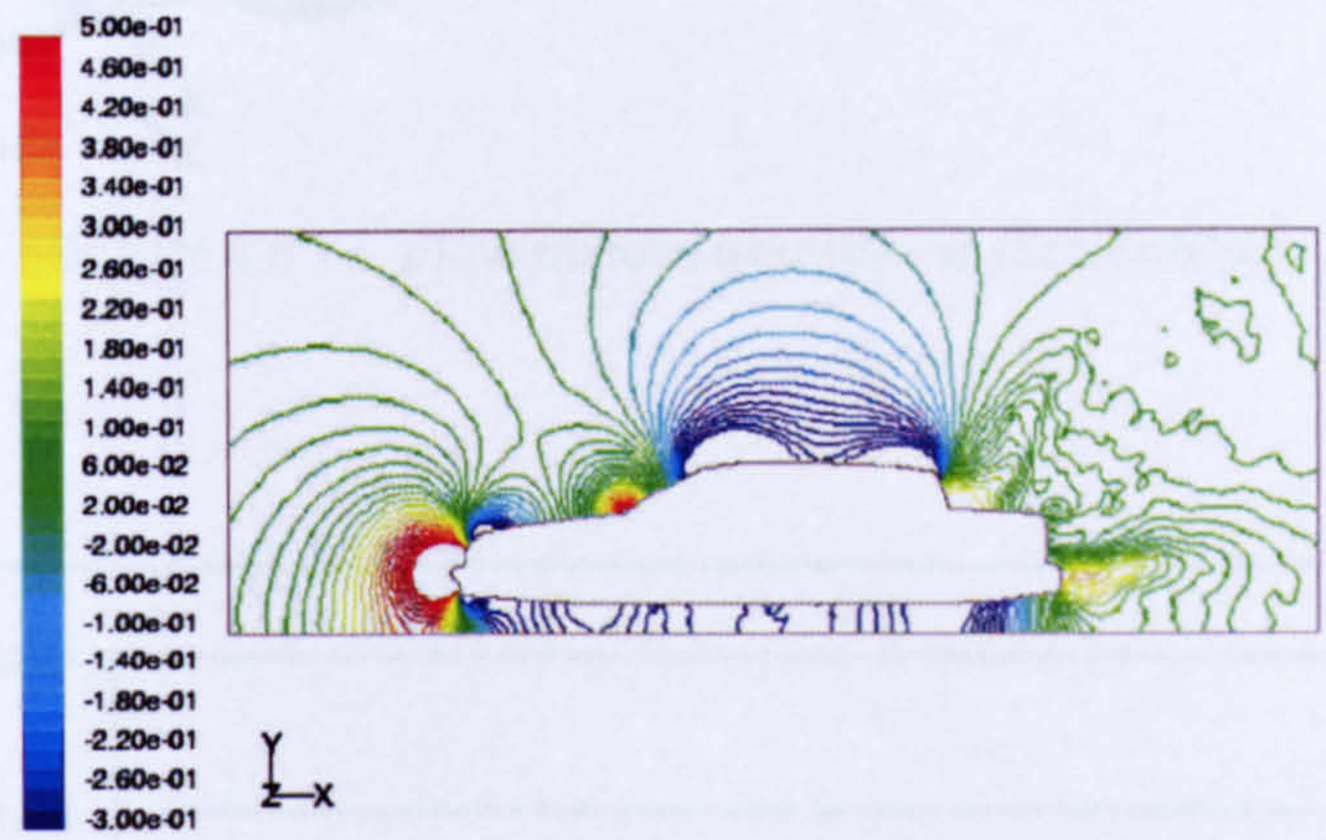

(c) Velocity Contours

Figure 4.4 Flowfield over the car in open air (Scale=60%)

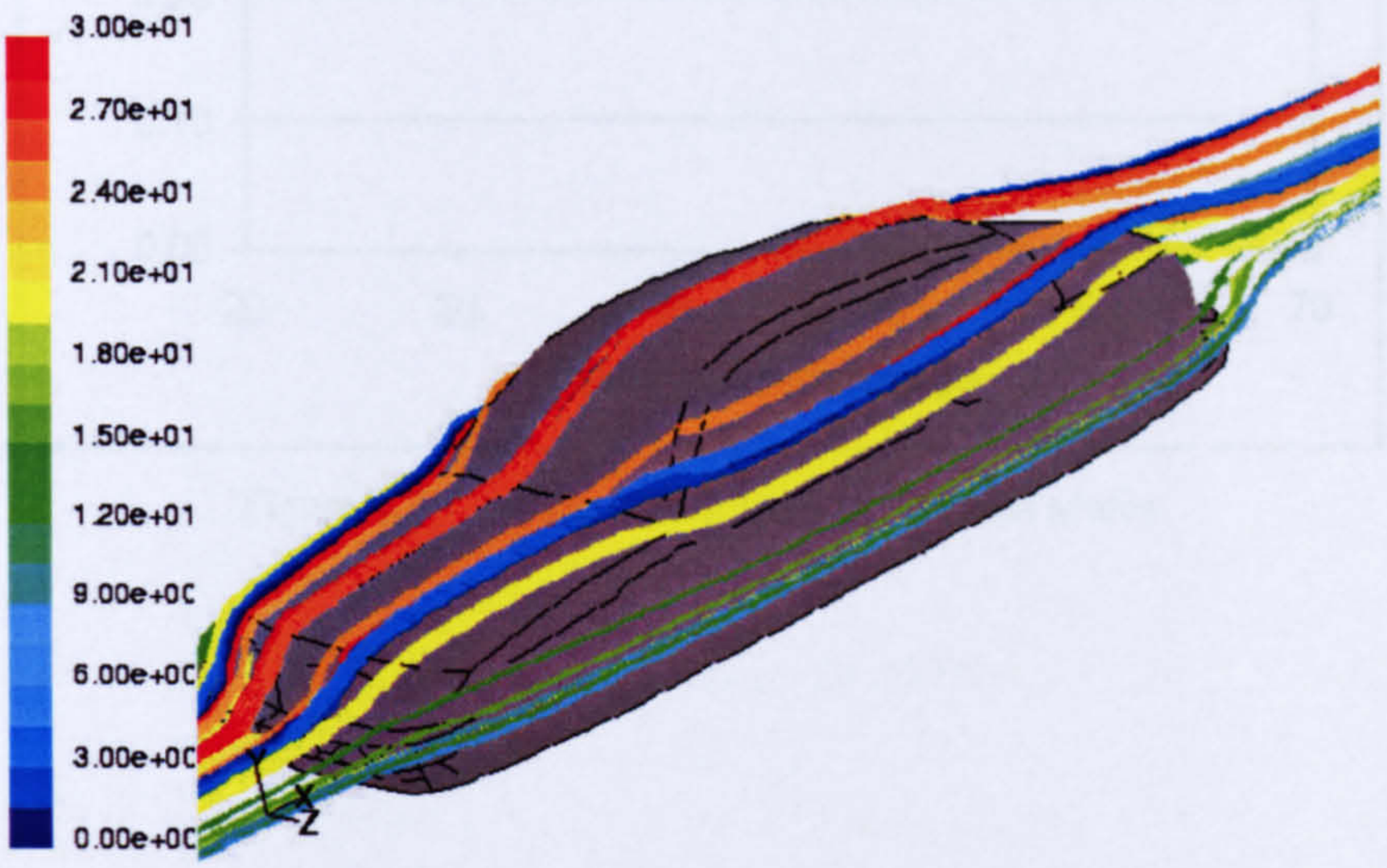

Figure 4.5 Flow ribbons over the car (Scale=30%)

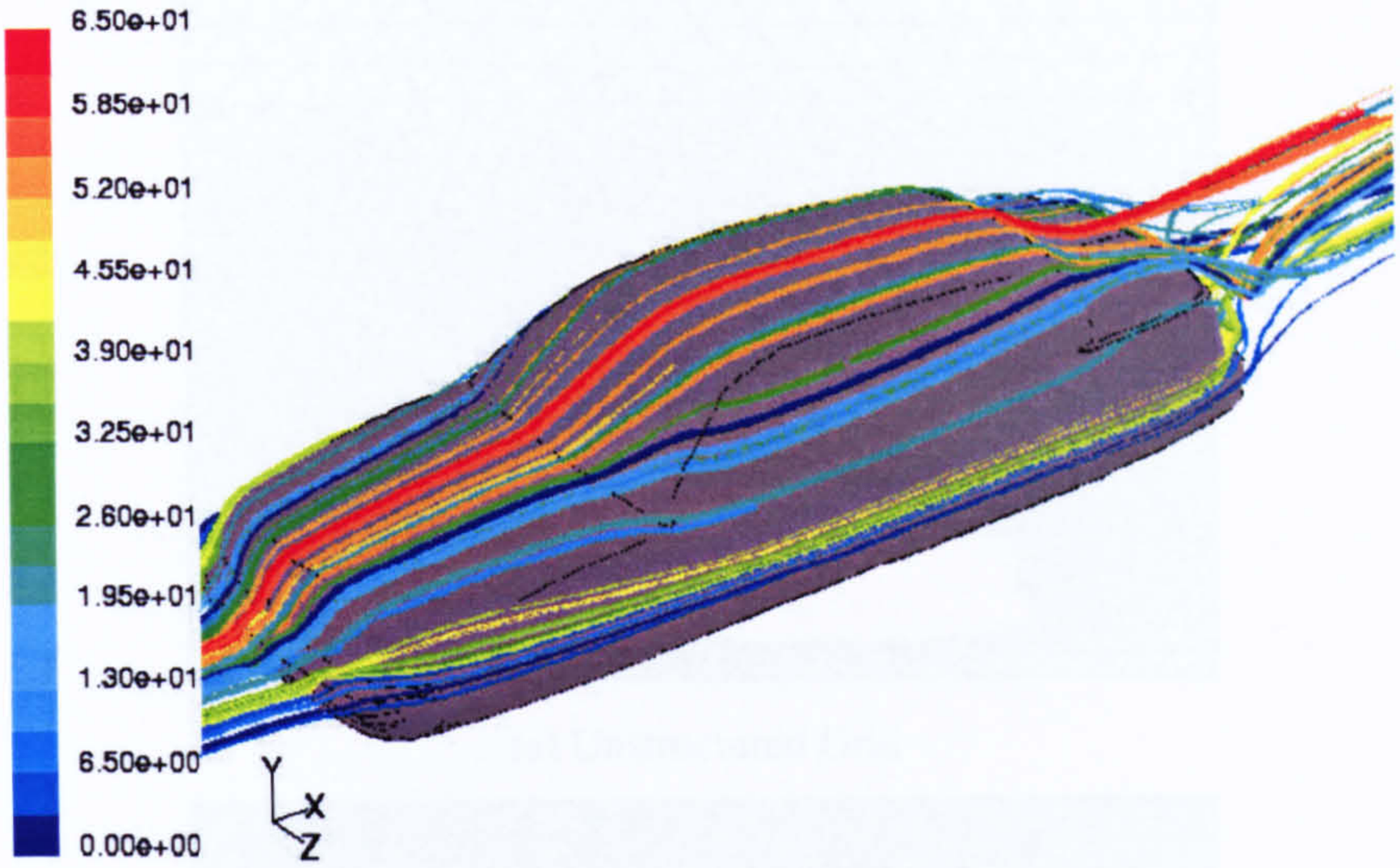

Figure 4.6 Flow ribbons over the car (Scale=60%)

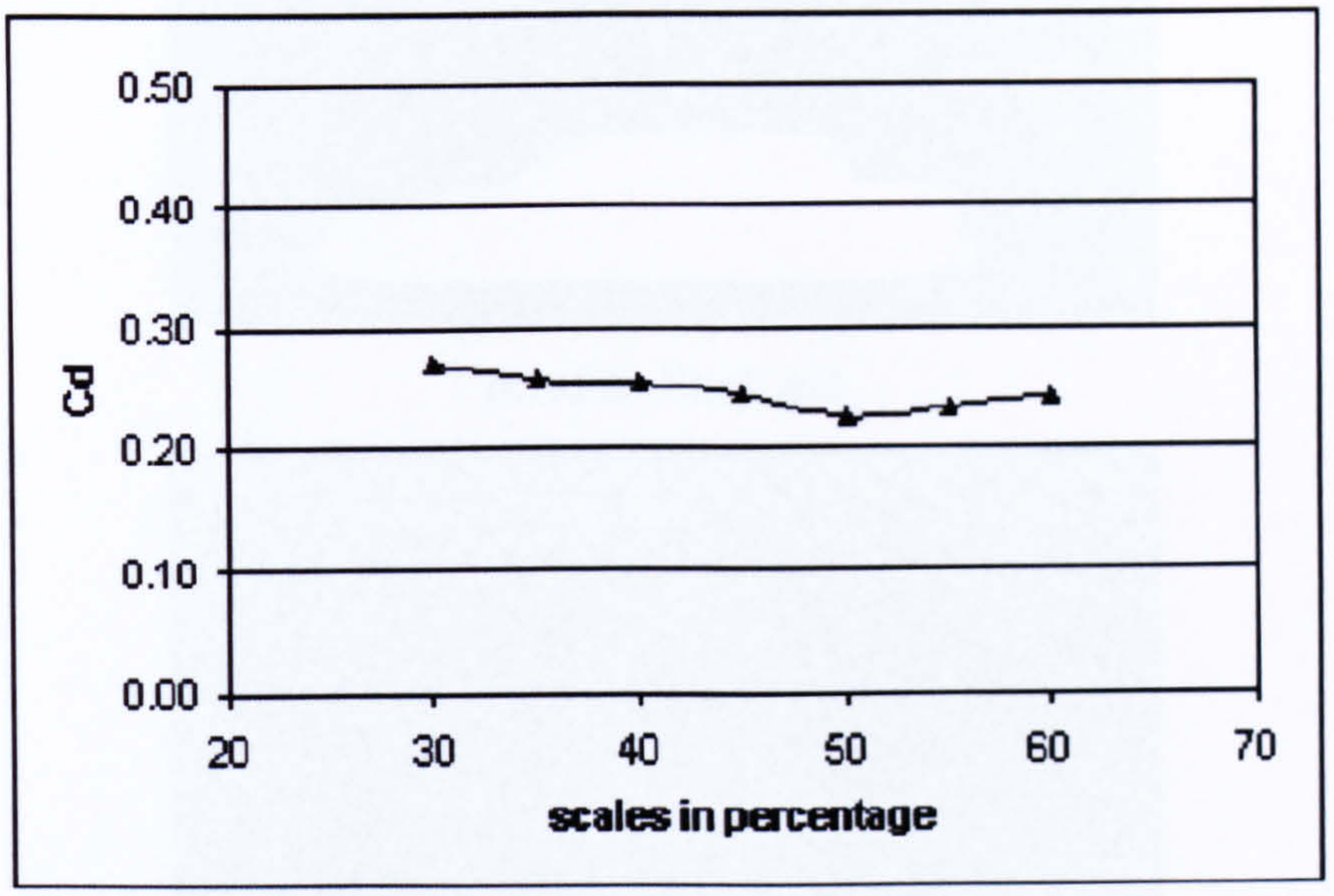

Figure 4.7 Drag coefficients in different scales

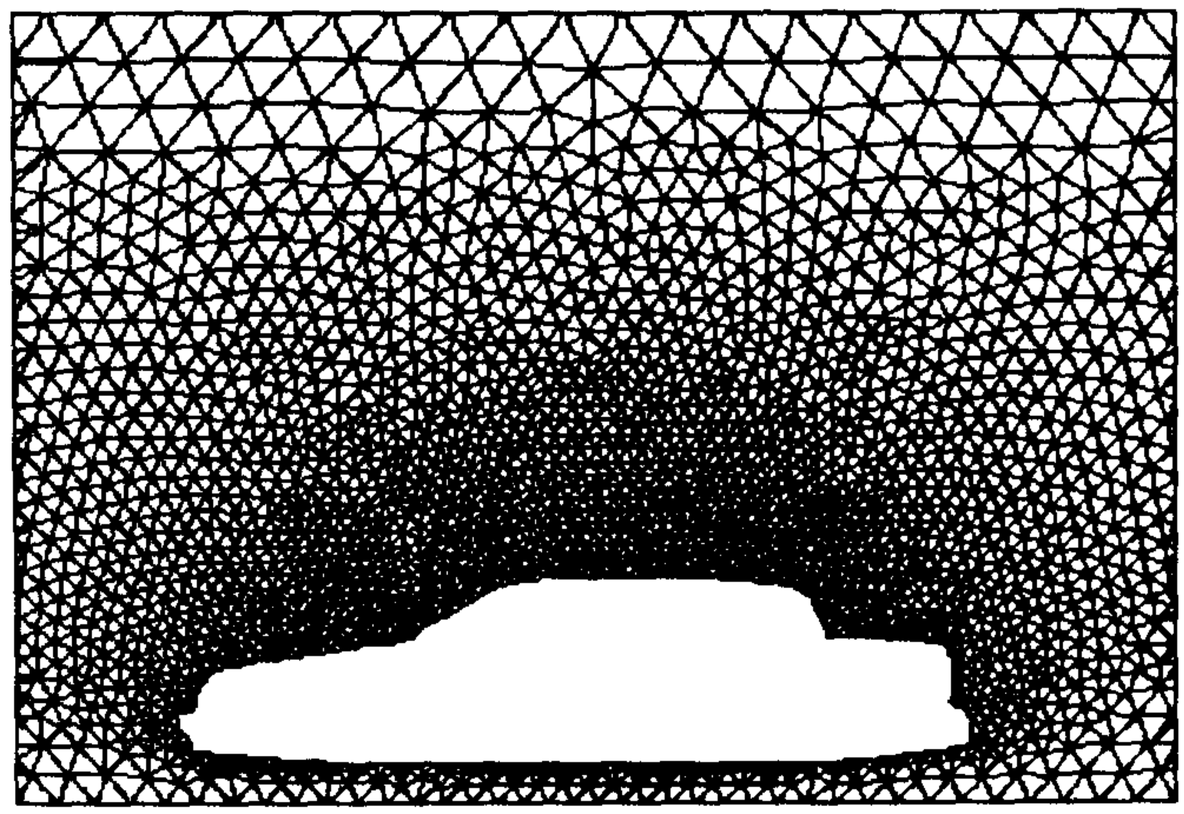

(a) Unstructured Grid

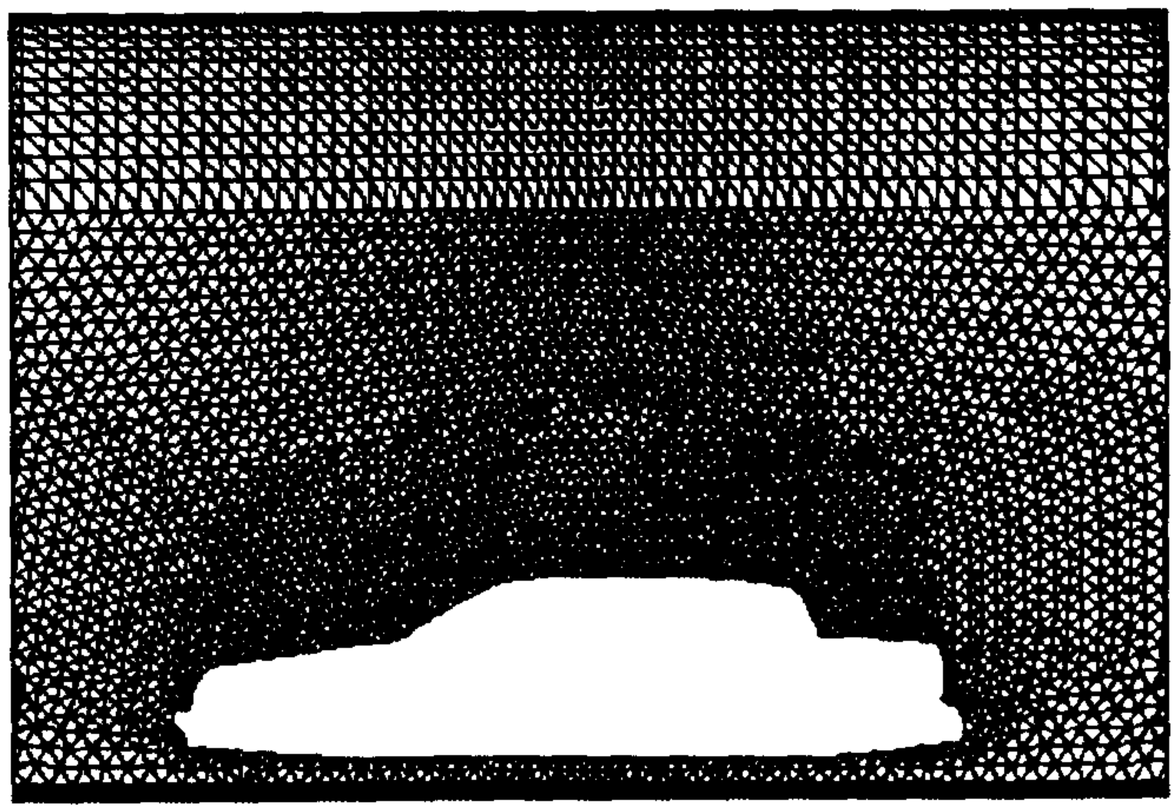

(b) Multi-Block grid

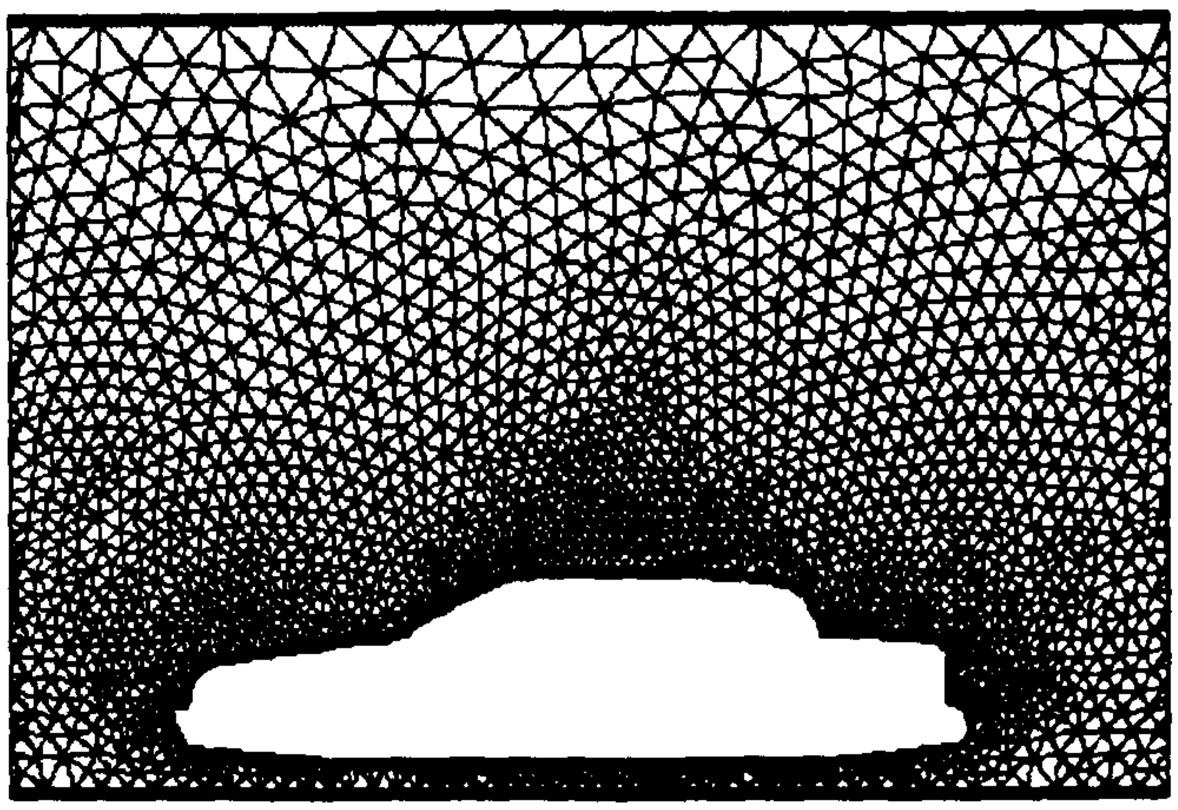

(c) Hybrid grid

Figure 4.8 Grids are used in the research

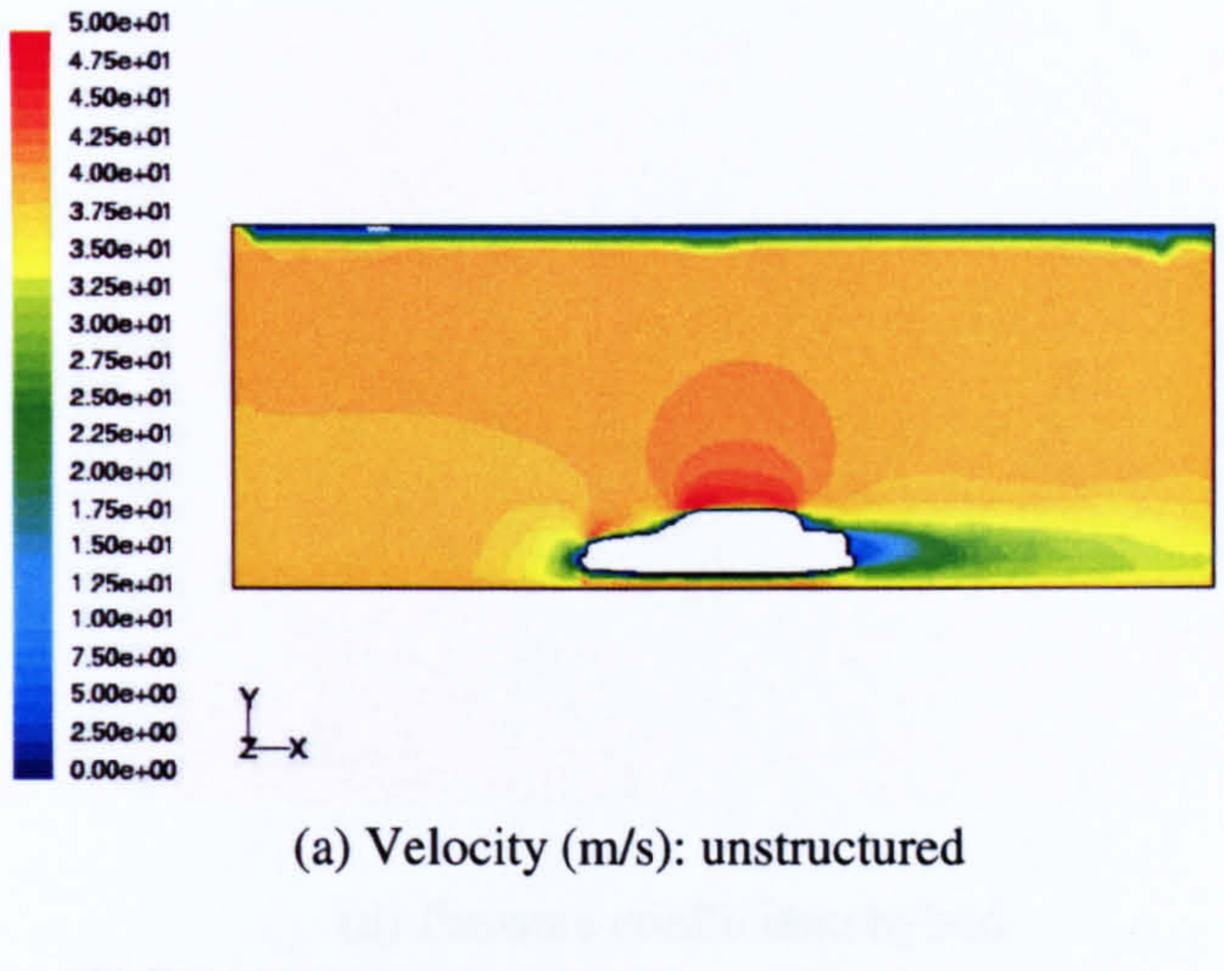

(a) Velocity (m/s): unstructured

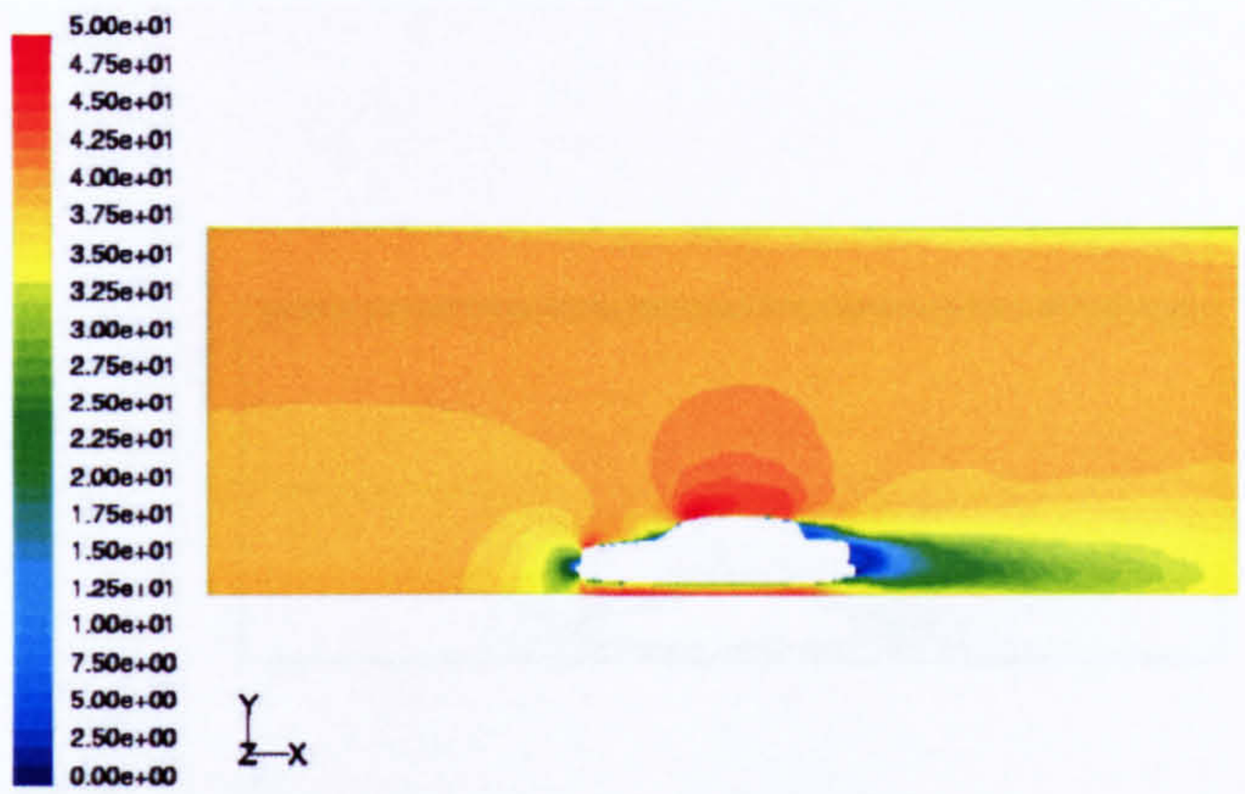

(b) Velocity (m/s): hybrid

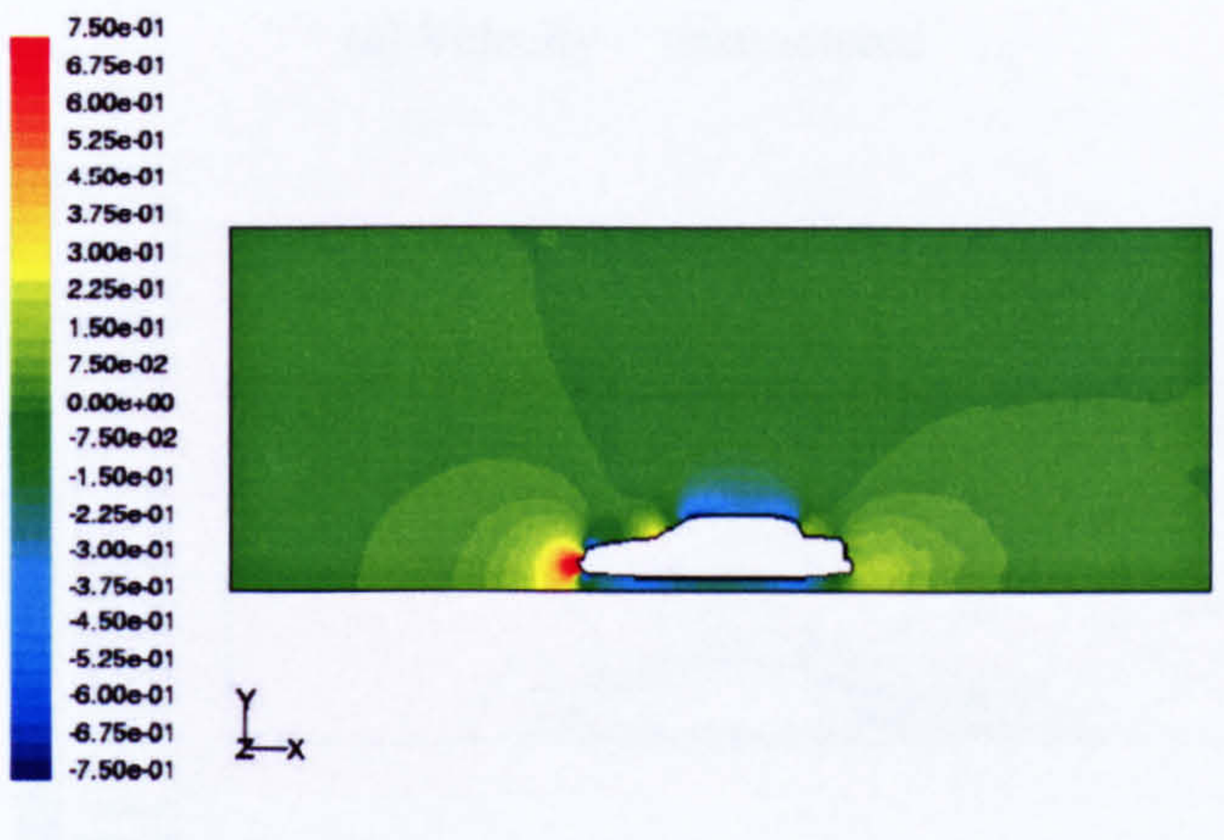

(c) Pressure coefficient: unstructured

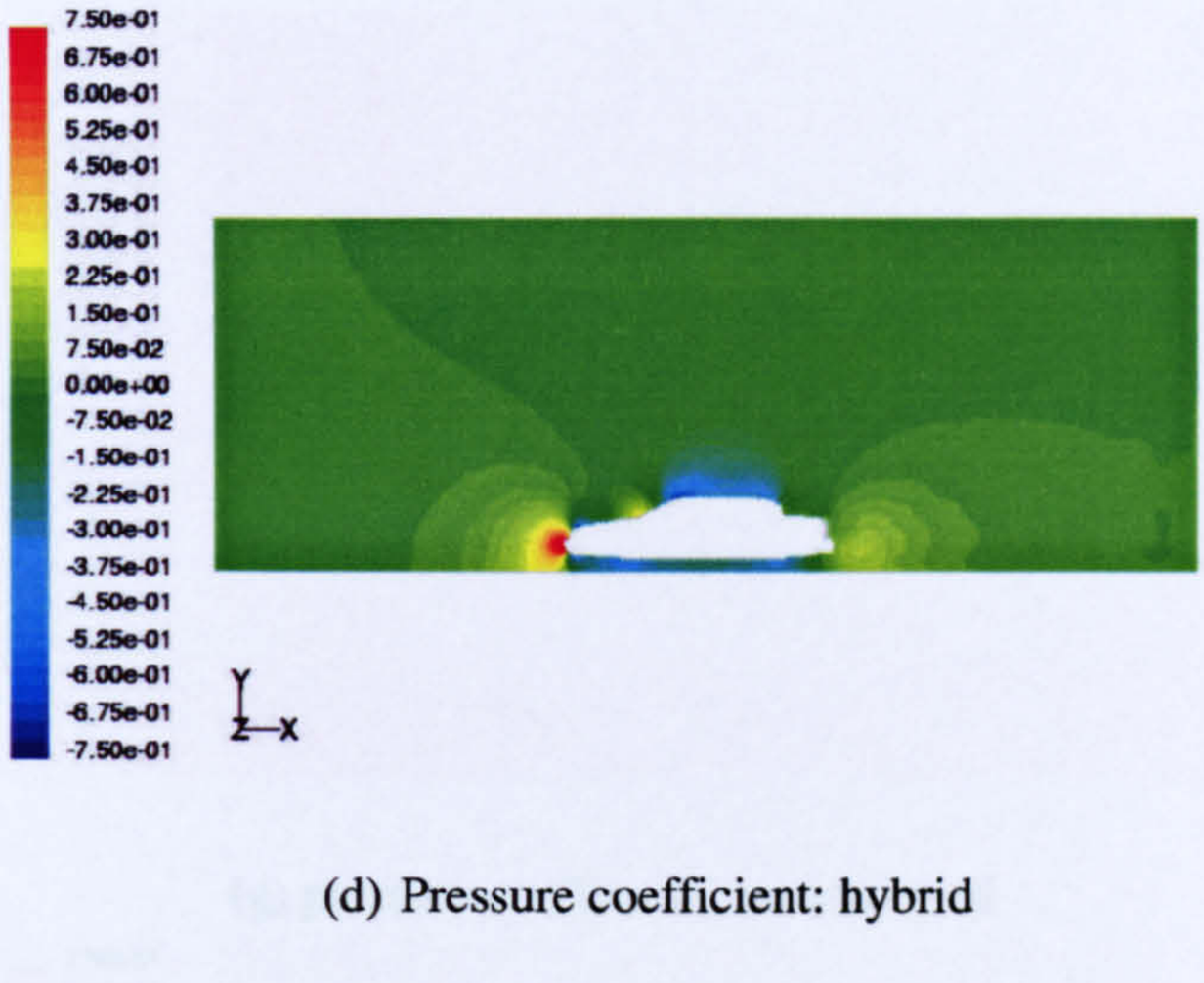

(d) Pressure coefficient: hybrid

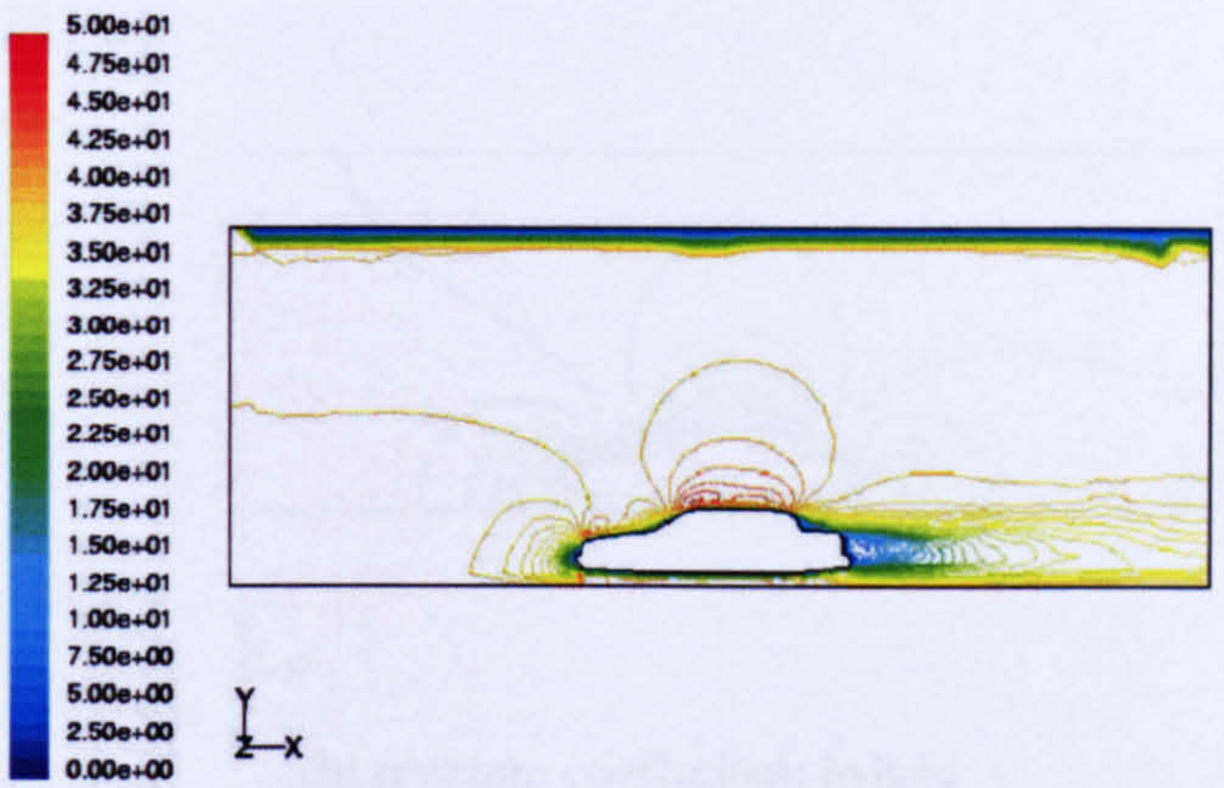

(e) Velocity : unstructured

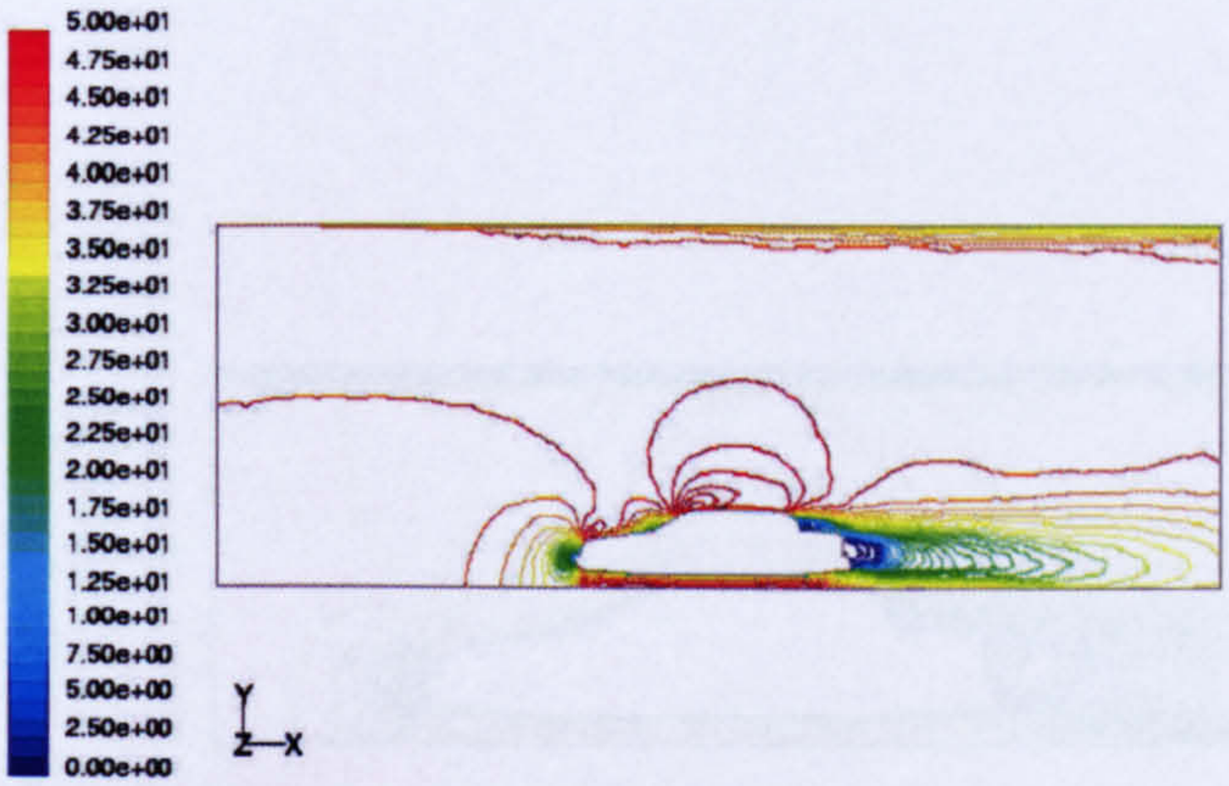

(f) Velocity: hybrid

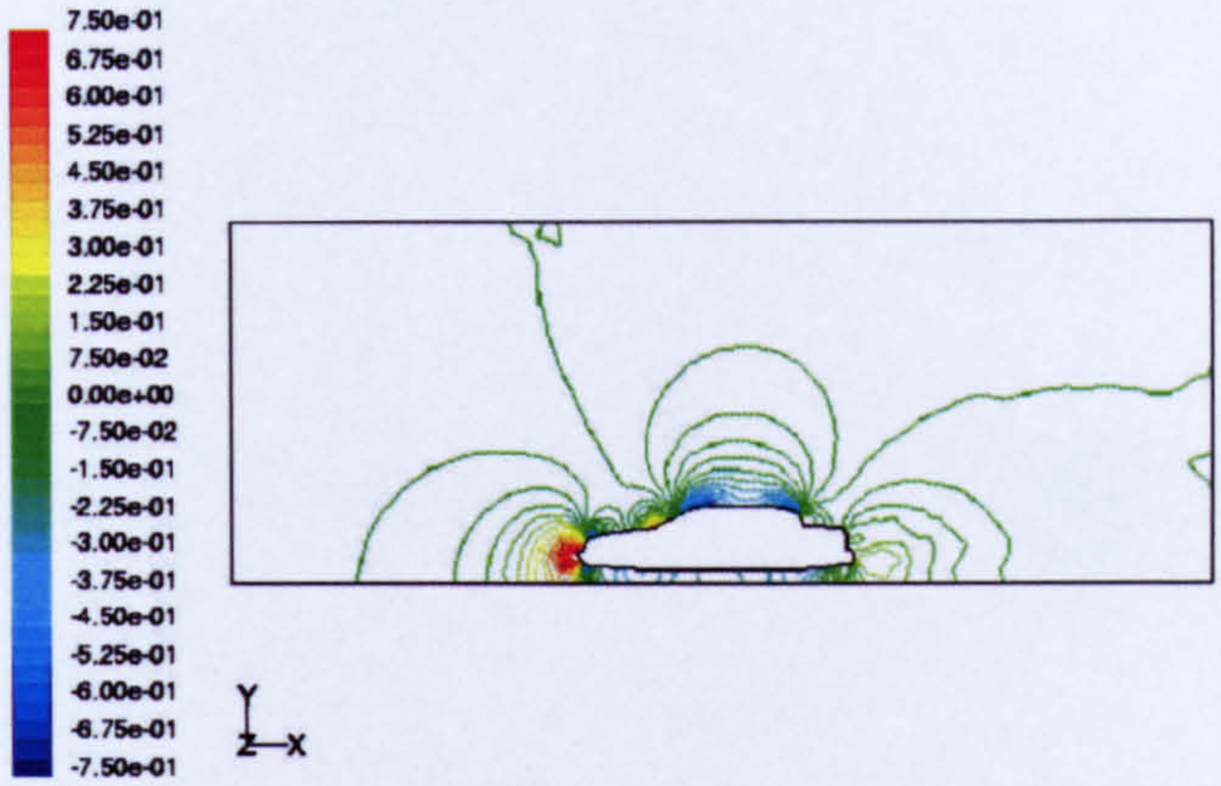

(g) pressure coefficient: unstructured

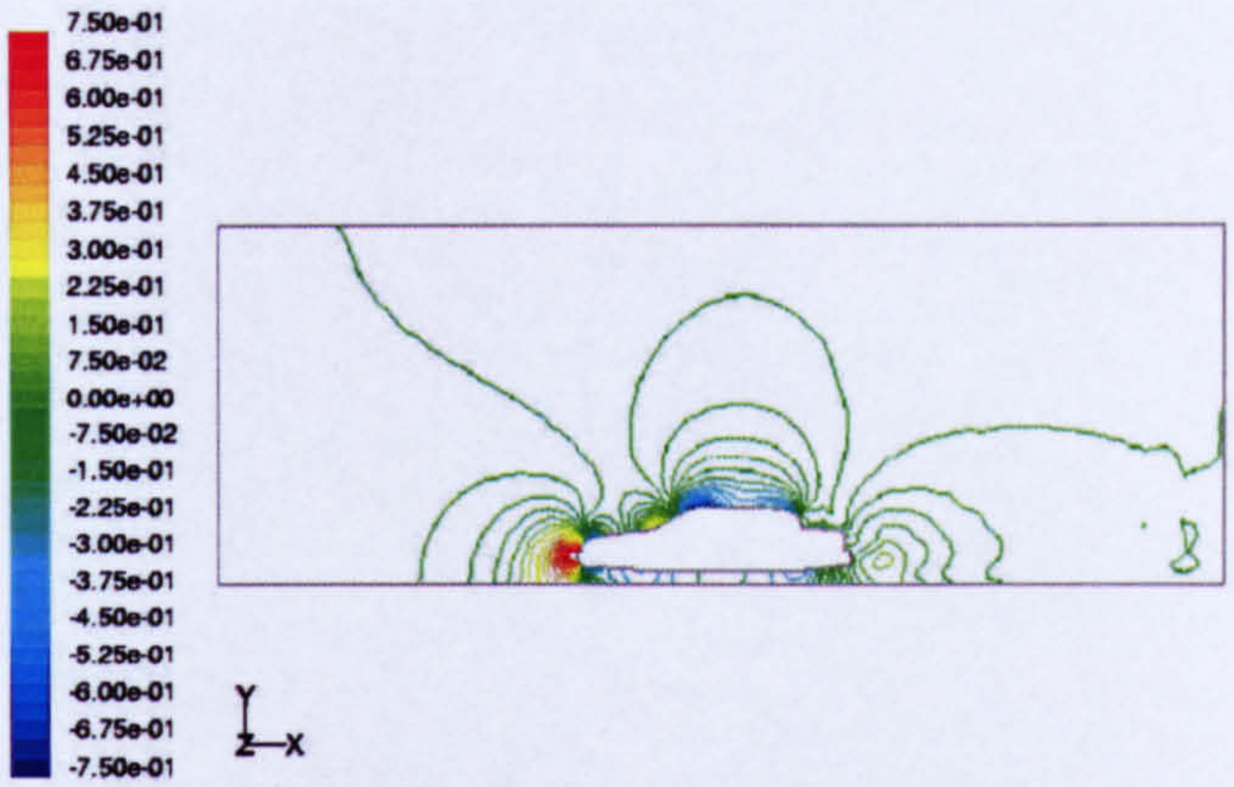

(h) pressure coefficient: hybrid

Figure 4.9 Car in the tunnel (no Strut, Scale=30%)

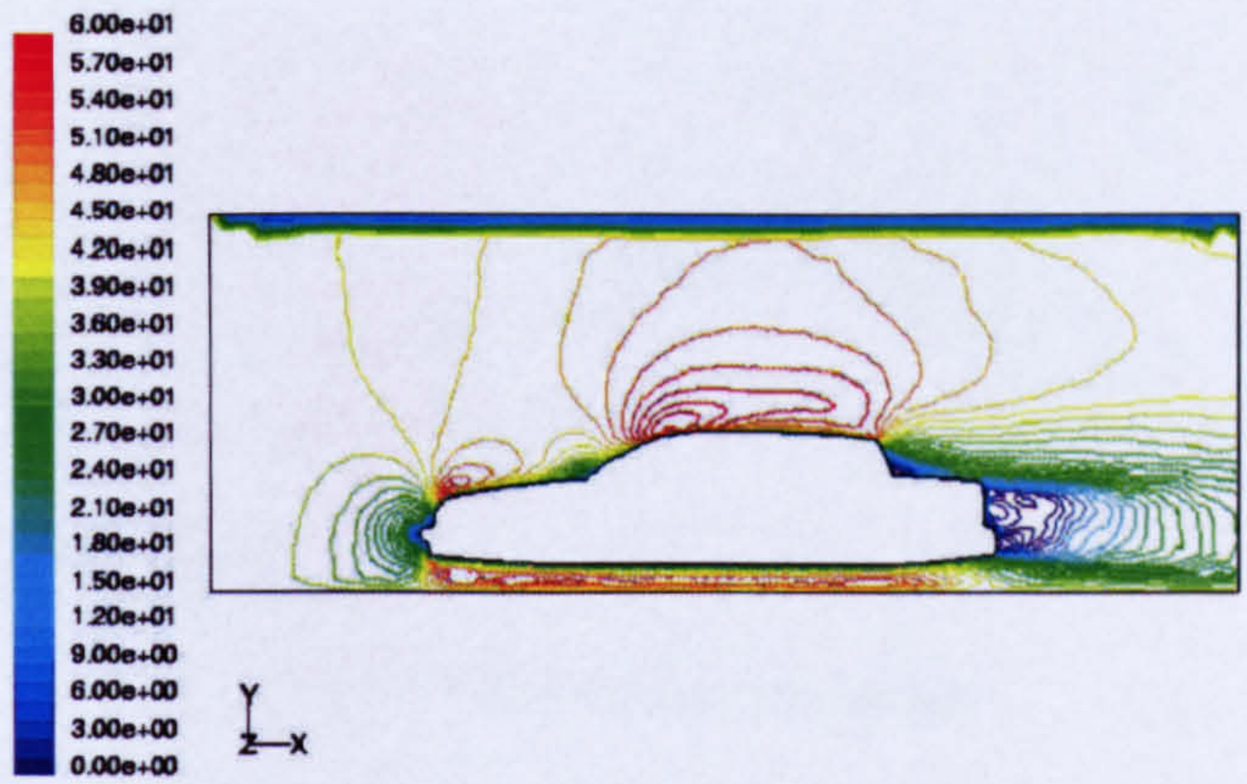

(a) velocity (m/s): unstructured

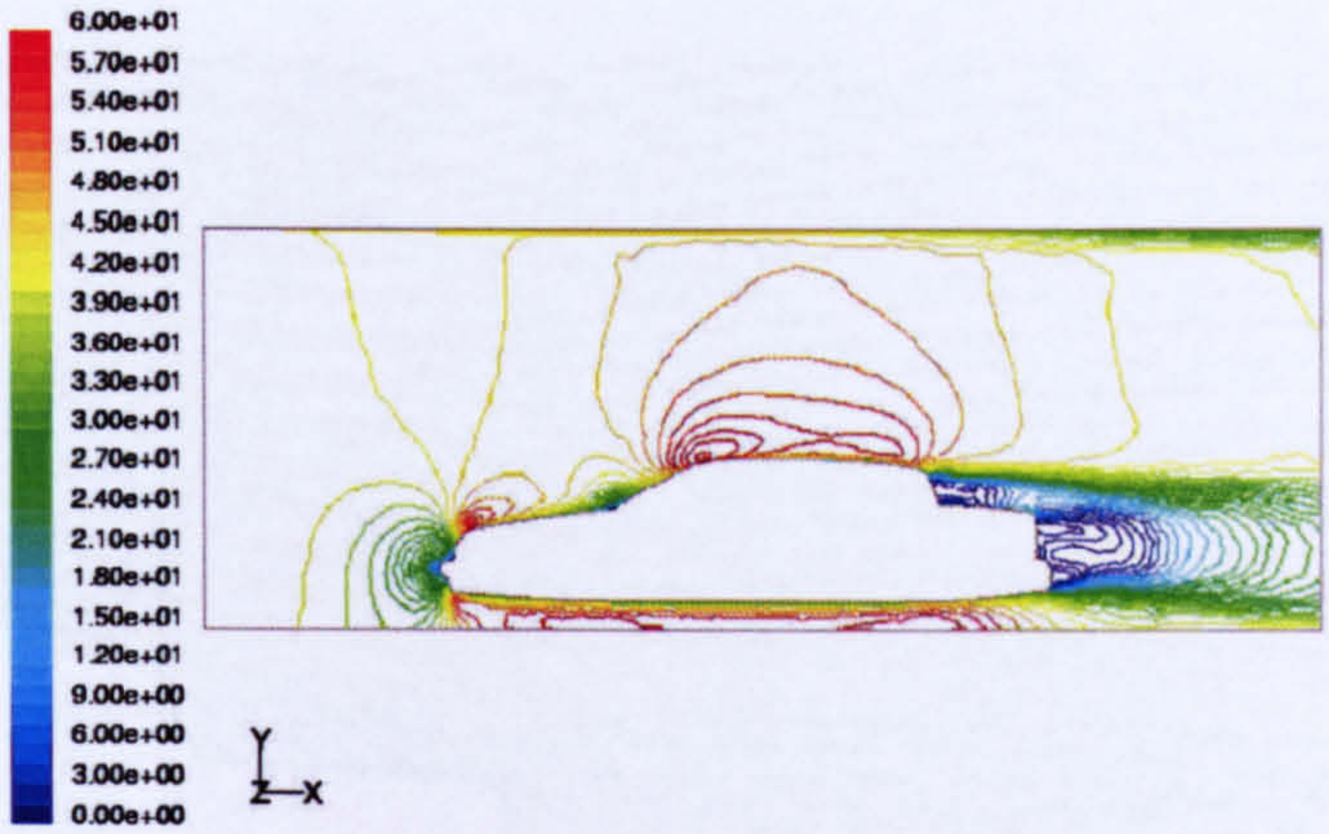

(b) Velocity (m/s): hybrid

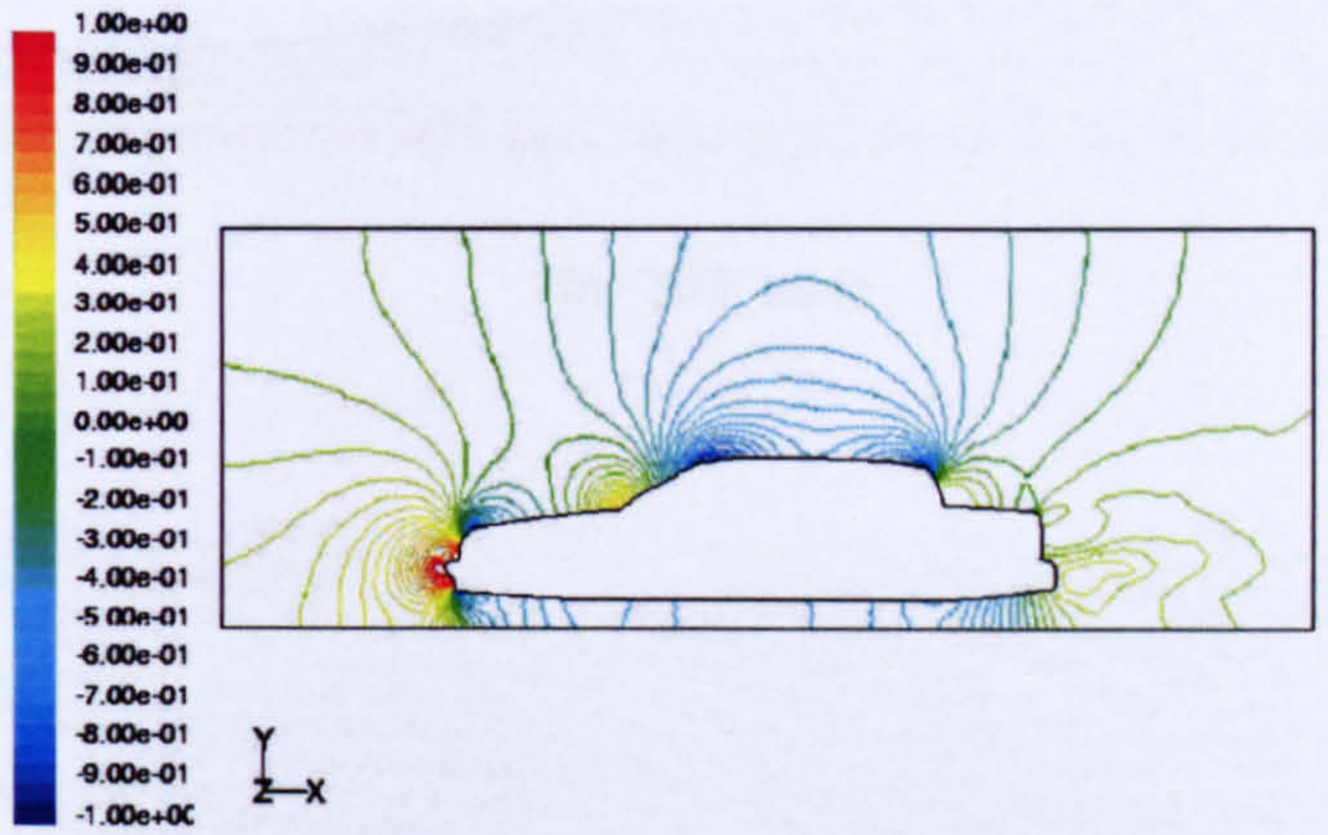

(c) Pressure coefficient: unstructured

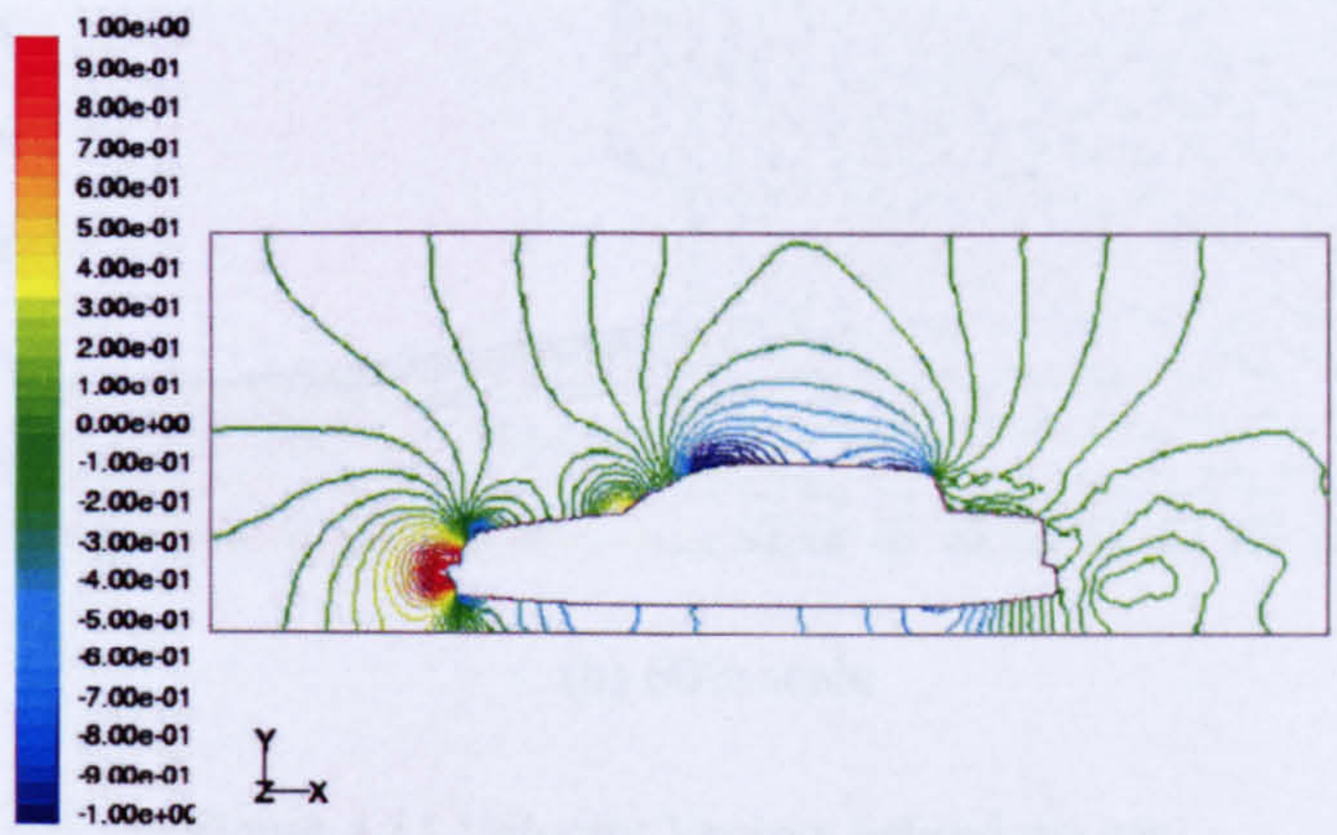

(d) Pressure coefficient: hybrid

Figure 4.10 Car in the tunnel (no Strut, Scale=60%)

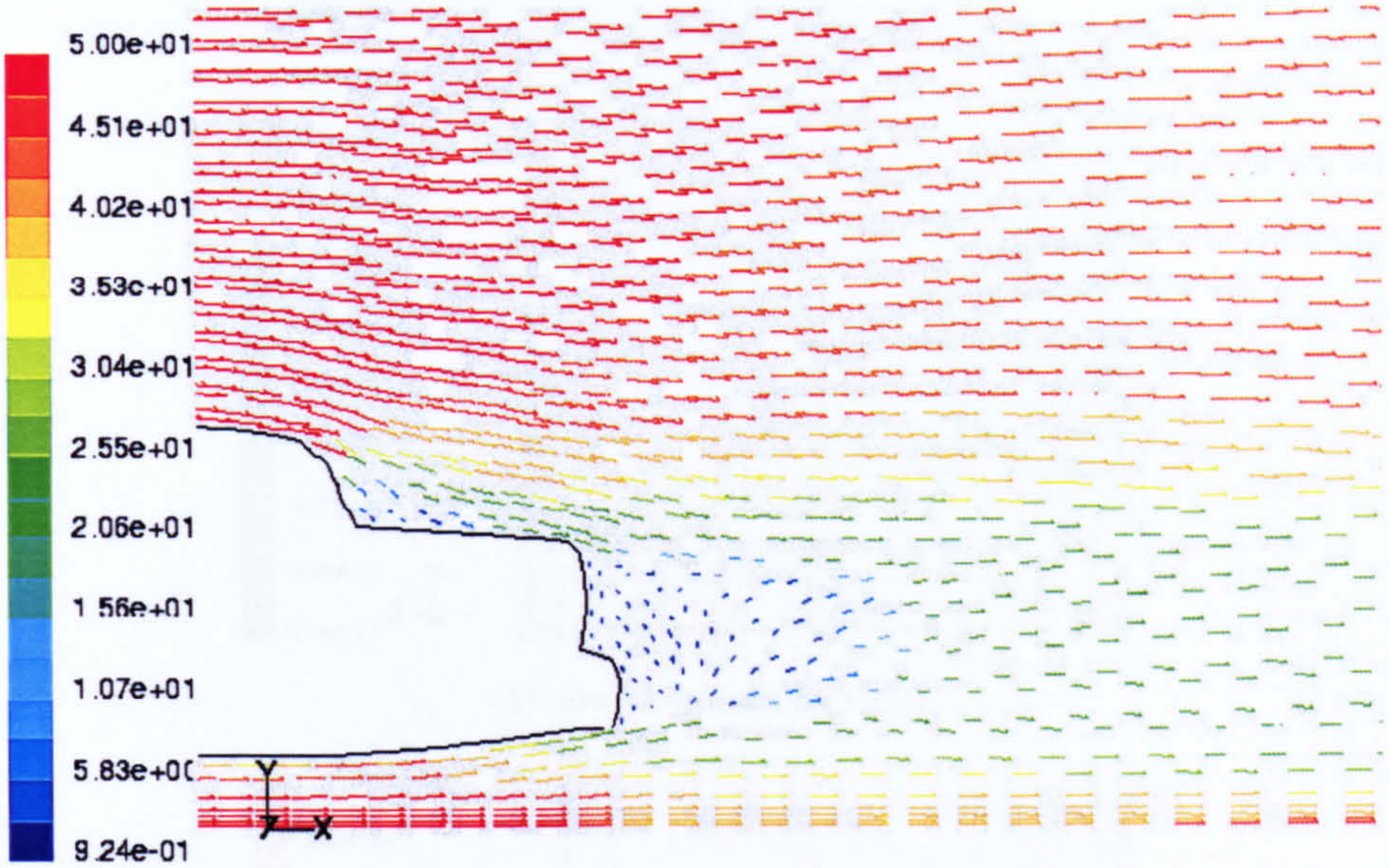

(a) 30% scale

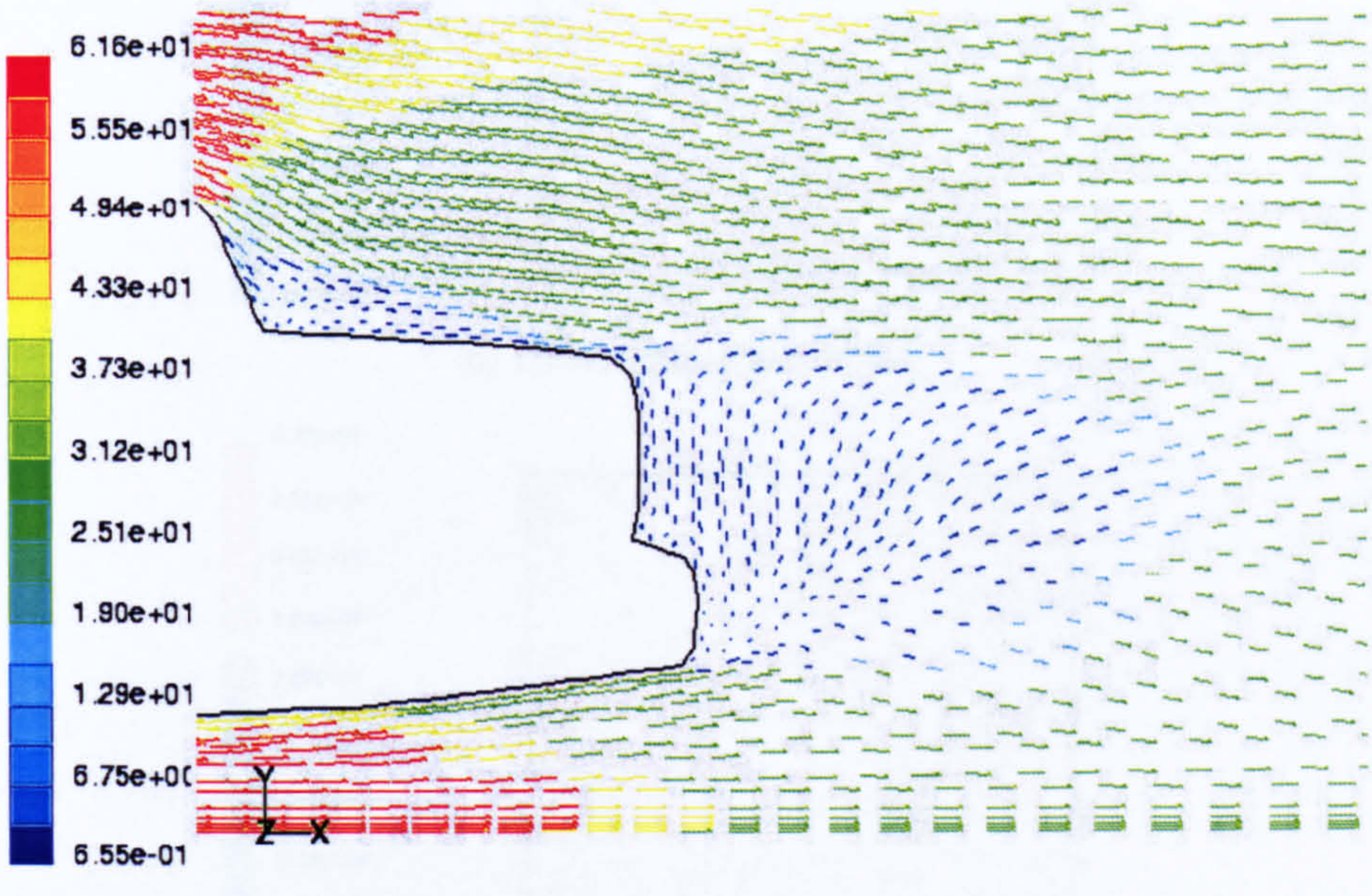

(b) 60% scale

Figure 4.11 Velocity Vectors behind the car

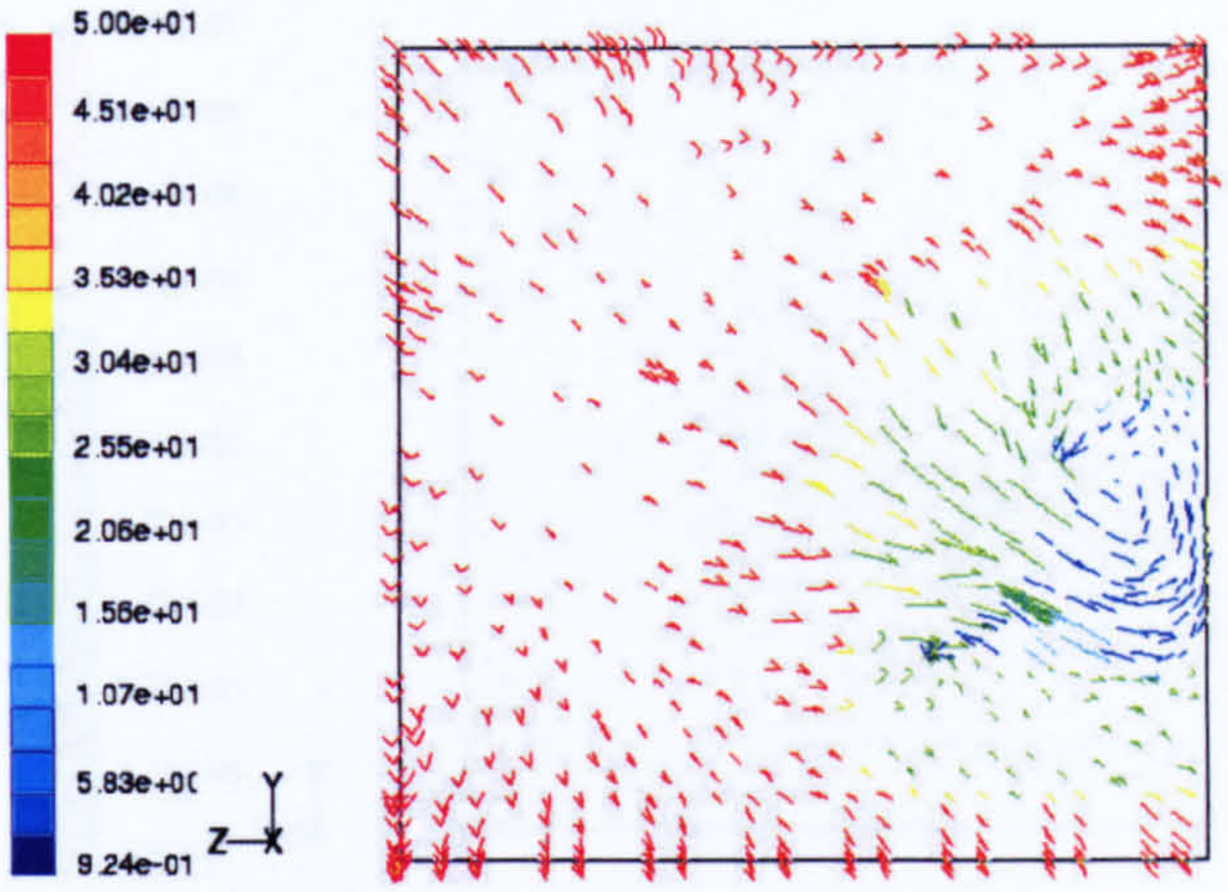

(a) xb=70mm(scale=30%)

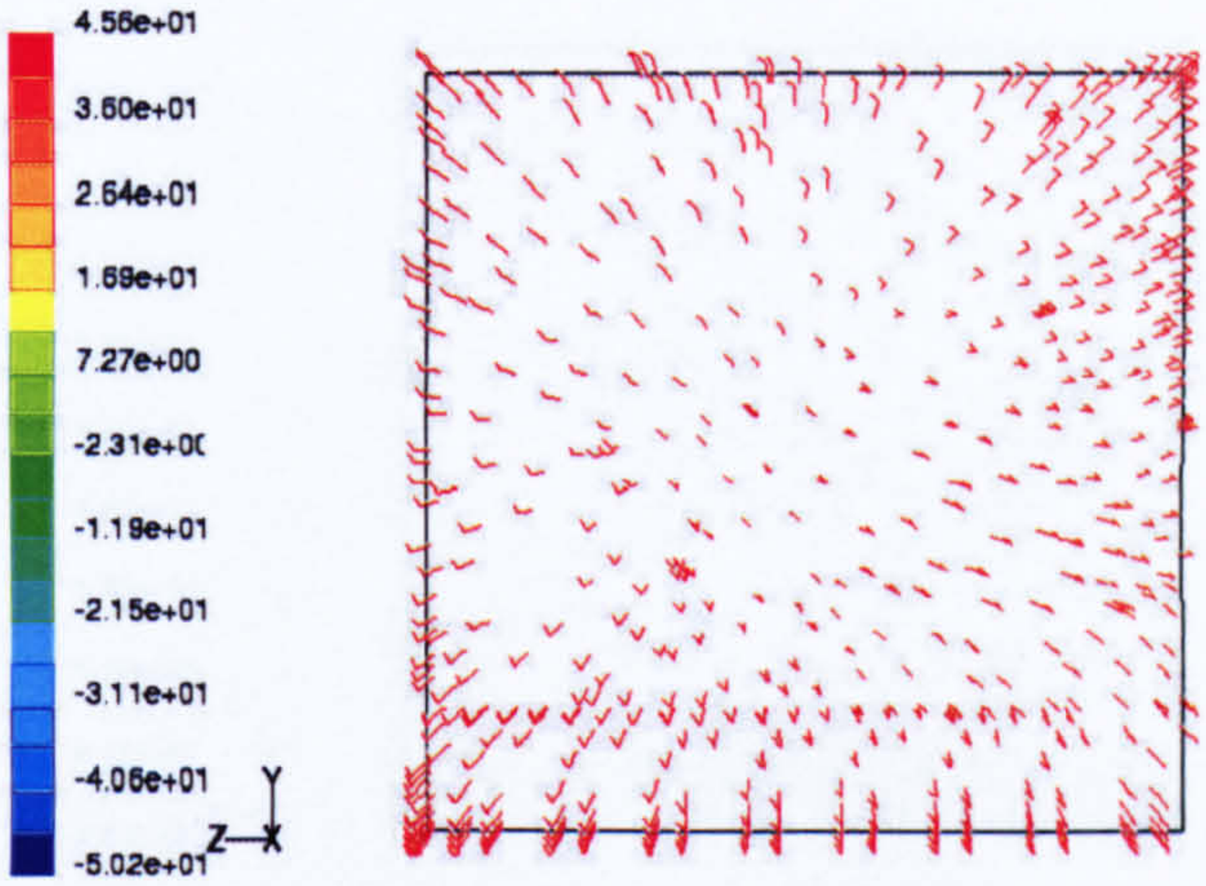

(b) xb=470mm(scale=30%)

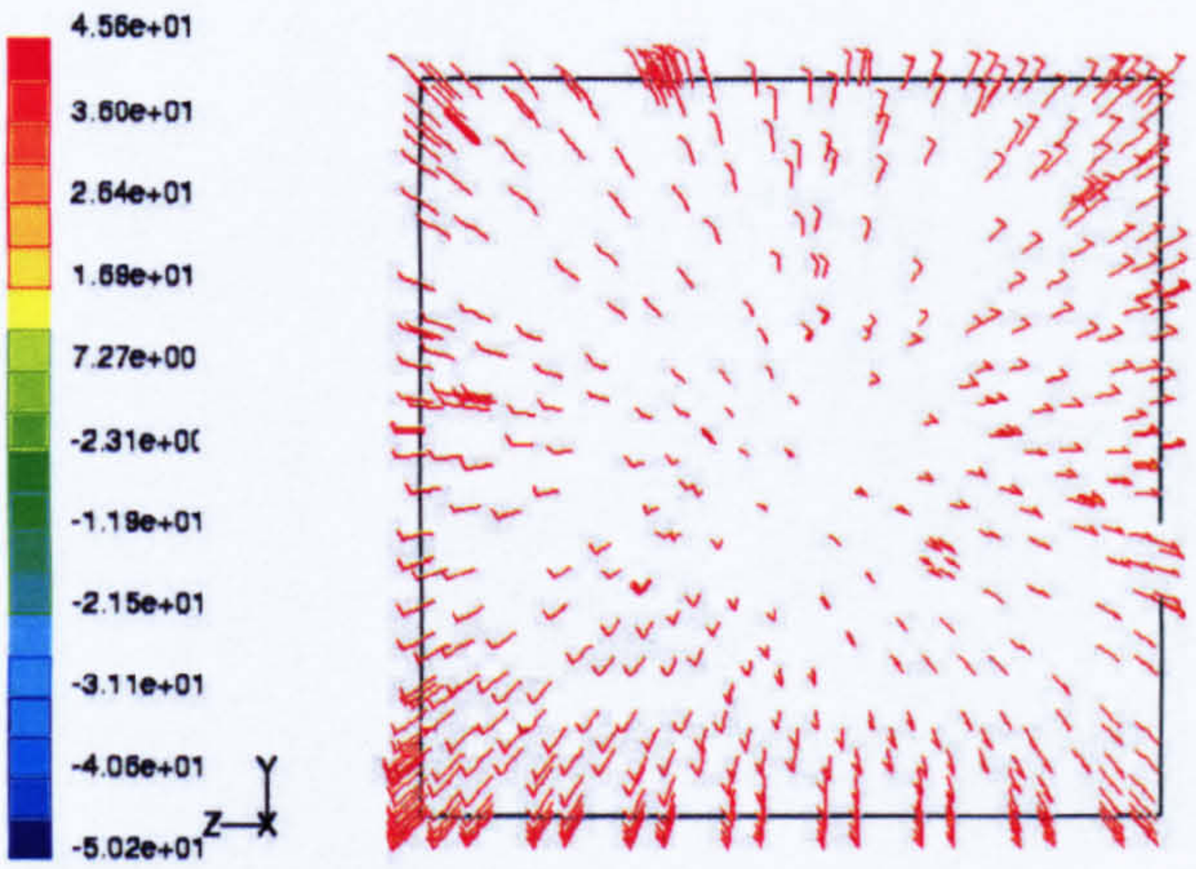

(c) xb=870mm(scale=30%)

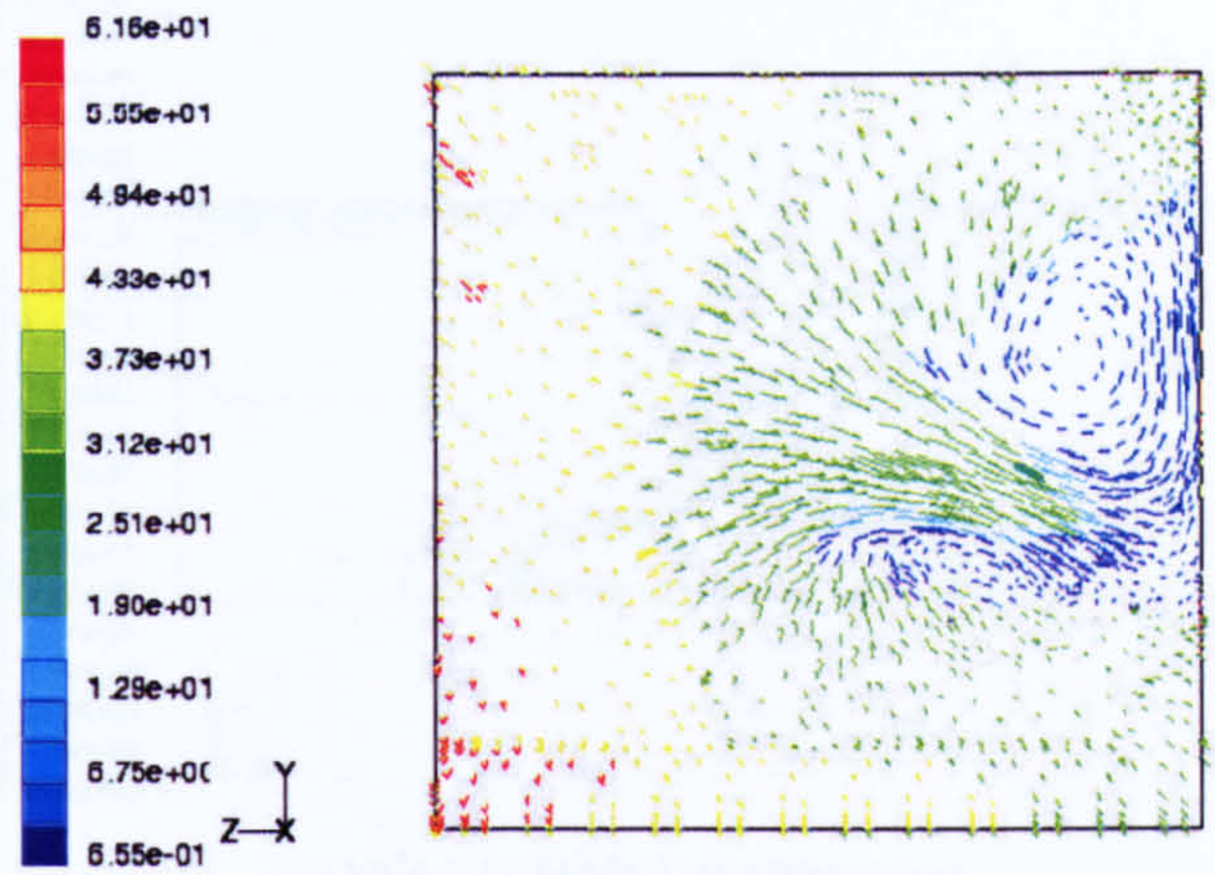

(d) xb=40mm(scale=60%)

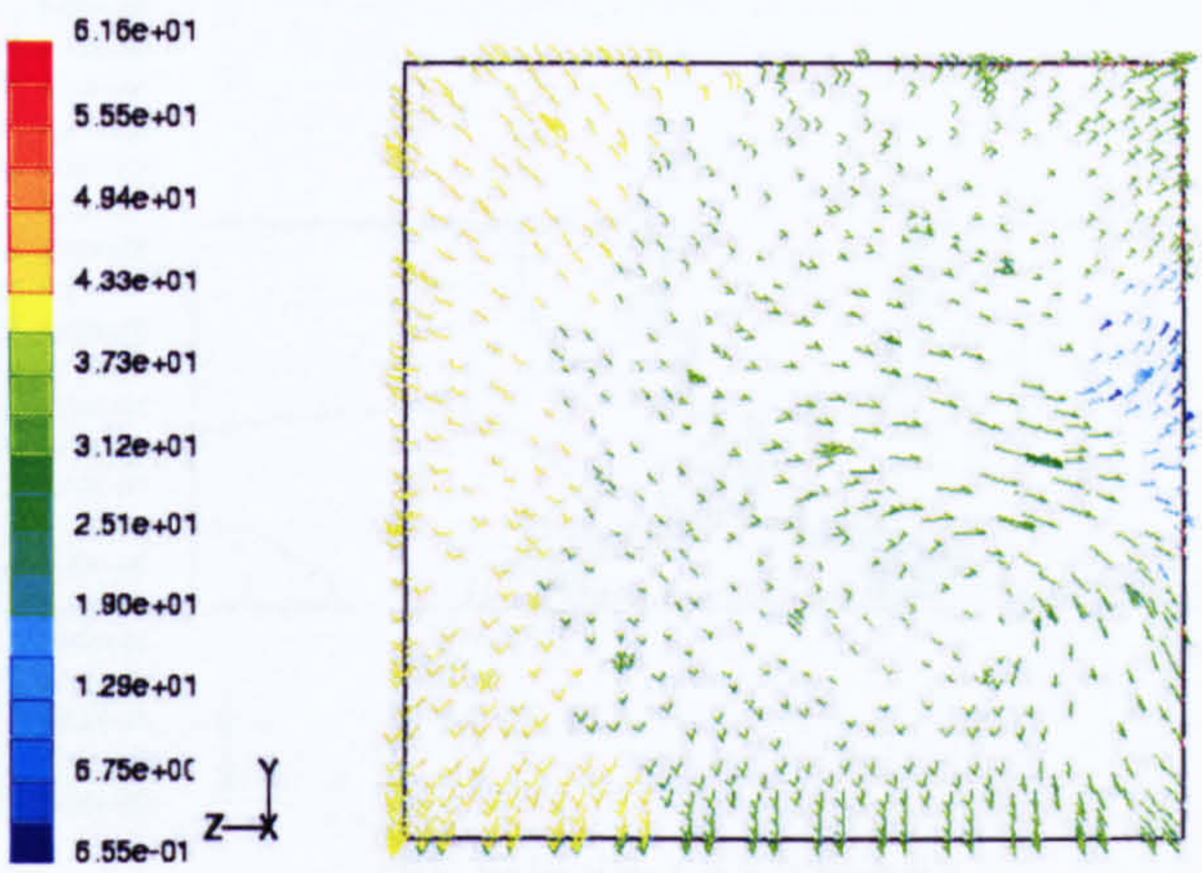

(e) xb=540mm(scale=60%)

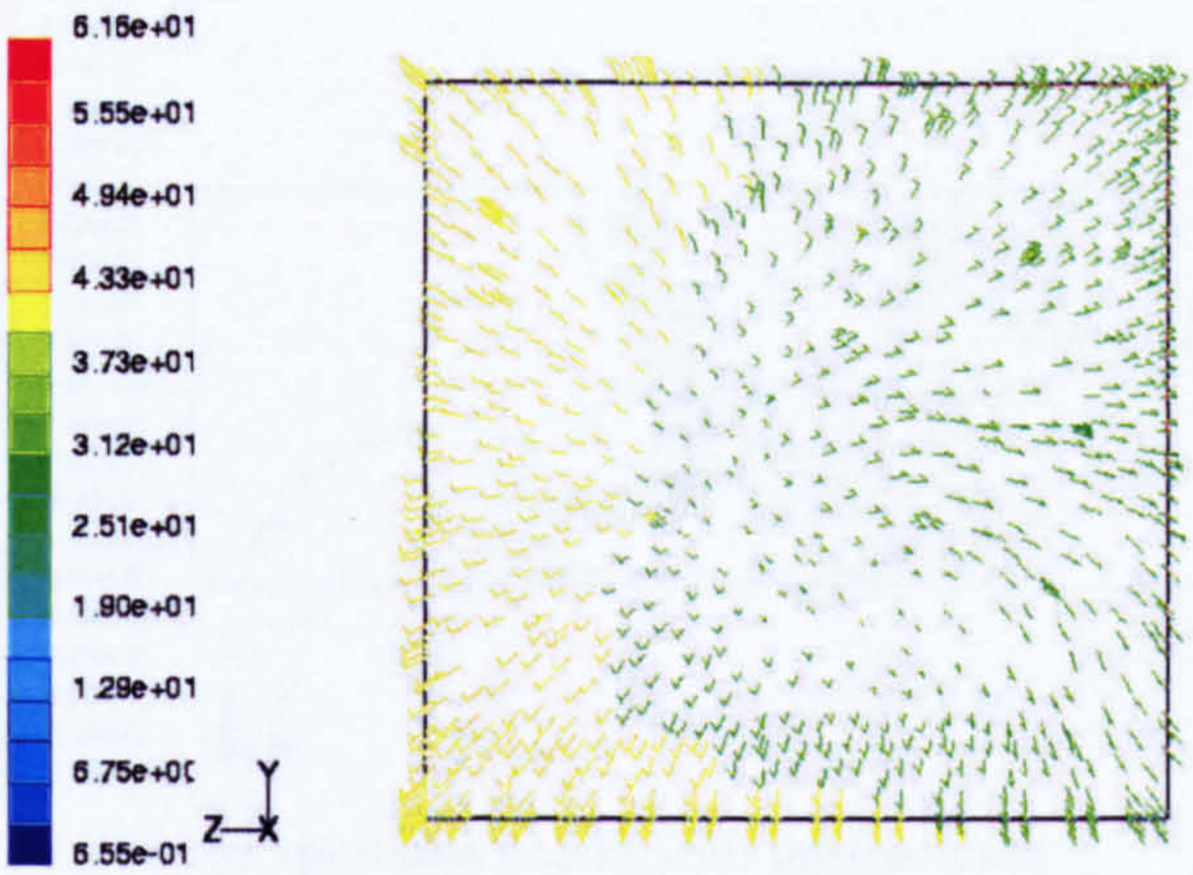

(f) xb=1040mm(scale=60%)

Figure 4.12 Velocity vectors (transverse section) behind the car

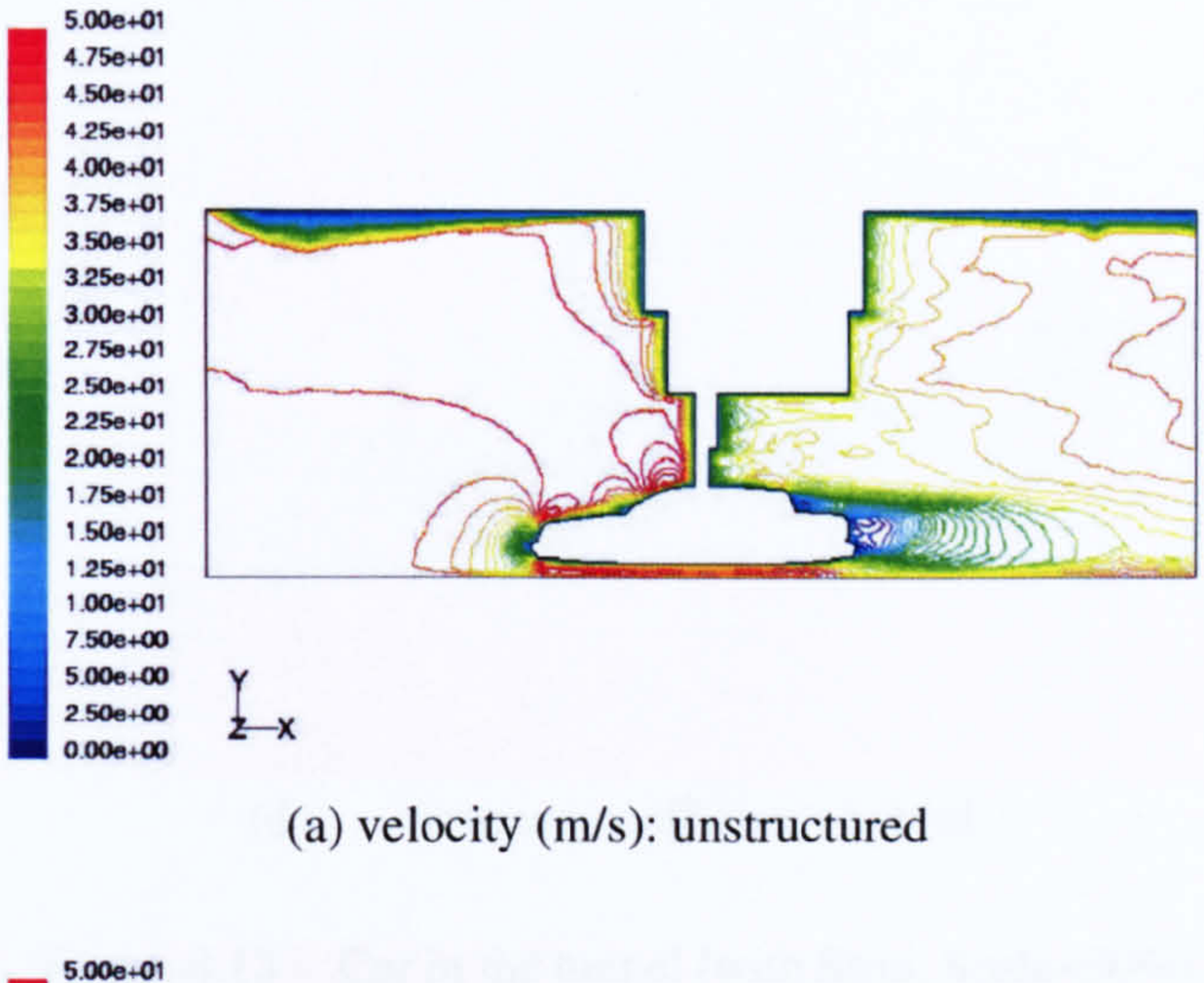

(a) velocity (m/s): unstructured

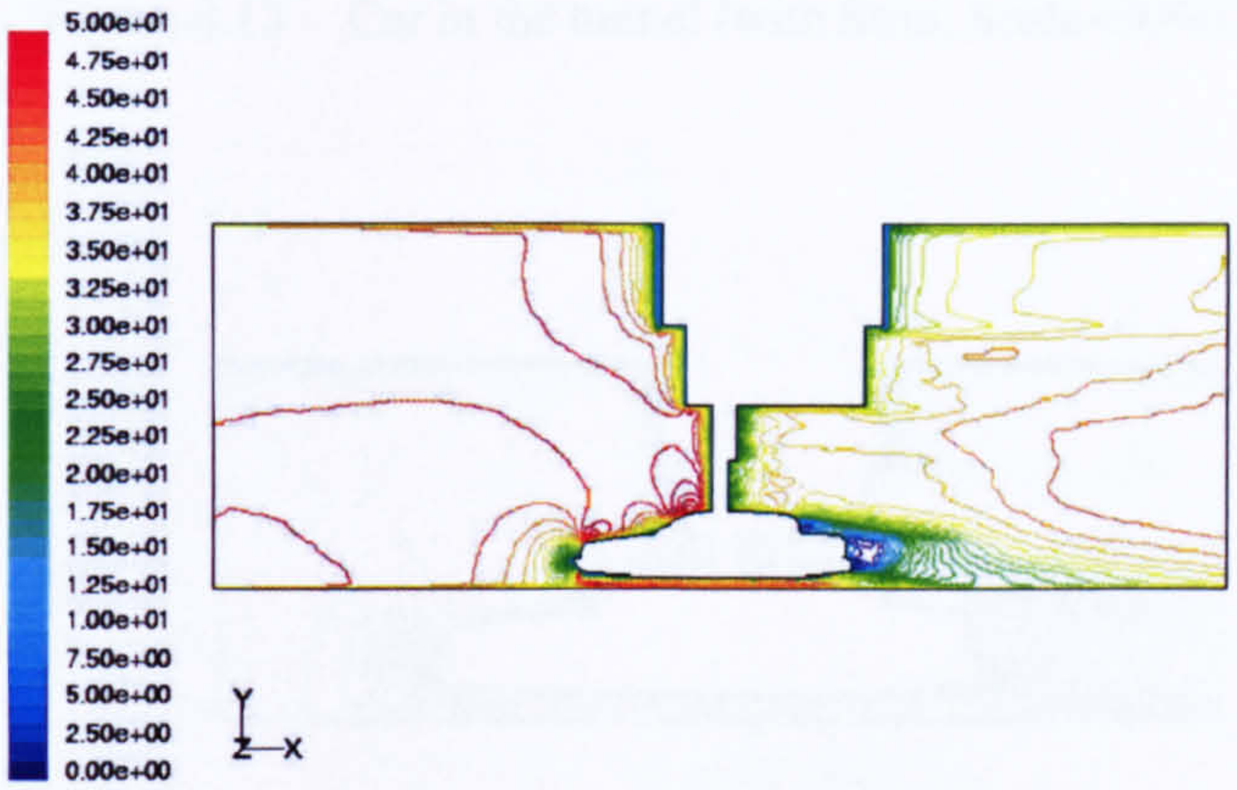

(b) velocity (m/s): hybrid

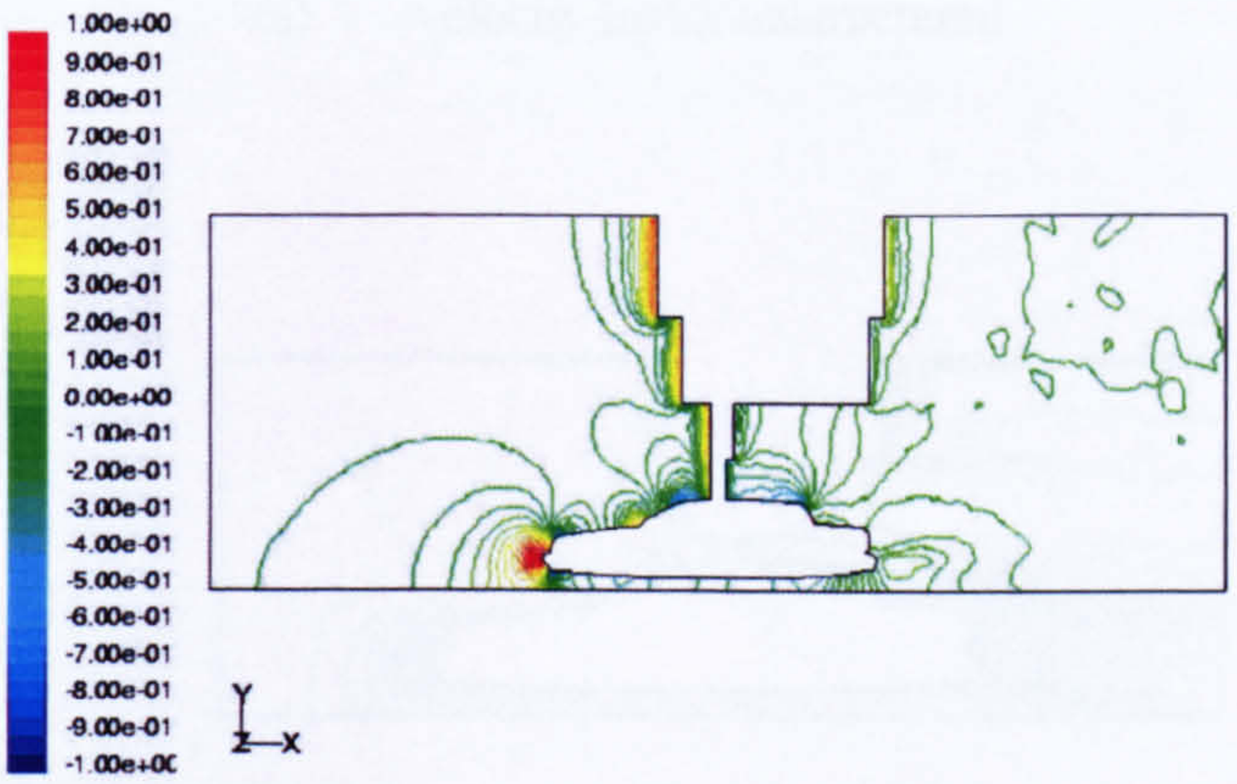

(c) pressure coefficient: unstructured

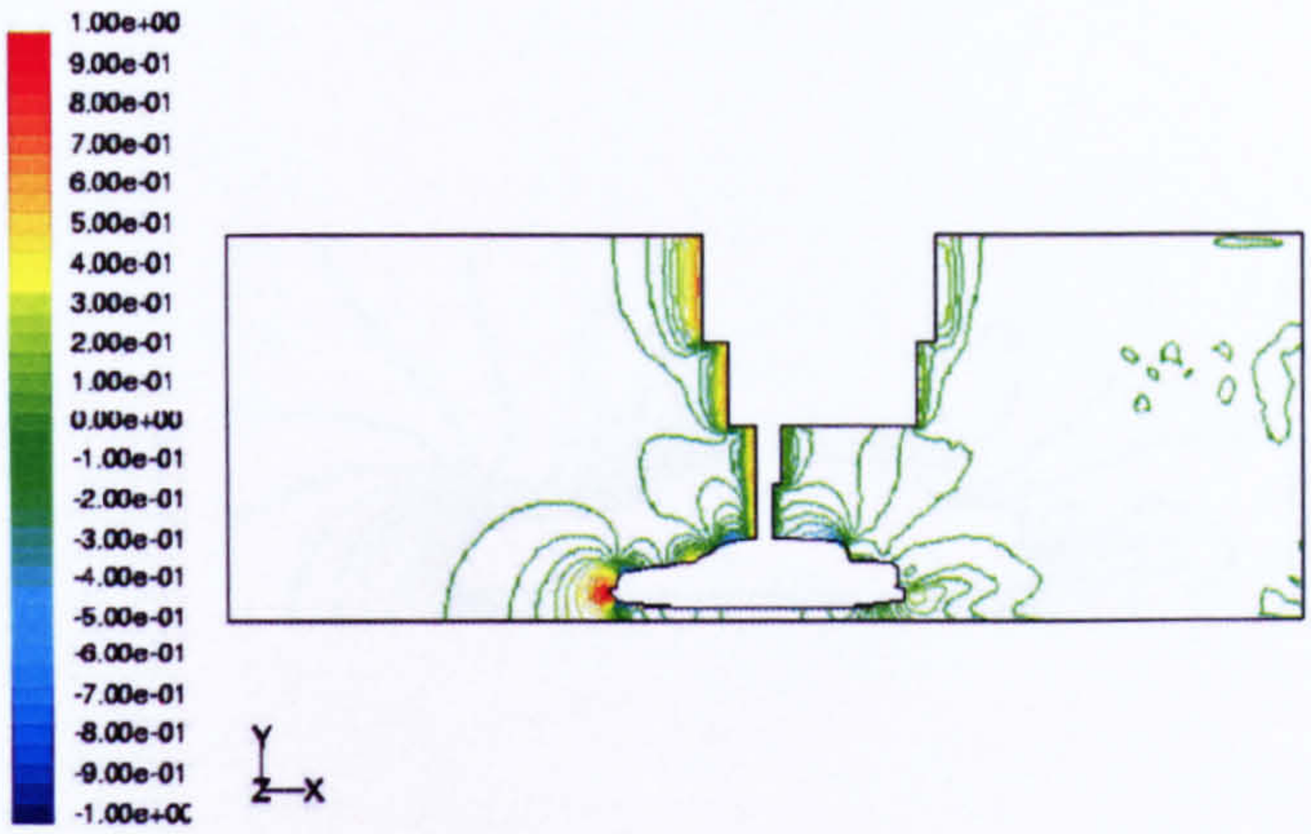

(d) pressure coefficient: hybrid

Figure 4.13 Car in the tunnel (with Strut, Scale=30%)

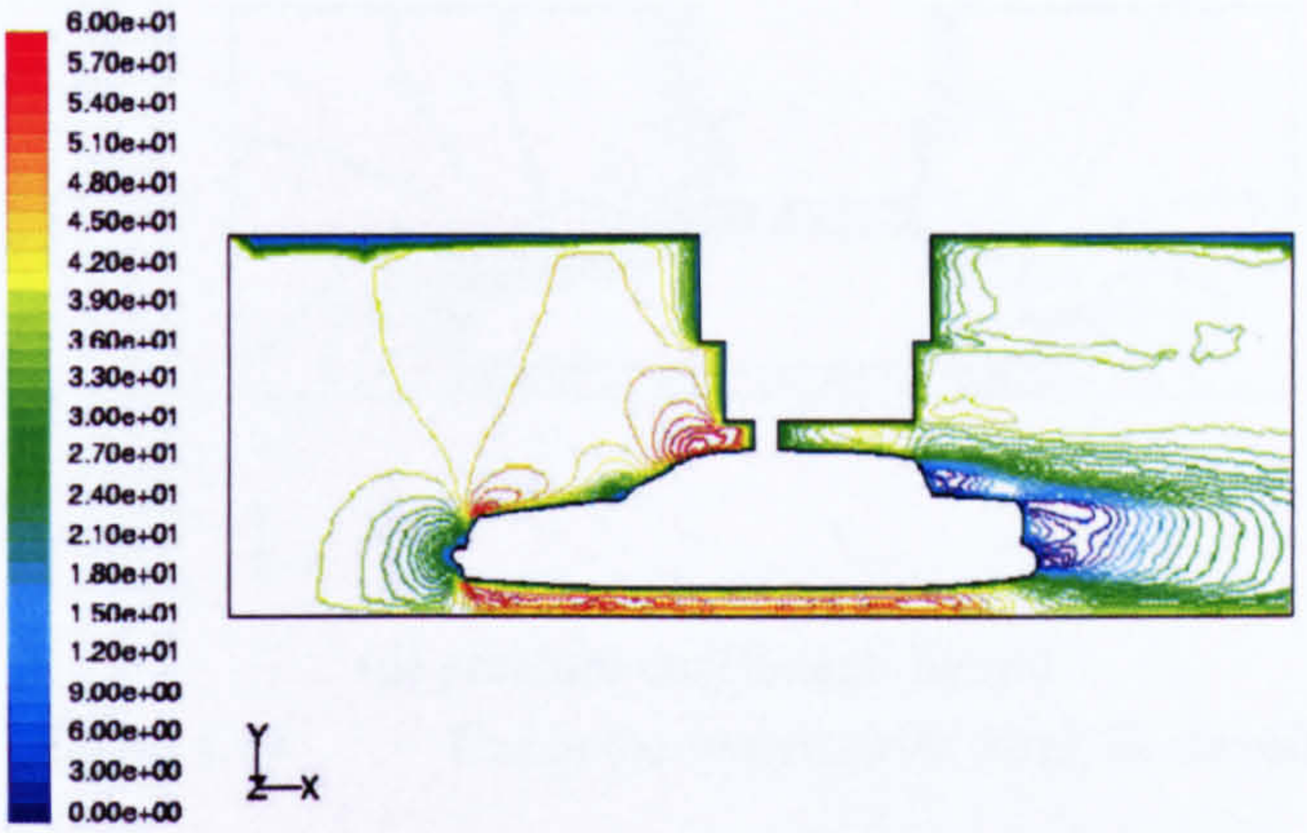

(a) velocity (m/s): unstructured

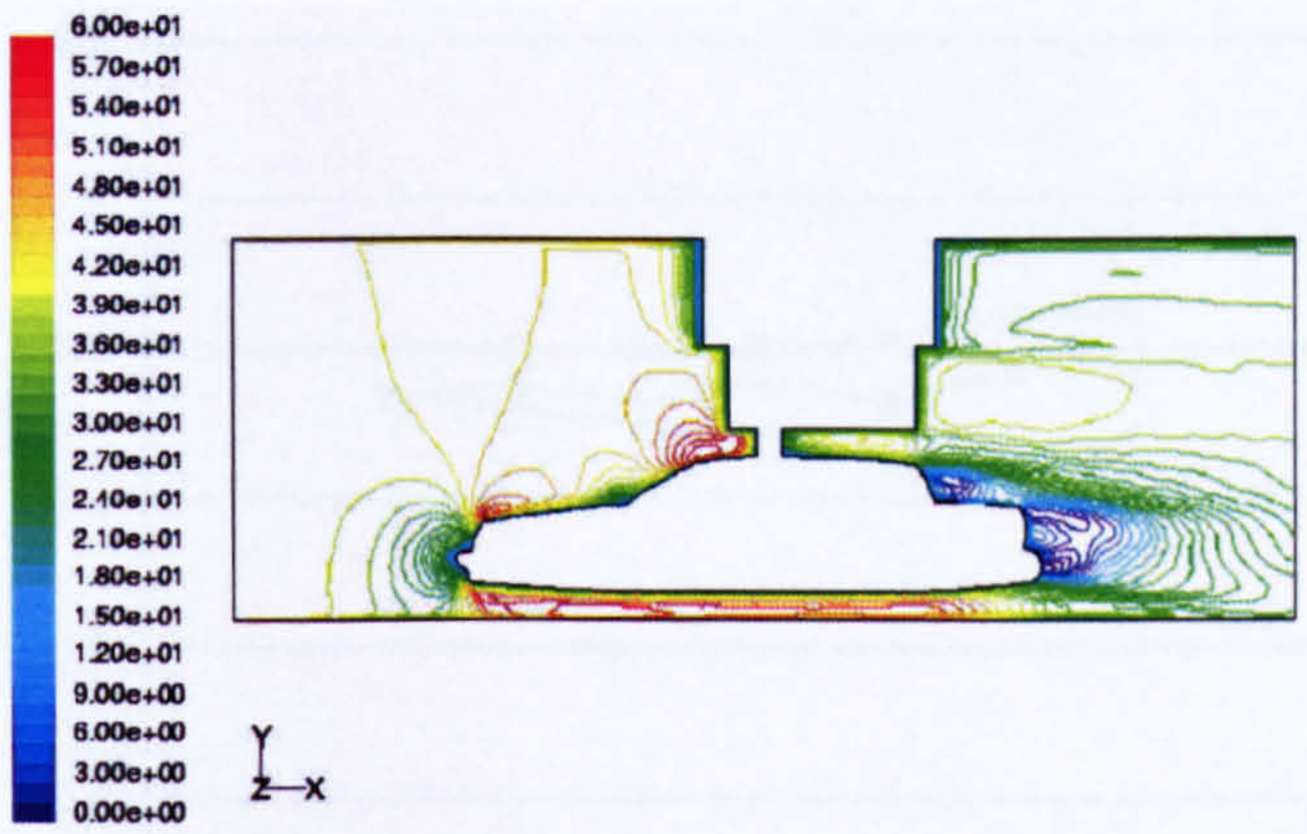

(b) Velocity (m/s): hybrid

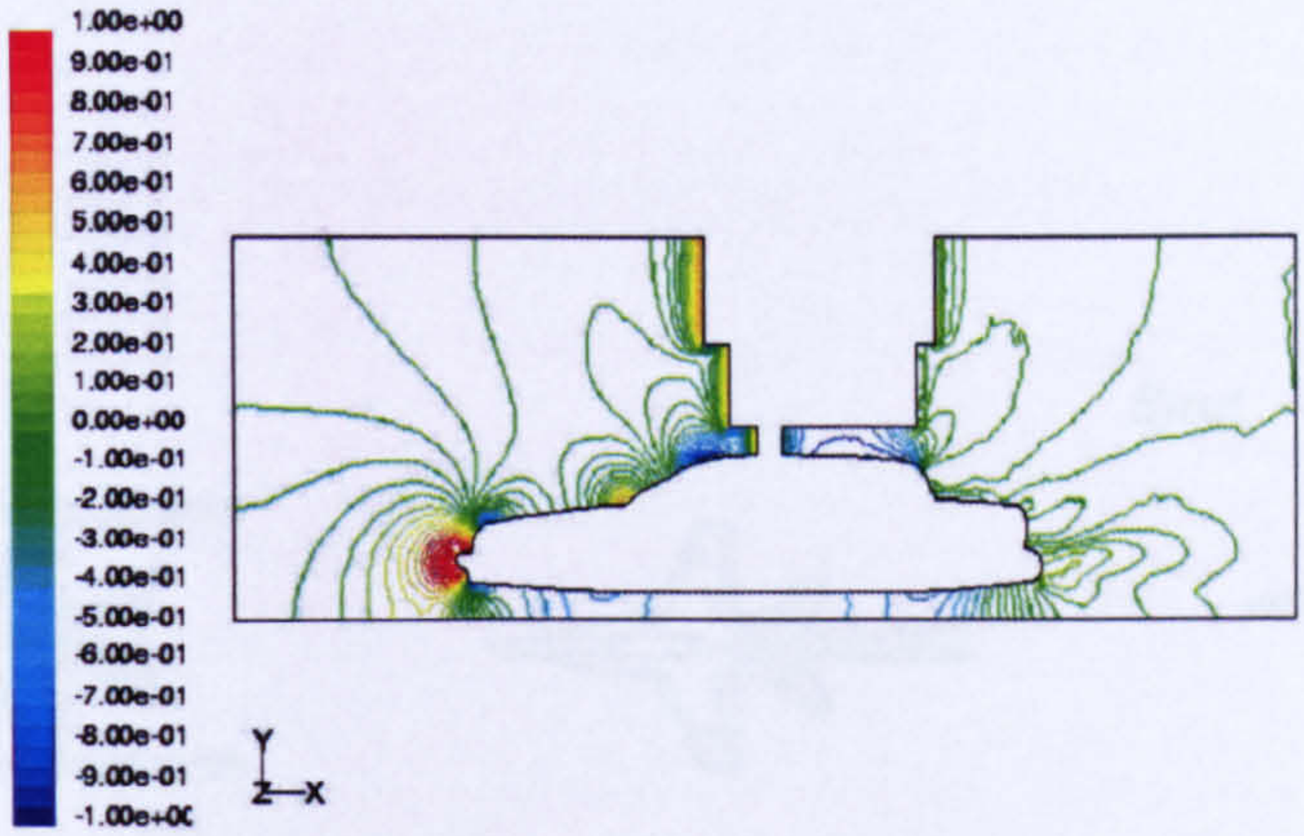

(c) pressure coefficient: unstructured

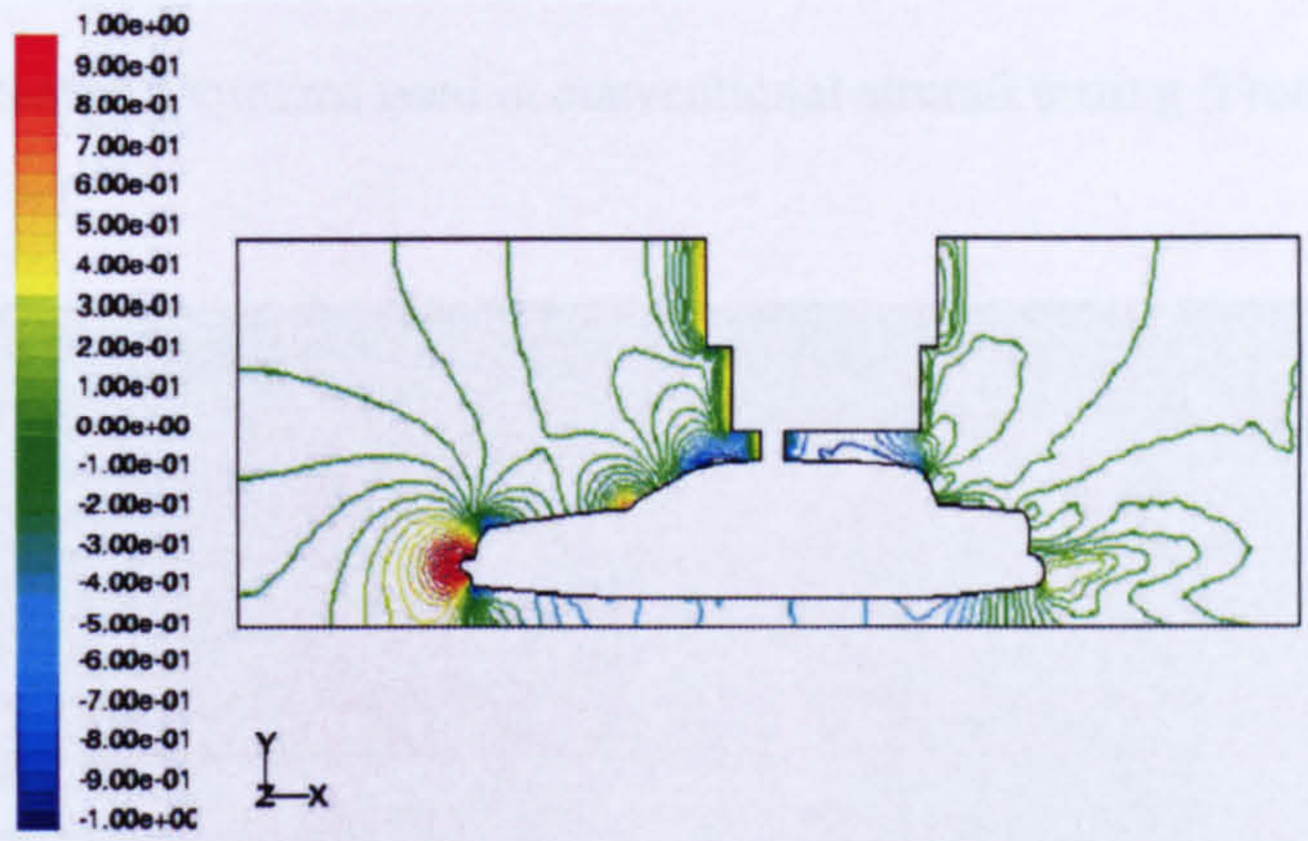

(d) pressure coefficient: hybrid

Figure 4.14 Car in the tunnel (with Strut, Scale=60%)

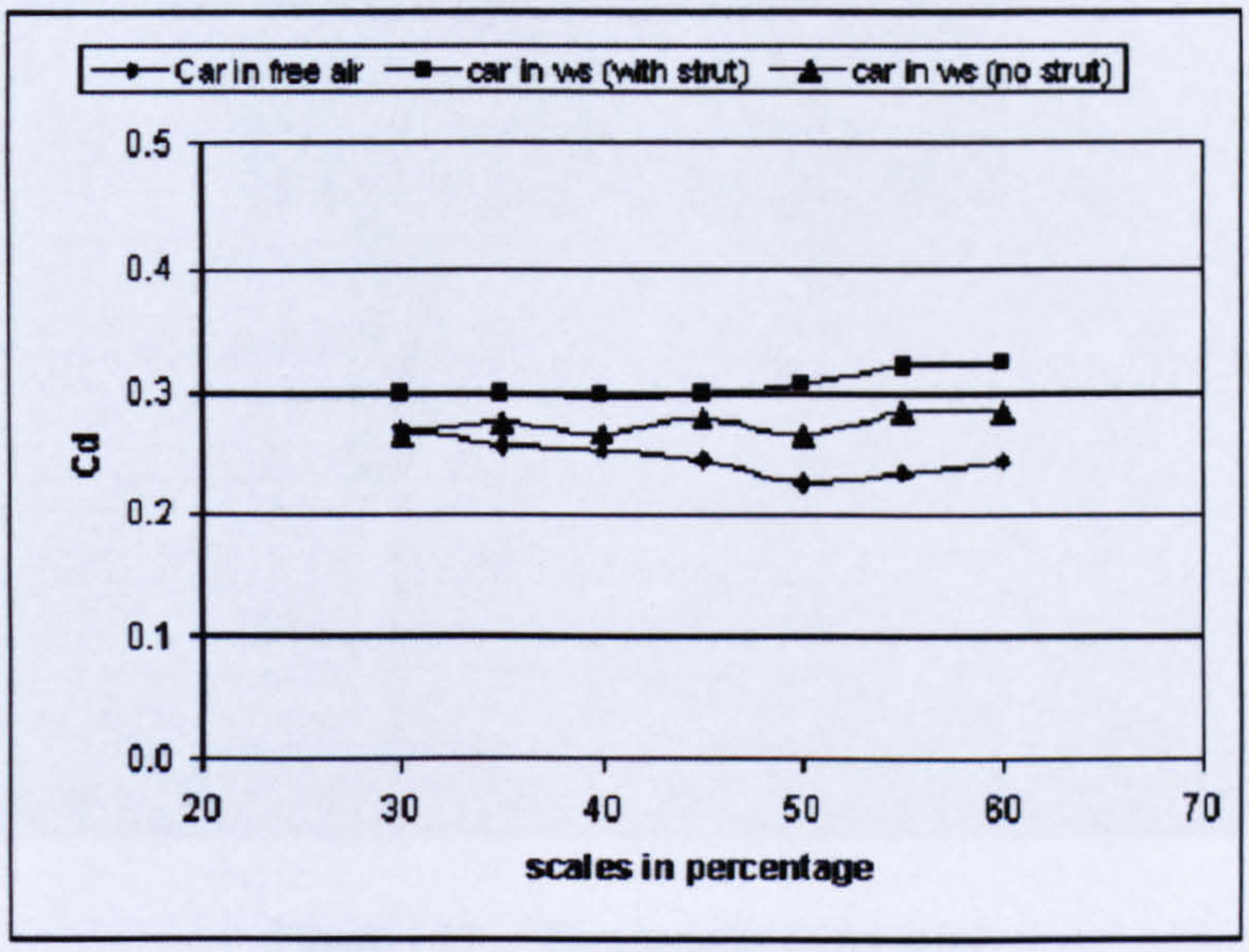

Figure 4.15 Coefficient comparison

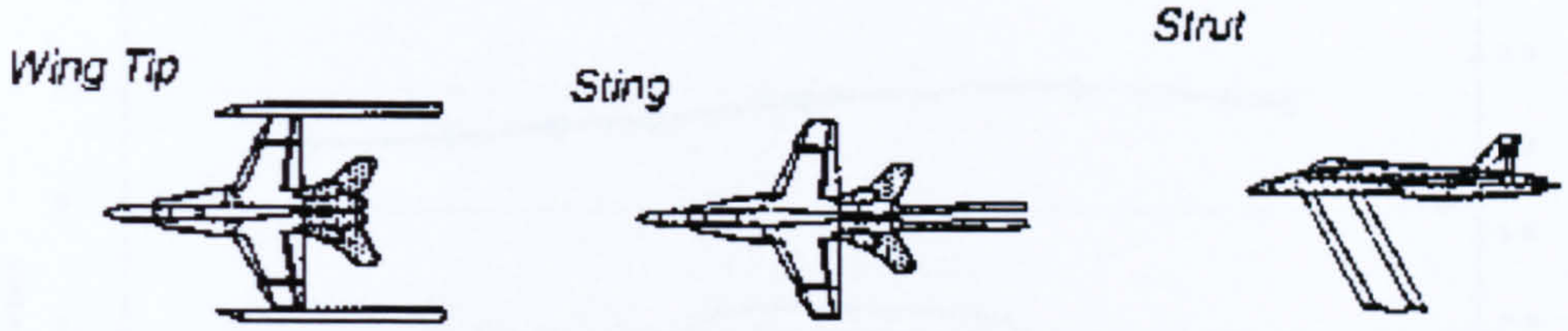

Figure 4.16 Support systems used in conventional aircraft testing (From Niewald 2000)

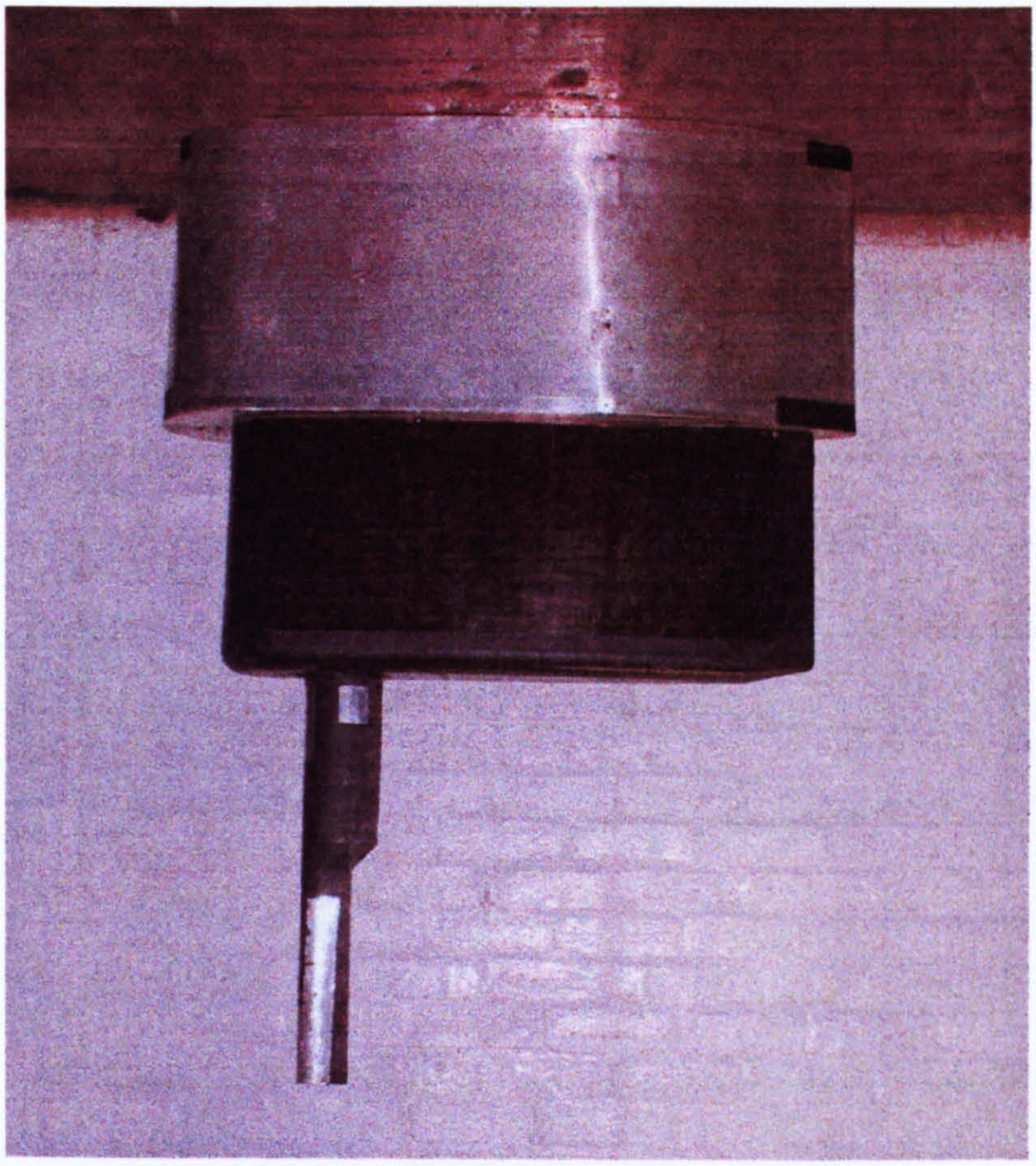

Figure 4.17 Photography of the strut

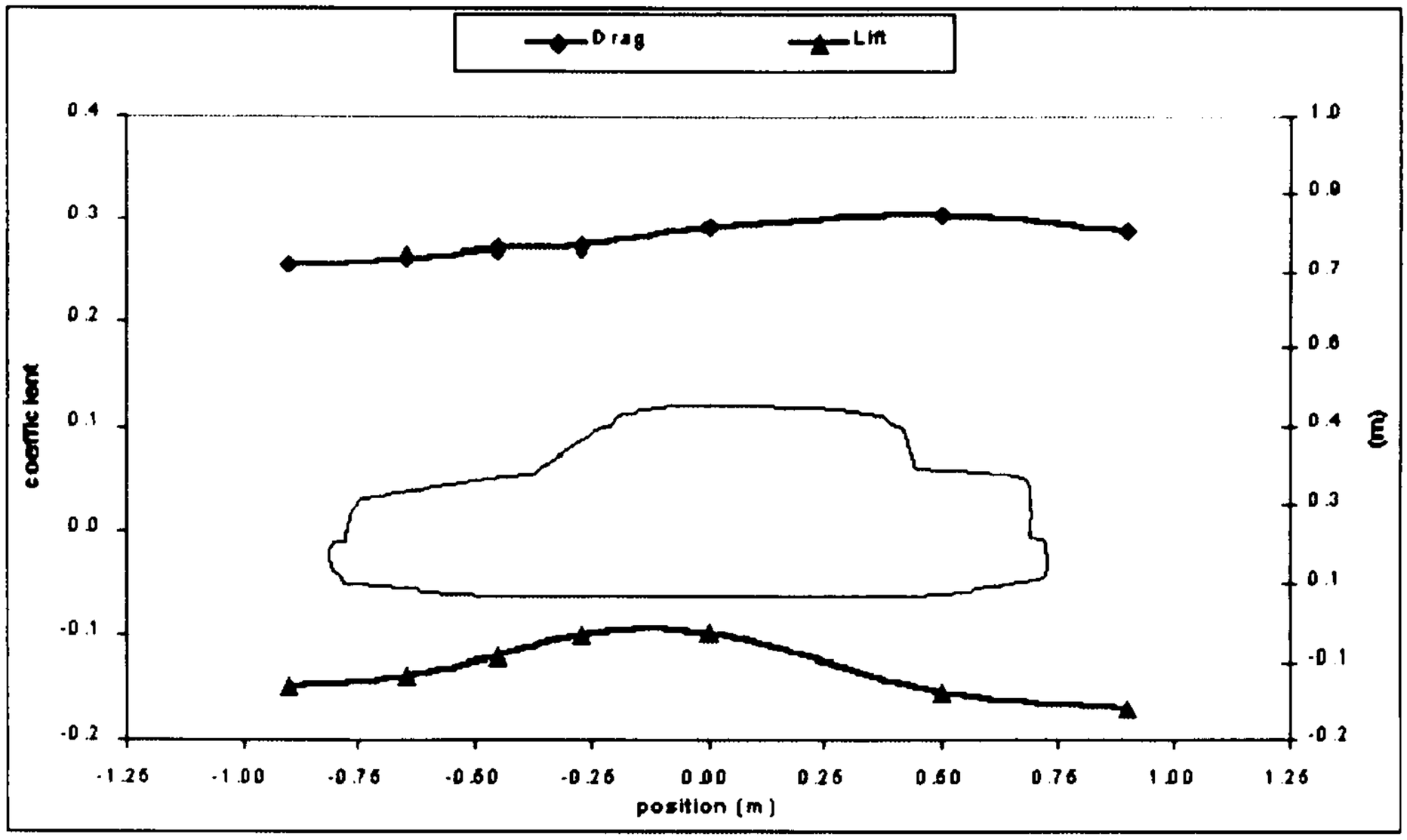

Figure 4.18 Effect of strut position on the drag and lift

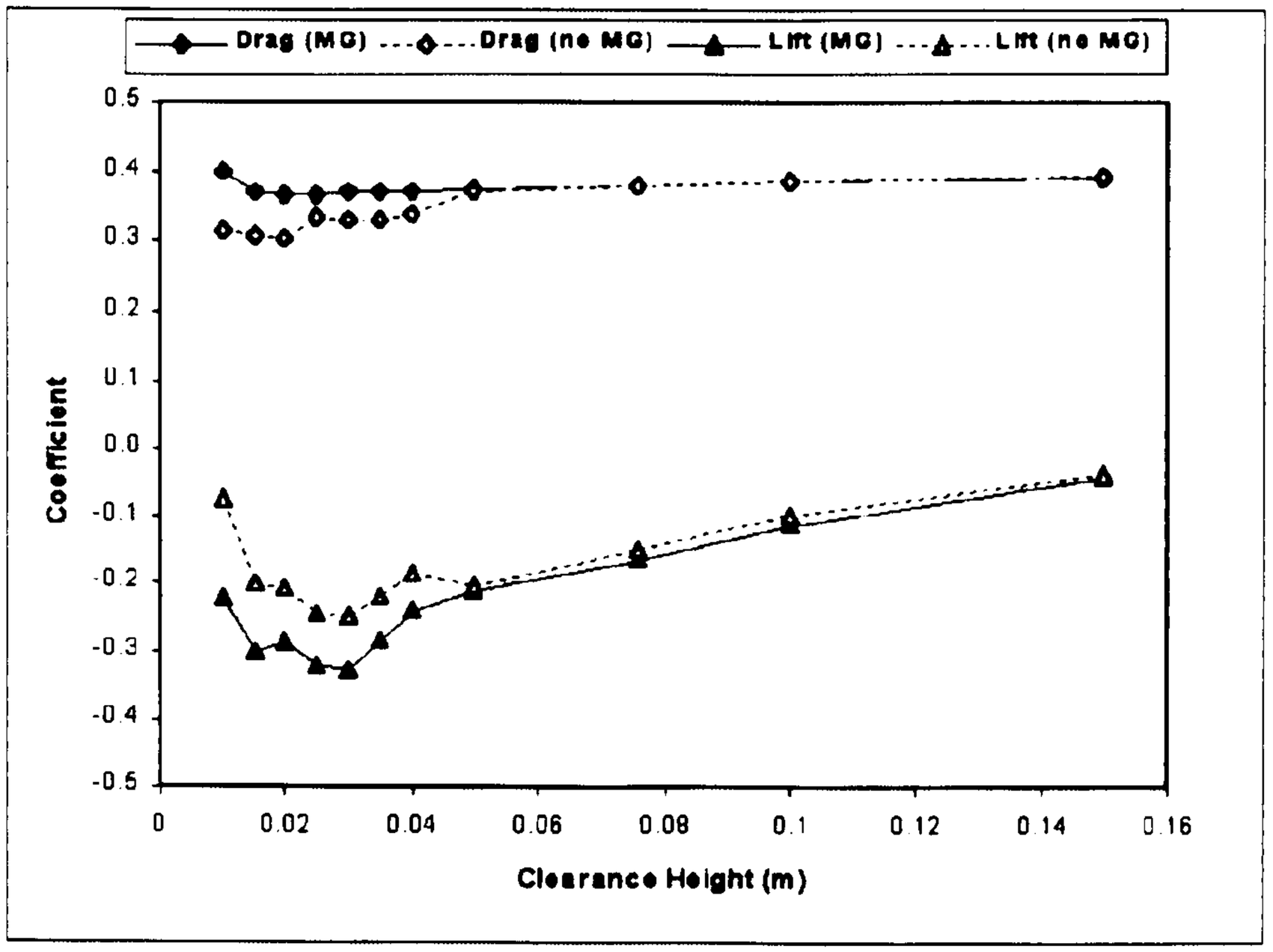

Figure 4.19 Clearance height effect on the coefficients

CHAPTER 5

BLOCKAGE CORRECTIONS AND CFD

5.1 Introduction

Wind tunnel testing is very important in the development of aerodynamics of aircrafts, road vehicles and other fluid dynamics machineries. The conditions under which a model is tested are actually different from those in free air in many ways, even though we accept the idea that there is no difference to having the model still and the air moving instead of vice versa (Rae et al 1984). Some of the differences have significant effects on the test results, for example, the longitudinal static pressure gradient and the open or closed boundaries in the working section usually produce extraneous forces on the test model that must be subtracted out. The former condition produces the drag force known as "buoyancy force", but in some wind tunnels, it is usually eliminated automatically by an expansion design in the working section. The latter may only be corrected by the methods of wind tunnel boundary or wall interference corrections. Rae and Pope (1984) outlined the several effects due to the presence of the lateral boundaries in the working section, some are as following:

- A constraint to the flow pattern about a body, known as "solid blockage". The presence of the model in the working section reduces the area through which the air must flow, and hence, by continuity, increase in velocity over the model. Solid

blockage usually causes the increase of dynamic pressure, the forces and moments at the same condition as the open air.

- A constraint to the flow pattern about the wake known as "wake blockage". When a road vehicle, a bluff body, is in the flow, the vehicle will have a big wake, in which the mean velocity is lower than the freestream. According to the laws of continuity, the velocity outside the wake in the working section must be higher than freestream in order that a constant volume of air may pass through the test section. This effect increases with an increase of wake size and increases the drag of the testing model.

- An alteration to the local angle of attack along the span. In the working section the angles of attack near the wing tips of a model with large span are increased excessively, making the tip stall start early.

- An alteration to the normal curvature of the flow about a wing so that the wing moment coefficient, wing lift and angle of attack are increased in the closed wind tunnel.

- An alteration to the normal downwash so that the measured drag and lift are in error. The closed jet makes the lift too large and drag small at a given geometric angle of attack. And many more.

Fortunately, only few corrections must be applied for most of tests in wind tunnels.

The aerodynamic test of the road vehicles is getting more and more popular in the vehicle design, especially for the formula one racing cars in which the aerodynamic features are

the vital factor in winning or losing. It's well known that the tests of road vehicles are quite different from the aircraft tests. There are fewer attitude changes, but the flowfield around the road vehicle may have quite different flow structures. The requirements of modelling the moving ground add more different characteristics. As a result, the corrections of test data for road vehicles may need quite different correction methods.

The fundamental problem of wall corrections concerns itself with the difference between the flow fields around a body immersed in a uniform oncoming stream of infinite lateral, upstream, and downstream extent, and around the same body in a stream confined or modified by wind tunnel walls, as shown in the previous chapter. Generally, the streamlines around a test model in a uniform flow depend on the shape of the body and on the aerodynamic forces acting on the body. In the open-air cases, it is defined as interference-free, for the distance increases laterally from the test model, the streamlines tend to approach the straight and parallel flow of the oncoming stream. If the wind tunnel walls are far enough away from a model being tested so that the flow perturbation due to the model is negligible, the same uniform parallel flow condition is obtained at the boundary and the flow around the model is therefore not affected by the tunnel boundaries. However, when the models influence is perceptible at the boundary, the flow within the tunnel is generally different from that which would be obtained in an unbounded stream. In the long history of wind tunnel test, people have tried to develop the methods to correct the wall effects, and the wall correction theory attempts to account for this difference under a set of simplifying assumptions and corresponding restrictions on the theory's range of applicability.

5.2 Blockage Correction Methods

The conventional wall correction methods are most developed on subsonic linear and inviscid flow hypothesis: potential theory. Most of these theories were published before 1950 and some appeared as early as 1920's. In many cases, the routine correction methods, such as those formulated by Prandtl and Glauert etc as early as the 1930's, have remained in use even in large high quality wind tunnels, in spite of the other novel and sophisticated methods that have been developed (Ewald 1998). Nevertheless, during this period, a large amount of theoretical and experimental studies of the tunnel wall interference were done, such as image correction methods, the panel methods, the boundary measurements methods and the recent computational fluid dynamics methods et al. The recent developments have been influenced by the rapid improvements in computing speed and power.

5.2.1 Classical Methods

Classical correction methods include the image methods and panel methods, which are generally based on the assumptions of potential flow and small blockage:

i) The flow considered is linear potential flow

ii) Perturbation flow at the tunnel boundaries

iii) Model whose dimensions generally are small relative to the tunnel and whose wakes extend straight downstream from the model

iv) Tunnel of constant cross-sectional area extending far upstream and downstream of the model, with boundaries parallel to the direction of the flow far upstream of the model,

and whose boundary condition for a given wall is either no flow normal to the wall or a constant pressure at the wall location.

Under those hypotheses, the methods are capable of representing the models by sources/sinks, doublets or vortices or their combinations. Figure 5.1 summarizes the representations of the elementary singularities. In the general case, a solid body can be represented by a source-sink system, a wake by a source, a wing by a lifting line vortex or a pair of trailing and so on.

Image methods:

In the image methods, the tunnel walls are taken as the mirrors, where the images can be produced. Figure 5.2 shows the image system for a singularity in a rectangular working section. The tunnel with a simple cross section provides the simplifications, permitting the application of analytical techniques. Therefore, the image methods are applicable in the relative simple tunnels, such as rectangular section tunnels. However, for the more complicated tunnels like the octagonal and elliptical tunnels, the researchers have extended the applications to the specific tunnels by the conformal transformation techniques.

The image methods are well developed and documented, and the corrections are usually available in many particular problems, like 2D/3D lift interference, 2D/3D blockage interference, 2D/3D wake blockage and so on, the details can be obtained in references (Rae et al 1984, Ewald 1998 etc).

Panel methods

Panel methods share the same fundamental theory and assumptions as the image methods. However, the panel methods have advantages over the image methods in both model and tunnel representation. The panel methods provide the tools capable of analysing a large and complex model, and modelling the wind tunnel directly, in which the arbitrary cross-section tunnels can be addressed, and even the support systems can also be included.

In the panel methods, the potential in the flows is the sum of the potentials of all panel singularities, while the interference velocity potential of the walls is the sum of all the wall panel potentials. The models and the tunnels can be represented by singularity distributions on their surfaces, in which the singularities are fundamental solutions of Laplace's equation. Figure 5.3 shows the panel discretisation of walls of working section including the settling chamber, contraction, and diffuser (Wang et al 2000), where a prescribed wake model was also used to represent the wind turbine and its wake. Then, the source strengths of the prescribed wake model were determined by the induced velocity, and by the boundary condition of zero normal velocity on the solid tunnel wall. Then the wake model is used to assess the basic effect of wind tunnel walls on wind turbine flow and performance.

The panel methods used to predict wall interference have in many cases replaced image methods for the closed-wall tunnels, and their use may be strengthened by the requirements: more accurate specification of the wall boundary conditions and more accurate representation of the fluid physics. The present trends in the development of panel methods are in both the wall representation and the physics modelling. Wall boundary condition descriptions have moved toward one- and two-variable methods,

while the flow physics modelling includes the treatment of separated wakes, vortex wake relaxation techniques, and the inclusion of compressibility in the flow equations for high-speed flows etc. The success of panel methods over a wide range of subcritcal flow conditions suggests their use not only in routine testing applications within their accepted range of validity, but also a touchstone against which advanced methods may be tested (Ewald 1998).

5.2.2 Boundary Measurement Methods

The ruthless competition makes the airplane manufacturers require more reliable prediction methods for the design of aircraft, therefore, advanced measurement methods and more reliable correction methods are urgently needed. It's known that the linear theory descriptions of the near-field flow around the model are increasingly inadequate as free-stream Mach number increases towards unity. This led to the idea of using wall pressures to determine the strengths of the singularities representing the model. Although the importance of the measurement of flow conditions at tunnel walls has been known for some time, but it's possible only when the sufficient computing power is available to make use of the information.

For the boundary measurement methods, numerical approximations include two methods when the effect of the wall boundary layers can be ignored: wall pressure signature method and two-variable method. For attached flows, the wall signature method is easy to apply and requires a small number of wall-pressure measurements on the tunnel walls. The model may be represented without difficulty by distributed singularities. The two-variable method, on the other hand, needs no model representation, but requires as many as

hundreds of wall pressure measurements (Ewald 1998). Figure 5.4 gives the typical arrangement of the pressure measurement points. It is usually inapplicable for most wind tunnels in the world.

5.2.3 Computational Fluid Dynamics (CFD) Methods

The advances in computer speed and memory and in numerical techniques make it possible to use complex CFD techniques in the wall interference corrections, while the demands of more accurate correction methods and increasing complicated test conditions accelerate CFD techniques utilized in the improvement of the wind tunnel wall interference corrections. Improvements and utilization of CFD techniques in assessing wind tunnel models are required for the following reasons:

i) The growing need for accuracy in wind tunnel testing mainly for commercial transport aircraft development. The aircraft manufacturer may need the accuracy of the drag measurement of 1 count due to the ruthless competition

ii) The recognition that the ability to test at flight Reynolds Numbers in some specific wind tunnels, such as the cryogenic wind tunnels, is only valuable if the wall interference corrections can be estimated with sufficient accuracy.

iii) The need to perform accurate wind tunnel assessment of CFD methods.

In tunnels with large models, the classical approach often fails to give the correction to the wall interference, since interaction between model and tunnel walls is strong, and the significant interference gradients develop about the model, and the linear wall boundary condition is not actually applicable. The boundary measurement methods are usually

limited in utility due to the requirements of too many pressure measurements on the tunnel walls.

Figure 5.5 outlines the general idea of the CFD correction method. Firstly, the CFD solver is used to simulate the aircraft model in the tunnel test conditions and in the free air. Secondly, the differences between the tunnel conditions and free air can be considered as incremental differences of the wall and support system effects. Finally, the differences are directly applied to the experimental data as the correction values.

In CFD correction methods, the test models and the tunnels are represented in real geometries. Therefore, the methods can deal with arbitrary complicated test models and tunnel cross-sections.

5.3 Blockage Corrections for Bluff Bodies

The flows around bluff bodies are quite different from and much more complicated than those of streamlined bodies. It's common that the bluff bodies have leading-edge separation with/without re-attachment and have large unsteady regions of separated flow further aft on the body. The physics of the interaction of the boundaries of a wind tunnel test section on these wake flows was explored by Maskell (1965), based on an analysis of measurements made on three-dimensional flat plates mounted normal to the flow. His results illustrated that the wall constraint in closed test sections was five times greater than predicted by the classical derivations for bodies with thin wakes. It was also clear that large separated flows from stalled wings and bluff bodies must be treated differently than the attached-flow cases.

In recent years, the major developments in wall corrections for bluff shapes have come through the development of boundary-measurement-based methods. Where the mathematical models that are used to represent the bodies in the test section are sufficiently general to extend to both bluff and streamlined shapes.

Ranzenbach et al (1999) proposed a wind tunnel boundary correction method using a wall signature method for a bluff body. The main idea is that there is a source/sink representation of the model and the wake, while the pressure distribution measured along the tunnel walls is used to determine the streamwise velocity distribution along the walls using Bernoulli's equation. Matching the flow velocity computed from the measured wall pressures and the mirror image method, the resulting source/sink distribution is obtained, which can be used to compute the velocity distribution induced by the tunnel walls.

5.4 CFD Application in Blockage Corrections

Many wall interference correction methods are based on the potential theory, which means the representation of the model in the tunnel is in the form of sources, sinks, doublets, vortices or their combinations. Here CFD methods refer to solving the Navier-Stokes equations with the advanced turbulence models. The representations of the tunnel walls and the model under test are high fidelity, based on the modern numerical geometry and mesh generation.

To validate the numerical consistency, a practice of the blockage effect for the numerical results in different blockages was presented here. Figure 5.6 gives the numerical prediction results of drag coefficients in free air and in tunnel with/without strut support. If

the CFD direct difference correction is employed, the drag coefficients in tunnel with/without strut should be corrected to the case of free air. The correction is very direct, and the differences are easy to get.

Now another correction is adopted. Following the correction method put forward by Ranzebach et al (1999), the correction expression for the drag coefficient is simply adopted as follow:

$$C_{dc} = \frac{C_{du}}{(1+\varepsilon)^2} \tag{5.1}$$

where C_{dc} Drag coefficient after correction

C_{du} Uncorrected drag coefficient

ε Blockage ratio (defined as the ratio of frontal area over the tunnel section area, in the case with strut, the frontal area include that of strut)

After correction, the drag coefficients are shown in Figure 5.7. The corrected drag coefficients are very close to the case in free air, except the very high blockage of 18.6% (70% scale model). In the numerical results, the correctable blockage for the case with strut is up to 60% model scale, the corresponding blockage ratio is 16.4%, and for the case without strut, the correctable blockage is up to 65% model scale, blockage ratio is 16.1%. When the model scale is up to 70%, the strong interference is produced by the wall restrictions, which is considered as uncorrectable area.

5.5 Concluding Remarks

Blockage and wall interference have been a difficult problem for tunnel engineers for a long time. In the long history of wind tunnel test, the different correction methods have been developed. Among the conventional correction methods, classical methods are easy to apply, but limited to the simple problems; and the boundary measurement methods are the advanced correction methods, but need too many measurements on the tunnel walls; CFD methods still require significant development.

In general, the classical correction methods are usually restricted to the small blockage case, or low Reynolds number or simple flow condition, while the boundary measurement methods are even applicable to bluff bodies, as shown by Ranzebach et al (1999).

In this chapter, the advanced CFD techniques are employed to assess the correction methods for the wind tunnel experimental data. The advantages of CFD techniques are that the test model and the tunnel walls can be represented in high fidelity. Once the numerical simulations have been completed, the direct difference compensation method can be made to correct the experimental data.

To prove the consistency and the feasibility of the correction, numerical investigations for different blockages have been conducted. Compared to the conventional correction approach, the CFD approach shows the very good results.

Figures of Chapter 5

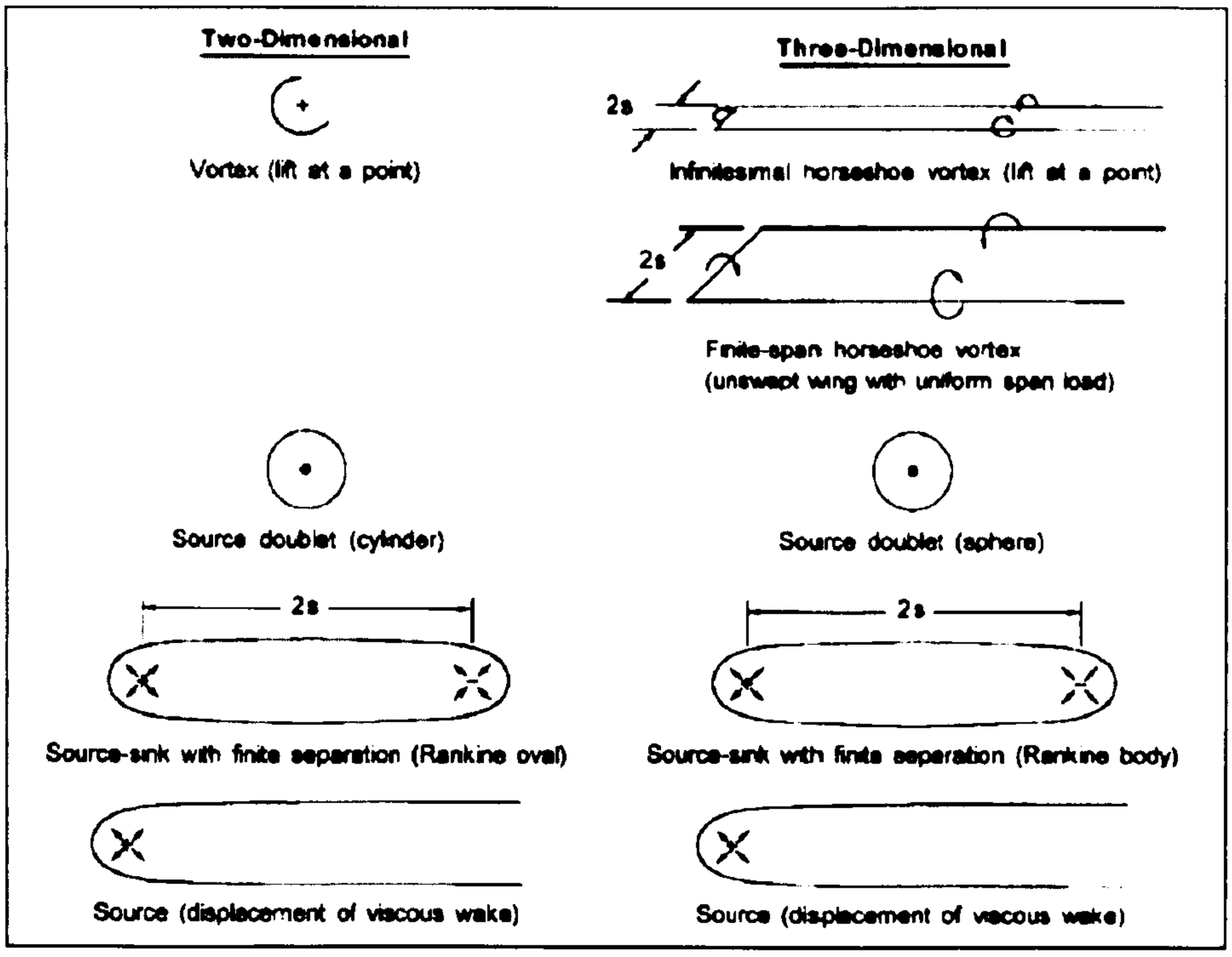

Figure 5.1 Model representation with elementary singularities (Ewald 1998)

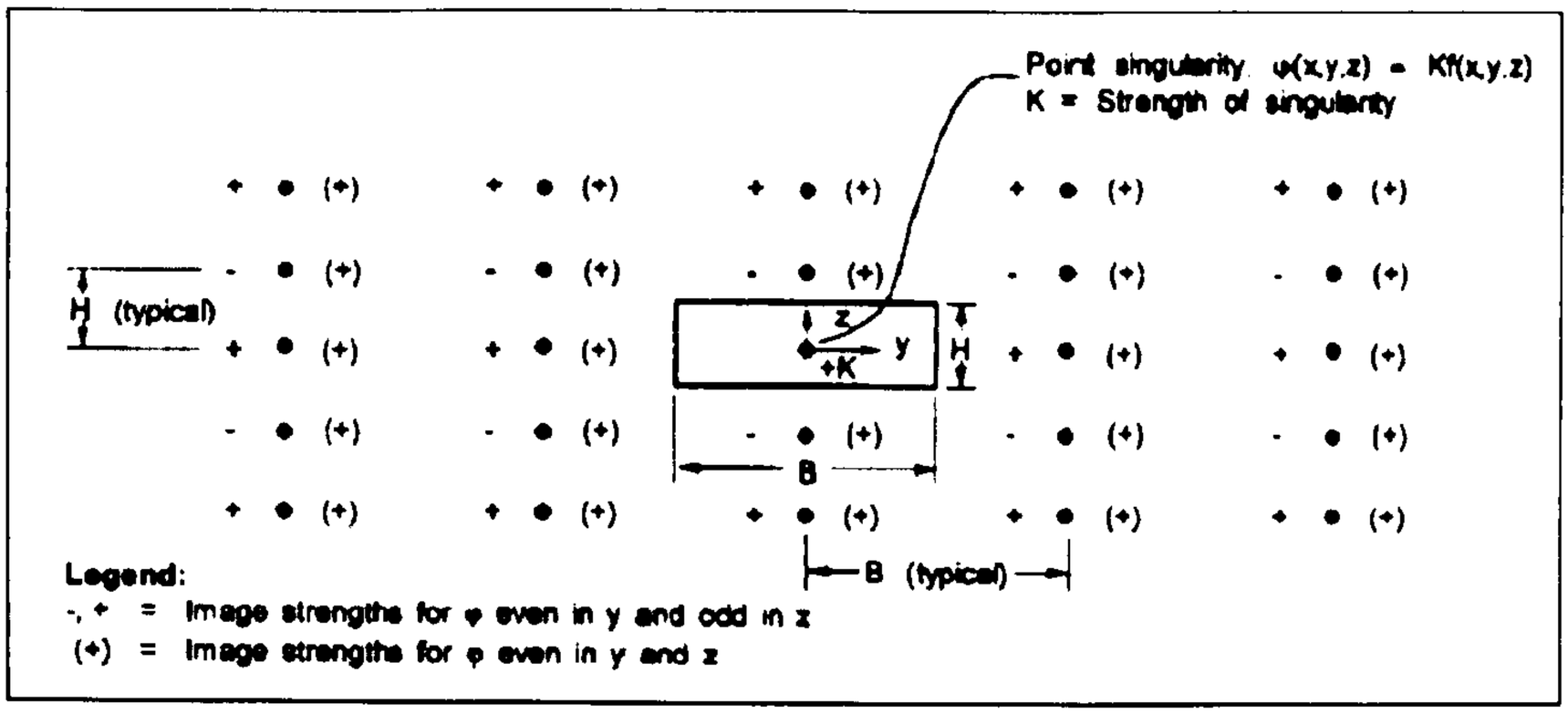

Figure 5.2 Image System for a Model in the Rectangular Working Section (Ewald 1998)

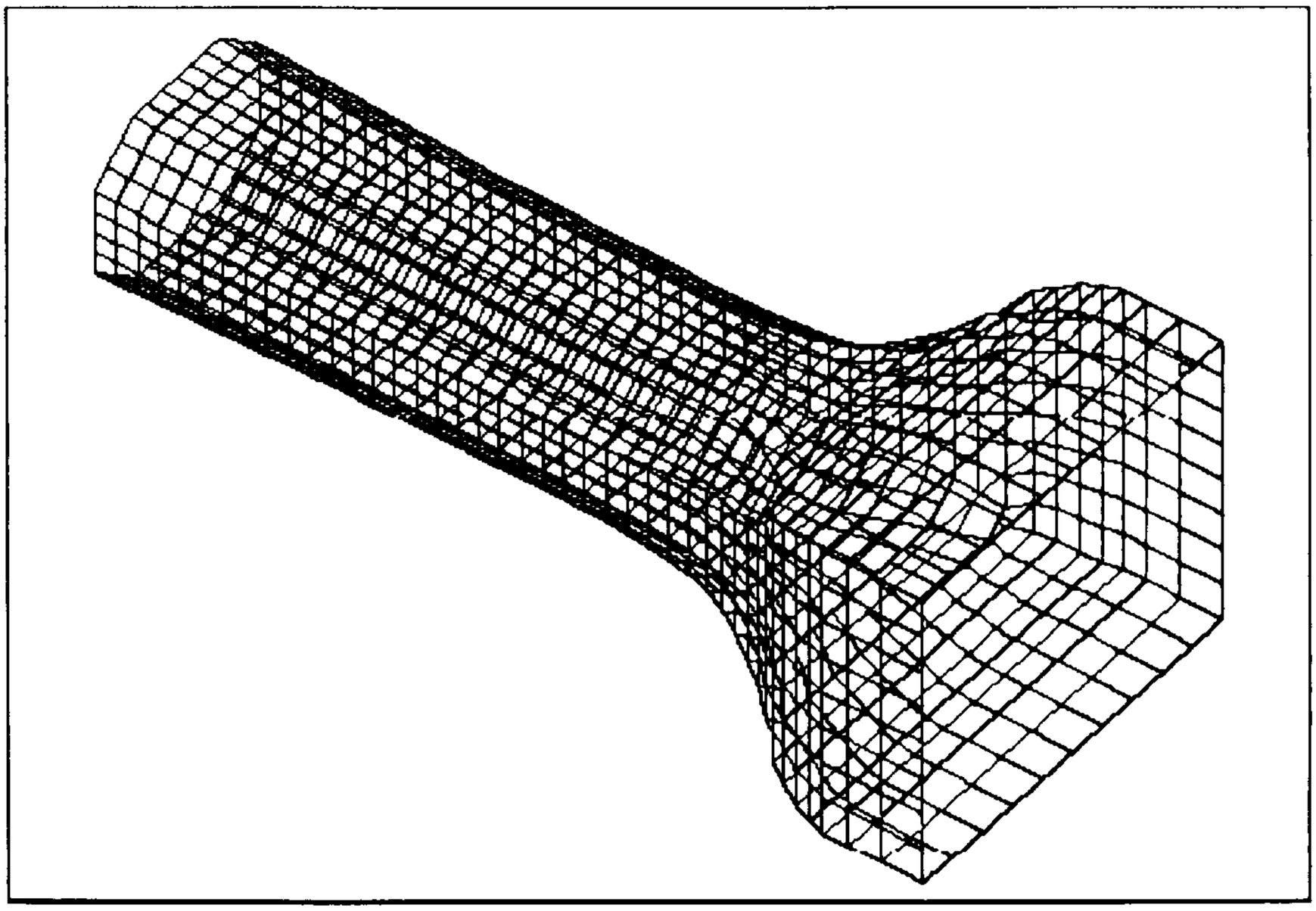

Figure 5.3 Panel discretisation of the wind tunnel settling chamber, contraction, working section and diffuser (From Wang etc 2000)

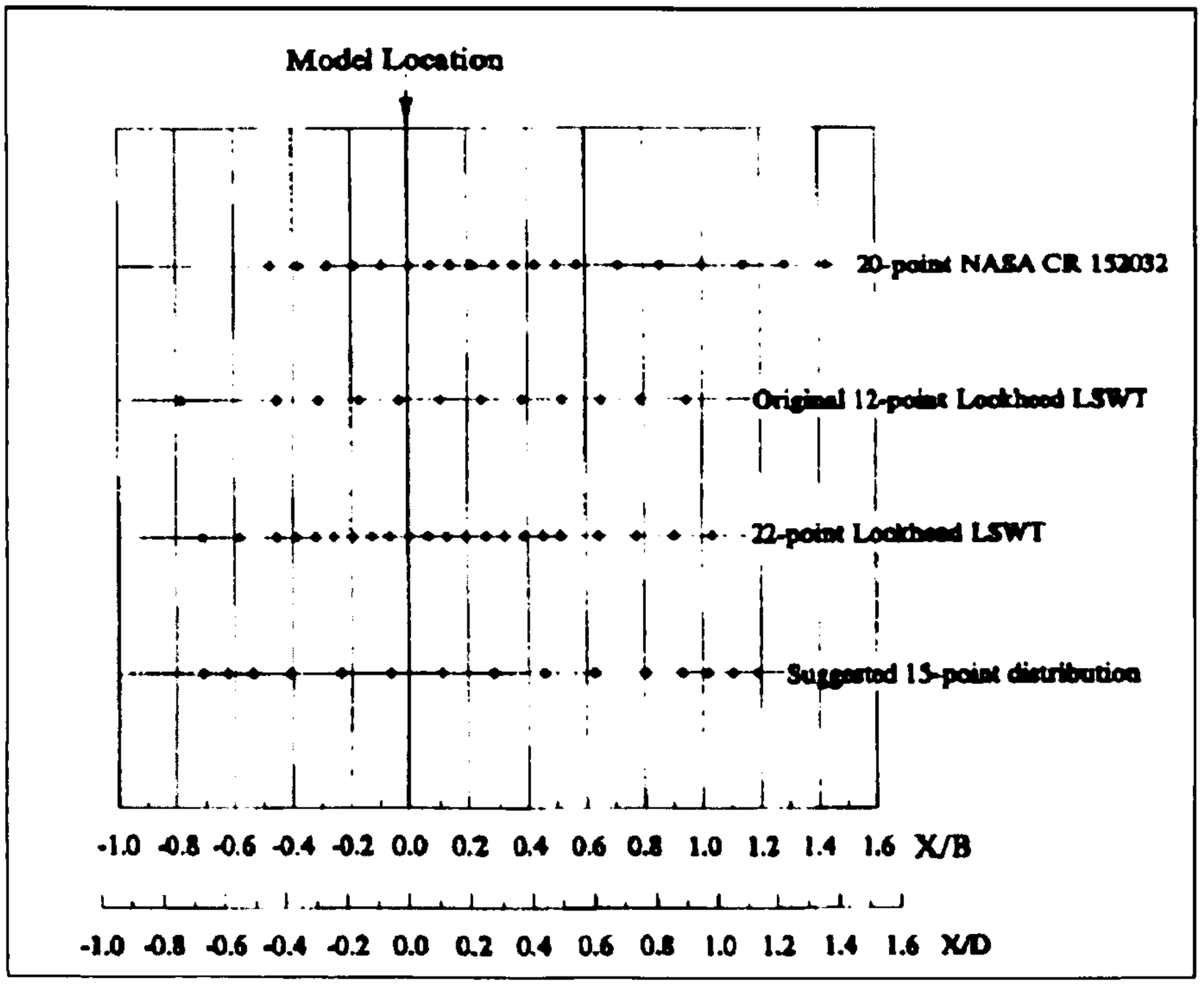

Figure 5.4 Typical orifice locations for the pressure signature method (from Ewald 1998)

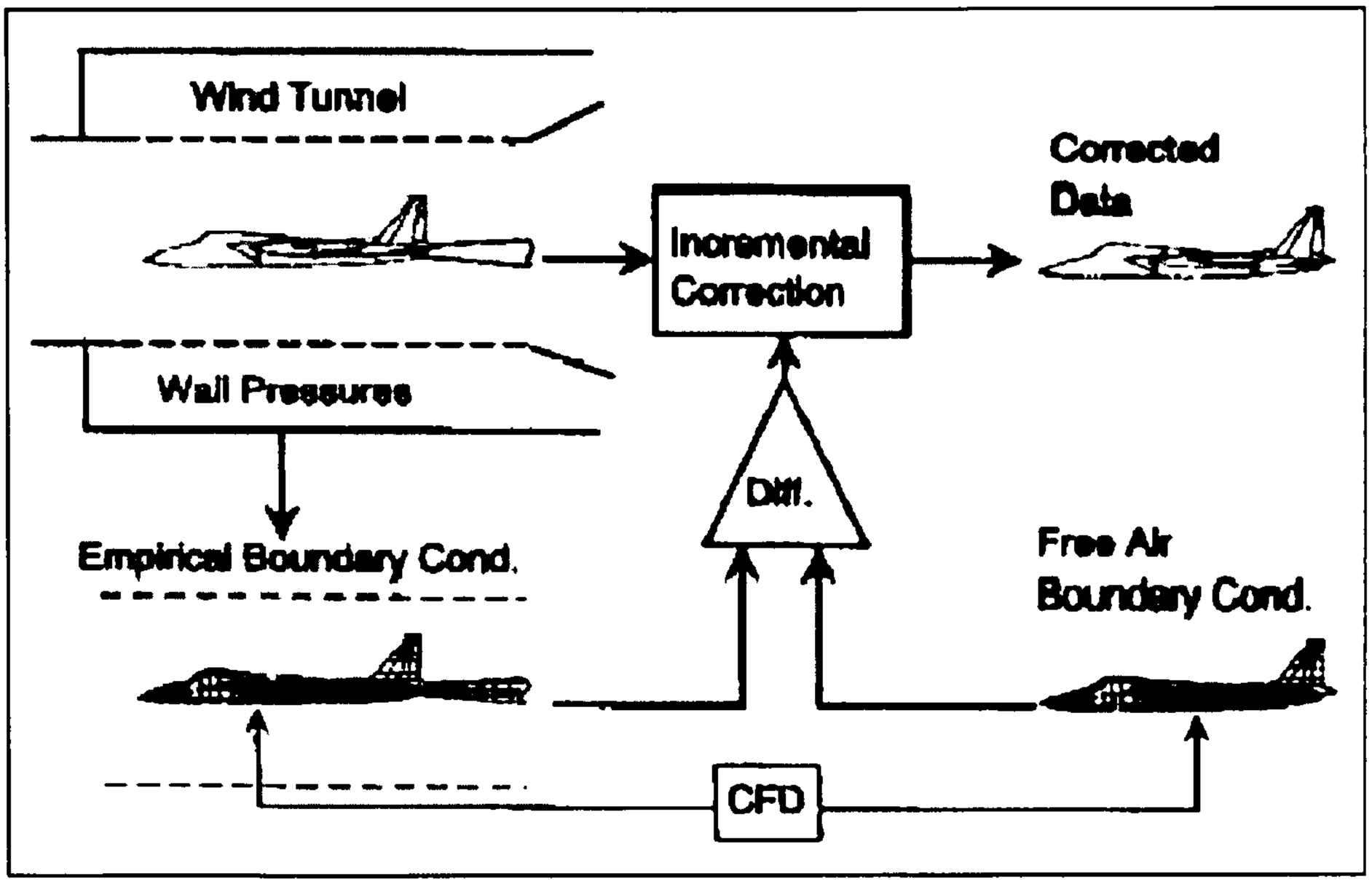

Figure 5.5 Boundary interference correction method (Ewald 1998)

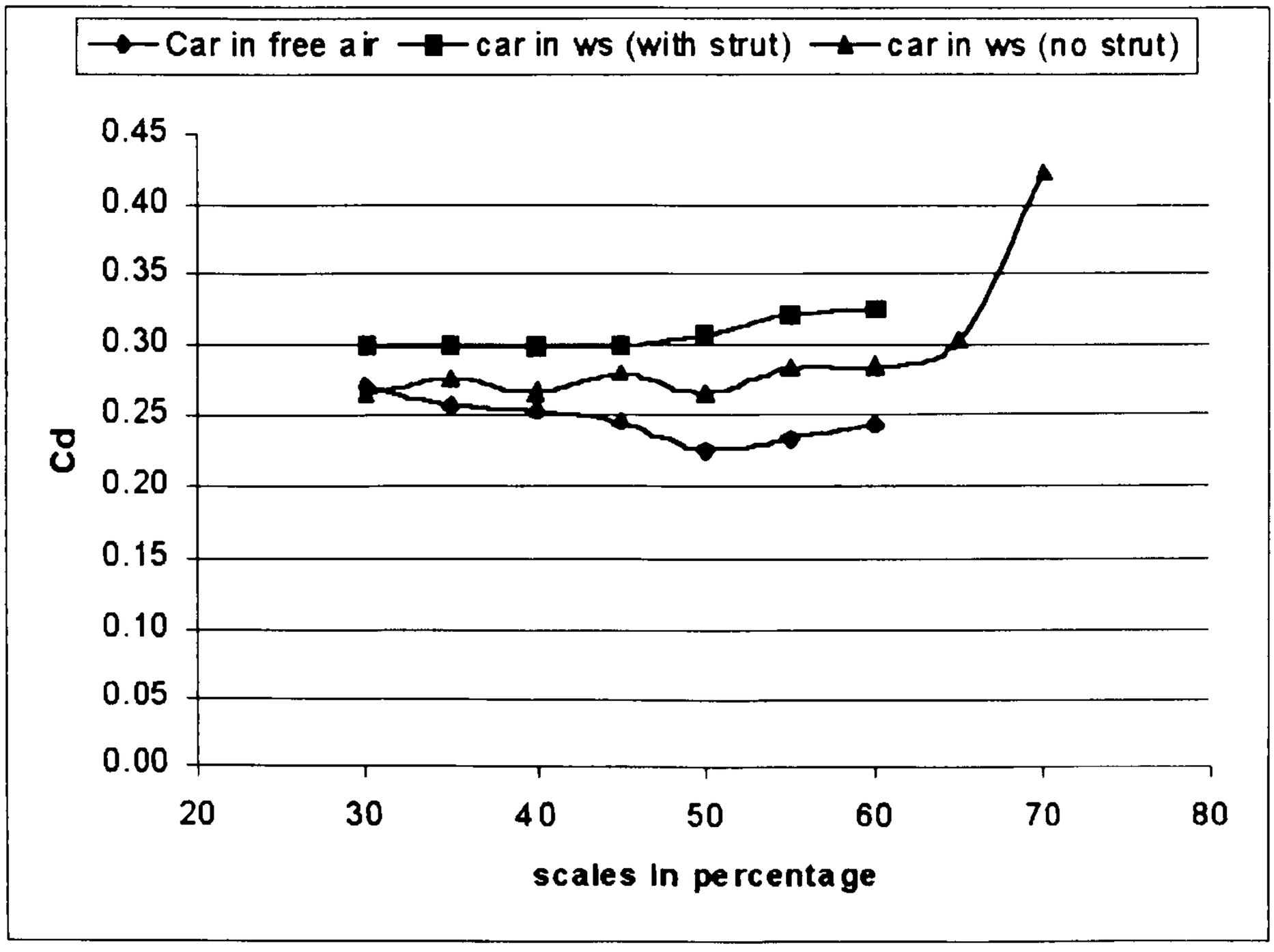

Figure 5.6 Numerical results of drag coefficient in different cases

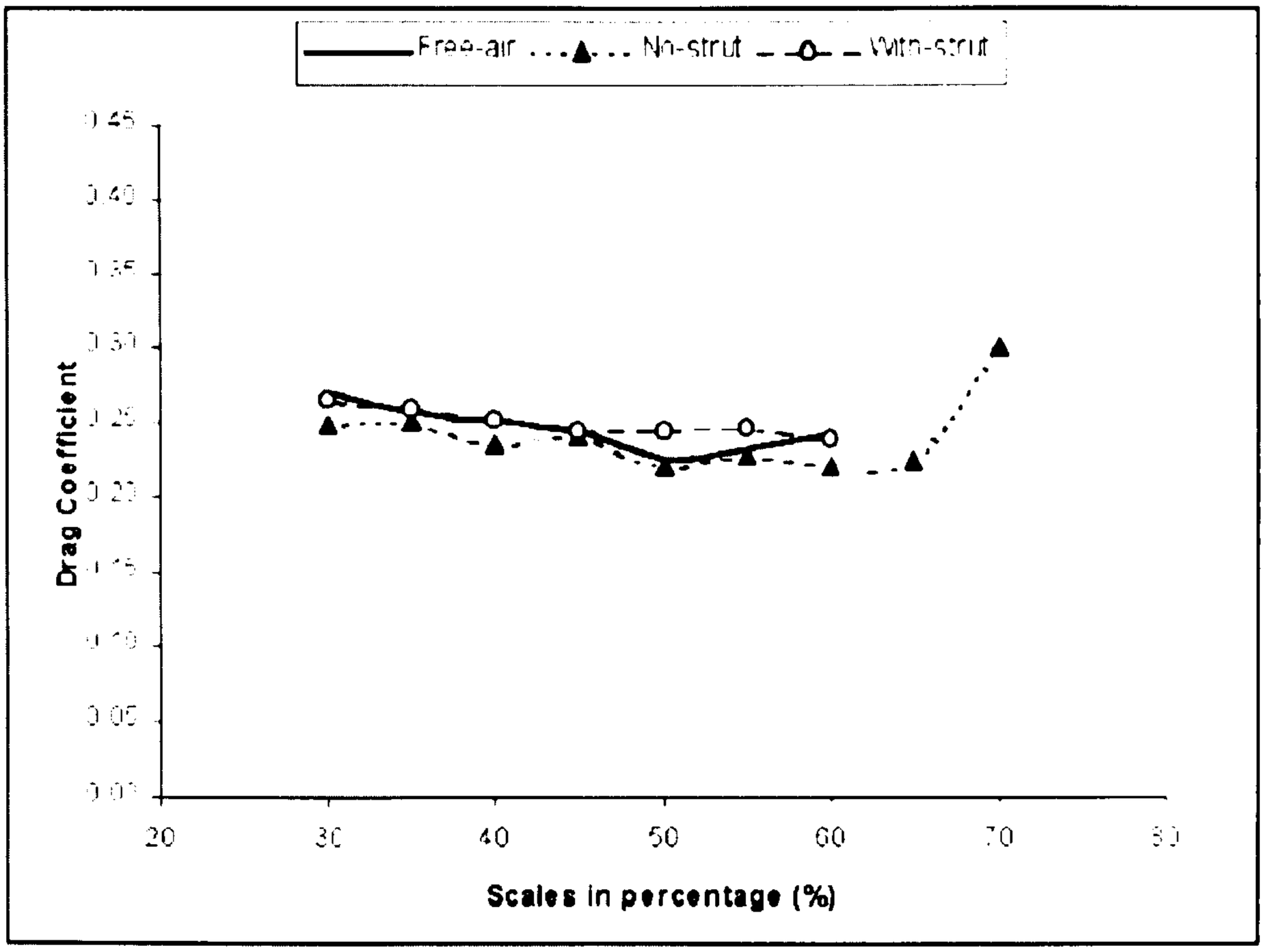

Figure 5.7 Drag coefficients after correction (numerical results)

CHAPTER 6

NUMERICAL SIMULATION (III): WORKING SECTION WITH DIFFUSER/CONTRACTION/SETTLING CHAMBER

6.1 Introduction

In Chapter 4, the detailed numerical simulation of a car in working section was given, where the boundary condition at the inlet of the working section was taken as velocity-inlet boundary condition, and the boundary condition at the exit was taken as pressure-outlet boundary condition. In other words, at the entry of the working section, the velocity inlet condition forces the velocity to be uniform and is kept constant during the numerical iteration. At the exit, the pressure-outlet condition was based on the following considerations: in the actual wind tunnel there is a gap between the working section and first diffuser, and it's open to the atmosphere, which means the pressure at the exit of working section is taken as the atmosphere (constant). In the working section of the Argyll Wind Tunnel, the exit is not far from the testing model (about 2.5m), and the flow at the exit should be fully-developed, where pressure outlet condition is suitable.

However, the inlet and outlet conditions in the numerical simulation may not be the same as or close to the actual circumstance. When the model is tested in the working section, the reduction of the flow passage will produce the blockage for the flows, and the flows at the model will change a great deal. Therefore, the velocity at the entry of working section may be affected and the flow no longer be uniform.

As for the exit condition, when the model is tested in the working section, especially for the bluff bodies, like a road vehicle, there is a big wake existing, and the wake vortices may be long lasting. The flows at exit of working section is therefore very complicated, and under-developed.

Therefore, the condition at exit of working section is significantly affected by model presence, and a single boundary condition is not enough to represent the flows at the exit of working section.

For the reasons mentioned above, the numerical simulation of wind tunnel should include the first diffuser, settling chamber and contraction to avoid the impractical condition. The numerical simulation of the wind tunnel will include all the parts of the wind tunnel, such as corners with cascades, the second diffuser, and even the fan. The comparisons of the cases with/without diffuser and contraction are also needed, in order to ensure the influence of the boundary conditions at entry and exit of working section.

Figure 6.1 gives the velocity and pressure coefficient contours for the working section and diffuser and contraction. The figure shows that the velocity in the working section is a uniform flow, but the velocity and pressure at the entry of working section are not so uniform due to the contraction influence. And the pressure at the exit is not the same as atmosphere at all, Figure 6.2 gives the velocity and pressure coefficient contours at the entry and exit.

6.2 Effect of Testing Model on Inlet and Exit Conditions

In this section, the effect of testing model on the inlet and exit conditions is investigated. The testing model presented in the working section produces the blockage of flow passage, and cause the changes of pressure and velocity in the working section, and the changes at the inlet and exit. Figure 6.3 gives the velocity and pressure coefficient contours for the entry and exit sections. Compared to Figure 6.2, the obvious differences can be seen: the velocity and pressure at exit of working section and the pressure at the entry of the working section are very different. The model presence in the working section seems to have effects on the velocity and pressure at the entry and exit of working section, i.e., the conditions at entry and exit for the case with no testing model show more uniform than those of with the test model.

Compared to Figure 6.4, which is the case without diffuser/contraction. The inlet and outlet conditions are forced to some given values, i.e., the velocity at entry of working section is set as a constant (figure 6.4a), and the pressure at exit is forced to be constant (figure 6.4d), they are quite different from the case with diffuser and contraction. Therefore, the numerical simulation including the working section only is different from the actual situation, and the implementation of the entry and exit boundary conditions may have effect on the aerodynamic characteristics of the model in the working section.

6.3 Numerical Simulation of Working Section with Diffuser/ Contraction

In this section, the case of the working section including 1st diffuser and contraction was investigated. Ideally, the numerical simulation of the wind tunnel under the test condition should include all the components of the wind tunnel, such as 1st and 2nd diffusers, fan, the corners with cascades, contraction and chamber room, and others. But, due to the computer memory limitation, the numerical simulation including all the wind tunnel components is not practical at present, and even not necessary for some cases.

Figure 6.5 shows the velocity and pressure coefficient contours at the vertical symmetrical plans of working section, 1st diffuser and contraction.

Figure 6.6 shows the velocity contours at the symmetrical plan of the working section (for scale=30%). The obvious differences have been seen between the cases with and without diffuser/contraction, especially in the wakes. For the case with diffuser/ contraction, the wake is much bigger than the case without diffuser/contraction. This is no wonder, because for the case of the working section only, the exit condition is not far from the model, and the pressure-outlet condition at exit forces the flow at exit to reach given pressure condition, and forces the wake behind the car to disappear very quickly as well.

To investigate the model size effect, a 55% model was investigated. Figure 6.7 gives the comparison of the velocity contours for the cases with and without diffuser/contraction. Again, the significant differences mainly occur in the wakes of the car, and only small effect occurs in the front area. For the case of working section only, the wake is much smaller than that of case of working section with diffuser/contraction.

Drag coefficients of the car in working section with and without diffuser/contraction give the more exact results. Table 6.1 gives the comparison.

Table 6.1 Drag coefficient comparisons

Model scale	Drag coefficient prediction by numerical simulation	
	Without diffuser/contraction	With diffuser/contraction
30%	0.299	0.296
55%	0.330	0.303

From table 6.1, the bigger the model size is, the bigger the effect of diffuser and contraction has. When the scale ratio is 30%, the drag coefficient without diffuser/contraction is 1% bigger than the case with diffuser and contraction, while the 55% model, the difference in drag coefficients becomes 8.9%.

Fukuda etc (1994) reported the improvement of vehicle aerodynamics by wake control, which was usually reached by changing the car rear end shape. In other word, the wake of road vehicle has significant effect on its aerodynamics. Figure 6.8 shows the velocity vectors behind the car for the 30% scale model in the cases with/without diffuser/contraction. Figure 6.9 shows the case of 55%. For 30% model, the case with/without diffuser/contraction doesn't give a much different wake, while for 55% model, the wakes show a big difference, which is responsible for the big difference in drag coefficient.

6.4 Concluding Remarks

This chapter investigates the effect of the inlet and outlet conditions numerically, the comparisons between the cases with and without diffuser/contraction in the numerical simulation show the effect on the results. According to the analysis of previous sections, the concluding remarks can be drawn as following:

1) The numerical simulation shows the uniform flow in the working section when the diffuser and contraction are included.
2) The velocity contours show, when the outlet boundary condition is given as pressure outlet condition at the exit of the working section, the suppression of outlet condition on the wakes is obvious. Figure 6.6 and 6.7 show the wake differences.
3) When the inlet and outlet conditions are given at the entry and exit of working section, they have effects on the numerical results of drag coefficients. And the bigger the model size is, the bigger the effect on the drag coefficient (Table 6.1).
4) Numerical simulations show that the wake structures have influence on the vehicle drag coefficient.

Figures of Chapter 6

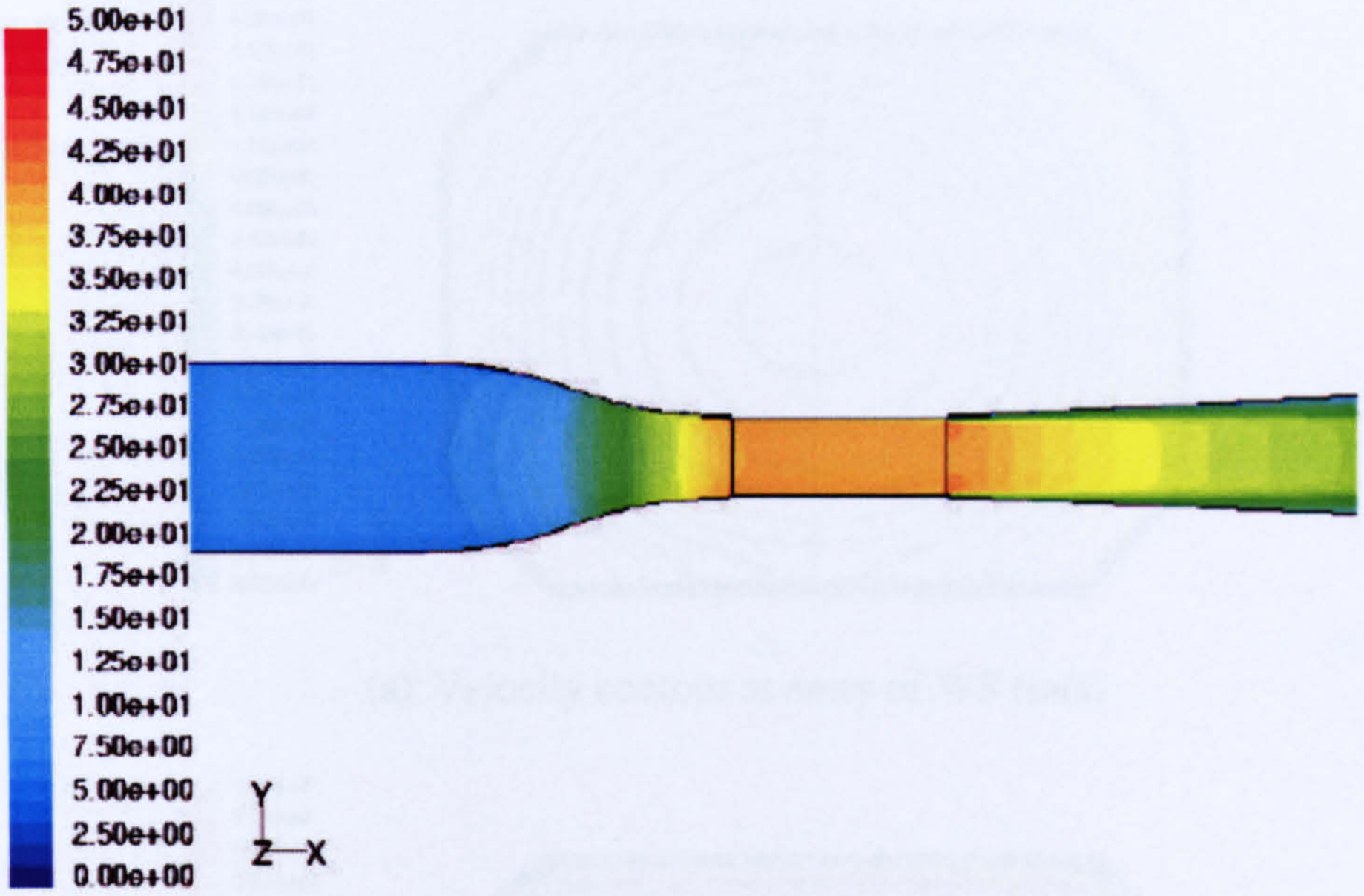

(a) velocity contour

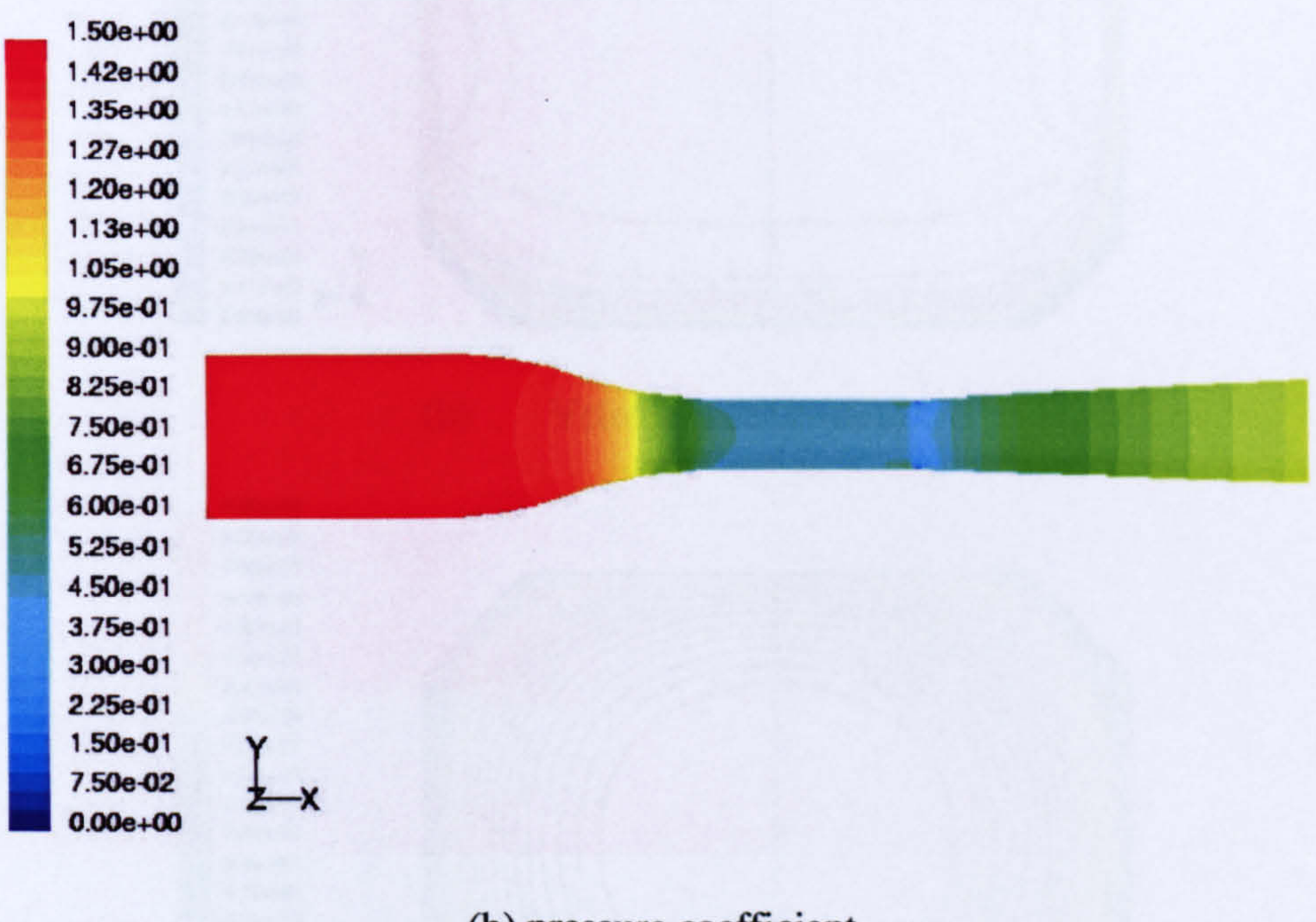

(b) pressure coefficient

Figure 6.1 Velocity and pressure contours of the working section, 1st diffuser and contraction

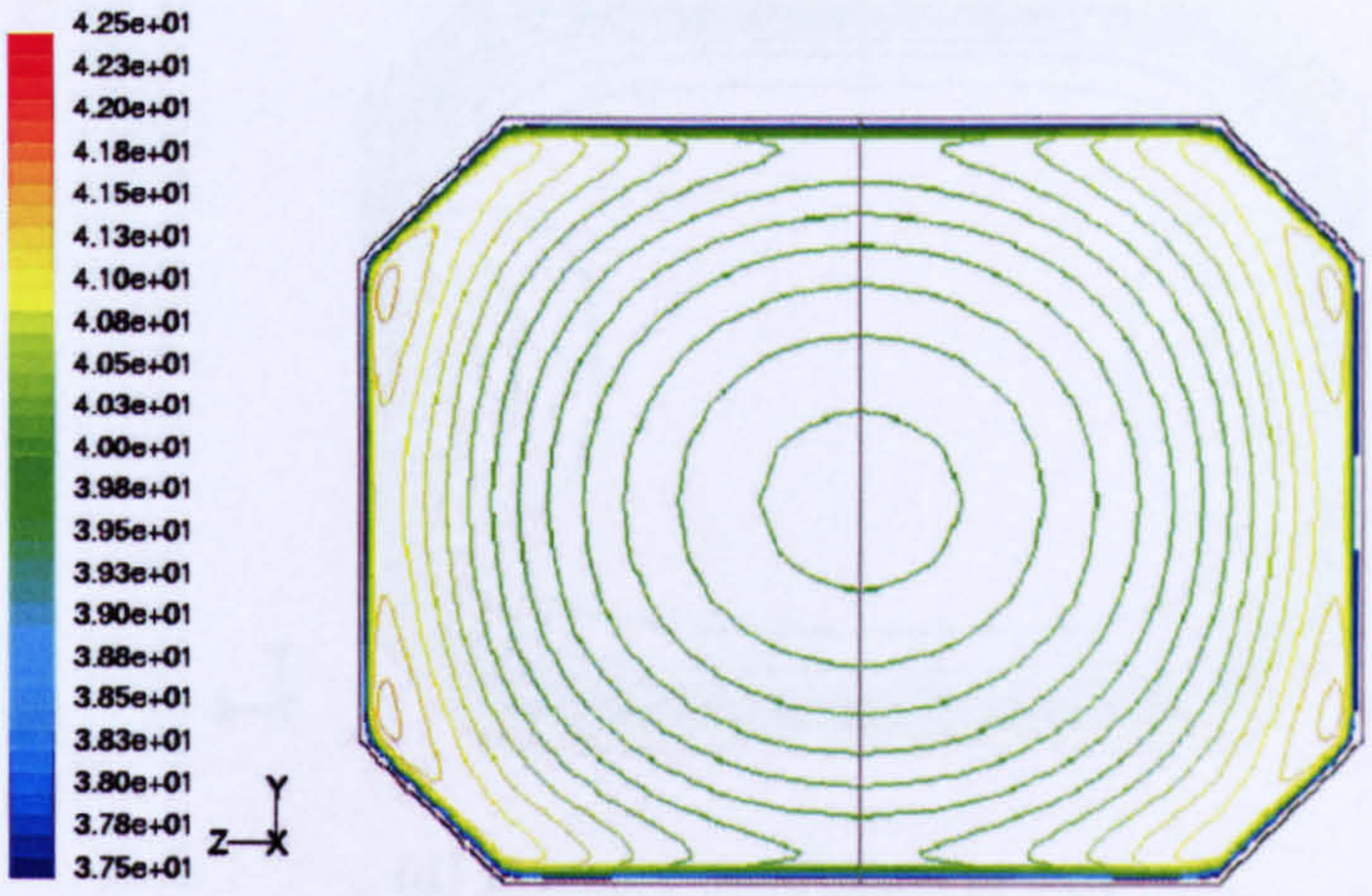

(a) Velocity contour at entry of WS (m/s)

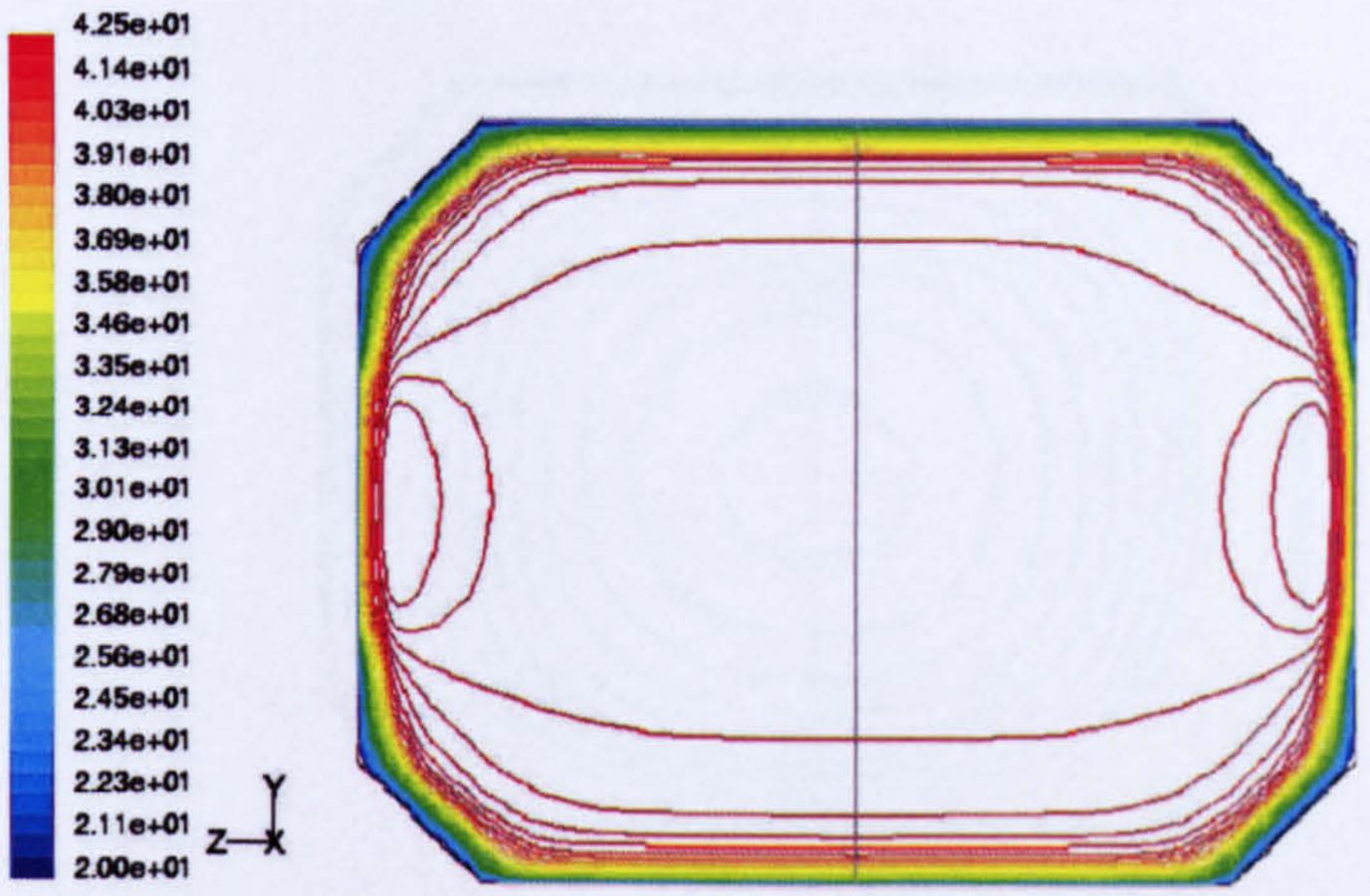

(b) Velocity at exit (m/s)

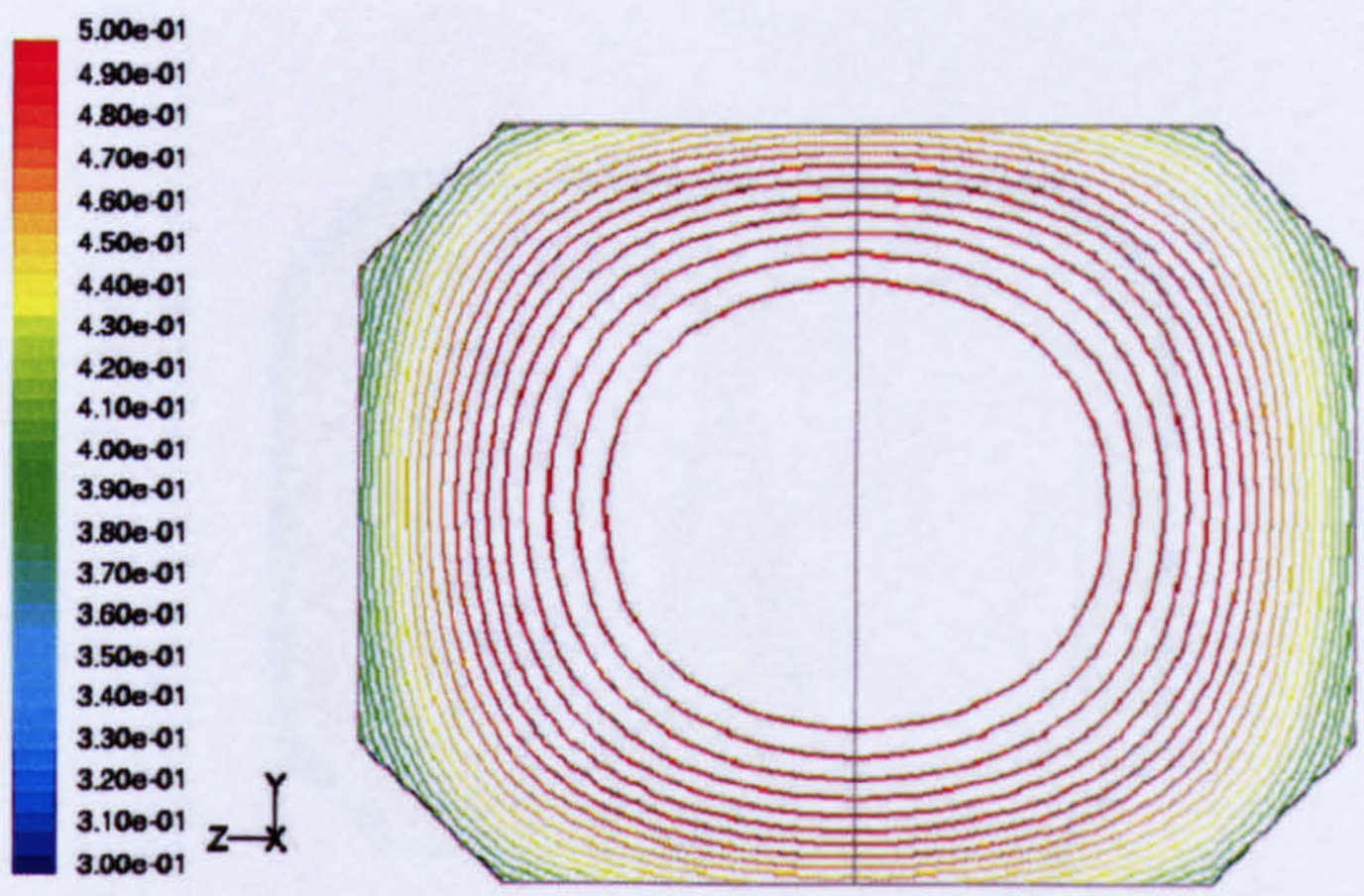

(c) Pressure coefficient at entry

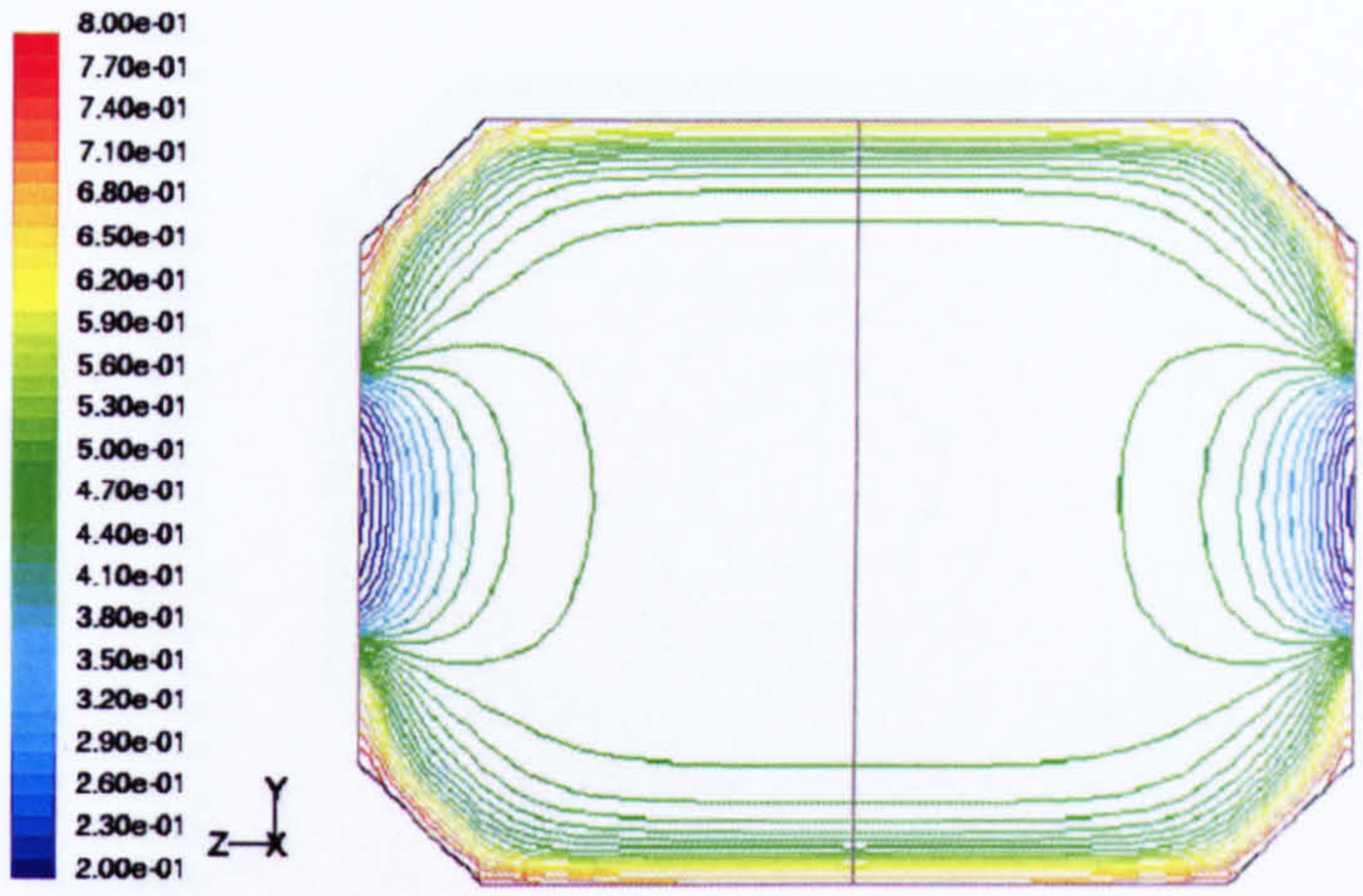

(d) pressure coefficient at exit

Figure 6.2 Velocity and Pressure Contours at Inlet and Outlet of the Working Section (case: no model, no strut, but with diffuser and contraction)

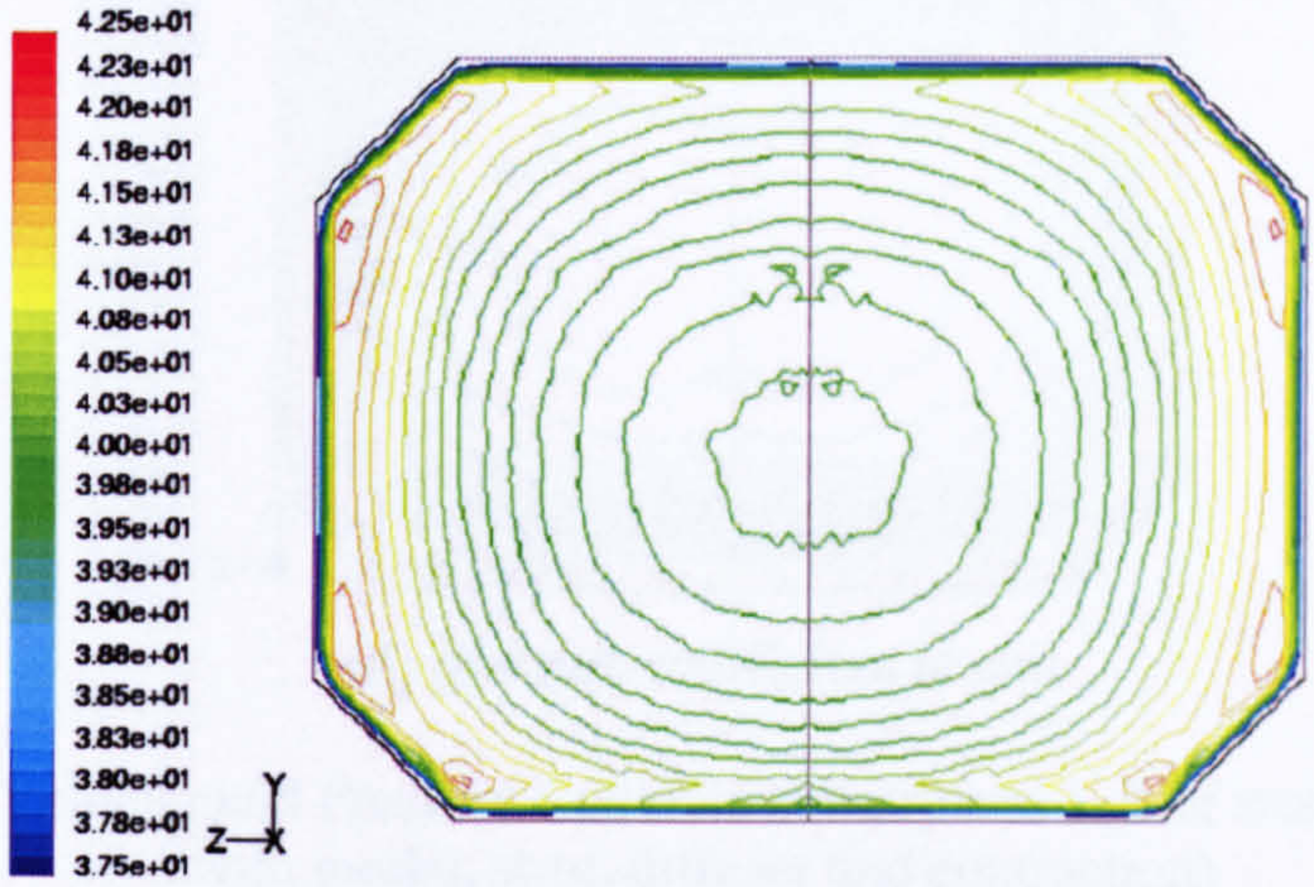

(a) velocity at entry of working section (m/s)

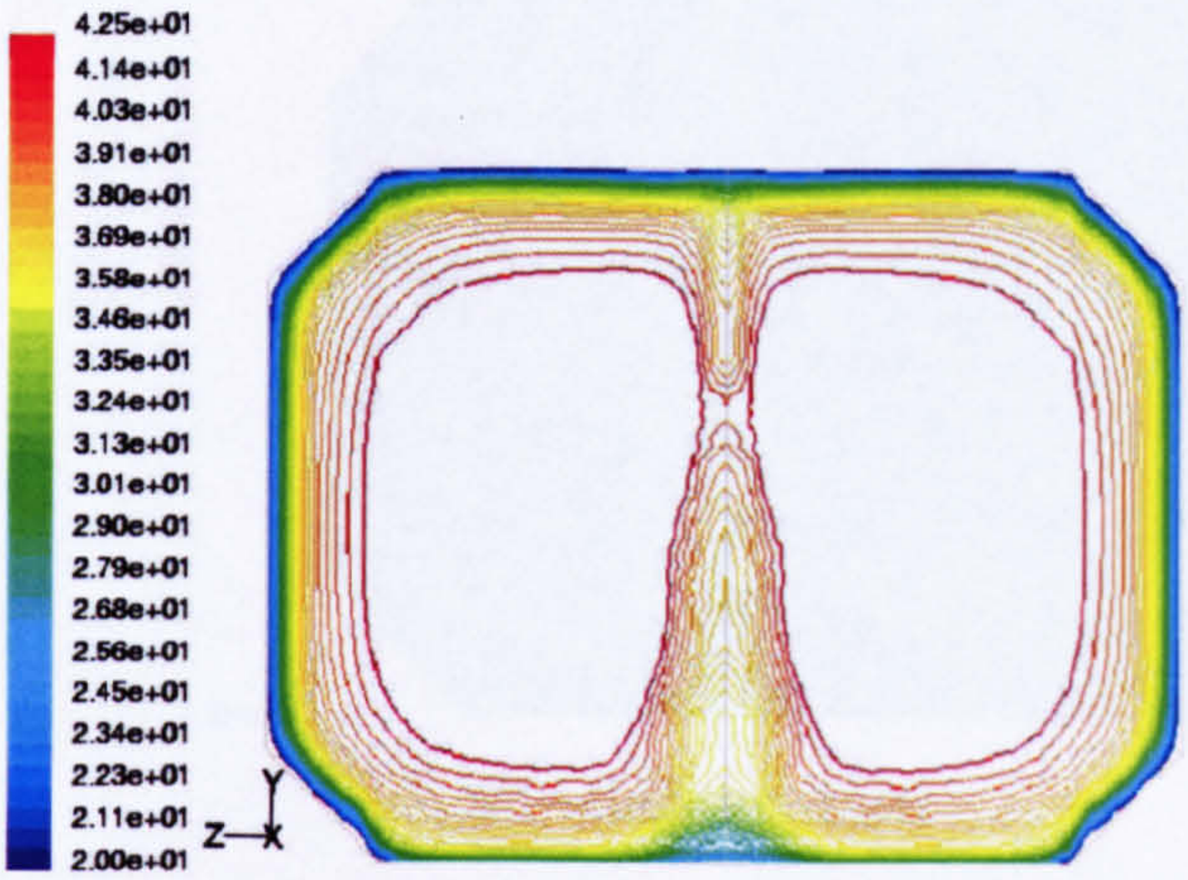

(b) velocity at exit of working section (m/s)

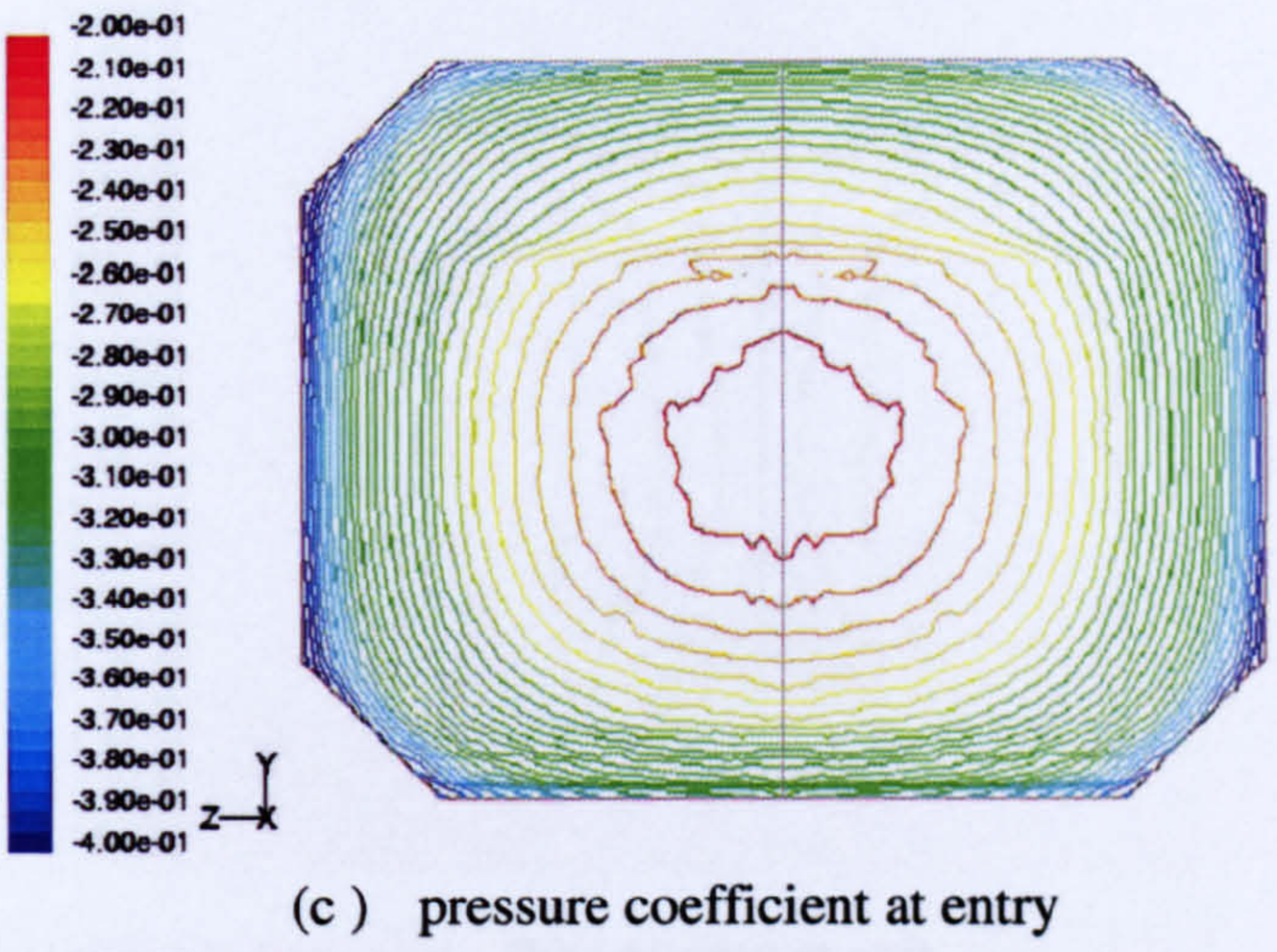

(c) pressure coefficient at entry

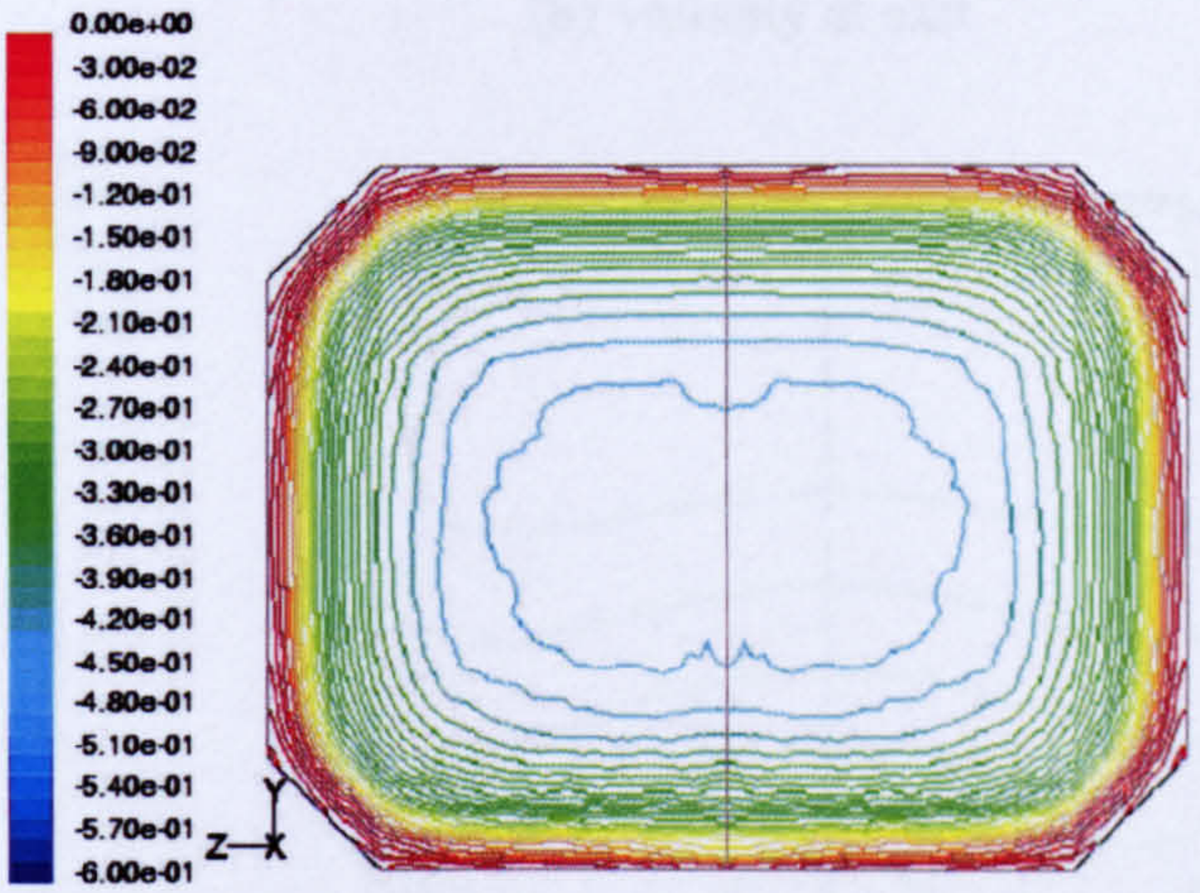

(d) pressure coefficient at exit

Figure 6.3 Velocity and Pressure Contours at entry and exit of working section (case: with model, strut, diffuser and contraction)

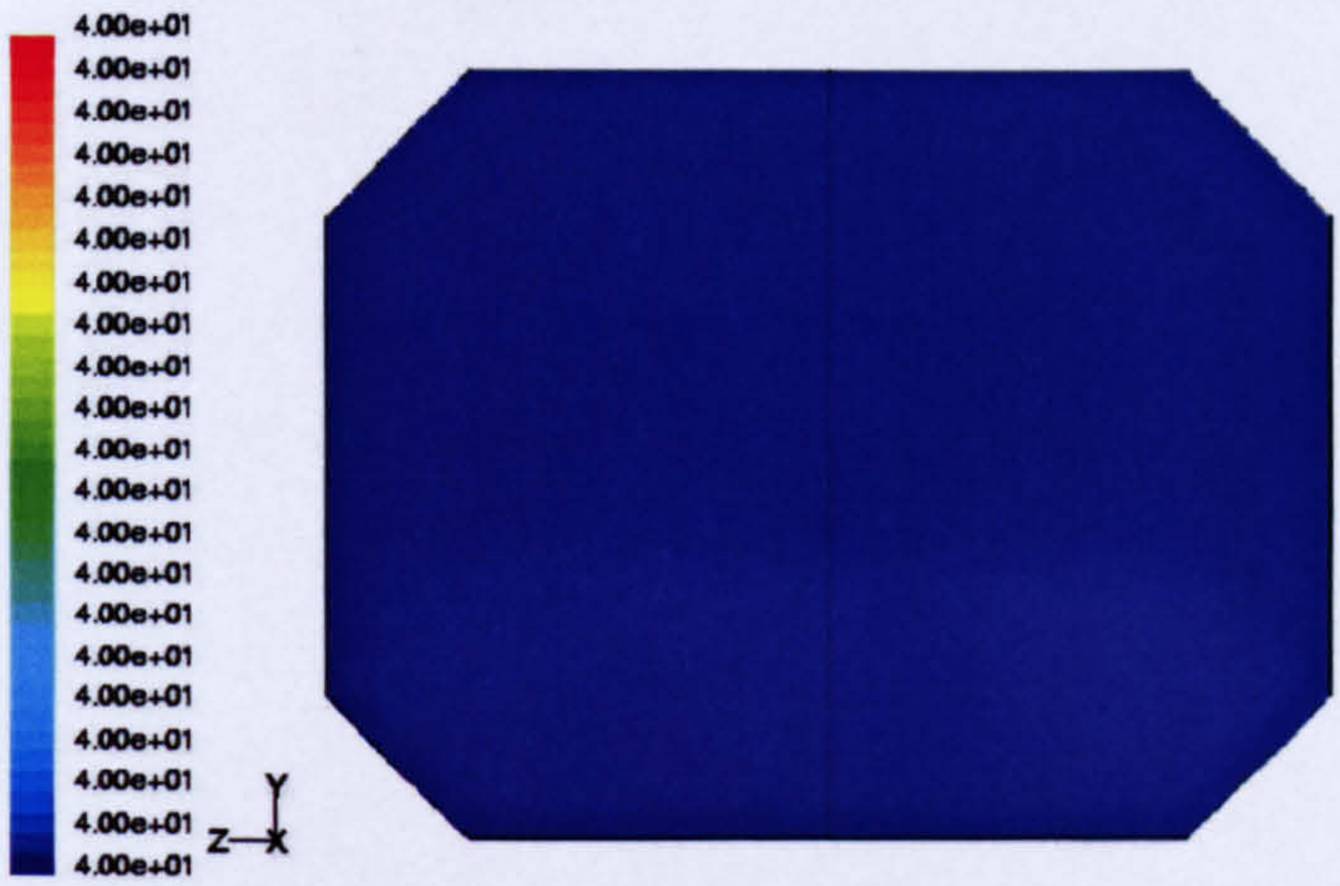

(a) velocity at entry

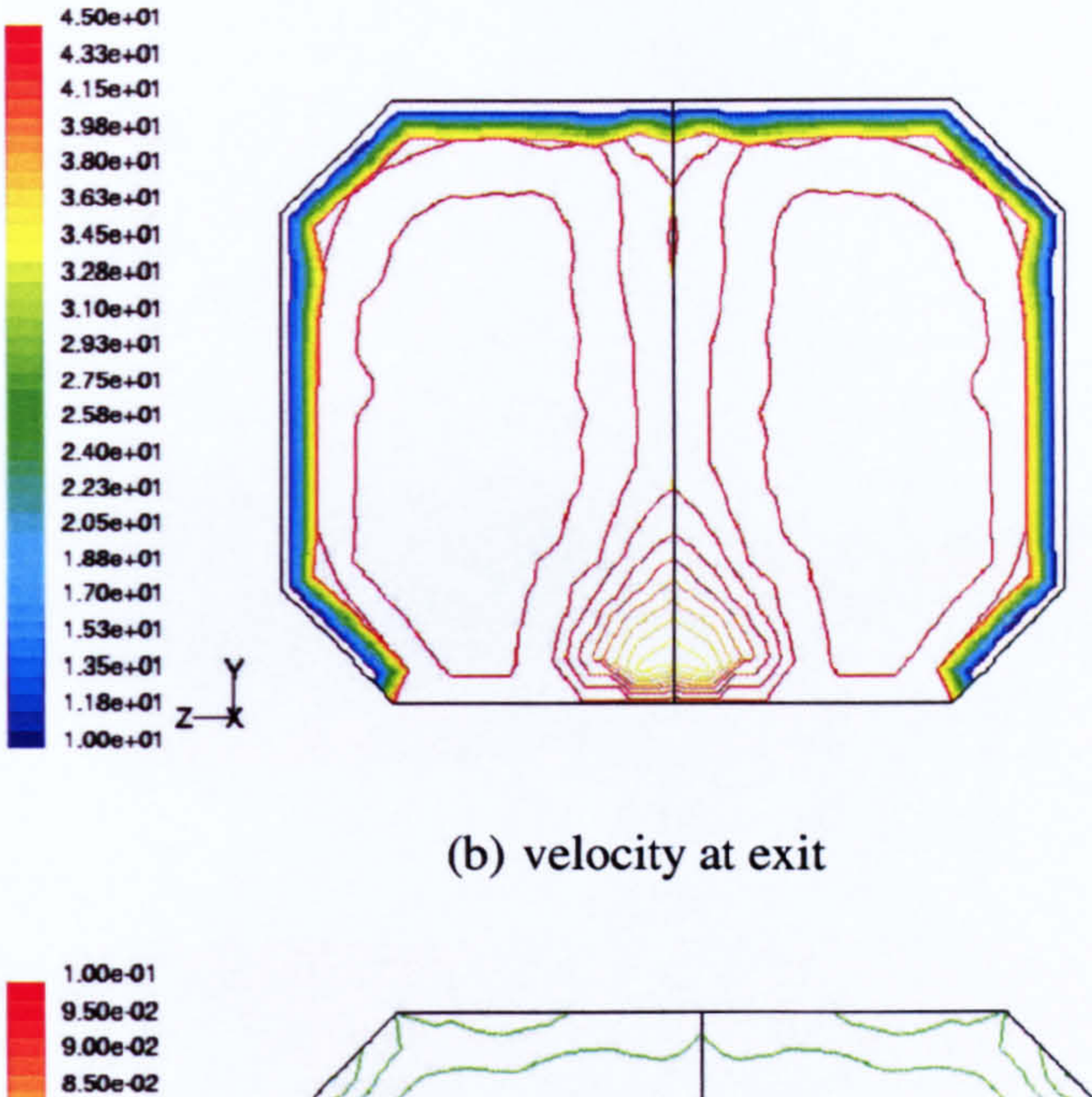

(b) velocity at exit

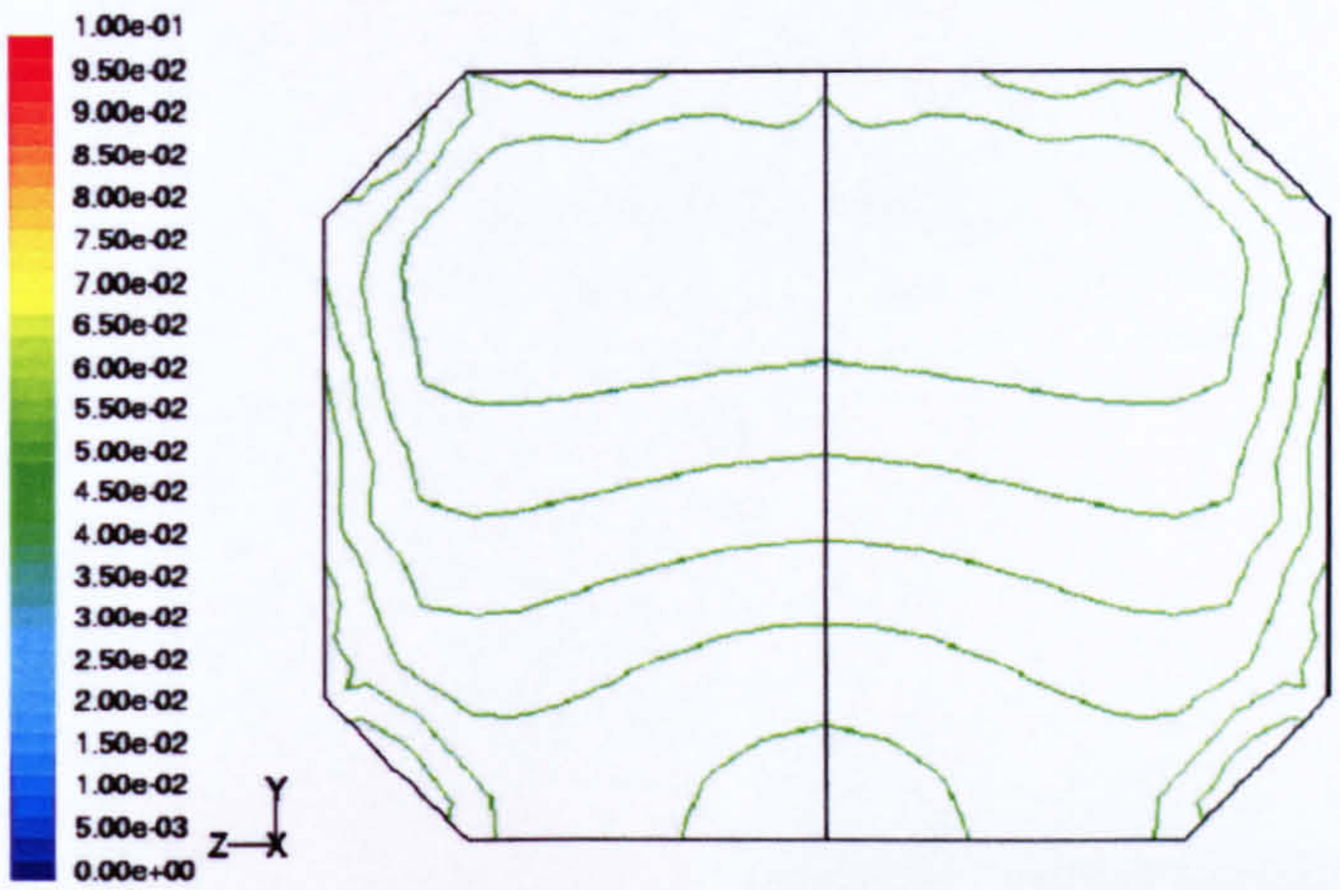

(c) pressure coefficient at entry

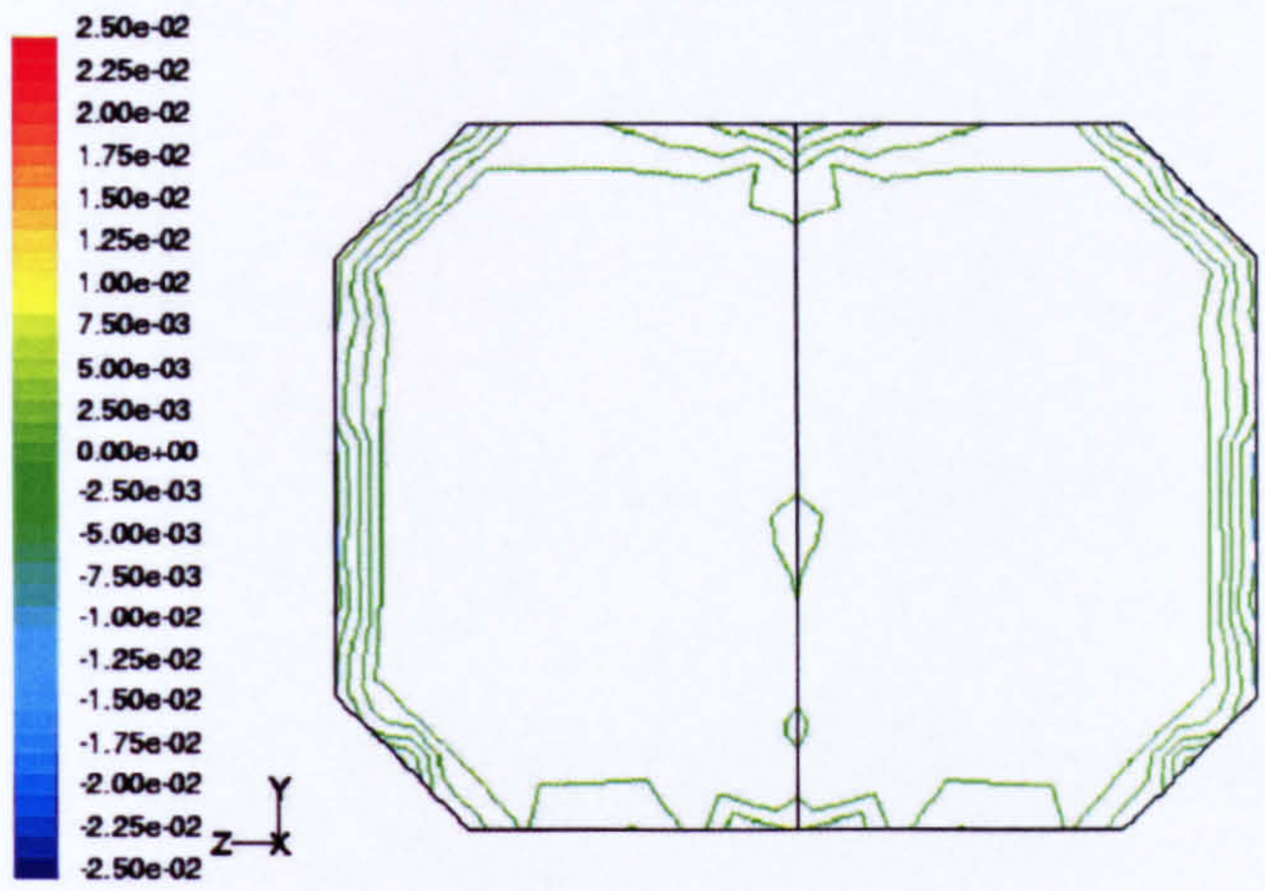

(d) pressure coefficient at exit

Figure 6.4 velocity and pressure contours at entry and exit of the working section (case: no diffuser, no contraction, but with model and strut)

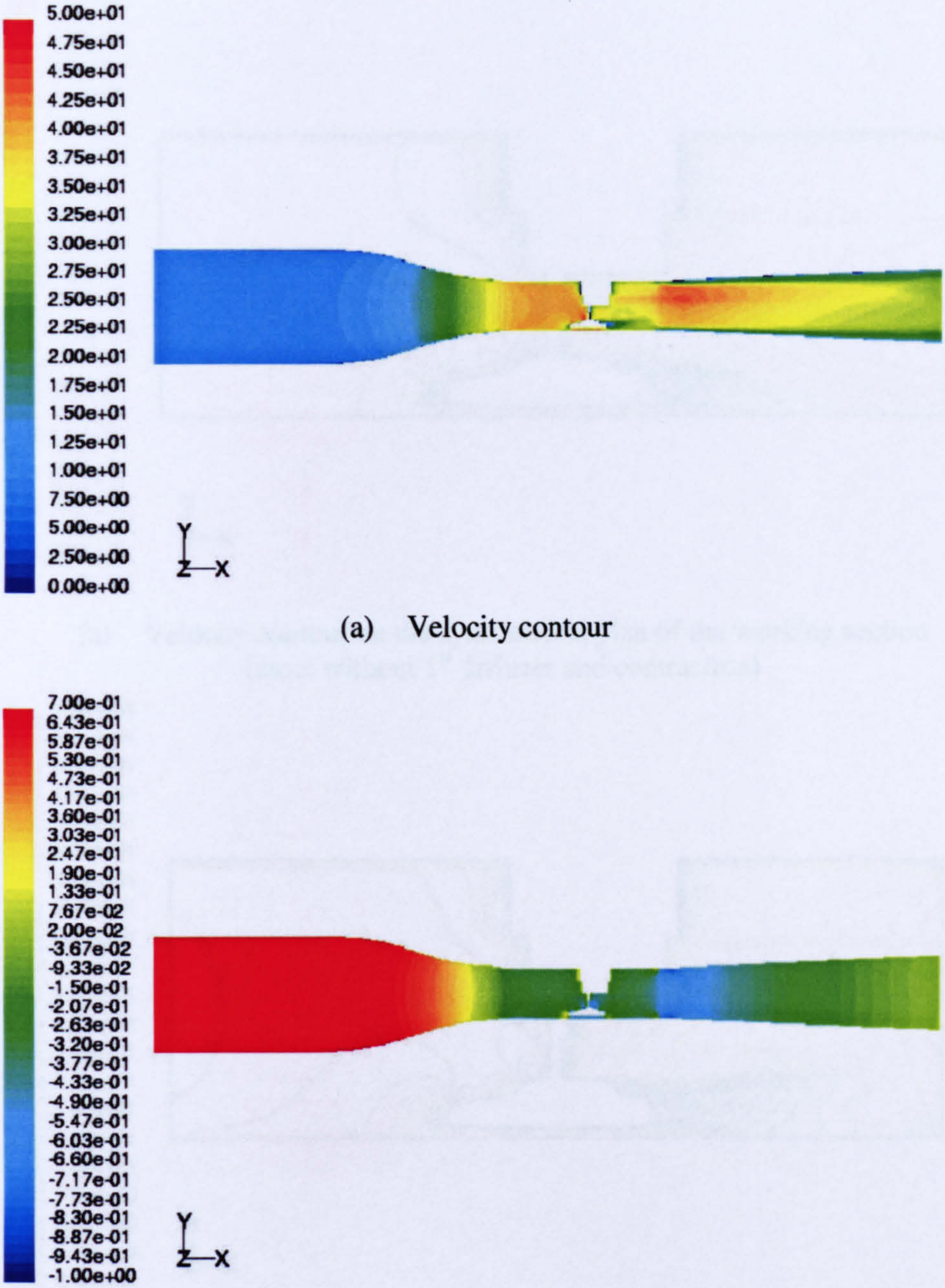

(a) Velocity contour

(b) Pressure coefficient contour

Figure 6.5 Velocity and pressure contours of the working section, 1st diffuser and contraction (30% scaled model)

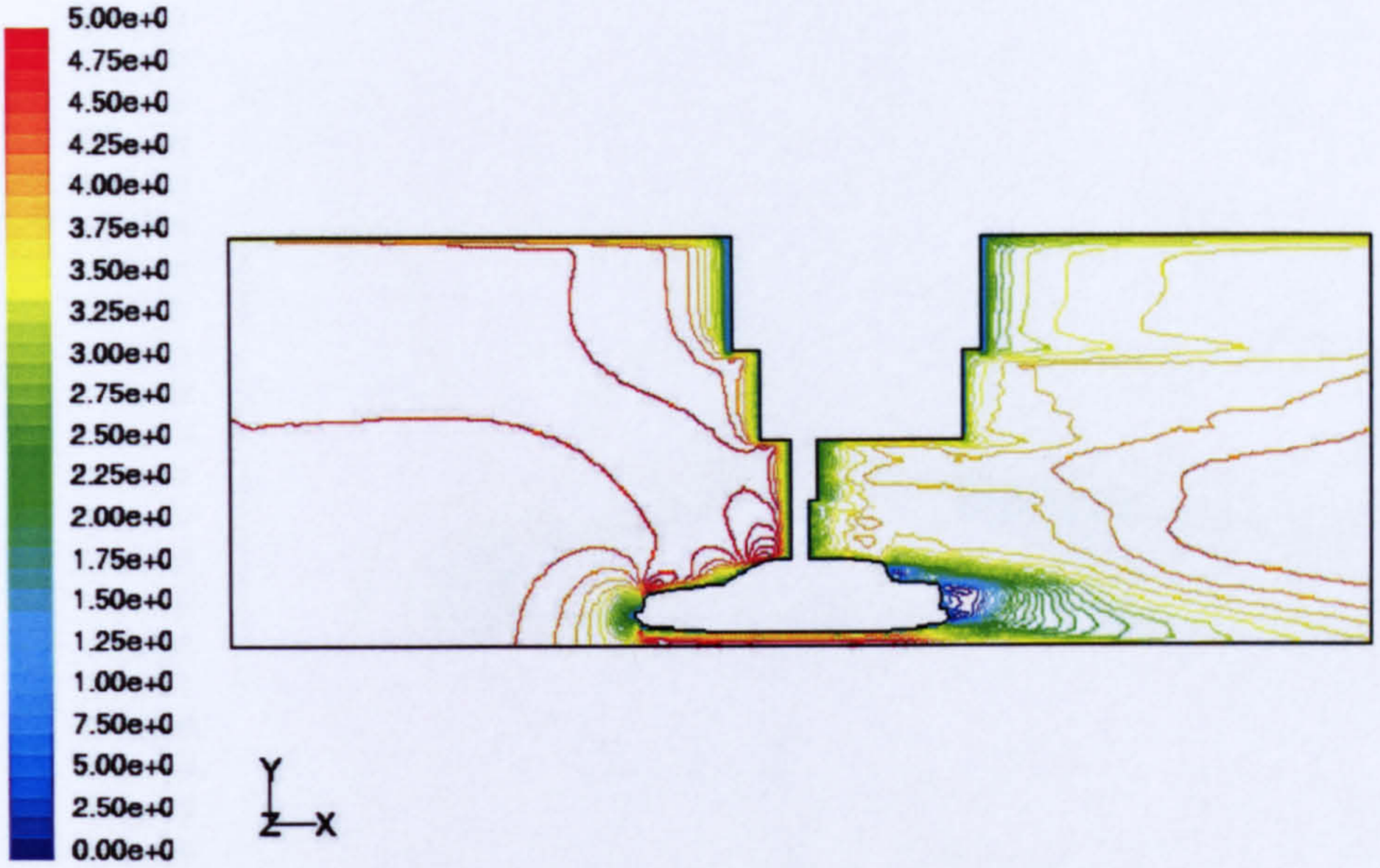

(a) Velocity contour on the symmetrical plan of the working section (case: without 1st diffuser and contraction)

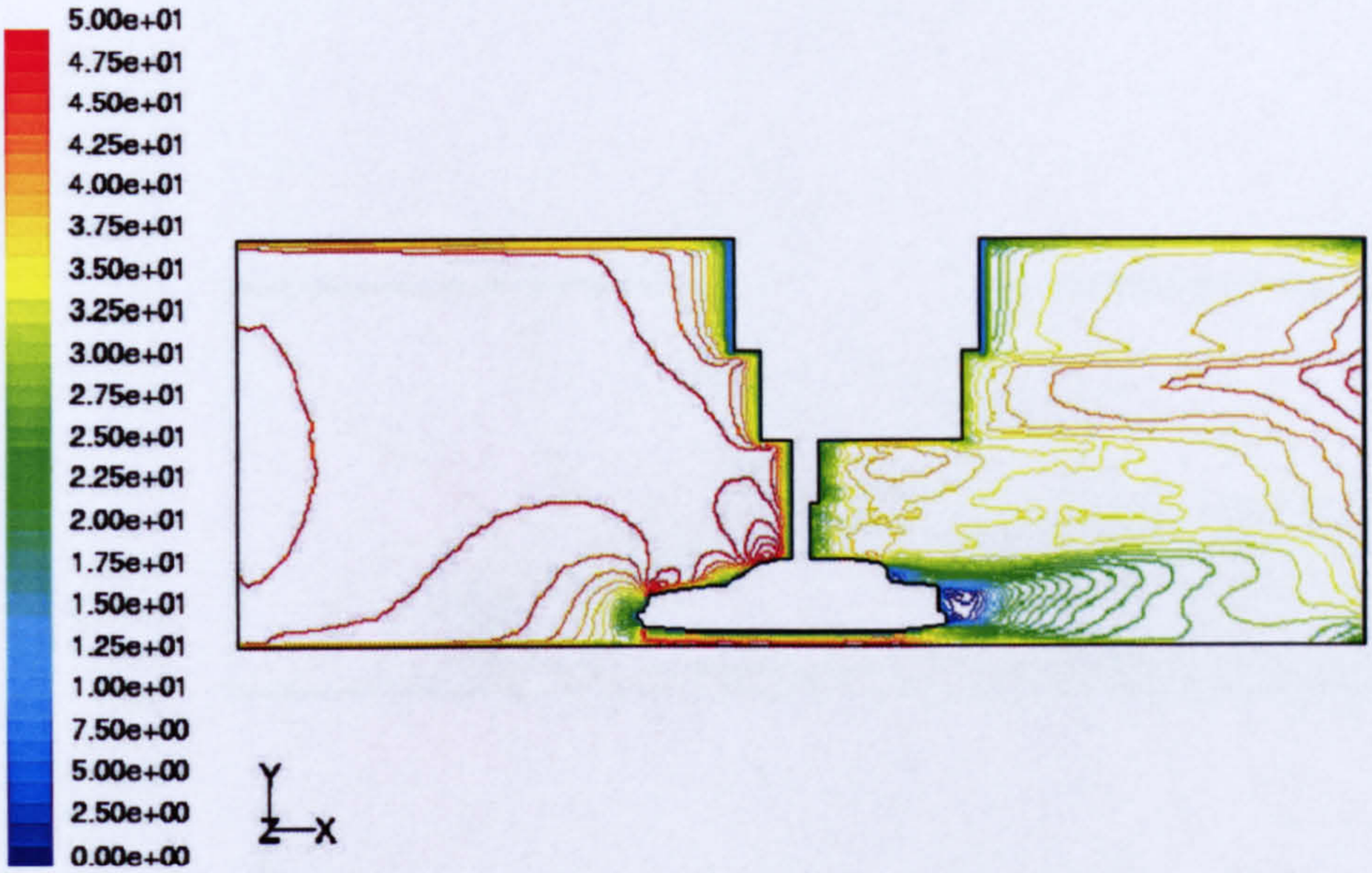

(b) Velocity contour on the symmetrical plan of the working section (case: with 1st diffuser and contraction)

Figure 6.6 Velocity contours at the symmetrical plan in the working section

(Scale=30%)

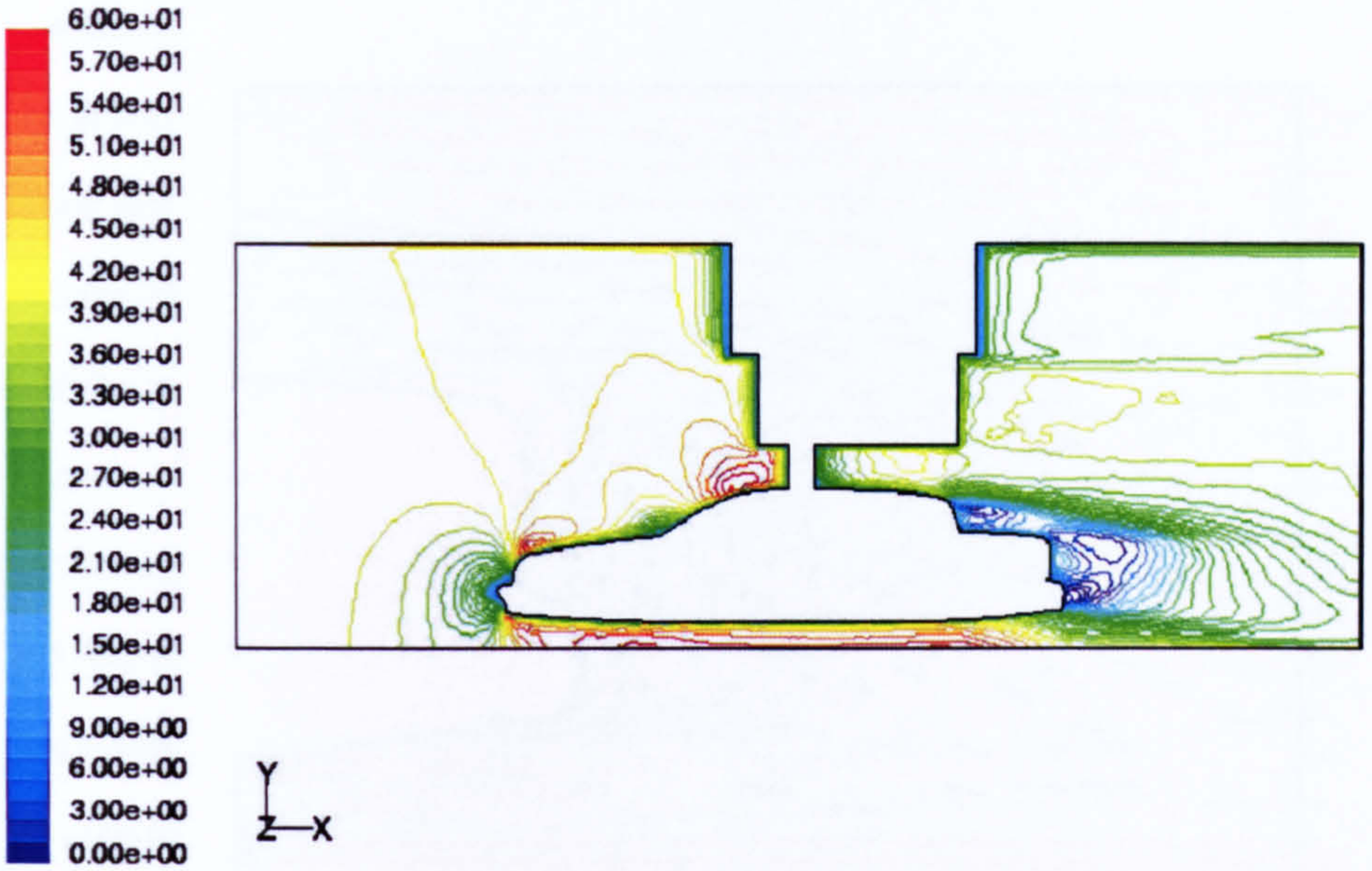

(a) Velocity contour on the symmetrical plan of the working section (case: without 1st diffuser and contraction)

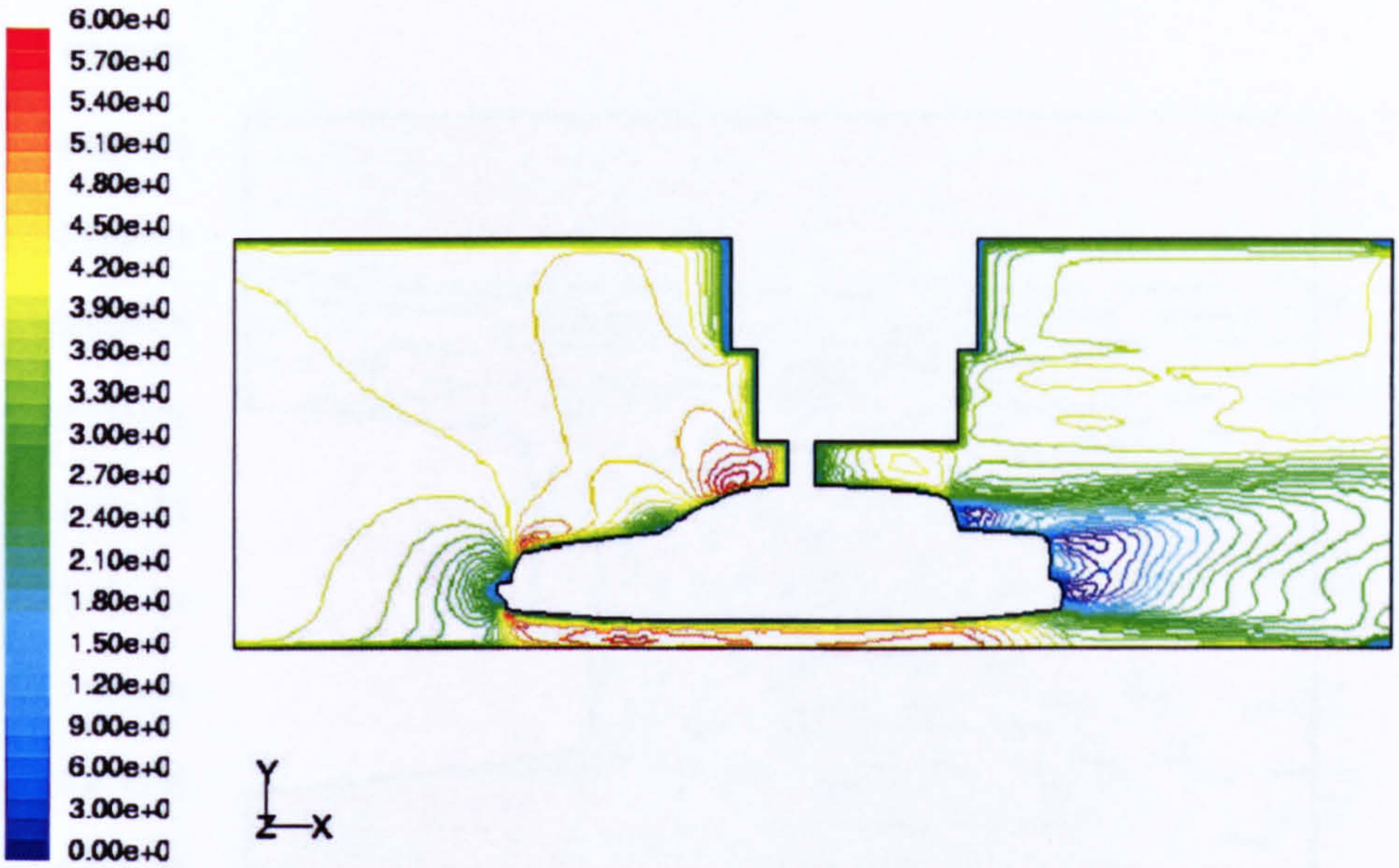

(b) Velocity contour on the symmetrical plan of the working section (case: with 1st diffuser and contraction)

Figure 6.7 Velocity contours at the symmetrical plan in the working section

(Scale=55%)

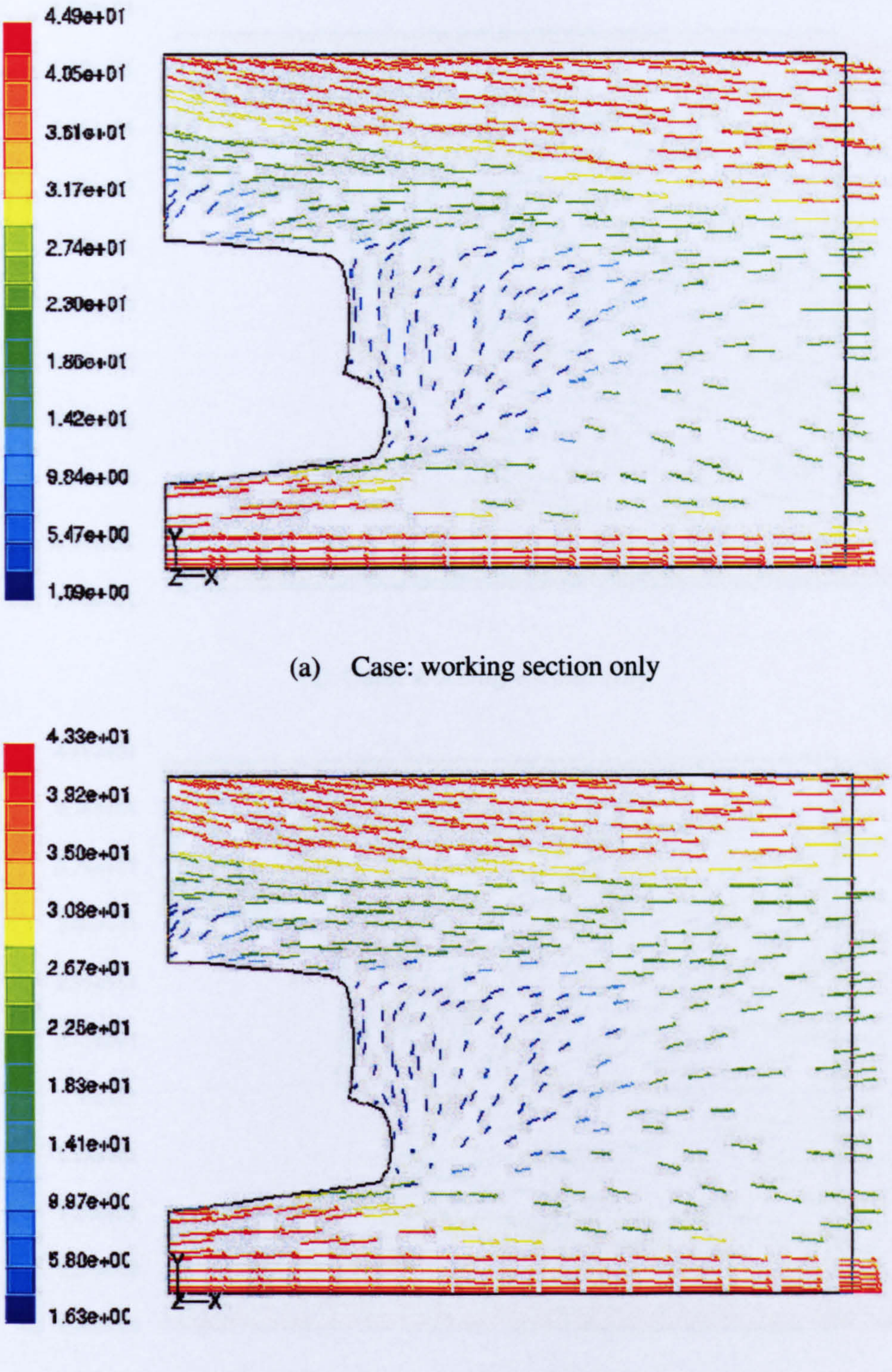

(a) Case: working section only

(b) Case: Working section with diffuser/contraction

Figure 6.8 Wake behind the car model (scale=30%)

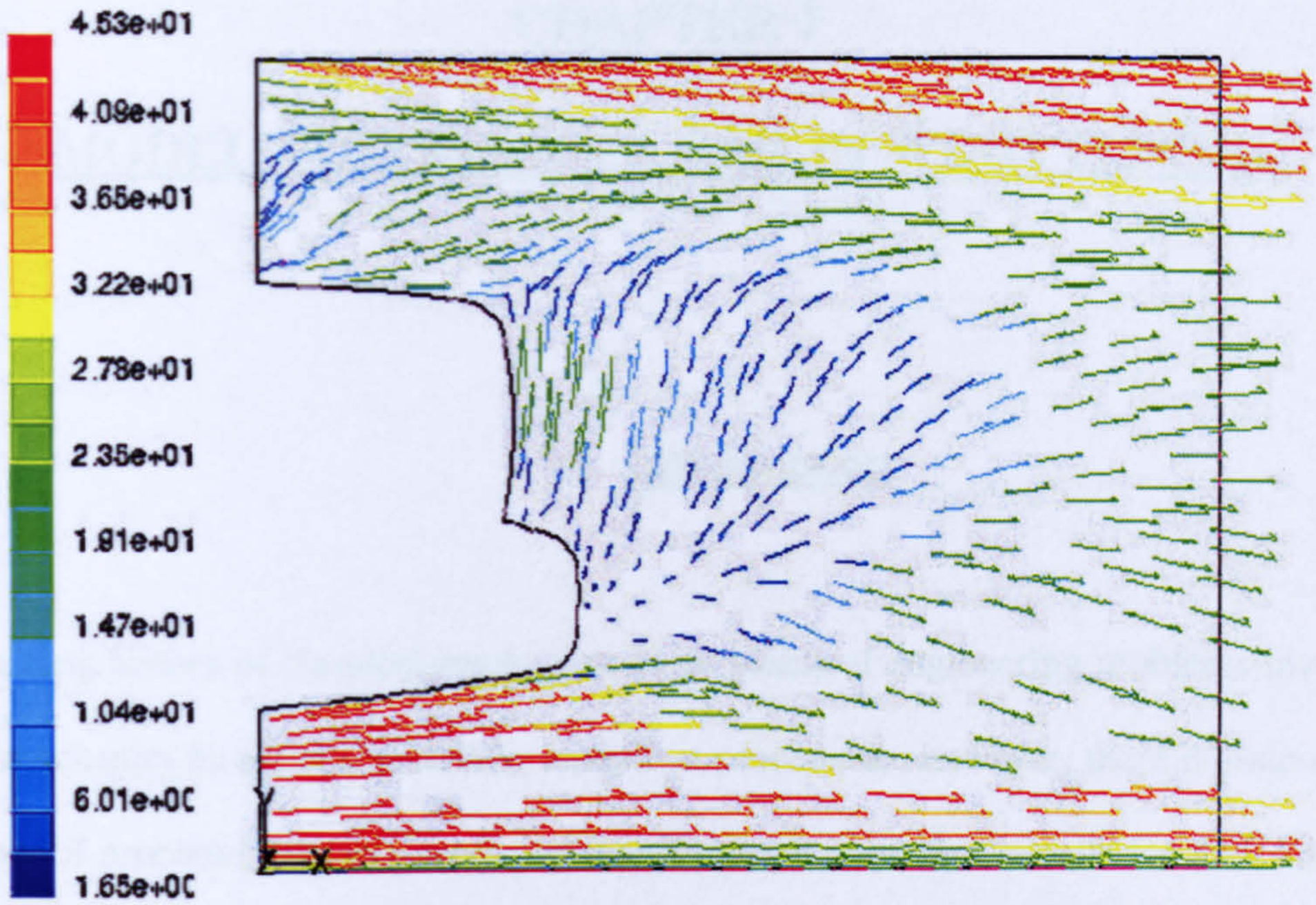

(a) Case: working section only

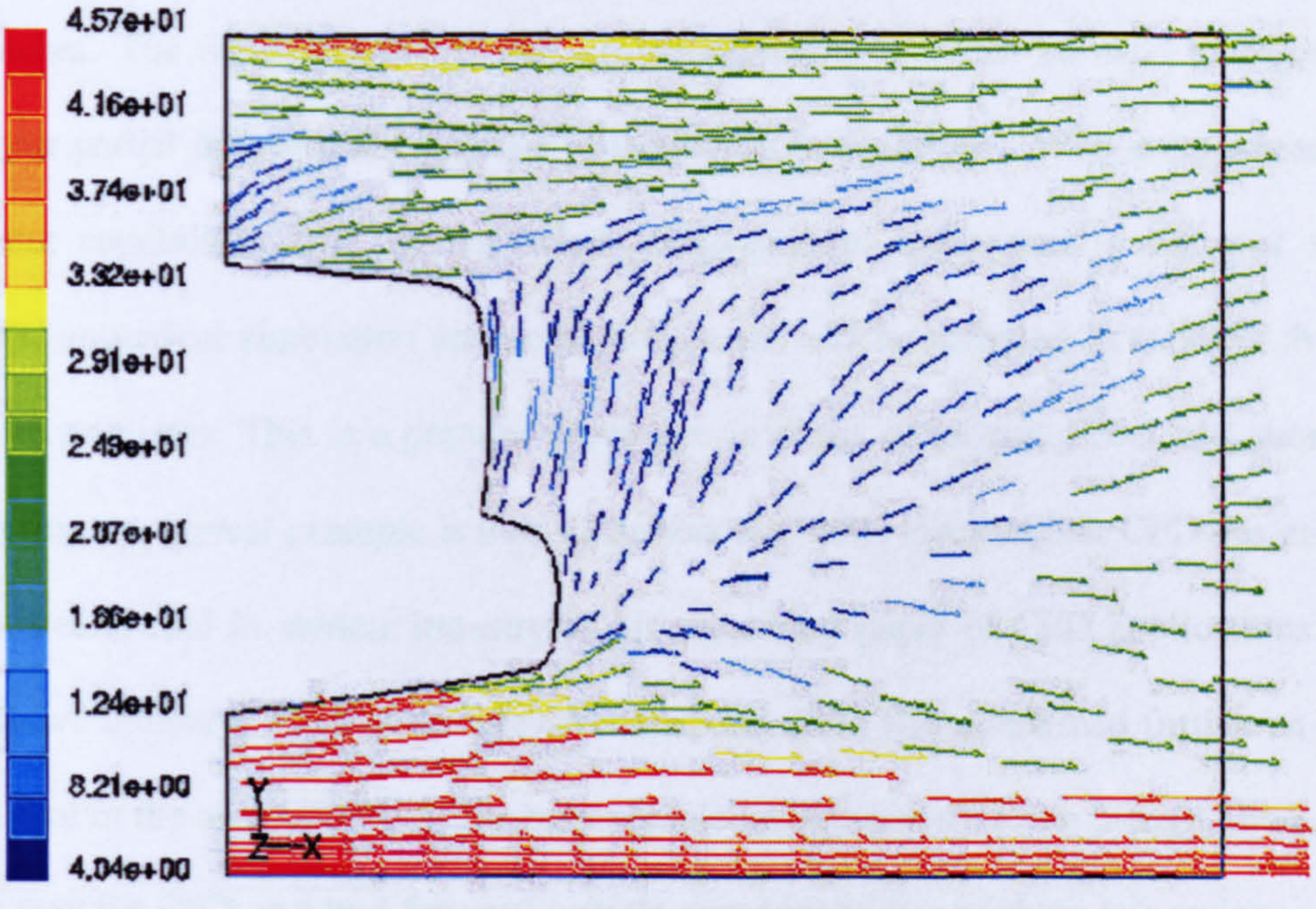

(b) Case: working section with diffuser/contraction

Figure 6.9 Wake behind the car model (scale=55%)

CHAPTER 7

MODEL TESTING OF A CAR IN WIND TUNNEL

7.1 Introduction

In the long history of classical mechanics, some practical engineering problems involving fluid mechanics have been solved by analytical procedures, however, there remain a large number of problems that rely on experimental data or numerical results for their solution. In modern fluid dynamics, the flows considered for analysis have become more complicated, therefore, very few problems can be actually solved by analytical approaches. The main problem is that no mathematical tool can be used to resolve the nonlinear partial differential equations (Navier-Stokes equations). With great advances in computer capabilities and the numerical computational techniques in the past several decades, numerical simulation and computation are widely accepted in tackling the fluid dynamic problems. This is a popular procedure in terms of reducing cost and shortening design time. A typical example is that, Dhaubhadel (1996) asserted that CFD has emerged as a powerful tool in vehicle industry in his reviewing paper of CFD applications in the automotive industry. Also, in the previous chapters CFD was confirmed further as a very useful tool in the computation of the road vehicle aerodynamics. Even though, there is still a long way for CFD as a tool for road vehicle aerodynamics, and there is a serious need of improvement of the prediction accuracy, reliability and the manipulation for CFD, particularly in handling the complicated fluid dynamic problems.

At present, for the complicated fluid dynamic problems, problem solving is generally achieved through the use of a combination of the analytical procedure, numerical simulation and experiment. There is no exception for automotive aerodynamic problems, like most complicated fluid dynamic problems, there are no analytical methods for road vehicle aerodynamics, and even the empirical methods for predicting vehicle aerodynamics haven't made any success, for the attempts to the empirical approaches have been abandoned (Hochu et al 1993). The most promising computation methods including modern computational fluid dynamics still have considerable limitations. Therefore, it is necessary to use wind tunnel testing.

For most of wind tunnel experiments, the models are the scaled models, i.e. 25-30% scale is the most popular scale in the wind tunnel testing of automobiles (Hucho 1993). The main advantages include: (i) scaled models are usually small, which are cheap and easy to manufacture and handle; (ii) scaled model can be tested in the small wind tunnels, therefore, the constructing and operating cost of wind tunnel is cheap and easy to access; (iii) the test environment is well adjusted and controlled. Even though, the scaled model tests have their own problems, such as blockage or wall interference; Reynolds number effect; model fidelity and even the use of wind tunnel data etc.

7.2 Methodologies of Model Testing

Model testing is an indispensable step for aerodynamic design, although CFD tools have replaced many wind tunnel tests for the reasons of reducing cost and accelerating the design process. But, wind tunnel experiments should be designed so that the results are widely applicable as possible, therefore, the tunnel engineer's careful plans for experiment

are needed, including model design and fabrication, test preparations, record of the reliable data, interpretation and use of test data. In a word, the model testing isn't simply recording the experimental data, but a whole procedure of careful planning for the testing.

To achieve this goal, dimensional analysis and the similitude are first considered to design the model and guide the operation, so that measurements made in a laboratory can be used to describe the behaviour of other similar systems. The laboratory systems are usually thought of as models and are used to study the phenomenon of interest under carefully controlled conditions. From these model studies, empirical formulations can be made. To do this, it is necessary to establish the relationship between the laboratory model and the "other" system, in which the similitude laws are applicable (in Appendix C the details of the dimensional analysis and the similitude laws are given).

7.3 Use of Wind Tunnel Data

For most wind tunnel testing, the model is usually manufactured smaller than the prototype, it's very difficult for the scaled model testing in wind tunnel to reach the same Reynolds number as the prototype, if it's not impossible. Therefore, for the scaled model test in wind tunnel, the tunnel engineers are often facing the problem of Reynolds number effect, i.e., how to use the wind tunnel data?

Rae and Pope (1984) mentioned in their book: data can easily be taken all day long, as long as they are not used to design airplanes. And also the difficulties lay: one side is that little correlation had been made between flight test and wind tunnel data available, which increases the difficulties to extrapolate the wind tunnel data to prototype; another side is

that any flight test and wind tunnel correlation always suffers from a great number of unknowns. The tunnel data suffer inexact or unknown Reynolds number extrapolation, uncertainties in corrections to the data such as tare and interference and wall effects, errors in duplicating the power on effects with fixed-pitch propeller, simulation of flow around or through jet engine nacelles, omission of manufacturing irregularities and small excrescences, and insufficient deflections of the model under load. The flight test data suffer from the pilot techniques, acceleration due to gusts, errors in average center of gravity locations, determination of true airspeed, and unknowns of propeller efficiencies and other power-plant effects.

Although the difficulties mentioned before are ever present, the use of wind tunnel data is feasible in some areas. In the long history of wind tunnel testing, tunnel engineers have accumulated the experience in using wind tunnel data. In their book, Rae and Pope (1984) summarised the fundamental extrapolation methods for wind tunnel data, including the boundary layer, scale effect on drag, lift curve, etc, and provided the general ways to use wind tunnel data.

McDonald et al (2000) reported their practice in wind tunnel data corrections in NASA Ames Research Center, aiming to improve the understanding of the pertinent aerodynamics and the extrapolation methods.

7.4 Car Model

In this research, a scaled car model (30%) was manufactured and tested in the Argyll Wind Tunnel. The car was a generic car, as shown in Figure 7.1.

The blockage of the 30% car model in the Argyll Wind Tunnel was 3.44%, lower than the recommended blockage of a conventional test 5%, even lower than the 3.9% of Han's test models (Han et al 1996), in which they thought the blockage effect could be ignored. But, in this model test, a strong supporting system was employed to hold the model firmly (see figure 4.17), and its frontal area was comparative to that of the car model. Therefore, the overall blockage in the working section is 6.1%, still smaller than 7.5% blockage of Rae & Pope's recommendation.

In the manufacture of the model, the model was actually sectioned into 10 sections, shown in figure 7.2, and some section profiles for model manufacturing are given in figure 7.3. Figure 7.4 is the photography of the manufactured model. Figure 7.5 shows the model installation in the working section.

It can be seen that the supporting system (strut) supports the test model from the tunnel ceiling. A force transducer is connected to the model and used to measure drag and lift. The strut has a computer controlled movement system to control the model moving up and down, in order to adjust the clearances of the car above the ground. In this test, the clearance varies from 0.01m to 0.20m (the scaled height of the actual car is 0.076m, corresponding to the prototype 0.25m). The following table gives the test cases.

Table 7.1 Test Cases

Clearance(m) / Speed	0.01	0.015	0.02	0.025	0.03	0.035	0.04	0.05	0.075	0.10	0.20
10m/s	O	O	O	O	O	O	O	O	O	O	O
15m/s	O	O	O	O	O	O	O	O	O	O	O
20m/s	O	O	O	O	O	O	O	O	O	O	O
25m/s	O	O	O	O	O	O	O	O	O	O	O
30m/s	O	O	O	O	O	O	O	O	O	O	O
35m/s	O	O	O	O	O	O	O	O*	O*	O*	O

Note: O- measuring drag and lift, O*- measuring drag and lift, as well as oil visualization.

Figure 7.6 shows the numerical model, comparing to the physical model in Figure 7.5.

7.5 Aerodynamics Test of Car

The aerodynamics test of the car model is carried on for different air speed and the different ground clearances. The test cases are listed in Table 7.1.

Figure 7.7 gives the comparisons of numerical simulations and experimental results for drag and lift coefficient in different air speeds. The good agreement is achieved in the drag coefficient prediction. Figure 7.8 shows the comparisons of numerical simulations and experimental results for drag and lift coefficient in different clearances. Again, the drag coefficient prediction is in the good agreement with the experiment.

In general, CFD can predict the drag of road vehicles in good accuracy, while for lift, CFD predictions, only in few cases, give very good prediction. In the automotive industry, it's generally accepted that lift forces are usually poorly predicted.

For the conventional road vehicle, the most important aerodynamics is drag, because the low drag coefficient is the target that the car manufacturers pursue, especially after two oil crises in 70's. For formula race cars, the drag coefficient is inherently important, but the lift is more important. Because large down force for formula 1 race car is the vital factor for increasing the cornering speed and, therefore, the overall speed.

In this research, CFD predicted the drag coefficient accurately, but a little poor prediction in lift coefficient.

7.6 Flow Visualisation

Flow visualisation has been a critical factor in understanding flow physics. In modern fluid dynamics test, the various tools for flow visualisation have been widely used, and these methods can be made quantitative even in complex and/or unsteady flow fields. For the qualitative visualization of flows, smoke and fluorescent oil/paint are widely used, while for the quantitative measurements of velocity, techniques have been developed for nonintrusive approaches, only relying on seeding the flow with particles and observing the motion of those particles. These seeded approaches include Laser Doppler Velocimetry (LDV), Particle Image Velocimetry (PIV), or even Doppler Global Velocimetry (DGV). More advanced techniques of unseeded visualisation in flow measurements have been

developed recently (Miles et al 1997), the laser-induced fluorescence from oxygen, flow tagging by oxygen excitation, and Reyleigh scattering are among them.

In this wind tunnel test, an oil with a fluorescent seeding was used to visualise the flowfield on the surface of the car model. The fluorescent powder was mixed up with the oil, and then put on the car model before each test run. During the test, the air flow would change the fluorescent oil on the car surface, and some particular pattern would be formed on the car surface. When the steady pattern was formed, the resulting flow patterns were photographed.

Figure 7.9 and 7.11 are the photographs taken of the fluorescent oil patterns on the car surface, from the front and rear views, respectively, while figure 7.10 and 7.12 give the pathlines of the corresponding numerical simulation near the car surface. For the flow visualization in the front part of the car, the numerical simulation gives an accurate pathline prediction (figure 7.9 and 7.10), and for the rear part, the numerical pathlines also show the same trend as the oil flow, but not in some particular areas. The oil flow near the underbody showed some uneven flows, where numerical simulation gave the continuous and smooth pathlines.

7.7 Concluding Remarks

From the comparisons between simulation and experiment, the following remarks can be made:

- CFD prediction of drag coefficients is quite reliable for the different oncoming streams and the different clearances. As a result, it's accepted that the prediction of drag coefficient can be done by CFD methods.

- For the lift coefficient prediction, the accuracy is not so high as drag coefficient. The main reason is that CFD has difficulties to predict the flows between the vehicle and ground properly, which has significant effect on the lift, while little effect on drag.

- Compared to the oil flow on the vehicle surface, CFD gives a quite good prediction of the pathlines near the car surface, especially for the front part of the car.

Figures of Chapter 7

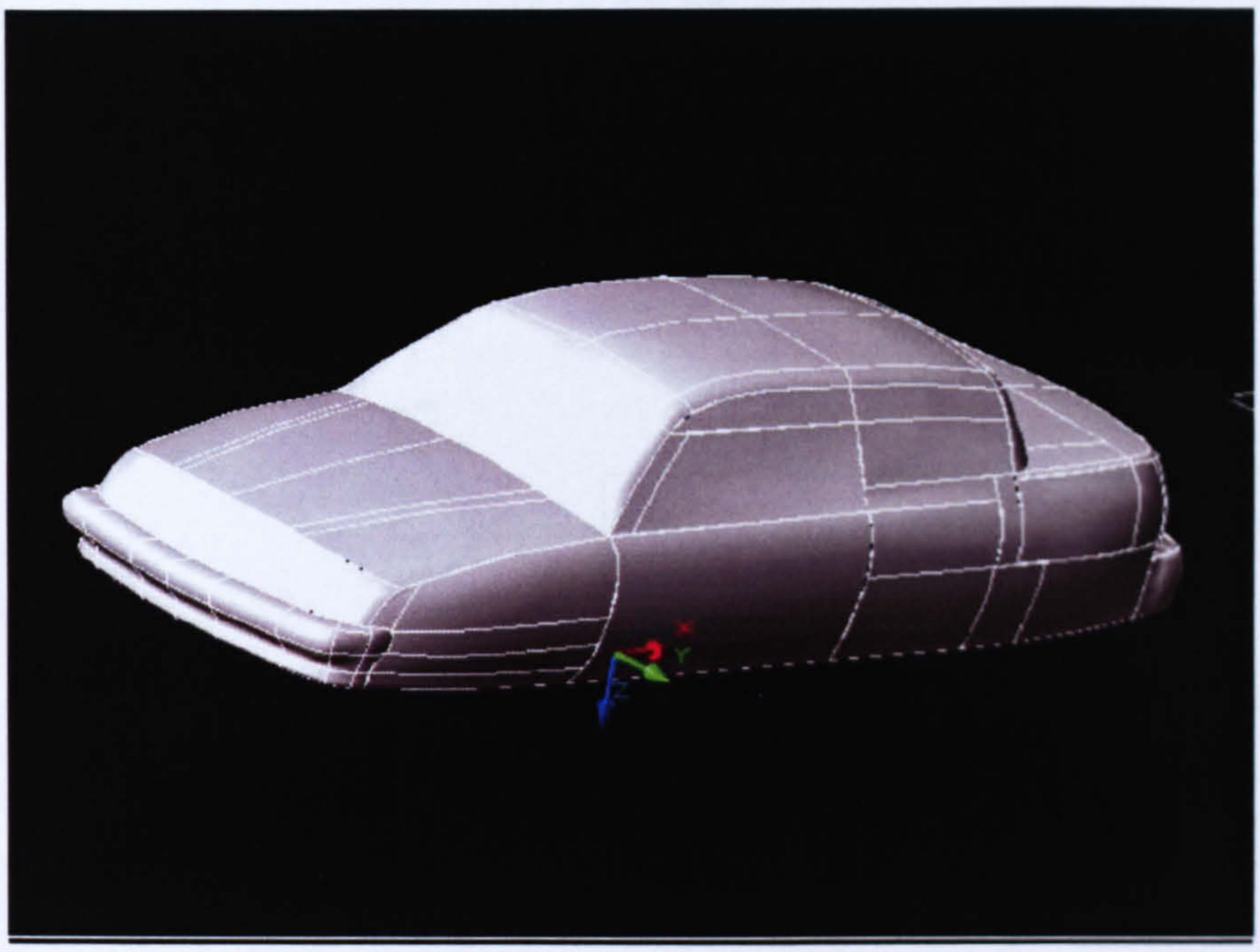

Figure 7.1 Image of the car (numerical model)

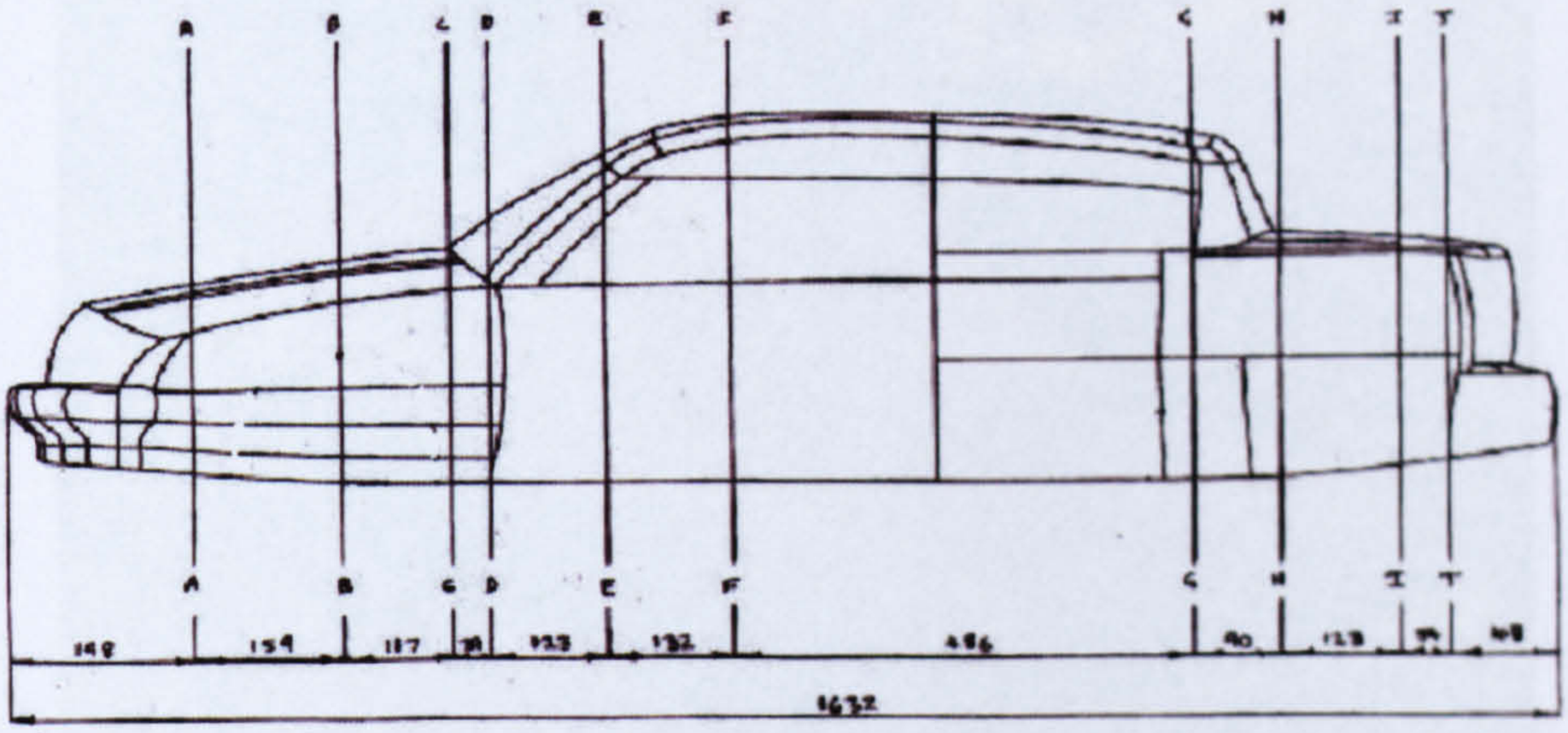

Figure 7.2 The section view of the 30% scaled car

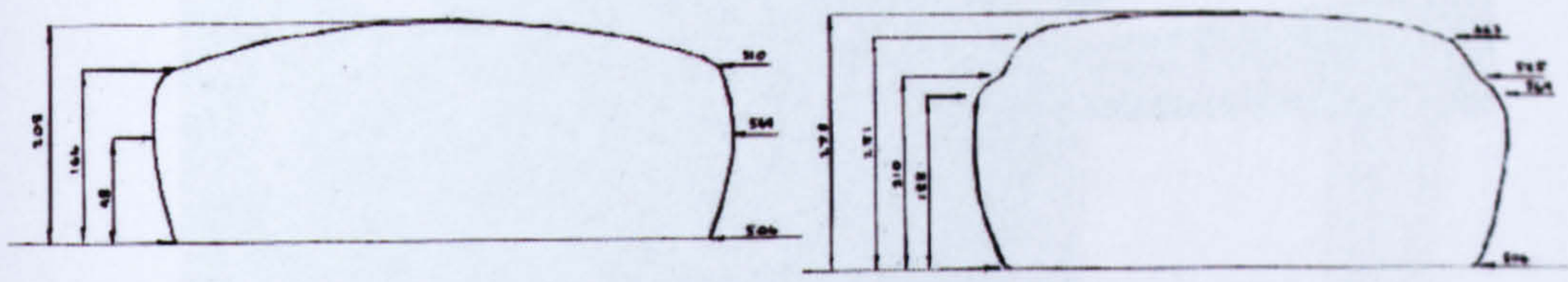

Section A-A

Section D-D

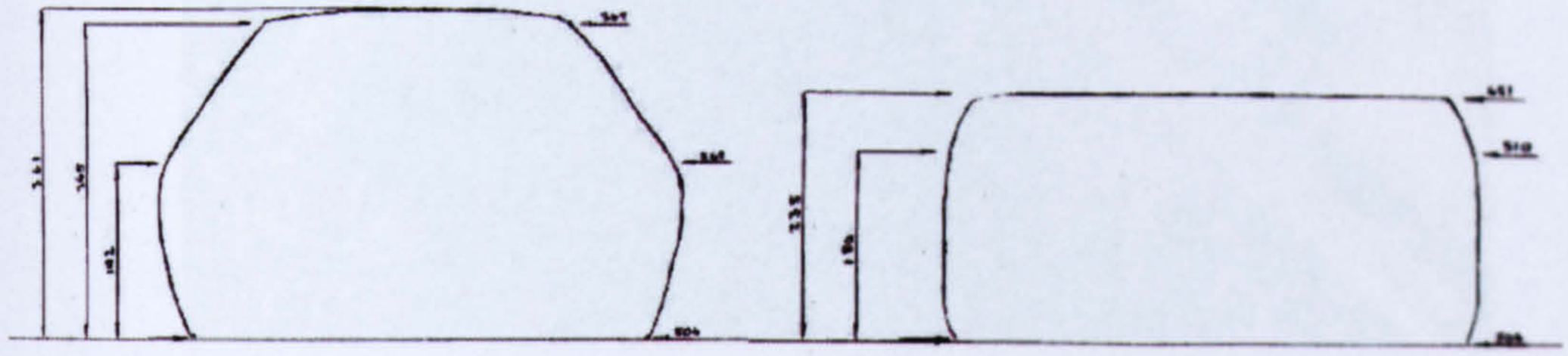

Section G-G

Section J-J

Figure 7.3 Some sections of the 30% car

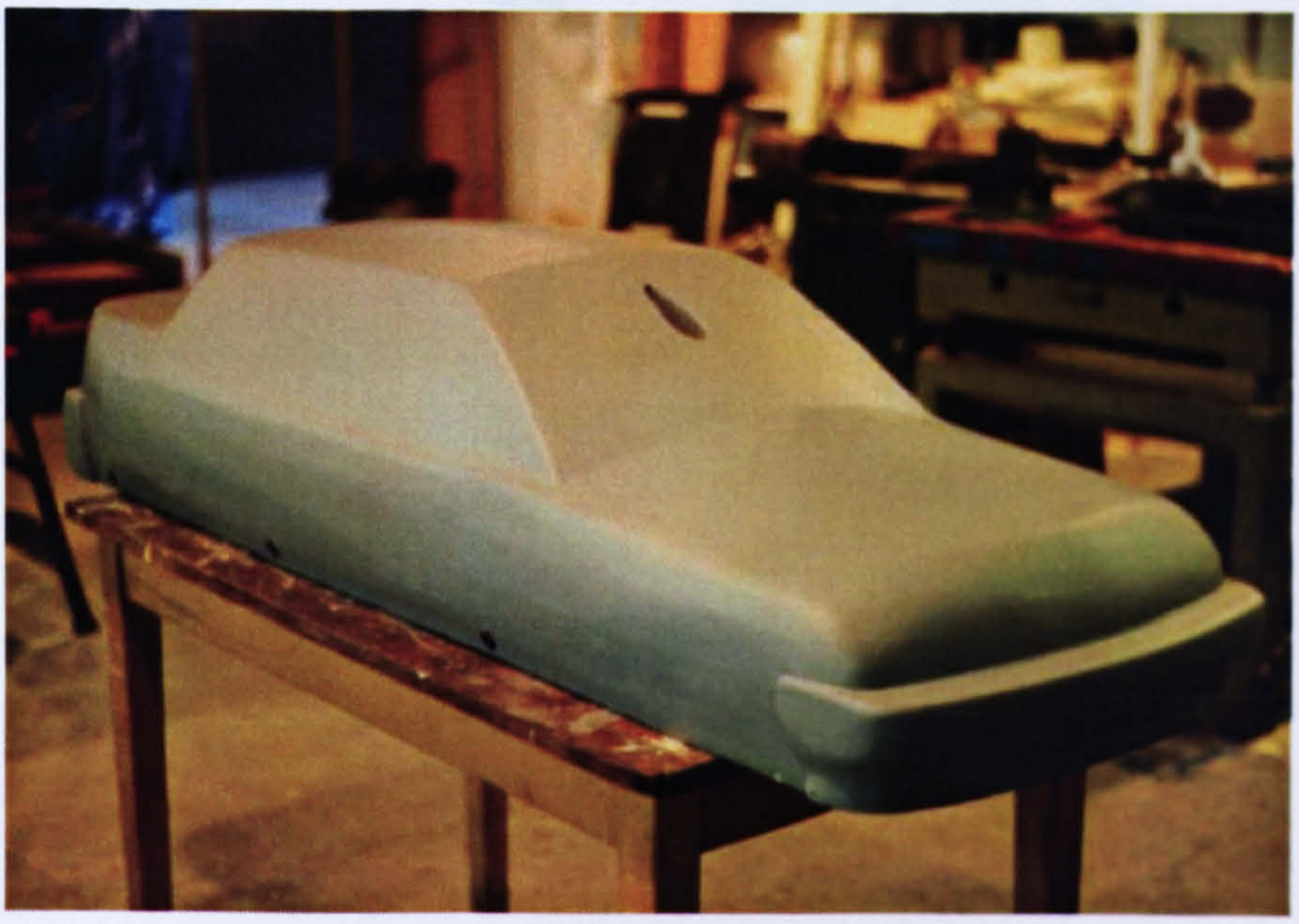

Figure 7.4 The manufactured 30% car model

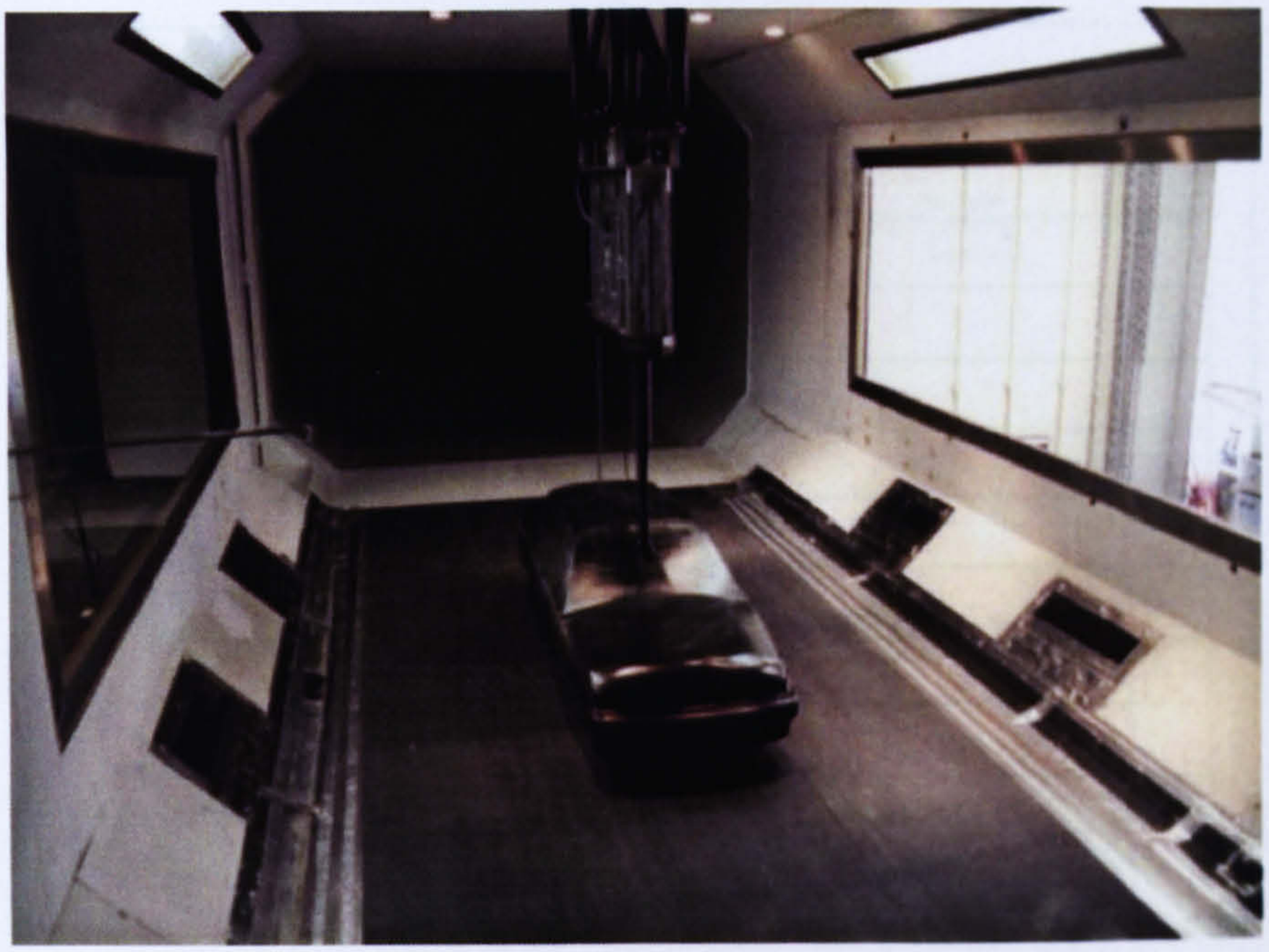

Figure 7.5 A Car Model in the Working Section

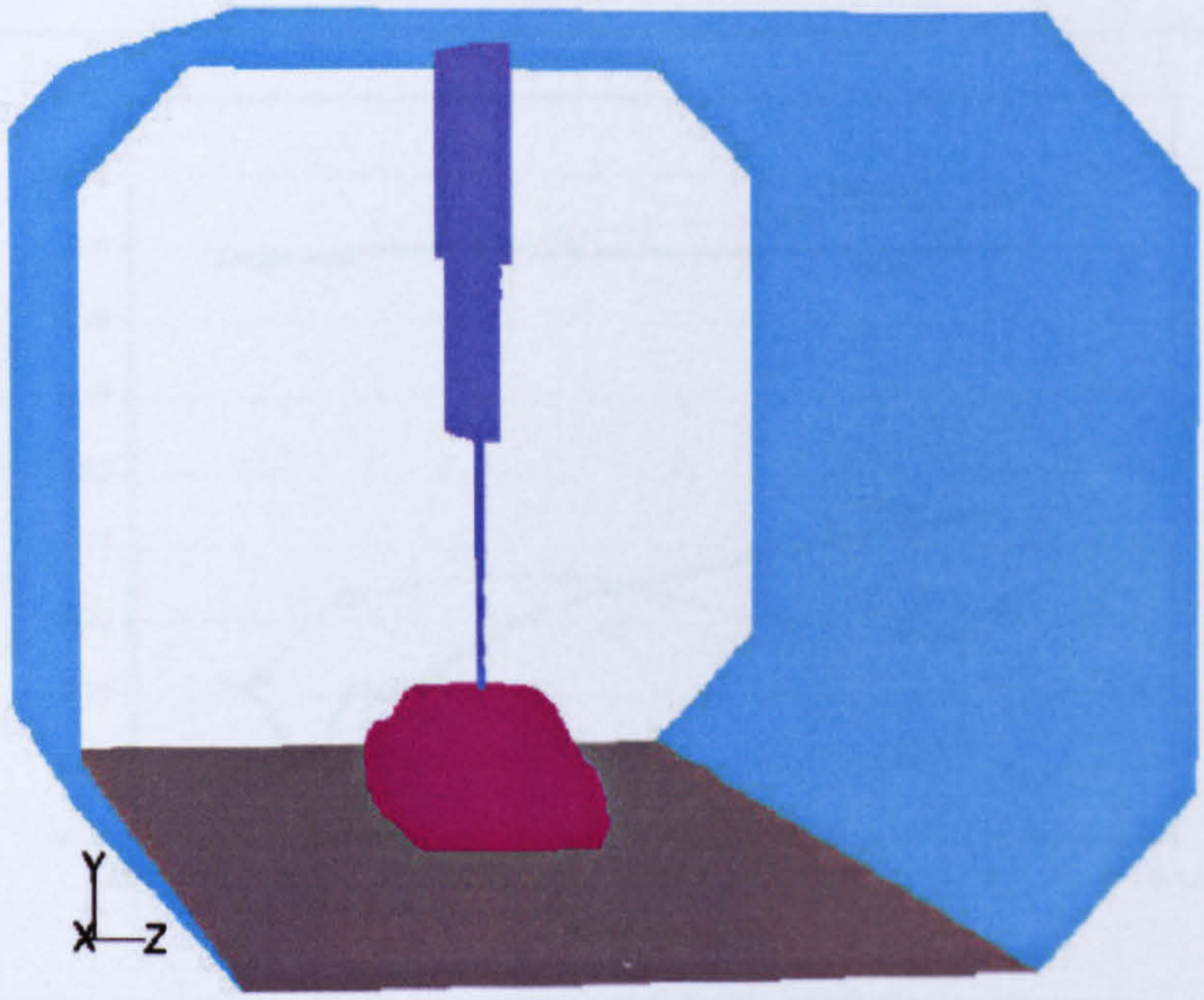

Figure 7.6 A Car Model in the Working Section (Numerical Model)

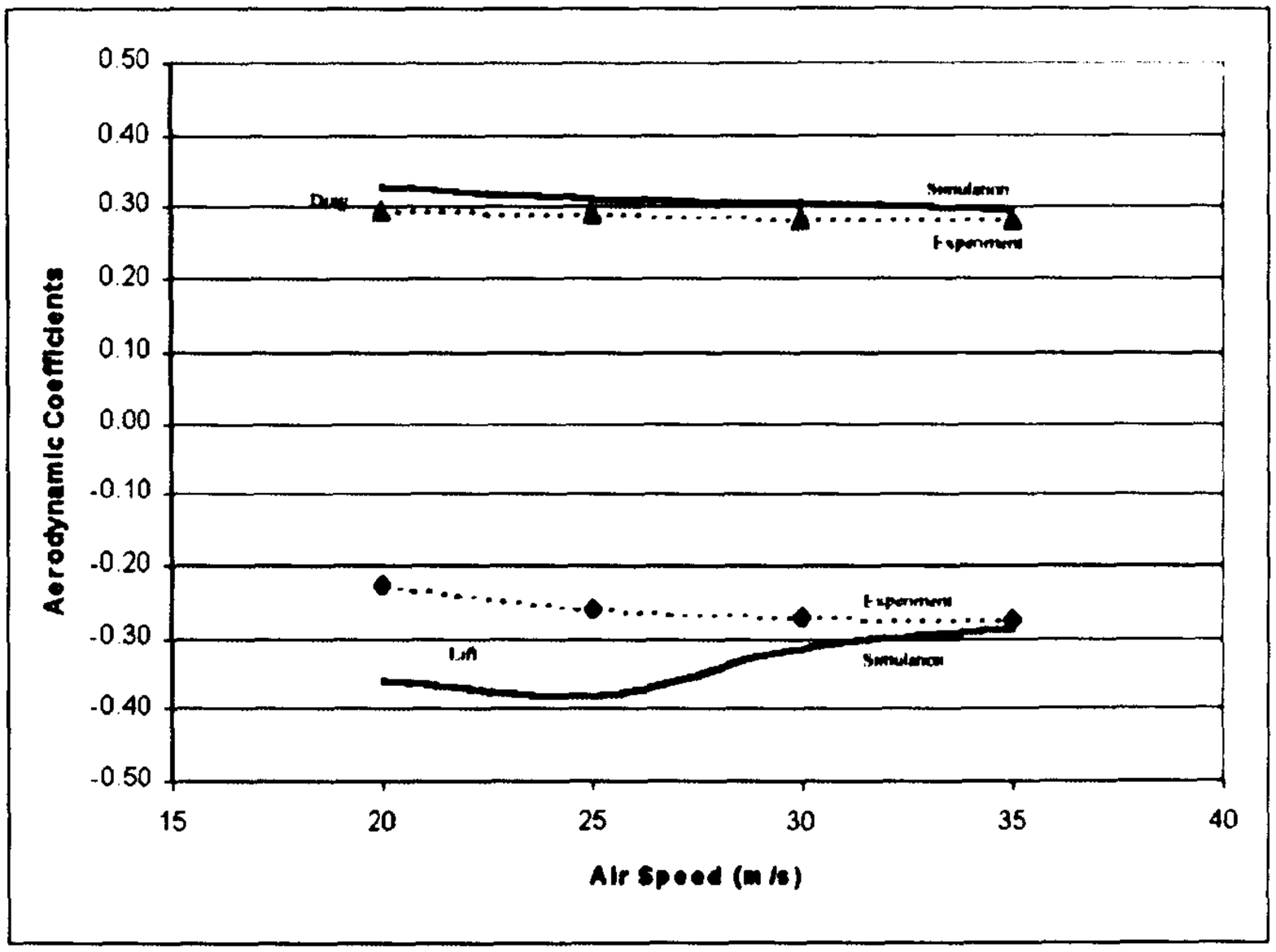

Figure 7.7 Drag and lift coefficient against the air speed

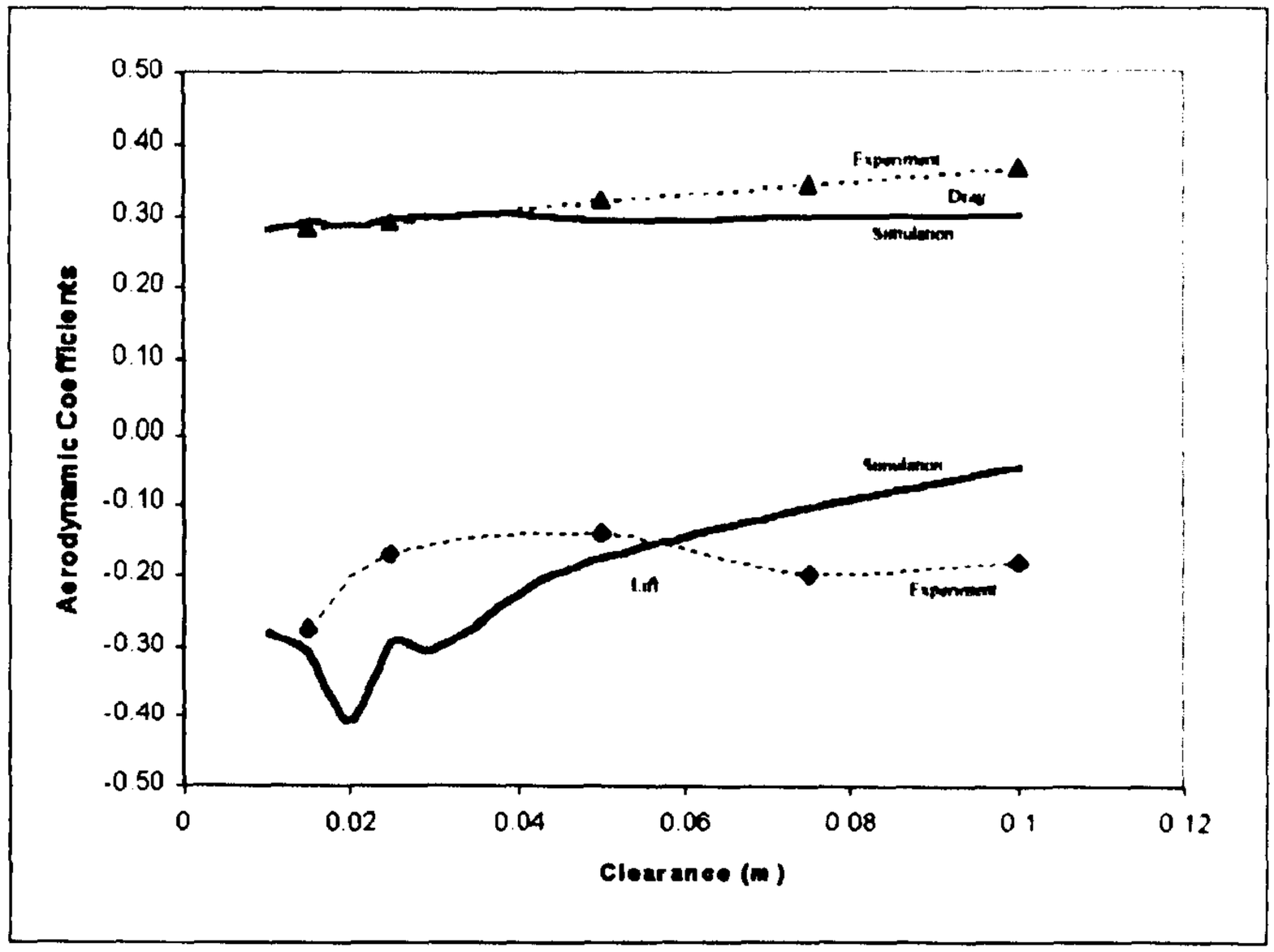

Figure 7.8 Drag and lift coefficients against the clearance

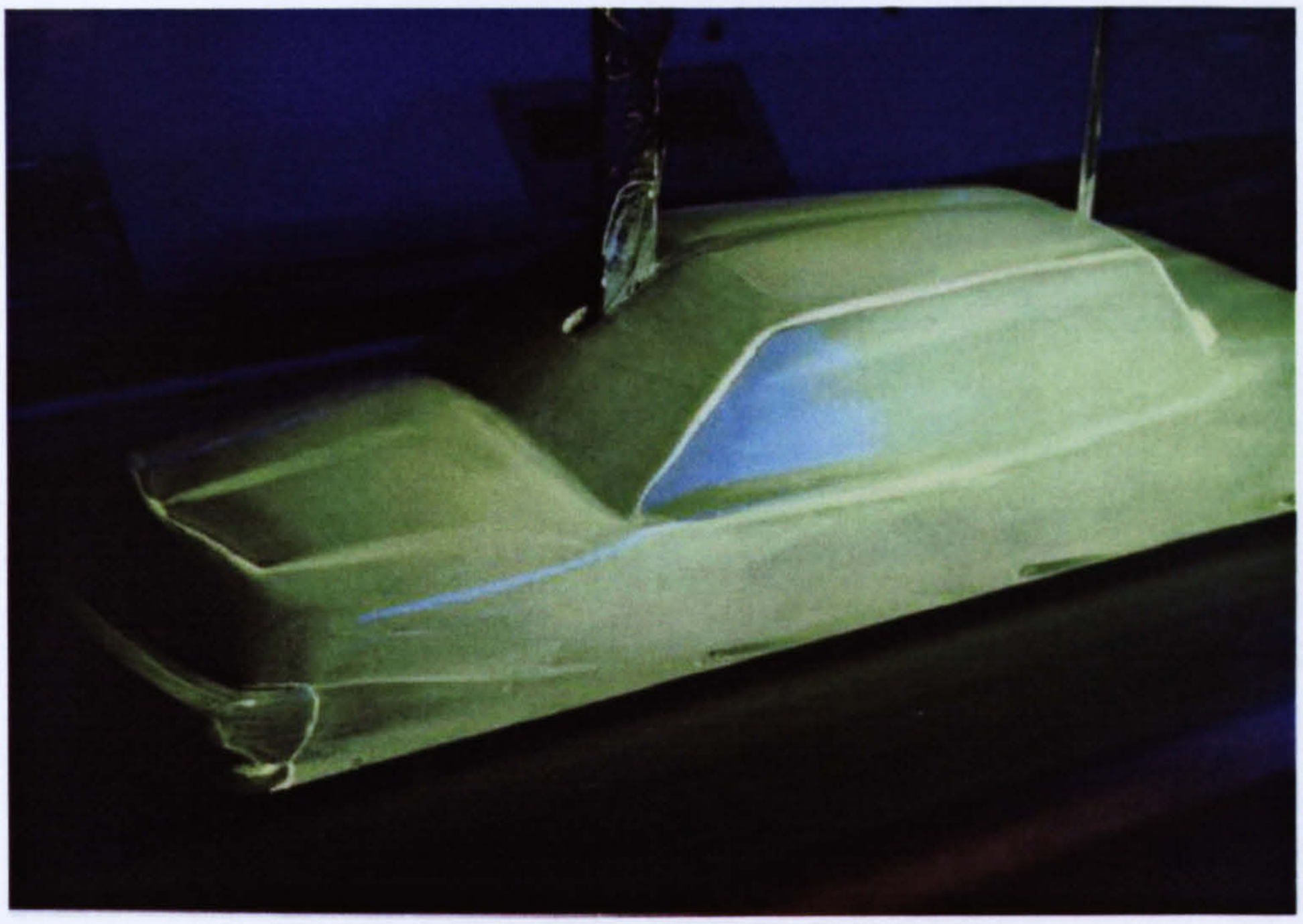

Figure 7.9 Flow visualization by fluorescent oil on car surface

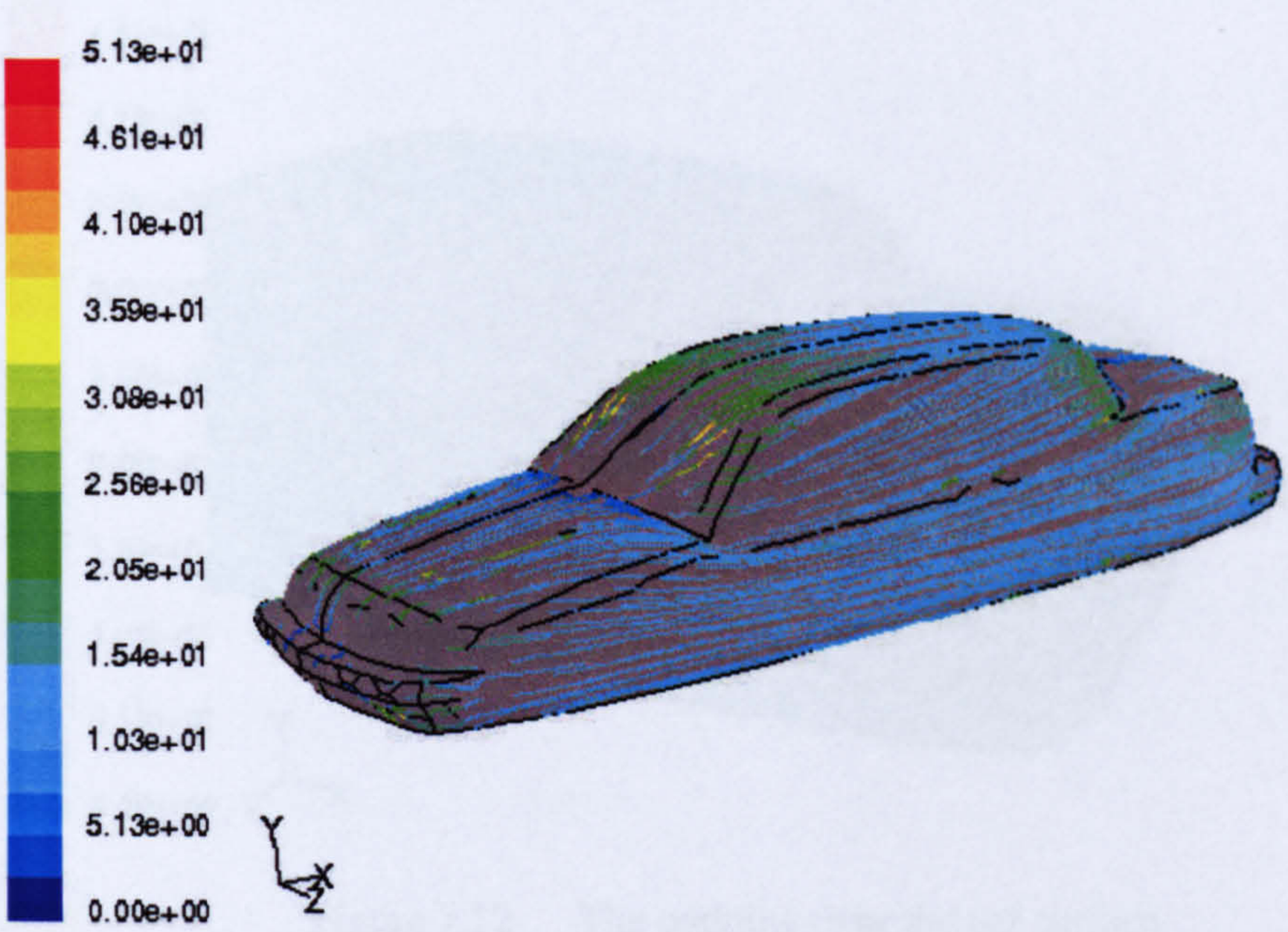

Figure 7.10 The pathline over the car surface

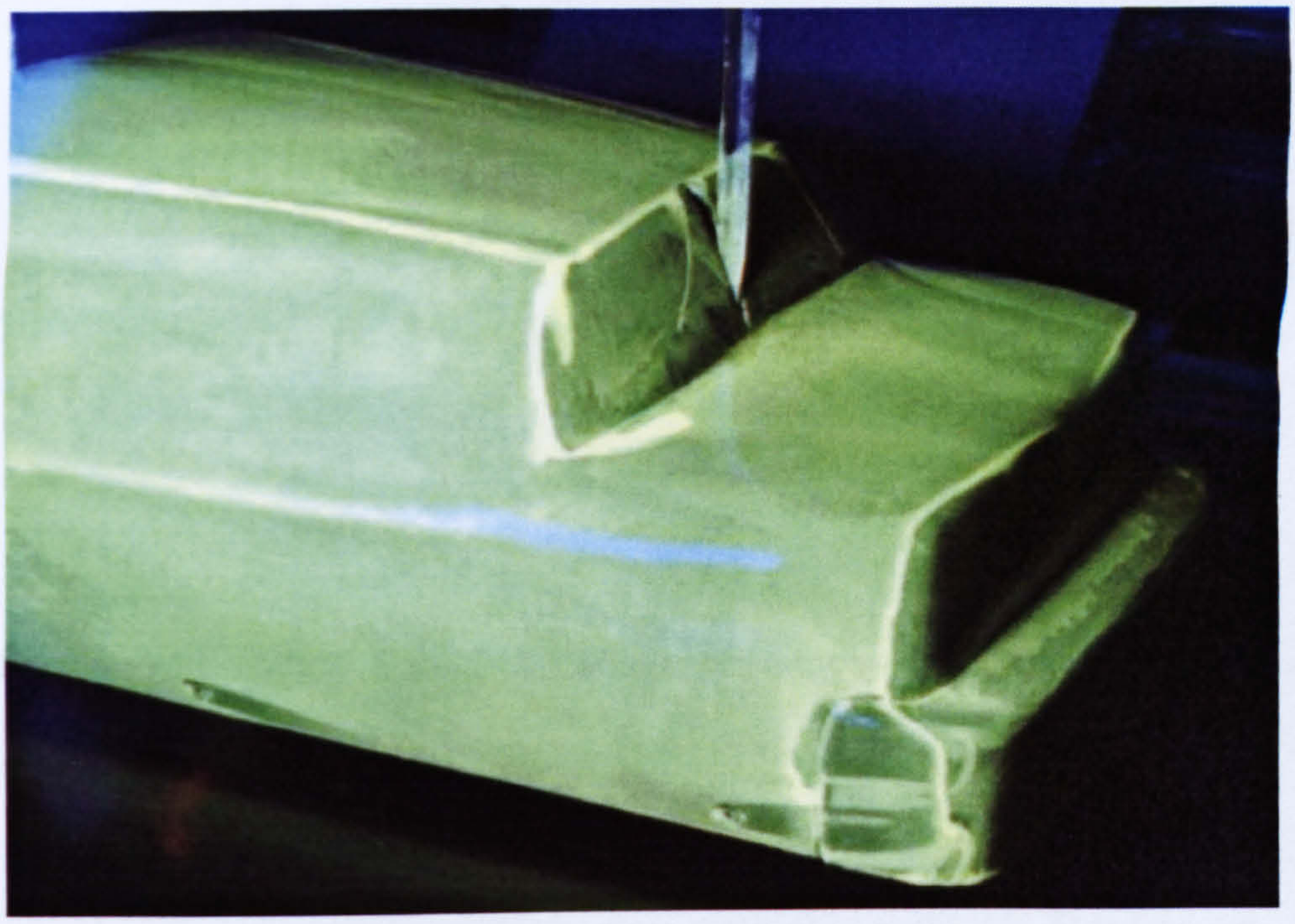

Figure 7.11 Flow visualization by fluorescent oil on car surface

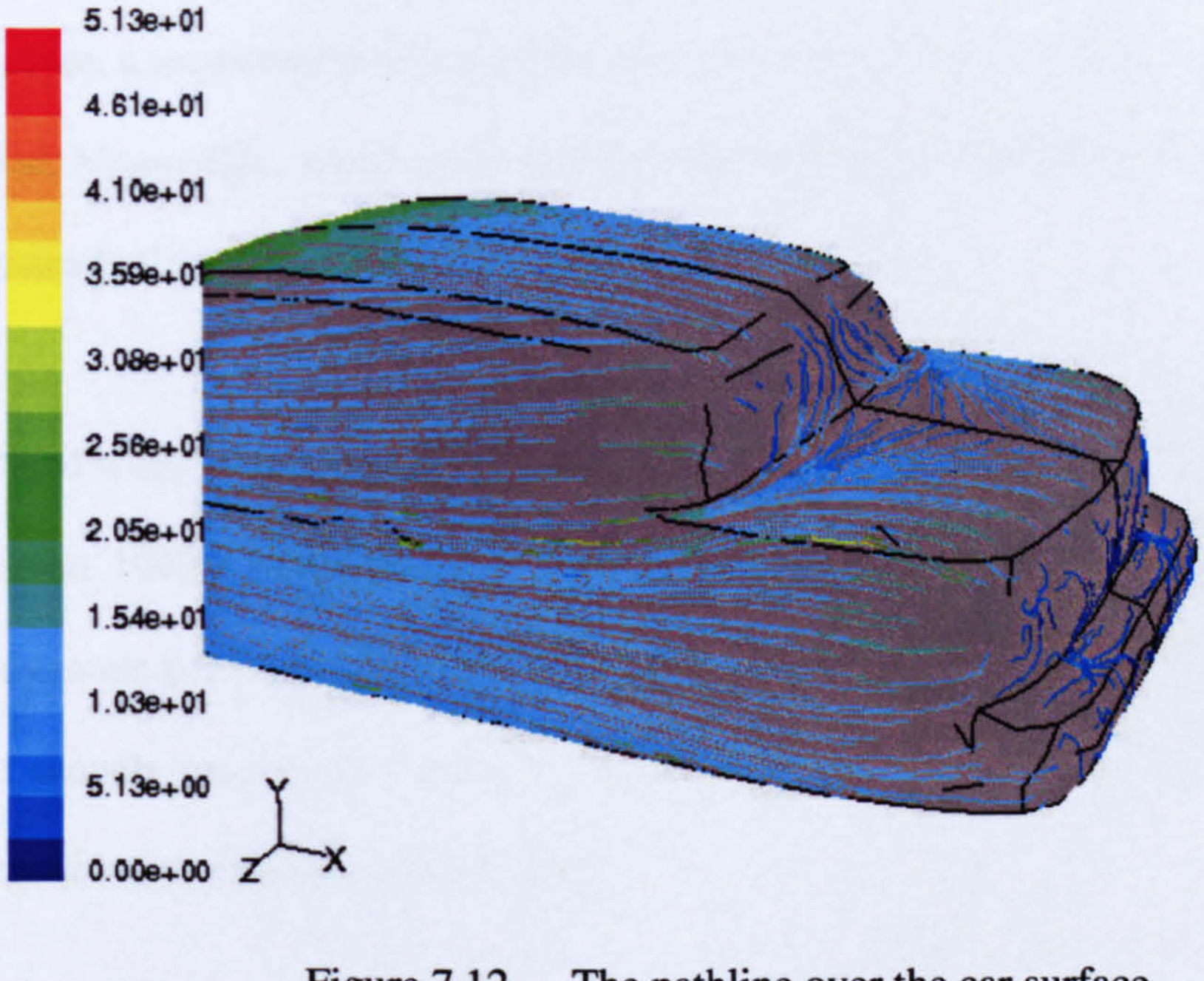

Figure 7.12 The pathline over the car surface

CHAPTER 8

CONCLUSIONS AND FUTURE WORK

8.1 Conclusions

Wind tunnels will continue to play an important role in aerodynamics test, and they won't be replaced fully by CFD tools in the foreseeable future although CFD has reduced the wind tunnel test in the early aerodynamic design stages. With the ruthless competition in aircraft and automotive industries, the requirements for wind tunnel testing are becoming more and more stringent. For civil aircraft, the accuracy of wind tunnel test should be 1-2 counts (Jameson etc 2001), and 20 counts for automotive test (Hucho et al 1993). Therefore, a requirement of a significant improvement to the current wind tunnel testing is needed. Meanwhile, advances in measurement are also needed for the complicated flows or unsteady flows (Passmore et al 2001).

CFD and wind tunnel simulations are complementary due to their own inherent limitations (Agarwal 1999). As progress is made towards using CFD tools in predicting absolute aerodynamic performance and certifying new technologies and concepts, the future role of wind tunnels may evolve more towards phenomena-based testing and development of code validation database (Kumar 2000).

In this research, CFD tools were used to complement and, therefore, enhance the wind tunnel test. As the first stage, the research work has finished the research on the numerical simulation of working section (including first diffuser and contraction/settling chamber),

the blockage correction and the effect of support system. The eventual goal was to form a powerful facility for aerodynamic testing by combining CFD tools and wind tunnel.

From the previous chapters, the general conclusions can be drawn:

i) CFD has emerged as a powerful tool in fluid dynamics research and applications. In aircraft industry, the whole bodies of aircraft have been analysed by CFD and the results show the very good agreements with experiment. In automotive industry, CFD application has made great progress, and the drag prediction is acceptable, while lift prediction may need some improvements.

ii) CFD is successfully used to simulate the working section, involving the first diffuser and contraction/settling chamber. The results show that the pressure and velocity in the working section can benefit from the design with an expansion. The boundary layer is well removed by the moving belt system in the Argyll Wind Tunnel.

iii) CFD simulation shows that the uniform flows could be obtained in the working section when the contraction and first diffuser are added on the simulation.

iv) CFD has reproduced the removal of boundary layer numerically. Further, a more simplified moving ground system could be gained by lowering the moving ground to be flush with tunnel floor, according to the CFD simulation results.

v) CFD predicts the drag coefficients of road vehicles well in general, but has some difficulties in predicting the lift coefficients.

vi) The blockage correction is also investigated by CFD computation. A CFD direct compensation method is applied in this research.

vii) CFD is used to investigate the strut effect on the test results. The numerical results show the significant effects on the test results. Besides, the strut positions have significant effects on the test results as well, and the effects may be best removed by CFD method.

viii) CFD simulation and wind tunnel test are complimentary due to their inherent limitations. Therefore, a more powerful facility for aerodynamic test is expected by combining CFD and wind tunnel.

8.2 Future Work

Future role of wind tunnels are shifting towards phenomena-based testing and development of code validation database (Kumar 2000), and the future wind tunnel testing will be more complicated in principle, more accurate and elaborate in measurement. Therefore, much work is needed in wind tunnel techniques, as well as CFD assisting wind tunnel testing.

From the previous chapters, CFD has shown its capabilities in supporting wind tunnel testing. It's feasible to form a more powerful facility for aerodynamic testing by the proper use of CFD in wind tunnels. Further research work is needed in following aspects:

i) Wind tunnel numerical simulation

Numerical simulation of wind tunnel should include the other parts of the wind tunnel, such as the corners and cascades, the 2nd diffuser and even the fan. The overall work will help to understand the wind tunnel, and a real numerical wind tunnel is being expected.

ii) Further CFD research of road vehicle aerodynamics

The flows around road vehicle are actually very complicated. The present CFD predicts drag quite accurately in general. But, more delicate CFD simulation and analysis are still needed, and special attention could pay to the complicated flow structures, such as wake vortex, unsteady flows, separations and reattachments, which are actually challenging the CFD community. In the future research, superior turbulence models, such as DES (LES+RANS), even LES, may be employed, in order to predict the vehicle aerodynamics more accurately, especially for the lift prediction.

iii) Further experiments and comparisons

In the present research, the wind tunnel testing only included the measurements of drag and lift, and the oil flows on the car surface for one scaled model. Future experiments should include different scale models and a delicate flowfield measurement and flow visualization. Besides, some appendices may be added on the car model, such as spoiler, tyres etc.

For the different scaled models, the tests aim at the blockage correction and the Reynolds number effect; for the flowfield measurement, the tests should include the pressure on car surface, and the velocity around the car. The advanced flowfield measurement and visualization are also needed.

REFERENCES

1. Agarwal R, 'Computational Fluid Dynamics of Whole-Body Aircraft', *Annual Review of Fluid Mechanics* 31:125-169 (1999)
2. Ahmed S.R, 'Wake Structure of Typical Automobile Shapes', *Journal of Fluids Engineering* 103: 162-169 (1981)
3. Ahmed S.R, 'Influence of Base Slant on the Wake Structure and Drag of Road Vehicles', *Journal of Fluids Engineering* 105: 429-434 (1983)
4. Ahmed S. R, Ramm G, Faltin G, 'Some Salient Features of the Time Averaged Ground Vehicle Wake', SAE Paper 840300 (1984)
5. Arnal P, Casalis G, 'Laminar-Turbulent Transition Prediction in Three-Dimensional Flows', *Progress in Aerospace Science* 36: 173-191 (2000)
6. Aroussi A, Aghil S, 'Characterisation of the Flow Field in a Passenger Car Model', *Optical Diagnostics in Engineering* 4: 1-15 (2000)
7. Ashill P.R, Goodyer M.J, Lewis M.C, 'An Experimental Investigation into the Rationale of the Application of Wind Tunnel Wall Corrections', ICAS 96-2.4.1: 798-808
8. Ayad S.S, 'Computational Study of Natural Ventilation', *Journal of Wind Engineering and Industrial Aerodynamics* 82: 49-68 (1999)
9. Baker C.J, Humphreys N.D, 'Assessment of the Adequacy of Various Wind Tunnel Techniques to Obtain Aerodynamic Data for Ground Vehicles in Cross Winds', *Journal of Wind Engineering and Industrial Aerodynamics* 60: 49-68 (1996)
10. Bardina J.E, Huang P.G, Coakley T.J, 'Turbulence Modelling Validation, Testing, and Development', NASA Technical Memorandum 110446 (1997)
11. Basara B, 'Computations of Automotive Flows Using the Second Moment Closure', *European Congress on Computational Methods in Applied Science and Engineering*, Barcelona, Sep. 1994
12. Beccaria M, Buresti G, Ciampa A, Lombardi G, Gentzsch G, Paap H G, Vicere A, 'High-Performance Road Vehicle Optimised Aerodynamic Design: Application of Parallel Computing to Car Design', *Future Generation Computer System* 15: 323-332 (1999)
13. Bosniakov S, 'Experience in Integrating CFD to the Technology of Testing in Wind Tunnels', *Progress in Aerospace Science* 34: 391-402 (1999)

14. Boswell B.A, Dutton J.C, 'Flow Visualization and Measurements of a Three-Dimensional Supersonic Separated Flow', AIAA Journal 39: 118-121 (2001)
15. Bradshaw P, Pankhurst R.C, 'The Design of Low-Speed Wind Tunnels', *Progress in Aeronautical Sciences* 5: 1-69 (1964)
16. Brain C, 'Simulation in Support of Test or Test in Support of Simulation', IMechE S555/008/98 (1998)
17. Bryson S, Levit C, 'The Virtual Wind Tunnel', *IEEE Computer Graphics and Applications* 12(4): 25-34 (1992)
18. Campbell T, Galbraith R.A.McD, Sheng W, Fleming A, 'The Application of Computational Fluid Dynamics (CFD) in the Aerodynamics Design of Race and Road Vehicles', SAE 2003-01-1250
19. Chapman J.R, Mark H, Pirtle M.W, 'Computers vs. Wind Tunnels for Aerodynamic Flow Simulations', *Astron. Aeronaut.* 13: 22-30 (1975)
20. Cheng L, Armfield S, 'A Simplified Marker and Cell Method for Unsteady Flows on Non-Staggered Grids', *International Journal for Numerical Methods in Fluids* 21: 15-34 (1995)
21. Choi D, Prasad D, Wang M, Pierce C, 'Evaluation of an Industrial CFD Code for LES Applications', Proceedings of the Summer Program 2000 (Center for Turbulence Research), 221-228 (2000)
22. Conlisk A.T, 'Modern Helicopter Aerodynamics', *Annual Review of Fluid Mechanics* 29: 515-567 (1997)
23. Conlisk A.T, 'Modern Helicopter Rotor Aerodynamics', *Progress in aerospace Science* 37:419-476 (2001)
24. Corda S, Stephenson M.T, Burcham F.W, Curry R.E, 'Dynamic Ground Effects Flight Test of an F-15 Aircraft', NASA Technical Memorandum 4604 (1994)
25. Craft T.J, 'Development in a Low-Reynolds-Number Second-Moment Closure and its Application to Separating and Reattaching Flows', *International Journal of Heat and Fluid Flow* 19: 541-548 (1998)
26. Cross A.G.T, 'The Use of Computational Fluid Dynamics in Support of Wind Tunnel Testing', IMechE S555/002/98 (1998)
27. Deloach R, 'The Modern Design of Experiments: A Technical and Marketing Framework', AIAA 2000-2691
28. Diana G, De Ponte S, Falco M, Zasso A, 'A New Large Wind Tunnel for Civil-Environmental and Aeronautical Applications', *Journal of Wind Engineering and Industrial Aerodynamics* 74-76: 553-565 (1998)
29. Durbin P.A, 'Separated Flow Computations with the κ-ε-v^2 Model' AIAA Journal 33: 659-664 (1995)
30. Ewald B.F.R. (editor), *Wind Tunnel Wall Correction*, AGARD AG-336, North Atlantic Treaty Organization, Oct. 1998

31. Fang F.M, Chen J.C, Hong Y.T, 'Experimental and Analytical Evaluation of Flow in a Square-to-Square Wind Tunnel Contraction', *Journal of Wind Engineering and Industrial Aerodynamics* 89:247-260 (2001)
32. Filippone A, *Advanced Topics in Aerodynamics* (internet book, 2003), Available website: http://aerodyn.org/
33. *FLUENT Manual*: http://sp81.msi.umn.edu:999/fluent/index.htm
34. Freitas C.J, 'Perspective: Selected Benchmarks from Commercial CFD Codes', *Journal of Fluids Engineering* 117: 208-218 (1995)
35. Fukuda H, Yanagimoto K, China H, Nakagawa K, 'Improvement of Vehicle Aerodynamics by Wake Control', *JSAE Review* 16:151-155 (1995)
36. *GAMBIT Manual*: http://sp81.msi.umn.edu:999/gambit/index.html
37. Gatski TB, Jongen T, 'Nonlinear Eddy Viscosity and Algebraic Stress Models for Solving Complex Turbulent Flows', *Progress in Aerospace Science* 36: 655-682 (2000)
38. Gordon R, Imbabi M.S, 'CFD Simulation and Experimental Validation of a New Closed Circuit Wind/Water Tunnel Design', *Journal of Fluids Engineering* 120: 311-318 (1998)
39. Ghani S.A.A.A, Aroussi A, Rice E, 'Simulation of Road Vehicle Natural Environment in a Climate Wind Tunnel', *Simulation Practice and Theory* 8:359-375 (2001)
40. Gosman A.D, 'Development in CFD for Industrial and Environmental Applications in Wind Engineering', *Journal of Wind Engineering and Industrial Aerodynamics* 81: 21-39 (1999)
41. Gresho P.M, 'Incompressible Fluid Dynamics: Some Fundamental Formulation Issues', *Annual Review of Fluid Mechanics* 23: 413-453 (1991)
42. Han T, 'Computational Analysis of Three-Dimensional Turbulent Flow around a Bluff Body in Ground Proximity', AIAA Journal 27: 1213-1219 (1989)
43. Han T, Sumamtran V, Harris C, Kuzmanov T, Huebler M, Zak T, 'Flow-Field Simulation of Three Simplified Vehicle Shapes and Comparisons with Experimental Measurements', SAE-960678 (1996)
44. Hess J.L, Smith A.M.O, 'Calculation of Non-Lifting Potential Flow About Arbitrary Three-Dimensional Bodies', Douglas Aircraft Report, ES 40622, 1962
45. Holscher N, Niemann H-J, 'Towards Quality Assurance for Wind Tunnel Tests: A Comparative Testing Program of the Windtechnologische Gesellschaft', *Journal of Wind Engineering and Industrial Aerodynamics* 74-76: 599-608 (1998)
46. Hoxey R.P, Roberston A.P, Richardson G.M, Short J.L, 'Correction of Wind Tunnel Pressure Coefficients for Reynolds Number Effect',

Journal of Wind Engineering and Industrial Aerodynamics 69-71: 547-555 (1997)

47. Hucho W.H, Sovran G, 'Aerodynamics of Road Vehicles', *Annual Review of Fluid Mechanics* 25, pp.485-537 (1993)
48. Hunt J.C.R, 'Industrial and Environmental Fluid Mechanics', *Annual Review of Fluid Mechanics* 23: 1-41 (1991)
49. Hwang R.R, Jaw S.Y, 'Second-Order Closure Turbulence Models: Their Achievements and Limitations", *Proceeding of National Science Council* (Taiwan) 22: 703-732 (1998), (Invited Review Paper)
50. Imaizumi T, 'On the Method of Multi-Suction-and-Blowing Ground Plane in Automotive Wind Tunnels', *JSAE Review* 17: 145-149 (1996)
51. Ito H, Kobayashi R, Kohama Y, 'The Low-Turbulence Wind Tunnel at Tohoku University', *Aeronautical Journal* (1992), pp.141-151
52. Iyer V, Everhart J.L, 'Application of Pressure-Based Wall Correction Methods to Two NASA Langley Wind Tunnel', AIAA 2001-2472
53. Jameson A, 'Optimum Aerodynamic Design via Boundary Control', *AGARD Report 803*(1994)
54. Jameson A, Vassberg J.C, 'Computational Fluid Dynamics for Aerodynamic Design: Its Current and Future Impact', AIAA 2001-0538
55. Jenkins L.N, 'An Experimental Investigation of the Flow over the Rear End of a Notchback Automobile Configuration', SAE paper 2000-01-0489
56. Johnson R.W (ed), *The Handbook of Fluid Dynamics*, 1998, CRC Press
57. Kader B, 'Temperature and Concentration Profiles in Fully Turbulent Boundary Layers', *International Journal of Heat Mass Transfer* 24:1541-1544 (1993)
58. Koike H, 'Evolution of CFD Software from Academic Code to Practical Engineering Software', *Journal of Wind Engineering and Industrial Aerodynamics* 81: 41-55 (1999)
59. Krajnovic S, Davidson L, 'Large-Eddy Simulation of the Flow Around a Round Vehicle Body', SAE 2001-01-0702
60. Kumar A, Hefner J.N, 'Future Challenges and Opportunities in Aerodynamics', *ICAS 2000 Congress* (2000)
61. Kuwahara K, 'Unsteady Flow Simulation and its Visualization' AIAA 99-3405
62. Kwon H-B, Park Y-W, Lee D-H, Kim M-S, 'Wind Tunnel Experimental on Korean High-Speed Trains Using Various Ground Simulation Techniques', *Journal of Wind Engineering and Industrial Aerodynamics* 89: 1179-1195 (2001)
63. Lamar J.E, Obara C.J, Fisher B.D, Fisher D.F, 'Flight, Wind-Tunnel, and Computational Fluid Dynamics Comparison for Cranked Arrow Wing (F-16XL-1) at Subsonic and Transonic Speeds', NASA/TP-2001-210629

64. Landman D, Britcher C.P, 'Experimental geometry Optimization Techniques for Multi-Element Airfoils', Journal of Aircraft 37: 707-713 (2000)

65. Lessard W.B, 'Analysis of Post-Support and Wind-Tunnel Wall Interference on Flow Field about Subsonic High-Lift High-Speed Research Configuration', NASA/TP-2000-210555

66. Liaw P.C, Lan C.E, Chen Y.S, 'Calculation of V/STOL Aircraft Aerodynamics with Defected Jets in Ground Effect', AIAA 93-3530-CP

67. Lin W.L, Chen C.J, 'Automatic Grid Generation of Complex Geometries in Cartesian Co-ordinates', *International Journal for Numerical Methods in Fluids* 28:1303-1324 (1998)

68. Lumley J, Blossey P, 'Control of Turbulence', *Annual Review of Fluid Mechanics* 30:311-327 (1998)

69. Malone M.B, Dwyer W.P, Crouse D, 'A 3D Navier-Stokes Analysis of a Generic Ground Vehicle Shape', AIAA 93-3512

70. Maskell, E.C, A Theory of the Blockage Effects on Bluff Bodies and Stalled Wings in a Closed Wind Tunnel, ARC R&M No. 3400, HMSO, London, 1965

71. Matsuno K, Satofuka N, Sudani N, Fukuda M, 'Numerical Simulation of Flowfields of the NAL Two-Dimensional Transonic Wind Tunnel', ICAS 96-2.4.2: 809-816 (1996)

72. McDonald H, Ross J, Driver D, Smith S, 'Wind Tunnel and Flight', *10th International Symposium on Applications of Laser Techniques to Fluid Mechanics* (2000)

73. McMasters J. H, Cummings R. M, 'Airplane Design- Past, Present, and Future', *Journal of Aircraft* 39: 10-17 (2002)

74. Mehta R.D, Bradshaw P, 'Design Rules for Small Low Speed Wind Tunnels', *Aeronautical Journal* 83: 443-449 (1979)

75. Miles R. B, Lempert W. R, 'Quantitative Flow Visualization in Unseeded Flows', *Annual Review of Fluid Mechanics 29:* 285-326 (1997)

76. Miyoshi H, 'Development and Achievement of NAL Numerical Wind Tunnel (NWT) for CFD Computations', *Proceedings of Supercomputing'94*, pp.685-692

77. Moin P, Mahesh K, 'Direct Numerical Simulation: A Tool in Turbulence Research', *Annual Review of Fluid Mechanics* 30: 539-578 (1998)

78. Mokry M, 'Wall Interference Correction to Drag Measurements in Automotive Wind Tunnels', *Journal of Wind Engineering and Industrial Aerodynamics* 56: 107-122 (1995)

79. Murakami S, 'Current Status and Future Trends in Computational Wind Engineering', *Journal of Wind Engineering and Industrial Aerodynamics* 67-68:3-34 (1997)

80. Nagano Y, Shimada M, 'Computational Modelling and Simulation of Turbulence Flows', *Computational Fluid Dynamics Review 1995*, pp.695-714

81. Niewald P. W, Parker S.L, 'Wind-Tunnel Techniques to Successfully Predict F/A-18E In-Flight Lift and Drag', *Journal of Aircraft* 37: 9-14 (2000)

82. Neyland V, Bosniakov S, Glazkov S, Ivanov A, Matyah S, Mikhailov S, Vlasenko V, ' Conception of Electronic Wind Tunnel and First Results of its Implementation', *Progress in Aerospace Science* 37: 121-145 (2001)

83. Nishi A, Miyagi H, 'Computer-Controlled Wind Tunnel for Wind-Engineering Applications', *Journal of Wind Engineering and Industrial Aerodynamics* 54-55: 493-504 (1995)

84. Okada Y, Nouzawa T, Nakamura T, 'CFD Analysis of the Flow in an Automotive Headlamp', *JSAE Review* 23:95-100 (2002)

85. Oran E.S, 'Matchsticks, Scramjets, and Black Holes: Numerical Simulation Faces Reality', AIAA Journal 40: 1481-494 (2002)

86. Ozawa H, Nishikawa S, Higashida D, 'Development of Aerodynamics for a Solar Race Car', *JSAE Review* 19: 343-349 (1998)

87. Paris J, Padovan J, 'Hierarchically Partitioned Solution Strategy for CFD Applications Part I—Theory', *Computer Methods in Applied Mechanics and Engineering* 126: 197-222 (1995)

88. Paris J, Padovan J, 'Hierarchically Partitioned Solution Strategy for CFD Applications Part II—Numerical Applications', *Computer Methods in Applied Mechanics and Engineering* 126: 223-237 (1995)

89. Pascarelli A, Piomelli U, Candler G.V, 'Multi-Block Large-Eddy Simulations of Turbulent Boundary Layers', *Journal of Computational Physics* 57: 256-279 (2000)

90. Passmore M.A, Richardson S, Imam A, 'An Experimental Study of Unsteady Vehicle Aerodynamics', IMechE, Vol.215, Part D, pp779-788 (2001)

91. Perot B, 'Turbulence Modelling Using Body Force Potentials', *Physics of Fluids* 11: 2645-2656 (1999)

92. Perzon S, Davidson L, 'On CFD and Transient Flow in Vehicle Aerodynamics', SAE Paper 2000-01-0873 (2000a)

93. Perzon S, Davison L, 'On Transient Modelling of the Flow Around Vehicles Using the Reynolds Equation', *ACFD 2000*, Beijing, China, 17-20th Oct. 2000 (2000b)

94. Piomelli U, 'Large-Eddy Simulation: Achievements and Challenges', *Progress in Aerospace Science* 35: 335-362 (1999)

95. Rae W.H, Pope A, *Low-Speed Wind Tunnel Testing* (2nd Edition), John Wiley & Sons (1984)

96. Ranzenbach R, Mairs C, Lasher B, 'Wind Tunnel Boundary Corrections Using the Wall Signature Method for a Bluff Body', AIAA 99-3164-CP
97. Roache P.J, 'Quantification of Uncertainty in Computational Fluid Dynamics', *Annual Review of Fluid Mechanics* 29:123-160 (1997)
98. Rogers S.E, Roth K, Nash S.M, 'CFD Validation of High-Lift Flows with Significant Wind-Tunnel Effects', AIAA 2000-4218
99. Romblad J.P, Leijon T.G, 'Dreamliner III-Summary of Wind Tunnel Tests and the First Phase of Test Driving of a Load Speed Record Vehicle', AIAA-99-3155
100. Ross J.C, Jorgenson C.C, Norgaard M, 'Reducing Wind Tunnel Data Requirements Using Neural Networks', NASA Technical Memorandum 112193 (1997)
101. Rubinstein R, Rumsey C.L, Salas M.D, Thomas J.L (Editors), *Turbulence Modelling Workshop*, ICASE Interim Report No. 37, NASA/CR-2001-210841 (2001)
102. Saltzman E.J, Ayers T.G, 'A Review of Flight-to-Wind Tunnel Drag Correction', *Journal of Aircraft* 19:189-238 (1982)
103. Sawley M.L, Richter R, 'Numerical Simulation of the Flow around a Formula 1 Racing Car', *EPFL SuperComputing Review*, Nov.97, also available: http://sic.epfl.ch/SA/publications/SCR/[illegible]
104. Schetz J.A, 'Aerodynamics of High-Speed Trains', *Annual Review of Fluid Mechanics* 33: 371-414 (2001)
105. Senior A.E, Zhang X, 'The Force and Pressure of a Diffuser-Equipped Bluff Body in Ground Effect', *Journal of Fluids Engineering* 123: 105-111 (2001)
106. Sheng W, Campbell T, Galbraith R.A.McD, 'The Application of CFD to Wind Tunnel of Vehicles', *International Test Expro 2002*, 14-16th, May 2002, Stuttgart, Germany
107. Sheng W, Galbraith R.A.McD, 'CFD Modelling of a Wind Tunnel Working Section for Automotive Work', submitted to *Journal of Automotive Engineering* (2003a)
108. Sheng W, Galbraith R.A.McD, 'CFD Computation in Support of Wind Tunnel Testing', Prepared to be published (2003b)
109. Spalart P.R, 'Strategies for Turbulence Modelling and Simulations', *International Journal of Heat and Fluid Flow* 21: 252-263 (2000)
110. Squire L.C, 'A Review of the Role of Some Small High-Speed Wind Tunnels in Aeronautical Research', *Progress in Aerospace Science* 34:107-166 (1998)
111. Su Y.X, 'Flow Analysis and Design of Three-Dimensional Wind Tunnel Contractions', AIAA Journal 29: 1912-1920 (1991)
112. Suga K, 'Recent Developments in Eddy Viscosity Modelling of Turbulence', *R&D Review of Toyota CRDL* (1998)

113. Swanson R.S, Gillis C.L, 'Wind-Tunnel Calibration and Correction Procedures for Three-Dimensional Models', NACA ARR No.L4E31, Oct. 1944

114. Tabbal S. A. A, Mestreau E, Montmayeur N, Masbernat F, Wolfhugel Y.F, Dumas J.C, 'CFD Aerodynamics of the French High-Speed Train', SAE Paper 920343

115. Taniguchi N, Ono K, Ikeda K, Yamada T, Komoriya T, 'Validation of CFD Commercial Codes for Vehicle Design and Development', SAE-2002-01-1297

116. van Dam C.P, 'Recent Experience with Different Methods of Drag Prediction', *Progress in Aerospace Science* 35: 751-798 (1999)

117. Walker E.L, Everhart J.L, Iyer V, 'Sensitivity Study of the Wall Interference Correction System (WICS) for Rectangular Tunnels', AIAA 2001-0159

118. Wang T.G, Coton F.N, 'Numerical Simulation of Wind Tunnel Wall Effects on Wind Turbine Flows', *Wind Energy* 3: 135-148 (2000)

119. Wang Z.Y, Plate E.J, Rau M, Keiser R, 'Scale Effects in Wind Tunnel Modelling', *Journal of Wind Engineering and Industrial Aerodynamics* 61: 113-130 (1996)

120. Weeks R, 'The Role of the Synthetic Environment', IMechE S555/001/98 (1998)

121. Wendt J.F (ed), Anderson J.D, *Computational Fluid Dynamics: An Introduction*, von Karman Institute Book, Springer 1996

122. Wilcox D.C, 'Reassessment of the Scale-Determining Equation for Advanced Turbulence Models', AIAA Journal 26: 1299-1310 (1988)

123. Wilcox D.C, *Turbulence Modelling for CFD*, DCW Industries (1993)

124. Wolf S.W.D, 'Adaptive Wall Technology for Improved Wind Tunnel Testing Techniques-- A Review', *Progress in Aerospace Science* 31: 85-136, (1995)

125. Wolf T, 'Design of a Variable Contraction for a Full-Scale Automatic Wind Tunnel', *Journal of Wind Engineering and Industrial Aerodynamics* 56: 1-21 (1995)

126. Wolfstein M, 'The Velocity and Temperature Distribution of One-Dimensional Flow with Turbulence Augmentation and Pressure Gradient', *International Journal of Heat Mass Transfer* 12: 301-318 (1969)

127. Yee H.C, Torczynsky J.R, Morton S.A, Visbal M.R, Sweby P.K, 'On Spurious Behaviour of CFD Simulations', *International Journal for Numerical Methods in Fluids* 30: 675-711 (1999)

128. Yokota C, Nakamura Y, Yada S, Funachi K, Kubo F, Ohkubo T, Watanabe T, 'Development of the 2001 Year Model Civic', *JSAE Review* 23: 387-399 (2002)

129. Yoshizawa A, *Hydrodynamic and Magnetohydrodynamic Turbulent Flows-Modelling and Statistical Theory*, Kluwer Academic Publishers (1998)

130. Zhou Q.B, 'A Simple Grid Generation Method', *International Journal for Numerical Methods in Fluids* 26: 713-724 (1998)

APPENDICES

Appendix A: N-S Equations and Turbulence Models

A1 Navier-Stokes Equations

In this research, only incompressible flow is considered. The Navier-Stokes equations are as follows:

Continuity equation:

$$\frac{\partial u_i}{\partial x_i} = 0 \qquad (i=1,2,3) \tag{A.1}$$

Momentum equation:

$$\rho\frac{\partial u_i}{\partial t} + \rho u_j \frac{\partial u_i}{\partial x_j} = -\frac{\partial p}{\partial x_i} + \mu\frac{\partial^2 u_i}{\partial^2 x_j} \qquad (i=1,2,3,\ j=1,2,3) \tag{A.2}$$

A2 RANS Equations

Continuity equation:

$$\frac{\partial U_i}{\partial x_i} = 0 \qquad (i=1,2,3,) \tag{A.3}$$

Momentum equation:

$$\rho\frac{\partial U_i}{\partial t} + \rho U_j \frac{\partial U_i}{\partial x_j} = -\frac{\partial P}{\partial x_i} + \frac{\partial}{\partial x_j}(2\mu S_{ji} - \overline{\rho u_j' u_i'}) \qquad (i=1,2,3,\ j=1,2,3) \tag{A.4}$$

Where:

Strain-rate tensor: $$S_{ij} = \frac{1}{2}(\frac{\partial U_i}{\partial x_j} + \frac{\partial U_j}{\partial x_i})$$

Reynolds stress tensor: $$\tau_{ij} = -\overline{\rho u_i' u_j'}$$

Equations (A.3) and (A.4) actually have ten unknowns, but only four equations are available. To close the RANS equations, the additional equations must be included.

Generally, we presume that the Boussinesq approximation is applicable, which relates the Reynolds stress tensor τ_{ij} to the strain-rate tensor S_{ji} by following formula:

$$\tau_{ij} = 2\mu_T S_{ij} - \frac{2}{3}\rho\kappa\delta_{ij} \tag{A.5}$$

where:

μ_T: turbulent viscosity

κ: turbulent kinetic energy

A3 Turbulence Models

Here give some widely used turbulence models, including Algebraic Model, S-A one equation model, Standard κ-ε model, RNG κ-ε model, Realizable κ-ε model and RSM. These turbulence models, except algebraic model, are all integrated into the Fluent solver.

A3.1 Algebraic Model

Prandtl's mixing-length hypothesis leads to the expression:

$$\tau_{xy} = \mu_T \frac{dU}{dy} \tag{A.6}$$

where μ_T is the eddy viscosity, given by

$$\mu_T = \rho l_{mix}^2 \left|\frac{dU}{dy}\right| \tag{A.7}$$

Prandtl further postulated that for the flows near solid boundaries the mixing length l_{mix} is proportional to the distance from the surface. This is a rather reasonable approximation over a limited portion of a turbulent boundary layer, and actually successful in many engineering applications.

A3.2 One Equation Model

Conventional one-equation model is based on the Prandtl's hypothesis in which the dissipation is defined as following:

$$\varepsilon = C_D \kappa^{3/2} / l \tag{A.8}$$

and the turbulent length scale remains the only part of the model, and the one-equation model has the form of following:

$$\rho\frac{\partial \kappa}{\partial t}+\rho U_j\frac{\partial \kappa}{\partial x_j}=\tau_{ij}\frac{\partial U_i}{\partial x_j}-C_D\rho\frac{\kappa^{3/2}}{l}+\frac{\partial}{\partial x_j}[(\mu+\mu_T/\sigma_k)\frac{\partial \kappa}{\partial x_j}] \tag{A.9}$$

where:

Reynolds stress tensor is given by:

$$\tau_{ij}=2\mu_T S_{ij}-\frac{2}{3}\rho\kappa\delta_{ij} \tag{A.10}$$

The eddy viscosity is:

$$\mu_T=\rho\kappa^{1/2}l \tag{A.11}$$

Generally, the C_D and σ_κ can be taken as the constant, but the length scale l must be specified. Later on, Spalart and Allmaras (1992) developed their one-equation turbulence model, including eight closure constants and three damping functions, the major improvement is that the scale length in eddy viscosity has been removed:

$$\frac{\partial \tilde{\nu}}{\partial t}+U_j\frac{\partial \tilde{\nu}}{\partial x_i}=C_{b1}[1-f_{t2}]\tilde{S}\tilde{\nu}-c_{w1}f_w(\frac{\tilde{\nu}}{d})^2+\frac{1}{\sigma}[\frac{\partial}{\partial x_k}\{(\nu+\tilde{\nu})\frac{\partial \tilde{\nu}}{\partial x_k}\}+C_{b2}\frac{\partial \tilde{\nu}}{\partial x_k}\frac{\partial \tilde{\nu}}{\partial x_k}] \tag{A.12}$$

Turbulent viscosity is calculated by:

$$\nu_t=\tilde{\nu}f_{v1} \tag{A.13}$$

The auxiliary relations and the constants are listed:

$$\begin{cases} f_{v1}=\dfrac{\chi^3}{\chi^3+C_{v1}^3} \\ f_{v2}=1-\dfrac{\chi}{1+\chi f_{v1}} \\ f_w=g[\dfrac{1+C_{w3}^6}{g^6+C_{w3}^6}]^{1/6} \\ \chi=\dfrac{\tilde{\nu}}{\nu} \\ g=r+C_{w2}(r^6-r) \\ r=\dfrac{\tilde{\nu}}{\tilde{S}\kappa^2d^2} \\ \tilde{S}=S+\dfrac{\tilde{\nu}}{\kappa^2d^2}f_{v2} \\ S=\sqrt{2\Omega_{ij}\Omega_{ij}} \end{cases} \tag{A.14}$$

The model constants are:

C_{b1}=0.1355

C_{b2}=0.622

C_{v1}=C.1

σ=2/3

κ=0.41,

$$C_{w1} = \frac{C_{b1}}{\kappa^2} + \frac{(1+C_{b2})}{\sigma}$$

C_{w2}=0.3

C_{w3}=2

The S-A model predicts the flowfield without the prior knowledge of the turbulence structure, and the turbulence model is getting more and more popular in aerodynamics.

A.3.3 Two Equation Models

It is said that the two equation turbulence models are complete, just because the models provide the computation of kinetic energy κ and the turbulent dissipation rate ε or the specific dissipation rate ω, and hence predict the flowfield with no prior knowledge of the turbulent structure (Agarwal 1999). Some conventional two-equation models are given as following.

A3.3.1 Standard κ-ε turbulence model

Turbulent kinetic energy:

$$\rho\frac{\partial \kappa}{\partial t} + \rho U_j \frac{\partial k}{\partial x_j} = \tau_{ij}\frac{\partial U_i}{\partial x_j} - \rho\varepsilon + \frac{\partial}{\partial x_j}[(\mu + \mu_T/\sigma_\kappa)\frac{\partial \kappa}{\partial x_j}] \qquad \text{(A.15)}$$

Turbulent dissipation rate:

$$\rho\frac{\partial \varepsilon}{\partial t} + \rho U_j \frac{\partial \varepsilon}{\partial x_j} = C_{\varepsilon 1}\frac{\varepsilon}{\kappa}\tau_{ij}\frac{\partial U_i}{\partial x_j} - C_{\varepsilon 2}\rho\frac{\varepsilon^2}{\kappa} + \frac{\partial}{\partial x_j}[(\mu + \mu_T/\sigma_\varepsilon)\frac{\partial \varepsilon}{\partial x_j}] \qquad \text{(A.16)}$$

Eddy viscosity is given:

$$\mu_T = \rho C_\mu \kappa^2/\varepsilon \qquad \text{(A.17)}$$

The constants are as follows:

$C_{\varepsilon 1}$=1.44, $C_{\varepsilon 2}$=1.92, C_μ=0.09, σ_κ=1.0, σ_ε=1.3

A3.3.2 RNG κ-ε Turbulence Model

The RNG κ-ε turbulence model is derived from the instantaneous N-S equations, using renormalization group (RNG) methods. The analytical derivation results in a model with constants different from those in the standard κ-ε model, and additional terms and functions in the transport equations for κ and ε. Though a little more computational effort needed, the benefits from RNG turbulence model are immediate (Fluent Manual):

- The RNG model has an additional term in its ε equation that significantly improves the accuracy for rapidly strained flows.
- The effect of swirl on turbulence is included in the RNG model, enhancing accuracy for swirling flows.
- The RNG theory provides an analytical formula for turbulent Prandtl numbers, while the standard κ-ε model uses user-specified, constant values.
- While the standard κ-ε model is a high-Reynolds-number model, the RNG theory provides an analytically-derived differential formula for effective viscosity that accounts for low-Reynolds-number effects. Effective use of this feature does, however, depend on an appropriate treatment of the near-wall region.

Turbulent Kinetic Energy Equation:

$$\rho\frac{\partial \kappa}{\partial t}+\rho U_j\frac{\partial \kappa}{\partial x_j}=\tau_{ij}\frac{\partial U_i}{\partial x_j}+\frac{\partial}{\partial x_j}(\alpha_\kappa \mu_{eff}\frac{\partial \kappa}{\partial x_j})-\rho\varepsilon \qquad \text{(A.18)}$$

Turbulent Dissipation Rate Equation:

$$\rho\frac{\partial \varepsilon}{\partial t}+\rho U_j\frac{\partial \varepsilon}{\partial x_j}=C_{1\varepsilon}\frac{\varepsilon}{\kappa}\tau_{ij}\frac{\partial U_i}{\partial x_j}+\frac{\partial}{\partial x_j}(\alpha_\varepsilon \mu_{eff}\frac{\partial \varepsilon}{\partial x_j})-C_{2\varepsilon}\rho\frac{\varepsilon^2}{\kappa}+R_\varepsilon \qquad \text{(A.19)}$$

Modelling the Effective Viscosity:

$$d(\frac{\rho^2\kappa}{\sqrt{\varepsilon\mu}})=1.72\frac{\hat{\nu}}{\sqrt{\hat{\nu}^3-1+C_\nu}}d\hat{\nu} \qquad \text{(A.20)}$$

where:

$$\hat{\nu}=\mu_{eff}/\mu$$

$$C_\nu \approx 100$$

When the Reynolds number is high, the equation (A.20) is degraded to equation (A.17).

The Consideration of the Inverse Effective Prandtl Numbers

The inverse effective Prandtl numbers, α_κ and α_ε, are computed using the following formula derived analytically by the RNG theory:

$$\left|\frac{\alpha-1.3929}{\alpha_0-1.3929}\right|^{0.6321}\left|\frac{\alpha+2.3929}{\alpha_0+2.3929}\right|^{0.3679}=\frac{\mu_{mol}}{\mu_{eff}} \tag{A.21}$$

where α_0=1.0. In the high-Reynolds-number limit (μ_{mol}/μ_{eff}<<1)), $\alpha_\kappa=\alpha_\varepsilon\approx 1.393$.

The main difference between the RNG and standard κ-ε models lies in the additional term in the ε equation given by

$$R_\varepsilon=\frac{C_\mu\rho\eta^3(1-\eta/\eta_0)}{1+\beta\eta^3}\frac{\varepsilon^2}{\kappa} \tag{A.22}$$

where

$\eta=S\,k/\varepsilon$, η_0=4.38, β=0.012.

and the model constants are:

$C_{1\varepsilon}$=1.42, $C_{2\varepsilon}$=1.68

A3.3.3 Realizable κ-ε Turbulence Model

The Realizable κ-ε turbulence model was developed to overcome the deficiencies of traditional κ-ε turbulence models by adopting a new eddy-viscosity formula for the variable C_μ and a new model equation for dissipation rate ε based on the dynamic equation of the mean-square vorticity fluctuation.

Turbulent Kinetic Energy Equation:

$$\rho\frac{\partial\kappa}{\partial t}+\rho U_j\frac{\partial k}{\partial x_j}=\tau_{ij}\frac{\partial U_i}{\partial x_j}-\rho\varepsilon+\frac{\partial}{\partial x_j}[(\mu+\mu_T/\sigma_\kappa)\frac{\partial\kappa}{\partial x_j}] \tag{A.23}$$

Turbulent dissipation rate:

$$\rho\frac{\partial\varepsilon}{\partial t}+\rho U_j\frac{\partial\varepsilon}{\partial x_j}=\frac{\partial}{\partial x_j}[(\mu+\mu_T/\sigma_\varepsilon)\frac{\partial\varepsilon}{\partial x_j}]+\rho C_1S_\varepsilon-\rho C_2\frac{\varepsilon^2}{\kappa+\sqrt{\nu\varepsilon}} \tag{A.24}$$

where

$$C_1 = \max[0.43, \frac{\eta}{\eta+5}]$$

and

$$\eta = S\kappa/\varepsilon$$

Modelling the Turbulent Viscosity

In Realizable κ-ε models, the eddy viscosity is computed from equation (A.17). The C_μ is not a constant any more, but taken as following form:

$$C_\mu = \frac{1}{A_0 + A_s \frac{\kappa U^*}{\varepsilon}} \tag{A.25}$$

where

$$U^* = \sqrt{S_{ij}S_{ij} + \tilde{\Omega}_{ij}\tilde{\Omega}_{ij}} \tag{A.26}$$

and

$$\tilde{\Omega}_{ij} = \Omega_{ij} - 2\varepsilon_{ijk}\omega_k \tag{A.27}$$

$$\overline{\Omega}_{ij} = \Omega_{ij} - \varepsilon_{ijk}\omega_k \tag{A.28}$$

where $\overline{\Omega}_{ij}$ is the mean rate-of-rotation tensor viewed in a rotating reference frame with the angular velocity ω_κ. The model constants A_0 and A_s are given by

$$A_0 = 4.04, \quad A_s = \sqrt{6}\cos\phi$$

where

$$\phi = \frac{1}{3}\cos^{-1}(\sqrt{6}W)$$

$$W = \frac{S_{ij}S_{jk}S_{ki}}{\tilde{S}}$$

$$\tilde{S} = \sqrt{S_{ij}S_{ij}}$$

$$S_{ij} = \frac{1}{2}(\frac{\partial U_j}{\partial x_i} + \frac{\partial U_i}{\partial x_j})$$

and the constants:

$$C_{1\varepsilon}=1.44,\ C_2=1.9,\ \sigma_\kappa=1.0,\ \sigma_\varepsilon=1.2$$

A3.3.4 κ-ω Turbulence Models

Another family of the two-equation turbulence models is the κ-ω turbulence models, which are based on the solving the equations of the turbulent kinetic energy κ and the specific dissipation rate ω. Wilcox (1988) formulated the standard κ-ω turbulence model:

Turbulent kinetic energy:

$$\rho\frac{\partial \kappa}{\partial t}+\rho U_j\frac{\partial k}{\partial x_j}=\tau_{ij}\frac{\partial U_i}{\partial x_j}-\beta^*\rho\kappa\omega+\frac{\partial}{\partial x_j}[(\mu+\sigma^*\mu_T)\frac{\partial \kappa}{\partial x_j}] \tag{A.29}$$

Specific dissipation rate:

$$\rho\frac{\partial \omega}{\partial t}+\rho U_j\frac{\partial \omega}{\partial x_j}=\alpha\frac{\omega}{\kappa}\tau_{ij}\frac{\partial U_i}{\partial x_j}-\beta\rho\omega^2+\frac{\partial}{\partial x_j}[(\mu+\sigma\mu_T)\frac{\partial \omega}{\partial x_j}] \tag{A.30}$$

Eddy viscosity:

$$\mu_T=\rho\kappa/\omega \tag{A.31}$$

The closure constants:

$\alpha=5/9$, $\beta=3/40$, $\beta^*=0.09$, $\sigma=0.5$, $\sigma^*=0.5$

A3.4 RSM Model

RSM models abandon the isotropic eddy-viscosity hypothesis (employed in Boussinesq hypothesis (A.5)), and solve transport equations for the Reynolds stresses directly, together with an equation for the dissipation rate. Since the RSM accounts for the effects of streamline curvature, swirl, rotation, and rapid changes in strain rate in a more rigorous manner than one-equation and two-equation models, they have greater potentials to give accurate predictions for complex flows. However, the fidelity of RSM predictions is still limited by the closure assumptions employed to model various terms in the exact transport equations for the Reynolds stresses. The modelling of the pressure-strain and dissipation-rate terms is particularly challenging, and often considered to be responsible for compromising the accuracy of RSM predictions.

The RSM might not always yield results that are clearly superior to the simpler models in all classes of flows to warrant the additional computational expense. However, use of the RSM is a must when the flow features of interest are the result of anisotropy in the

Reynolds stresses. Among the examples are cyclone flows, highly swirling flows in combustors, rotating flow passages, and the stress-induced secondary flows in ducts.

The exact equations of Reynolds stress tensor τ_{ij} are as follows:

$$\frac{\partial \tau_{ij}}{\partial t} + U_k \frac{\partial \tau_{ij}}{\partial x_k} = -\tau_{ik} \frac{\partial U_j}{\partial x_k} - \tau_{jk} \frac{\partial U_i}{\partial x_k} + \varepsilon_{ij} - \Pi_{ij} + \frac{\partial}{\partial x_k}[\nu \frac{\partial \tau_{ij}}{\partial x_k} + C_{ijk}] \qquad \text{(A.32)}$$

where:

Pressure strain:

$$\Pi_{ij} = p'(\frac{\partial u_i'}{\partial x_j} + \frac{\partial u_j'}{\partial x_i}) \qquad \text{(A.33)}$$

Dissipation:

$$\varepsilon_{ij} = 2\mu \overline{\frac{\partial u_i'}{\partial x_k} \frac{\partial u_j'}{\partial x_k}} \qquad \text{(A.34)}$$

Turbulent Diffusion:

$$C_{ijk} = \overline{\rho u_i' u_j' u_k'} + \overline{p' u_i'} \delta_{jk} + \overline{p' u_j'} \delta_{ik} \qquad \text{(A.35)}$$

For the dissipation ε_{ij}, most modelers use the Kolmogorov hypothesis of local isotropy, which has the following relationship:

$$\varepsilon_{ij} = \frac{2}{3} \rho \varepsilon \delta_{ij} \qquad \text{(A.36)}$$

where:

$$\varepsilon = \nu \overline{\frac{\partial u_i'}{\partial x_k} \frac{\partial u_i'}{\partial x_k}} \qquad \text{(A.37)}$$

With regard to the turbulent diffusion C_{ijk}, Launder Reece and Rodi (1975) proposed a general closure approximation as follow:

$$C_{ijk} = -C_s' \frac{\kappa}{\rho \varepsilon} [\tau_{im} \frac{\partial \tau_{jk}}{\partial x_m} + \tau_{jm} \frac{\partial \tau_{ik}}{\partial x_m} + \tau_{km} \frac{\partial \tau_{ij}}{\partial x_m}] \qquad \text{(A.38)}$$

A well known RSM model is the LRR model, proposed by Launder, Reece and Rodi (1975), and most newer RSM models are mostly based on the LRR model. The LRR model is as follows:

Reynolds-Stress tensor:

$$\frac{\partial \tau_{ij}}{\partial t} + U_k \frac{\partial \tau_{ij}}{\partial x_k} = -P_{ij} + \frac{2}{3}\rho\varepsilon\delta_{ij} - \Pi_{ij} - C_s \frac{\partial}{\partial x_k}[\frac{\kappa}{\varepsilon}(\tau_{im}\frac{\partial \tau_{jk}}{\partial x_m} + \tau_{jm}\frac{\partial \tau_{ik}}{\partial x_m} + \tau_{km}\frac{\partial \tau_{jk}}{\partial x_m})] \tag{A.39}$$

Dissipation rate ε:

$$\rho\frac{\partial \varepsilon}{\partial t} + \rho U_j \frac{\partial \varepsilon}{\partial x_j} = C_{e1}\frac{\varepsilon}{\kappa}\tau_{ij}\frac{\partial U_i}{\partial x_j} - C_{e2}\rho\frac{\varepsilon^2}{\kappa} - C_\varepsilon \frac{\partial}{\partial x_k}[\frac{\kappa}{\varepsilon}\tau_{km}\frac{\partial \varepsilon}{\partial x_m}] \tag{A.40}$$

Pressure-strain correlation is:

$$\begin{aligned}\Pi_{ij} = {} & C_1\frac{\varepsilon}{\kappa}(\tau_{ij} + \frac{2}{3}\rho\kappa\delta_{ij}) - \hat{\alpha}(P_{ij} - \frac{2}{3}P\delta_{ij}) - \hat{\beta}(D_{ij} - \frac{2}{3}P\delta_{ij}) \\ & - \hat{\gamma}\rho\kappa(S_{ij} - \frac{1}{3}S_{kk}\delta_{ij}) + \left[0.125\frac{\varepsilon}{\kappa}(\tau_{ij} + \frac{2}{3}\rho\kappa\delta_{ij}) - 0.015(P_{ij} - D_{ij})\right]\frac{\kappa^{3/2}}{\varepsilon}\end{aligned} \tag{A.41}$$

The auxiliary relations are:

$$\begin{cases} P_{ij} = \tau_{im}\dfrac{\partial U_j}{\partial x_m} + \tau_{jm}\dfrac{\partial U_i}{\partial x_m} \\ D_{ij} = \tau_{im}\dfrac{\partial U_m}{\partial x_j} + \tau_{jm}\dfrac{\partial U_m}{\partial x_i} \\ P = \dfrac{1}{2}P_{kk} \end{cases} \tag{A.42}$$

Appendix B: Near-Wall Treatments

Flows are significantly affected by the presence of walls, especially the presence of the complicated geometries in the flows. Obviously, the mean velocity field is affected through the no-slip condition that has to be satisfied at the wall. When very close to the wall, viscous damping reduces the tangential velocity fluctuations, while kinematic blocking reduces the normal fluctuations. Toward the outer part of the near-wall region, however, the turbulence is rapidly augmented by the production of turbulence kinetic energy due to the large gradients in mean velocity.

The near-wall modelling significantly impacts the fidelity of numerical solutions, inasmuch as walls are the main source of mean vorticity and turbulence. After all, it is in the near-wall region that the solution variables have large gradients, and the momentum and other scalar transports occur most vigorously. Therefore, accurate representation of the flow in the near-wall region largely determines the successful predictions of wall-bounded turbulent flows.

It is shown that the near-wall region can be largely subdivided into three layers. In the innermost layer, called the "viscous sublayer", the flow is almost laminar, and the molecular viscosity plays a dominant role in momentum and heat or mass transfer. In the outer layer, called the fully-turbulent layer, turbulence plays a major role. Finally, there is an interim region between the viscous sublayer and the fully turbulent layer where the effects of molecular viscosity and turbulence are equally important. Fig.B1 illustrates these subdivisions of the near-wall region, plotted in semi-log coordinates.

Traditionally, there are two approaches to modelling the near-wall region. In one approach, the viscosity-affected inner region (viscous sublayer and buffer layer) is not resolved. Instead, semi-empirical formulae called "wall functions" are used to bridge the viscosity-affected region between the wall and the fully-turbulent region. The use of wall functions obviates the need to modify the turbulence models to account for the presence of the wall.

In another approach, the turbulence models are modified to be suitable for the low Reynolds number flows and to enable the viscosity-affected region to be resolved with a mesh all the way to the wall, including the viscous sublayer. In Fluent, three near-wall treatments are integrated: standard wall function, non-equilibrium wall function and enhanced near-wall treatment.

B1. Standard Wall Function

The standard wall function is based on the proposal of Launder and Spalding, and has been most widely used for many industrial flows. In general, the mean velocity near wall satisfies the logarithmic law:

$$U^* = \frac{1}{\kappa}\ln(Ey^*) \tag{B.1}$$

where:

$$U^* = \frac{U_p C_\mu^{1/4} \kappa_p^{1/2}}{\tau_\omega / \rho} \tag{B.2}$$

$$y^* = \frac{\rho C_\mu^{1/4} \kappa_p^{1/2}}{\mu} \tag{B.3}$$

and

U_p	Mean velocity of the fluid at point P
κ_p	Turbulence kinetic energy at point P
y_p	Distance from point P to the wall
μ	Dynamic viscosity of the fluid

But the logarithmic law is valid only when y* is bigger than 30, so when the calculation region is very near the wall, the laminar stress-strain relationship is employed instead.

$$U^* = y^* \tag{B.4}$$

Where:

$\kappa=0.42$	Von Karman constant
$E=9.81$	Empirical constant

B2. Non-equilibrium wall function

Generally speaking, the standard wall functions are simple, and work reasonably well for a broad range of industrial flows; but, they tend to become less reliable when the flow situations depart too much from the ideal conditions of the constant-shear and local equilibrium hypotheses. Therefore, when the near-wall flows are subjected to severe pressure gradients, or when the flows are in strong non-equilibrium, the predictions with standard wall functions are likely questionable.

In Fluent, the non-equilibrium wall functions are available, which improve the standard wall functions in two aspects:

(i) Launder and Spalding's log-law for mean velocity is sensitized to pressure-gradient effects

(ii) The two-layer-based concept is adopted to compute the budget of turbulence kinetic energy ($\overline{G}_k$, $\bar{\varepsilon}$) in the wall-neighboring cells.

The logarithmic law is given:

$$\frac{\tilde{U}C_\mu^{1/4}\kappa^{1/2}}{\tau_w/\rho} = \frac{1}{\kappa}\ln(E\frac{\rho C_\mu^{1/4}\kappa^{1/2}y}{\mu}) \tag{B.5}$$

where:

$$\tilde{U} = U - \frac{1}{2}\frac{dp}{dx}[\frac{y_v}{\rho\kappa\sqrt{k}}\ln(\frac{y}{y_v}) + \frac{y-y_v}{\rho\kappa\sqrt{k}} + \frac{y_v^2}{\mu}] \tag{B.6}$$

and y_v is the physical viscous sublayer thickness, and is computed from

$$y_v = \frac{\mu y_v^*}{\rho C_\mu^{1/4}\kappa_P^{1/2}} \tag{B.7}$$

where $y_v^* = 11.225$.

At the same time, the non-equilibrium wall function employs the two-layer concept in computing the budget of turbulence kinetic energy at the wall-adjacent cells, which is needed to solve the k equation at the wall-neighboring cells. The wall-neighboring cells are assumed to consist of a viscous sublayer and a fully turbulent layer. The following profile assumptions for turbulence quantities are made:

$$\tau_t = \begin{cases} 0, & y < y_v \\ \tau_w, & y > y_v \end{cases} \qquad k = \begin{cases} (\frac{y}{y_v})k_P, & y < y_v \\ k_P, & y > y_v \end{cases} \qquad \tau_t = \begin{cases} \frac{2\nu\kappa}{y^2}, & y < y_v \\ \frac{\kappa^{3/2}}{C_l y}, & y > y_v \end{cases} \tag{B.8}$$

where $C_l = \kappa C_\mu^{-3/4}$

Then the cell-averaged production of turbulent kinetic energy, $\overline{G}_k$, and the cell-averaged dissipation rate, $\bar{\varepsilon}$, can be computed from the volume average of G_k and ε of the wall-adjacent cells.

$$\overline{G}_k = \frac{1}{y_n}\int_0^{y_n} \tau_t \frac{\partial U}{\partial y} dy = \frac{1}{\kappa y_n} \frac{\tau_w^2}{\rho C_\mu^{1/4} \kappa_P^{1/2}} \ln(\frac{y_n}{y_v}) \tag{B.9}$$

and

$$\bar{\varepsilon} = \frac{1}{y_n}\int_0^{y_n} \varepsilon \, dy \tag{B.10}$$

The turbulence kinetic energy budget for the wall-neighboring cells is effectively sensitized to the proportions of the viscous sublayer and the fully turbulent layer, which varies widely from cell to cell in highly non-equilibrium flows. It effectively relaxes the local equilibrium assumption (production = dissipation) that is adopted by the standard wall function in computing the budget of the turbulence kinetic energy at wall-neighboring cells. Thus, the non-equilibrium wall functions, in effect, partly account for non-equilibrium effects neglected in the standard wall function.

B3. Enhanced Near-Wall Treatment

For the numerical computation, the standard wall functions may indeed give reasonably accurate predictions for many flows of high-Reynolds-number, whilst the non-equilibrium wall functions further extend the applicability of the wall function approach by including the effects of pressure gradient and strong non-equilibrium. However, the wall function approach becomes less reliable when the flow conditions depart too much from the ideal conditions underlying the wall functions, such as the pervasive low-Reynolds-number or near-wall effects, massive transpiration through the wall, severe pressure gradients leading to boundary layer separations, strong body forces, high three-dimensionality in the near-wall region etc.

In Fluent, a near-wall modelling method is provided hopefully to overcome the difficulties that wall function approach has. The near-wall modelling method combines a two-layer model with enhanced wall functions, i.e. when the near-wall mesh is fine enough to resolve the laminar sublayer (typically $y^+ \approx 1$), the enhanced wall treatment will be identical to a two-layer zonal model, in which the low Reynolds number turbulence model is employed in the near-wall region. However, the restriction that the near-wall mesh must be sufficiently fine everywhere might impose too large a computational requirement. As a result, one would like to have a near-wall formulation that can be used with coarse meshes as well as fine meshes. Hopefully, the excessive error should not be incurred for intermediate meshes that are too fine for the near-wall cell centroid to lie in the fully turbulent region, but also too coarse to properly resolve the sublayer. To achieve the goal of having a near-wall modelling approach that will possess the accuracy of the standard two-layer approach for fine near-wall, Fluent actually combines a two-layer model with enhanced wall functions

B3.1 Two-Layer Model

The two-layer model is an integral part of the enhanced wall treatment, and is used to specify both ε and the turbulent viscosity in the near-wall cells. In this approach, the whole domain is subdivided into a viscosity-affected region and a fully-turbulent region. The demarcation of the two regions is determined by a wall-distance-based, turbulent Reynolds number Re_y:

$$\mathrm{Re}_y = \frac{\rho y \sqrt{\kappa}}{\mu} \tag{B.11}$$

In the fully turbulent region, given by Re_y>200, the conventional turbulence models are employed, while in the viscosity-affected near-wall region, identified by Re_y<200, the one-equation turbulence model of Wolfstein (1969) is employed.

B3.2 Enhanced Wall Functions

The enhanced wall function is used to formulate the law-of-the wall as a single wall law for the entire wall region, in which blends the linear (laminar) and logarithmic (turbulent) laws-of-the-wall using a function suggested by Kader (1993). This approach allows the fully turbulent law to be easily modified and extended to take into account other effects

such as pressure gradients or variable properties. This formula also guarantees the correct asymptotic behavior for large and small values of y^+ and reasonable representation of velocity profiles in the cases where y^+ falls inside the wall buffer region ($3 < y^+ < 10$).

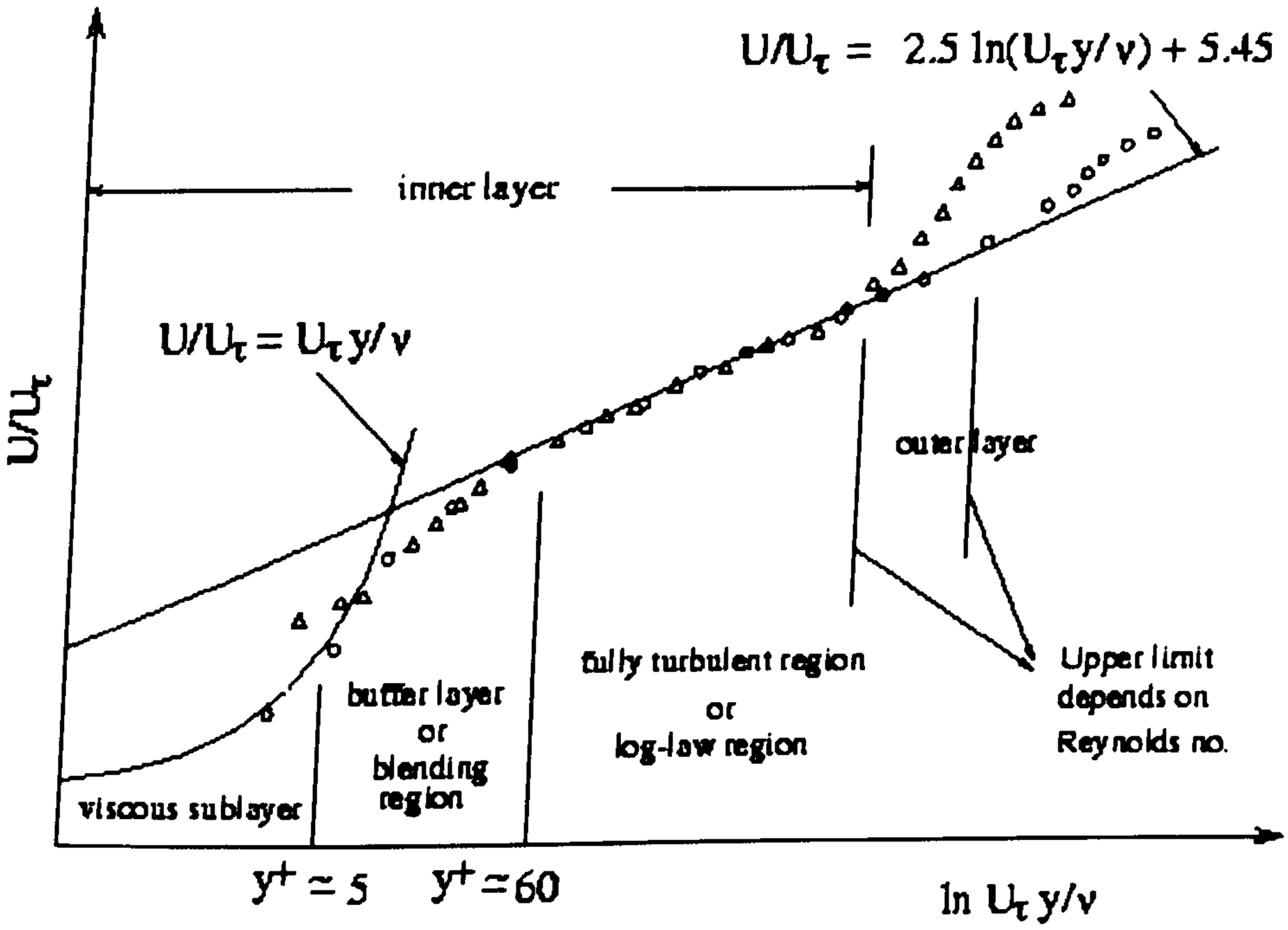

Fig. B1 Subdivisions of the Near-Wall Region (Fluent Manual)

APPENDIX C: Dimensional Analysis and Similitude Laws

C1. Dimensional Analysis

The practical problems are usually related to many variables, especially for the fluid dynamic problems, in which the pertinent variables include the three general groups:

Geometry:

The geometric characteristics can be usually represented by a series of volumes, surfaces, lengths and angles. For most problems in fluid dynamics the geometry of the system plays an important role and a sufficient number of geometric variables must be included to describe the system.

Material Properties:

Generally, the response of a system to external factors such as forces/moment, pressures, and the changes in temperature is dependent on the nature of the materials. The material properties are usually included in the variables.

External Effects:

Any variable cause a change in the system is included in the external effects. In the fluid dynamics, variables would be related to the pressures, velocities, external forces, temperature etc.

As mentioned before, the problems with all these variables can seldom be resolved. In solving any practical problem, the variables must be reduced to a minimum, which is very practical and important, because some variables are not independent and some are trivial. Only those independent variables are of interest in solving practical problems.

Dimensional analysis is a very important tool in reducing the theoretical and experimental work. Take a simple example, considering an incompressible steady flow of a car model in the working section and the drag is considered to be of the most interest. Now we assume the fluid is Newtonian fluid (note that most cases in practical problems, the fluid can be

taken as Newtonian fluid), and the working section is horizontal. The general relationship can be expressed as:

$$F_d = f(L, \rho, \mu, V) \tag{C.1}$$

where: F_d Drag force per unit frontal area of the car

L Characteristic length of the car (here taken as the length of the car)

V Fluid velocity in the pipe

ρ Fluid density

μ Kinematic viscosity

Following Buckingham Pi theorem, we have first Pi term:

$$\Pi_1 = F_d L^a V^b \rho^c \tag{C.2}$$

Since this combination is to be dimensionless, i.e.

$$(FL^{-2})(L)^a (LT^{-1})^b (FL^{-4}T^2)^c = F^0 L^0 T^0 \tag{C.3}$$

The conditions that satisfy equation (C.3) are: a=0, b= -2 and c= -1

$$\Pi_1 = \frac{F_d}{\rho V^2} \tag{C.4}$$

The second Pi term can be expressed as:

$$\Pi_2 = \mu L^a V^b \rho^c \tag{C.5}$$

or

$$(FL^{-2}T)(L)^a (LT^{-1})^b (FL^{-4}T^2)^c = F^0 L^0 T^0 \tag{C.6}$$

so, a= -1, b= -1, c= -1

Second Pi term is:

$$\Pi_2 = \frac{\mu}{LV\rho} \tag{C.7}$$

Rewrite (C.6) and (C.7) in more general term:

$$\Pi_1 = \frac{F_d}{1/2 \rho V^2} \tag{C.8}$$

$$\Pi_2 = \frac{\rho VL}{\mu} \tag{C.9}$$

The first term is actually the drag coefficient, and the second term the Reynolds number. So we have:

$$\frac{F_d}{1/2 \rho V^2} = \phi(\frac{\rho VL}{\mu}) \tag{C.10}$$

or

$$C_d = \phi(R_e) \tag{C.11}$$

where: C_d Drag coefficient

R_e Reynolds number

The meaning of Equation (C.10) or (C.11) is that drag coefficient is only the function of Reynolds number, but the drag per frontal area is the function of four independent variables. Suppose we want to investigate the drag characteristics of the car, according to equation (C.1), we have to vary each of 4 parameters to measure the corresponding drag.

- Design different sizes of model: varying L
- Use different working fluid: varying μ
- Use different working fluid: varying density ρ
- Test model in different speed: varying velocity V

Then another difficulty is to find out the relationship of the measured data, it's not easy at all. But by equation (C.10) or (C.11), the problem becomes much easier, the varying parameter is Reynolds number, which is reached easily by varying speed in wind tunnel. The more important issue for equation (C.10) and (C.11) is they have wider applications, i.e., the same Reynolds number will give the same test results without regard to the size of the scaled model.

C2. Similitude Laws

Models are widely used in many engineering projects, such as the models of aircrafts, ships, rivers, dams, harbors etc. A model is actually a representation of a physical system that may be used to predict the behavior of the system in the scaled sizes (bigger or smaller) for which is easy to handle in the laboratory.

In fluid dynamics, there are many variables arising in fluid dynamics problems. Fortunately, not all the variables would be encountered in all problems. In the previous section, the combinations of the variables into the common dimensionless forms are more useful.

It's supposed that any given problem of a prototype can be described in terms of a set of Pi terms as:

$$\Pi_1 = \phi(\Pi_2, \Pi_3, \cdots, \Pi_n) \tag{C.12}$$

and a similar relationship can be written for the model:

$$\Pi_{1m} = \phi(\Pi_{2m}, \Pi_{3m}, \cdots, \Pi_{nm}) \tag{C.13}$$

if the model is designed and operated under the following conditions:

$$\begin{cases} \Pi_{2m} = \Pi_2 \\ \Pi_{3m} = \Pi_3 \\ \quad . \\ \quad . \\ \quad . \\ \Pi_{nm} = \Pi_m \end{cases} \tag{C.14}$$

and the prediction equation is:

$$\Pi_1 = \Pi_{1m} \tag{C.15}$$

Equation (C.14) is actually the similitude law.

According to the similitude law above, it's necessary that the similarity requirement between the model and prototype must be satisfied which is the requirement of the Pi Theorem. If we have two length variables l_1 and l_2, the resulting similarity requirement is:

$$\frac{l_1}{l_2} = \frac{l_{1m}}{l_{2m}} \tag{C.16}$$

so that

$$\frac{l_{1m}}{l_1} = \frac{l_{2m}}{l_2} \tag{C.17}$$

The ratio l_{1m}/l_1 or l_{2m}/l_2 can be defined as the length scale. For most of the models there will be only one length scale and all lengths are fixed in accordance with this scale, but for some special cases, there are different length scale in different directions, such as some river models, the length of river is very long, but the depth is small, if using the same length scale, the model will be too long to be seated in the laboratory, or too shallow in depth that the flow may be affected mainly by roughness of river bed. The practical way is using small length ratio for the length of the river and big ratio for the depth of the river.

For the car testing, the testing model is immersed in the fluid. The similitude law requires geometric and Reynolds number similarity, then the general formulation for these problems is:

$$\Pi = \phi(\frac{l_i}{l}, \frac{\varepsilon}{l}, R_e) \tag{C.18}$$

where: l is a characteristic length of the system, and l_i is the other pertinent lengths, ε/l id the relative roughness of the surfaces.

According to Equation (C.18), the model design requires the similarity in geometry and roughness, and the scale ratio is λ ($\lambda = \frac{l_m}{l}$), and the model test should be in the same Reynolds number, i.e.,

$$\frac{\rho_m V_m l_m}{\mu_m} = \frac{\rho V l}{\mu} \tag{C.19}$$

since the conventional working fluid in wind tunnels is air, the same fluid as the prototype encounters, i.e., $\rho_m = \rho$ and $\mu_m = \mu$. So we have:

$$V_m = \frac{l}{l_m} V \tag{C.20}$$

If the model is designed as the ratio of 10%, in order to keep the same Reynolds number, the velocity for the test should be 10 times of that of the prototype. If the velocity of the prototype is 100mph, the model test velocity should be 1000mph or 444m/s (supersonic!). In practice, there are two problems in the model test: one is that supersonic wind tunnels are not many and not easy to access; another is that the prototype is in low air speed, the air can be considered as incompressible fluid, but the model is in supersonic flow, the flow must be treated as compressible fluid. There is no similar pattern in low speed flow and supersonic flow. In practice, it is very difficult for scaled model to keep the same Reynolds number as the Prototype. What the tunnel engineers do is get the Reynolds number as high as possible.

Fortunately, much experience has been accumulated in the wind tunnel testing. The experienced tunnel engineers can effectively extrapolate the test data to the prototype. From this standpoint, it's actually a matter of the use of wind tunnel data.